

**Instrumentation, fabrication techniques and  
method development for  
sample introduction, preparation and extraction on  
centrifugal microfluidic devices in motion**

David A. Duford

Department of Chemistry  
McGill University  
Montreal, Quebec, Canada  
April 2012

A thesis submitted to McGill University  
in partial fulfillment of the requirements of the degree of  
Doctor of Philosophy

## Abstract

A growing number of pollutants are being shown to have a large environmental and health impact resulting in stricter legislative limits. Increased environmental monitoring is forcing analytical chemists to consider automating and miniaturizing current standard methods. Instrumentation and sample handling techniques for centrifugal microfluidic devices in motion have been developed with the objective of integrating multi-step reactions into a single device for the analysis of environmental solid samples.

In order to study and optimize centrifugal microfluidic devices in motion, motorized stages integrating a camera, strobe and a variety of other peripheral components were developed. These allowed precise control of the devices throughout the methods' spin sequences and simultaneous acquisition of a series of stop action photographs of the devices.

Non-contact methodologies for sample introduction, preparation and extraction on centrifugal microfluidic devices in motion are presented. To achieve this, hybrid fabrication techniques including the use of 3D printers were investigated and a World-to-Disk interface permitting the introduction of a solution gradient to a spinning device was developed. The interaction of integrated mobile magnets with a series of fixed magnets placed below the spinning devices was also investigated resulting in the development of both a magnetically actuated solid sample preparation and a magnetically actuated liquid-solid extraction technique. New automated and miniaturized methods for the analysis of environmentally important species such as polycyclic aromatic hydrocarbons and pesticides in solid samples are presented.

## **Abrégé**

Les polluants ont des impacts importants sur la santé et l'environnement résultant à des restrictions accrues des limites législatives. Cette surveillance environnementale accrue pousse les chimistes analytiques vers l'automatisation et la miniaturisation des méthodes de référence actuelles. L'analyse d'échantillons environnementaux solides bénéficiera de cette envolée par le développement de nouveaux instruments et techniques de manipulation d'échantillon via des dispositifs microfluidiques centrifuges qui intègrent des réactions à étapes multiples sur un dispositif unique.

Afin d'étudier et d'optimiser les dispositifs microfluidiques centrifuges en mouvement, des plateformes motorisées qui incluent une caméra, une lumière stroboscopique et une variété d'autres composantes périphériques ont été développées. Celles-ci ont permis le contrôle efficace des dispositifs tout au long des séquences giratoires et l'acquisition simultanée de séries de photographies en arrêt sur image.

Des méthodologies sont présentées pour l'introduction, la préparation et l'extraction d'échantillons sur des dispositifs microfluidiques centrifuges en mouvement. Ceci fut réalisé grâce à la recherche de techniques de fabrication hybrides incluant l'utilisation d'imprimantes 3D menant au développement d'une interface permettant l'introduction de solutés à concentrations variables aux dispositifs en mouvement. De plus, l'interaction d'aimants mobiles intégrés avec une série d'aimants fixes placée sous les dispositifs en mouvement a mené au développement des techniques de préparation d'échantillons solides par force

magnétique et d'extraction liquide-solide d'échantillons par force magnétique. De nouvelles méthodes automatisées et miniaturisées ont été développées pour l'analyse d'espèces environnementales importantes telles que les hydrocarbures polycycliques aromatisés et les pesticides dans des échantillons solides.

## Contributions to Original Knowledge

- 1) New types of integrated motorized stages were designed and constructed for the study of centrifugal microfluidic devices.
- 2) A hybrid device was made from both subtractive and additive manufacturing techniques taking advantage of the characteristics of each.
- 3) Non-contact sample introduction, metering, and distribution of liquids to centrifugal microfluidic devices while they were in motion was achieved using a “Centrifugal Liquid Addition Distributor” (CLAD).
- 4) Magnetically actuated solid sample preparation for crushing and grinding solids in spinning centrifugal microfluidic devices was demonstrated on crystal samples.
- 5) Magnetically actuated liquid-solid extraction in spinning centrifugal microfluidic devices was demonstrated and applied to soil samples.
- 6) An automated method and miniaturized chemical device were developed for an absorbance-based determination of pyrene in soil samples integrating sample preparation and detection. A reduction in sample and reagent volumes was achieved.
- 7) An automated method and two centrifugal microfluidic devices were developed for the enzyme inhibition-based determination of carbofuran pesticide residues in vegetable and soil samples integrating sample preparation, sedimentation, multiple reaction steps and detection. A reduction in sample and reagent volumes was achieved.

## **Contributions of Authors**

In addition to the introduction and conclusion, the contents of this thesis are presented as a thesis chapter of unpublished work (Chapter 2), two thesis chapters that are being prepared for submission to peer-reviewed journals (Chapters 3 and 7) and three published manuscripts (Chapters 4–6).

Prof. Eric D. Salin of McGill University supervised all of the work presented, and was available for project guidance and direction throughout.

The experiments described in Chapters 2, 3 and 5 were designed, conducted, and interpreted by the author under the supervision of Prof. Salin, the only exception being the programming code of the servo motor by Dan (Donna) Peng, an undergraduate student under the immediate supervision of the author.

Chapter 4 is a result of collaboration with an undergraduate student, Adam P. Bouchard. The author contributed to the conception and design of the experiments, instructed and advised on instrumental aspects of the work, performed preliminary experimental work, supervised subsequent experimental work, equally shared in data analysis, wrote the manuscript, submitted the manuscript and replied to reviewers/editors. Adam P. Bouchard contributed to the conception and design of the experiments, performed experimental work and shared in data analysis.

Chapters 6 and 7 are the result of collaboration with a fellow graduate student, Ms. Yongqing Xi. The author contributed to the design of the experiments, instructed and advised on instrumental aspects of the work, supervised the experimental work, helped with data analysis, wrote the

manuscripts, submitted the manuscripts and replied to reviewers/editors. Yongqing Xi contributed to the conception and design of the experiments and carried out the analysis (experimental work) as well as processed and analyzed the data.

Though appearing as the second name on two of the published manuscripts, these manuscripts rightfully indicate that “these authors should be considered equal contributors”. The author of this thesis generously gave the honour of appearing first to his co-authors while remaining a primary author of the research. Likewise, this thesis is the only one in which these manuscripts have been reprinted.

The author of this doctoral thesis wrote all the texts and created all the figures and videos including those appearing in the three published manuscripts, while the listed co-authors aided in the editing process. These published manuscripts are reproduced with permission and waivers from the publishers and co-authors have been submitted.

## **Acknowledgments**

“The road to success is paved with the will to never stop learning.” I wrote this anonymous quote in my High School yearbook some 15 years ago and have strived to live up to it academically, spiritually and socially. This thesis is just a few more bricks in that road for which it would have been impossible to pave without the help (and patience) of the following people.

First, I would like to express my sincere gratitude to my supervisor, Prof. Eric D. Salin. His incredible patience, understanding and guidance were truly inspiring. I would also like to thank Prof. David H. Burns and Prof. Cameron D. Skinner for providing supervision and advice as members of my committee.

Members of the library and department's technical staff (Fred Kluck, Jean-Philippe Guay, Richard Rossi, Weihua Wang, Georges Kopp and Chantal Marotte) also deserve many thanks for their continuous battle finding articles, filling paperwork as well as repairing and troubleshooting all types of instruments.

Thank you to former and current lab members. Special thanks to Dan (Donna) Peng for her help with the servo motor, to Erin J. Templeton for editorial help, to Adam P. Bouchard for collaborating with the CLAD project and Yongqing Xi for collaborating with the PAH and pesticide projects.

I very gratefully acknowledge scholarship support from the “Natural Science and Engineering Research Council of Canada” (NSERC), the “Fonds québécois de la recherche sur la nature et les technologies” (FQRNT) and McGill University’s “Richard H. Tomlinson Fellowship”.

To my family for their continued support by their words of encouragement, generous meals and going to my adventurous wedding in Mexico.

And lastly, to my wife, Dulce Aline Carboney Palafox, whose love, encouragement and support has always been unconditional, wholehearted and absolute. You are my eternal best friend.

## Table of Contents

Abstract .....	ii
Abrégé .....	iii
Contributions to Original Knowledge .....	v
Contributions of Authors .....	vi
Acknowledgments .....	viii
Table of Contents .....	x
List of Figures .....	xvi
List of Tables .....	xxiv
List of Equations .....	xxv
Abbreviations .....	xxvii
CHAPTER 1: Introduction .....	1
1.1 Theoretical Concepts & Literature Review .....	2
1.1.1 Sample Preparation and Extraction .....	2
1.1.2 Magnetism .....	5
1.1.3 Microfluidics .....	7
1.1.3.1 Magnetism in Microfluidics .....	9
1.1.4 Centrifugal Microfluidics .....	10
1.1.4.1 Liquid Flow Rates .....	14
1.1.4.2 Capillary Burst Valves .....	17
1.1.4.3 Sedimentation .....	18
1.1.4.4 Magnetism in Centrifugal Microfluidics .....	19
1.1.4.5 Spectroscopic Detection .....	20
1.2 Objectives .....	21
1.3 Thesis Outline .....	21
1.4 References .....	23
CHAPTER 2: Instrumentation .....	29
2.1 Motorized Stages .....	29
2.1.1 Motors and Drives .....	33
2.1.2 Spindle Shafts .....	34

2.1.3 Fixed Magnet Base.....	37
2.1.4 Cameras and Lenses .....	38
2.1.5 Strobes .....	41
2.1.6 Computer Interfacing .....	42
2.1.6.1 DC Motor Control.....	44
2.1.6.2 Servo Motor Control.....	46
2.1.6.3 Peripherals Control .....	48
2.1.6.4 Trigger Breakout Box .....	48
2.1.7 System Software .....	50
2.1.8 Safety Shields.....	51
2.1.9 Summary of Motorized Stages .....	52
2.2 Centrifugal Microfluidic Devices: Subtractive Manufacturing Techniques and Components.....	53
2.2.1 Subtractive Manufacturing Techniques .....	53
2.2.1.1 Laser Cutting .....	53
2.2.1.2 CNC Cutting and Milling.....	54
2.2.1.3 Lamination Sealing Techniques .....	56
2.2.2 Components and “Mobile Magnets” .....	57
2.2.2.1 “Mobile Magnet” Composition, Coatings and Encapsulation.....	58
2.2.2.2 Acid Resistivity and Elemental Analysis by ICP-AES.....	62
2.3 References.....	69
CHAPTER 3: Comparison of 3D Printing Technologies for Rapid Prototyping and Additive Manufacturing of Centrifugal Microfluidic Devices .....	71
3.1 Abstract.....	71
3.2 Introduction .....	72
3.3 Experimental .....	78
3.3.1 Designing Test Structures .....	78
3.3.2 Manufacturing Test Structures.....	78
3.3.2.1 Fused Deposition Modeling (FDM) .....	79
3.3.2.2 Film Transfer Imaging (FTI) .....	80
3.3.2.3 PolyJet Modeling (PJM) .....	81

3.3.3 Studying Test Structures .....	81
3.3.3.1 Study 1: Precision, Accuracy and Ability to Retain Liquid .....	81
3.3.3.2 Study 2: Surface Finish and Chemical Resistivity .....	82
3.3.3.3 Study 3: Ability to “Print” Capillary Burst Valves .....	84
3.4 Results and Discussion .....	85
3.4.1 Designing Test Structures .....	85
3.4.2 Manufacturing Test Structures.....	89
3.4.3 Studying Test Structures .....	92
3.4.3.1 Study 1: Precision, Accuracy and Ability to Retain Liquid .....	92
3.4.3.2 Study 2: Surface Finish and Chemical Resistivity .....	97
3.4.3.3 Study 3: Ability to “Print” Capillary Burst Valves .....	102
3.4.4 Summary of Results .....	108
3.5 Conclusions .....	110
3.6 References .....	112
CHAPTER 4: Non-Contact Addition, Metering, and Distribution of Liquids into Centrifugal Microfluidic Devices in Motion .....	114
4.1 Abstract.....	116
4.2 Introduction .....	116
4.3 Experimental Section .....	119
4.3.1 Reagents .....	119
4.3.2 Device Design and Fabrication.....	119
4.3.2.1 Centrifugal Liquid Addition Distributor (CLAD).....	119
4.3.2.2 Centrifugal Disk Base .....	122
4.3.3 Instrumentation .....	122
4.4 Results and Discussion .....	123
4.4.1 Liquid Addition and Distribution .....	123
4.4.2 Gradient.....	126
4.5 Conclusions .....	127
4.6 Acknowledgments .....	128
4.7 References.....	128

CHAPTER 5: Magnetically Actuated Solid Sample Preparation for Centrifugal Microfluidic Devices .....	130
5.1 Abstract.....	131
5.2 Introduction .....	131
5.2.1 Centrifugal Microfluidics .....	132
5.2.2 Magnets.....	133
5.3 Experimental .....	134
5.3.1 Instrumentation.....	134
5.3.1.1 Macroscopic Stage .....	134
5.3.1.2 Magnets .....	135
5.3.1.3 Manufacturing Centrifugal Devices .....	138
5.3.2 Reagents .....	139
5.3.3 Procedure .....	139
5.4 Results & Discussion .....	140
5.4.1 Enhanced Dissolution.....	140
5.4.2 Induced Temperature .....	142
5.5 Conclusions .....	143
5.6 Acknowledgment.....	143
5.7 Supporting Information.....	143
5.8 References.....	146
CHAPTER 6: Automated Liquid-Solid Extraction of Pyrene from Soil on Centrifugal Microfluidic Devices.....	147
6.1 Abstract.....	148
6.2 Introduction .....	149
6.3 Experimental .....	150
6.3.1 Standards and Reagents .....	150
6.3.2 Device Fabrication.....	151
6.3.3 Valves.....	155
6.3.4 Centrifugal System .....	157
6.3.5 Detection System .....	157
6.4 Results and Discussion .....	158

6.5 Acknowledgements .....	164
6.6 References .....	165
CHAPTER 7: Enzyme Inhibition-Based Determination of Pesticide Residues in Vegetable and Soil in Centrifugal Microfluidic Devices .....	166
7.1 Abstract .....	166
7.2 Introduction .....	167
7.3 Experimental .....	169
7.3.1 Standards, Reagents and Samples .....	171
7.3.2 Device Fabrication .....	172
7.3.3 Valves .....	175
7.3.4 Centrifugal System .....	177
7.3.5 Detection System .....	181
7.3.6 Methods .....	181
7.4 Results and Discussion .....	183
7.5 Conclusion .....	193
7.6 References .....	194
CHAPTER 8: Conclusion and Suggestions for Future Work .....	197
8.1 Summary of Thesis Work .....	197
8.2 Suggestions for Future Work .....	198
8.2.1 Instrumentation .....	199
8.2.1.1 Proposed Additions to the Motorized Stages .....	199
8.2.1.2 Future Centrifugal Microfluidic Devices .....	201
8.2.2 Potential Applications .....	203
8.3 References .....	206
Appendix A: Additional Instrumentation Details .....	208
Appendix B: LabVIEW Virtual Instruments Code .....	215
Appendix C: 3D Printing and CLAD – Additional Designs and Details .....	222
Appendix D: Links to Supplementary Videos .....	240

Appendix E: Temperature Increase Within a Chamber Containing a Mobile Magnet – Experimental and Theoretical Calculations.....	243
E.1 Experimental Design and Results.....	243
E.2 Theoretical Calculations .....	247
E.2.1 Work Done by a Magnet <i>Spinning</i> on its Own Axis .....	247
E.2.2 Work Done by a Magnet <i>Shaking</i> Back and Forth in Chamber .....	248
E.2.3 Total Work Done by a Magnet Spinning and Shaking.....	250
Appendix F: Absorbance and Statistics .....	251
F.1 Signal Measurements .....	251
F.2 Error Propagation and Noise .....	253
F.3 Signal-to-Noise and Relative Standard Deviation .....	258
F.3.1 Absorbance RSD and Concentration RSD .....	260
F.4 Limit of Detection .....	262
F.5 Comparison Methods.....	264
F.5.1 <i>F</i> -test – Comparison of Variance.....	264
F.5.2 Student's <i>t</i> -test – Comparison of Means .....	264
F.6 Multiwavelength Ratiometric Blank Estimation Technique .....	265
F.7 References .....	267
Appendix G: Sedimentation Rate and Stokes' Law .....	268
G.1 Stokes' Law.....	268
G.2 Application of Stokes' Law to Centrifugal Microfluidics.....	269
G.2.1 Application to the Sedimentation of Soil .....	270
G.3 References .....	274

## List of Figures

Figure 1-1. Classification of extraction techniques .....	4
Figure 1-2. Magnetization BH curve (hysteresis loop). Dotted line is for a ferromagnetic material that is exposed to a magnetic field for the first time. ....	6
Figure 1-3. The number of publications per year containing the terms “microfluidic*” and “centrifugal microfluidic*” found in a search of the Scopus <sup>TM</sup> database in 2012. ....	11
Figure 1-4. Visual representation of variables affecting the flow rate of solution in centrifugal microfluidic devices.....	16
Figure 2-1. Photographs of motorized stages. (a) Stage v1.0, DC motor, (b) Stage v2.0, servo motor, (c) Stage v3.0, servo motor. ....	30
Figure 2-2. Schematic of DC motor Stage v1.0 integrating (a) laptop computer with LabVIEW National Instruments software and drivers, (b) Firewire 800 ExpressCard for interfacing camera, (c) USB6212 data acquisition device, (d) digital direction control circuit, (e) electronic forward-brake-reverse controller, (f) signal isolator controller, (g) DC motor drive, (h) DC motor, (i) spindle shaft, (j) centrifugal microfluidic device, (k) LED (l) retro-reflective sensor and reflective tape, (m) camera and macro lens. Figure components are not to scale.....	31
Figure 2-3. Schematic of servo motor Stage v2.0 and Stage v3.0 integrating (a) desktop computer with LabVIEW National Instruments software and drivers, (b) PCI-7342 card for interfacing motor, (c) Firewire 800 PCI card for interfacing camera, (d) UMI-7764 breakout box, (e) VM26-PM breakout box, (f) servo drive, (g) servo motor, (h) spindle shaft, (i) fixed magnets base, (j) centrifugal microfluidic device, (k) USB6009 data acquisition device, (l) peristaltic pump, (m) solenoid valve attached to a rotameter to control and measure gas flow rate, (n) camera and macro lens, (o) strobe light, (p) USB4000 spectrometer and fiber optic, (q) trigger breakout box. Figure components are not to scale. ....	32
Figure 2-4. Custom made spindle shafts. (a) Spindle shaft for Stage v1.0 DC motor. (b) Adaptor show in green to attach the original DC motor shaft to Stage v2.0 servo motor spindle. (c) Redesigned one-piece spindle shaft for Stage v3.0 servo motor. ....	36
Figure 2-5. Photographs of spindle shafts and relative space below the centrifugal devices on the stages. (a) Stage v2.0 with the combination of the shaft from Stage v1.0 and an adaptor. (b) Stage v3.0 with ease of access to below the centrifugal devices. ....	37

Figure 2-6. Fixed magnet base. (a) Sketch of magnets in fixed base and corresponding flux lines. (b) Photograph of fixed magnet base on Stage v2.0. A reticule is added beneath the base to include relative size and magnification of the acquired images. ....	38
Figure 2-7. Wiring diagram of USB6212 for DC motor control. ....	45
Figure 2-8. DC motor digital direction control circuit diagram. ....	46
Figure 2-9. Bridging wire connection diagram between Parker Automation VD26-PM breakout box and National Instruments UMI-7764 breakout box. ....	47
Figure 2-10. Trigger breakout box. (a) Circuit diagram, (b) Photograph of Stage v2.0 trigger breakout box. (c) Photograph of Stage v3.0 trigger breakout box. ....	49
Figure 2-11. Safety shields. (a) Top view of first shield surrounding Stage v1.0. (b) Bottom view of first shield. (c) Side view of second shield surrounding Stage v3.0. ....	52
Figure 2-12. Nomenclature for the direction of magnetization of rectangular and ring magnets. Dotted rectangle highlights the direction of magnetization used as “mobile magnets” and in the “fixed magnet base” ....	59
Figure 2-13. “Mobile magnets”. (a) Ni plated NdFeB bar, (b) Teflon encapsulated NdFeB discs, (c) Epoxy coated Ni plated NdFeB bar, (d) Alnico bar, (e) Tefzel coated Alnico bar ....	60
Figure 2-14. Teflon encapsulation schematic diagram. Two halves of the illustrated encapsulation were fused together with a total of six disc magnets inserted into the circular cavities, three on each side. ....	61
Figure 2-15. Elemental composition of the extractant for the reagent blanks, vial blanks and all of the “mobile magnets”. Error bars $\pm 1\sigma$ . ....	65
Figure 2-16. Elemental composition of the extractant for the poorly performing “mobile magnets”. Error bars $\pm 1\sigma$ . ....	66
Figure 2-17. Elemental composition of the extractant for the best performing “mobile magnets”. Error bars $\pm 1\sigma$ . ....	67
Figure 3-1. Example of the complexity possible in structures manufactured by 3D printing taking a computer generated design (left) and rapidly making a finished product (right). ....	74
Figure 3-2. Microscope with boom stand and camera. Entire system at 90 degrees to sample (left) and zoom view of boom stand set at 22 degrees to sample (right). ....	82
Figure 3-3. Experimental set-up in fume hood for chemical resistivity study. ....	84
Figure 3-4. Multiple views schematic drawing of one set of designed reservoirs and capillary burst valve (dimensions in mm). ....	88

Figure 3-5. Structure 1 (a) Drawings of design that was saved as *.STL and sent to all three printers (dimensions in mm) dotted area in right hand drawing corresponds to area in right hand photographs taken at 16.8x magnification, (b) photos of <i>uPrint</i> part, (c) photos of <i>V-Flash</i> part, and (d) photos of <i>Alaris</i> part.....	90
Figure 3-6. Structure 2, top view. (a) Drawing of design that was saved as *.STL and sent to all three printers (dimension in mm), (b) photo of <i>uPrint</i> part, (c) photo of <i>V-Flash</i> part, and (d) photo of <i>Alaris</i> part. Photographs were taken with backlighting and 16.8x magnification. ....	94
Figure 3-7. Vertical cross-sectional view of Structure 2 (a) Drawing of design, (b) photograph of cut cross section of the <i>uPrint</i> part (dimensions in mm). Dotted area highlights the empty spaces within the part. ....	96
Figure 3-8. Chemical resistivity study effect on structures. Photographs of 30 structures after exposure to different solvents.....	99
Figure 3-9. Selection of structures manufactured by the <i>uPrint</i> by FDM technology after chemical resistivity testing. ....	101
Figure 3-10. Structure 1 at 150x magnification. Dotted rectangles on the left hand drawings represents the magnified area shown in each photograph on the right. Designed dimensions were of (a) 1000 x 1000 $\mu\text{m}$ (b) 500 x 500 $\mu\text{m}$ (c) 400 x 400 $\mu\text{m}$ (d) 300 x 300 $\mu\text{m}$ (e) 200 x 200 $\mu\text{m}$ (f) 150 x 150 $\mu\text{m}$ (g) 100 x 100 $\mu\text{m}$ . ....	103
Figure 3-11. Structure 3 at 16.8x magnification. Dotted rectangle on the left hand drawing represents the magnified area shown in each photograph on the right. (a) Magnified view of 1000 and 500 $\mu\text{m}$ round and square sets of three channels. (b) Magnified view of 500, 400 and 300 $\mu\text{m}$ sets of three channels. (c) Magnified view of 300, 200, 150 $\mu\text{m}$ sets of three channels. The smaller 100, 75 and 50 $\mu\text{m}$ sets of three channels are not observed in any all three printers.....	104
Figure 3-12. Structure 3 comparison of round and square channels of <i>Alaris part</i> . Top drawing shows drawing with dotted highlighted channels photographed below.....	106
Figure 3-13. Structure 4 built on <i>Alaris</i> printer showing material blocking reservoirs and valves. ....	108
Figure 4-1. Journal's table of content figure of CLAD .....	115
Figure 4-2. (a) Cut isometric view of Centrifugal Liquid Addition Distributor (CLAD) including (all in mm): (i) cup, (ii) hole (radius 1.0), (iii) peg (inner radius 1.25, outer radius 1.75) and (iv) centre hole (radius 7.5). (b) Top view of centrifugal microfluidic platform including CLAD and disk base (radius 60.0 mm) – highlighted rectangle is enlarged in (c). (c) Disk base features: (i) Receiving Reservoir (radius 2.59 x 1.40 deep), (ii) Viewing Channel (1.00 wide x 1.40 deep x 10.50 long), (iii) Flow Choke (0.40 wide x	

0.10 deep x 1.41 long), (iv) Collection Reservoir (radius 7.00 x 1.40 deep), (v) vent. (d) Cut side view drawing of liquid deposition mechanism: (i) Peristaltic pump tubing, (ii) continuous stream of liquid broken by rough surface of CLAD, (iii) hole in CLAD cup into disk base, (iv) Receiving Reservoir, (v) Viewing Channel and (vi) Collection Reservoir. ....	120
Figure 4-3. Schematic of experimental setup. (a) Peristaltic pump and tubing, (b) camera and lens, (c) centrifugal microfluidic platform including CLAD and disk base, (d) beakers containing dyed water samples, (e) spindle shaft, and (f) servo motor. ....	121
Figure 4-4. High speed digital images of rotating CLAD and disk base at 600 rpm (10 Hz) at varying times after pump has started showing deposition process. (a) 1.7 s illustrating minimum liquid addition of 15 $\mu\text{L}$ per channel, (b) 4.9 s, (c) 9.7 s, (d) 14.5 s. ....	125
Figure 4-5. Gradient on a disk. (a-g) Series of digital images showing part of the 220 $\mu\text{L}$ Viewing Channel, from yellow to blue. ....	127
Figure 5-1. (a,b,c) Centrifugal device and macroscopic stage (motor shaft and fixed magnet base).....	136
Figure 5-2. Photograph of device including magnets, solvent and solid sample before (left) and after (right) rotation. ....	137
Figure 5-3. Movement of “mobile magnets” enclosed in extraction chamber. Magnet positions in circled regions are illustrated in adjacent drawings. .	138
Figure 5-4. Visual comparison of extraction chambers containing 0.10 g $\text{K}_3[\text{Fe}(\text{CN})_6]$ and 1.0 mL water (a) without “mobile magnet” (b) with “mobile magnet” (device rotating at 1000 rpm). ....	141
Figure 5-5. Dissolution time of 0.10 g $\text{K}_3[\text{Fe}(\text{CN})_6]$ in 1.0 mL of water at different rotational speeds using the magnetically driven solid sample preparation centrifugal device. ....	142
Figure 6-1. (a) Exploded view of device showing following five layers 1) bottom PMMA, 2) adhesive layer including rectangular passive valves, 3) middle PMMA with chambers into which cylindrical capillaries are epoxied, 4) adhesive layer, 5) top PMMA with vent holes. (b) Photograph of device with 10 sets of chambers. (c) Enlarged view of one set of chambers. (d) Schematic of chambers including 1) magnetically actuated liquid-solid extraction unit, 2) filtration unit, 3) detection unit, 4) rectangular passive capillary valve at a radial distance of 29 mm, 5) cylindrical passive capillary valve at a radial distance of 47 mm, 6) vent holes and vent lines (0.1 mm deep x 1 mm wide), 7) “mobile magnet” agitator. ....	153
Figure 6-2. Schematic of detection system: 1) light source, 2) fiber optic, 3) collimating lens, 4) integrated detection cell, 5) focusing lens, 6) fiber optic, 7) photodiode array spectrometer for detection at 334 nm. ....	154

- Figure 6-3. (a) Burst frequencies of hexane as a function of different channel widths of the rectangular passive capillary valves at a radial distance of 29 mm adhesive. (b) Burst frequencies of hexane as a function of different inner diameter of the cylindrical passive capillary valves at a radial distance of 47 mm. Inserts of both (a) and (b) show cross-sectional geometry of channels..... 156
- Figure 6-4. (a) Extraction time efficiency study and comparison to conventional method. A pyrene extraction plateau equivalent to conventional method is obtained in 10 minutes. (b) High speed images of spinning device showing the “mobile magnet” movement in top inner extraction chamber. The “mobile magnet” spins upon its own axis as well as back-and-forth in the extraction chamber..... 161
- Figure 6-5. Table of Contents Graphical Abstract..... 164
- Figure 7-1. Enzyme inhibition-based determination of pesticide residues. The multi-step reaction is divided into multiple chambers. (a) Complete reaction process without inhibitor pesticide results in a coloured product. (b) Complete reaction process with high concentration of inhibitor pesticide results in no coloured product. Chamber labels at left refer to chambers of Figure 7-2(iii), location of each subsequent step..... 170
- Figure 7-2. Centrifugal microfluidic device components and features. (a) Vegetable analysis centrifugal microfluidic device. (b) Soil analysis centrifugal microfluidic device. .... 173
- Figure 7-3. Soil analysis centrifugal microfluidic device. (a) Cut isometric side view of device. Highlighted area is enlarged in (b). (b) Zoom side view of one set of chambers (1) Chamber 1 - Extraction Chamber, (2) Chamber 2 - for interaction with enzyme, (3) Chamber 3 - for ESC complex formation and detection cell, (4) two 200  $\mu\text{m}$  rectangular passive capillary valve, (5) cylindrical passive capillary valve with protruding snorkel into Chamber 2, (6) vent holes and vent lines, (7) “mobile magnet” agitator. (c) Isometric view of one set of chambers (shown without top layer)..... 177
- Figure 7-4. Schematic of experimental set-up. (a) Strobe, (b) camera and lens, (c) soil centrifugal microfluidic device, (d) fixed base with six fixed magnets (see also Figure 7-5), (e) spindle shaft and (f) servo motor..... 178
- Figure 7-5. Magnet position and flux lines of the six fixed magnets in fixed base seen through a top semi-transparent view of centrifugal device..... 180
- Figure 7-6. Optimization of operating parameters. (a) Effect of enzyme concentration on absorbance. Obtained with pH 7.71 phosphate buffer, 25 mg/L substrate, 40 mg/L chromatic reagent. (b) Effect of substrate concentration on absorbance. Obtained with pH 7.71 phosphate buffer, 12 U/mL enzyme, 40 mg/L chromatic reagent. (c) Effect of chromatic reagent concentration on absorbance. Obtained with pH 7.71 phosphate

buffer, 12 U/mL enzyme, 50 mg/L substrate. (d) Stability of the ESC complex. Obtained with pH 7.71 phosphate buffer, 4 U/mL enzyme, 20 mg/L substrate, 32 mg/L chromatic reagent, and detected by Varian UV-VIS spectrometer in kinetic mode.....	184
Figure 7-7. Burst frequency of buffer as a function of different inner diameter cylindrical passive capillary valves at a radius of 42 mm from the centre of the disk and of length of 4.5 mm .....	189
Figure 8-1. Envisioned hybrid centrifugal microfluidic device containing (a) deep pocket for solid and liquid sample introduction, (b) “mobile magnet” for magnetically actuated sample preparation and liquid-solid extraction, (c) partial lid to minimize splash while allowing liquid addition, (d) filter. ....	202
Figure A-1. Dimensions of spindle shaft for Stage v1.0 DC motor.....	208
Figure A-2. Dimensions of spindle shaft top ring used to hold centrifugal devices of different thicknesses. ....	209
Figure A-3. Dimensions of adaptor used to attach the original DC motor shaft to Stage v2.0 servo motor spindle.....	210
Figure A-4. Dimensions one-piece spindle shaft for Stage v3.0 servo motor. .	211
Figure A-5. Dimension of fixed magnet base.....	212
Figure A-6. Dimensions of close focus zoom lenses. (a) Computar #54-363, dimension in mm. (b) Navitar Zoom 7000 #58-240, dimensions in inches. ....	213
Figure A-7. Digital acquisition (DAQ) screw terminal configuration for both USB6009 and USB6212 (National Instruments User manuals). ....	214
Figure B-1. VI Front Panel for control of DC motor Stage v1.0.....	215
Figure B-2. VI Block Diagram for control of DC motor Stage v1.0 .....	216
Figure B-3. VI Front Panel for control of servo motors Stage v2.0 and Stage v3.0 .....	217
Figure B-4. VI Block Diagrams for “continuous snap” (top) and “stop and snap” (bottom) modes of operation of servo motors (continued in Figure B-5). Bottom “save image at” sub-VI is detailed in Figure B-6 .....	218
Figure B-5. VI Block Diagrams for “continuous snap” (top) and “stop and snap” (bottom) modes of operation of servo motors (continued from Figure B-4). ....	219
Figure B-6. Sub-VI Front Panel and Block Diagram for control of camera.....	220
Figure B-7. VI Front Panel and Block Diagram for control of peristaltic pump. .	221
Figure C-1. Structure 1: Dimensions (mm) of square channels (width and height of channels are of 1000, 500, 400, 300, 200, 150 and 100 $\mu$ m respectively). Each channel was 15 mm long. A 1 mm space was included between each channel. ....	222
Figure C-2. Structure 2: Precise 100 $\mu$ L volume well with a 20 x 20 mm base	223

Figure C-3. Structure 3: Round and square 5 mm long channels. The diameter (for round) or height and width (for square) of the channels were of 1000, 500, 400, 300, 200, 150, 100, 75 and 50 $\mu\text{m}$ . Three replicates of each size were included. ....	224
Figure C-4. Structure 4: Entire device including reservoirs and “printed” capillary valves manufactured in one step. Seven different versions of this structure were designed, each with a different size capillary burst valve (500, 300, 200, 150, 100, 75, and 50 $\mu\text{m}$ ). Each of the seven versions contained 15 iteration of the same size valve. ....	225
Figure C-5. <i>uPrint</i> ABS raw and extruded material (left) and “printed” support structure (right) at 16.8x magnification .....	226
Figure C-6. Design of prototype filters. A series of posts or columns with diminishing diameter and distance between them were staggered over a small area. Entire test device (left), zoom of filter (middle) and <i>uPrint</i> failed test print (right) are shown.....	227
Figure C-7. First 3D prototype. The lip design was originally made by stacking a series of smaller concentric circles in SolidWorks.....	228
Figure C-8. Second 3D design included the original lip and two scoops which were opposite one another to balance the devices .....	229
Figure C-9. Lip and scoop design details (a) Zoom view of design lip and one scoop. (b) Zoom view of <i>uPrint</i> part after printing but before removal of support structure. (c) Photograph of entire device manufacture on the <i>V-Flash</i> . (c) Zoom view of <i>V-Flash</i> scoop. ....	229
Figure C-10. First prototype mini-centrifugal device (80 mm diameter) designed with one lip and one test hole that had two drain channels. This design was to deliver liquid to one chamber with the device turning clockwise and a to a second chamber with the device turning counter-clockwise.....	230
Figure C-11. Second prototype mini-centrifugal device designed with one lip at its perimeter and eight draining holes to segment the added liquid to eight separate chambers. ....	231
Figure C-12. Double lip mini-centrifugal device designed to be able to simultaneously add two different liquids to a moving device. ....	232
Figure C-13. In order to be able to measure the amount of liquid draining through each hole and to compare the distribution of liquid, U-shaped channels with inlet and vent holes was designed to act as a base for the mini-centrifugal device.....	233
Figure C-14. Joining the 80 mm mini-centrifugal device (here with one lip) and the 120 mm base with integrated U-shaped channels could have been done post-production or as seen here at the design stage and manufacture as a single part.....	234

Figure C-15. Composite part joining 80 mm mini-centrifugal device (here with two lips) and the 120 mm base with integrated U-shaped channels at the design stage. Alternating the radial distance from the centre of the inlet holes, four U-shaped channels were to collect liquid from the inner lip and four from the outer lip. ....	235
Figure C-16. (a) <i>uPrint</i> part with one lip and eight U-shaped channels. (b) Zoom of one U-shaped channel. (c) Schematic of U-shaped channel design including (i) inlet hole inside and under lip, (ii) vent hole and potentially outlet, (iii) integrated scale for measuring and comparing liquid distribution between U-shaped channels and (iv) alignment hole included but not used. ....	236
Figure C-17. Liquid deposition mechanism drawing (left – cut side view) and photograph (right). (a) Peristaltic pump tubing, (b) continuous stream of liquid broken by rough surface of CLAD, (c) hole in CLAD cup into disk base, (d) Receiving Reservoir, (e) Viewing Channel and (f) Collection Reservoir. ....	237
Figure C-18. Top view of CLAD with location of holes. Dotted circle represents the radial distance at which liquid was added (10.5 mm). ....	237
Figure D-1. QR code and link to supplementary video to Chapter 3. The sections of the video showing the <i>V-Flash</i> and the <i>Alaris</i> were taken from their respective promotional videos. ....	240
Figure D-2. QR codes and links to supplementary video to Chapter 4 .....	241
Figure D-3. QR codes and links to supplementary video to Chapter 5. ....	242
Figure E-1. Experimental set-up for the determination of the temperature in the chamber of centrifugal device with and without a “mobile magnet”. (a) Interfacing components of two stages operated simultaneously. (b) Secondary view of experimental set-up. (c) Temperature determination test device with thermocouple and counter weight. (d) Sample of one of over 4000 pictures obtained displaying the temperature inside chamber. ....	244
Figure E-2. Calibration curve of the DC motor between the applied voltage and the resulting rotational speed (angular velocity) .....	245
Figure E-3. Plot of temperature in chamber of centrifugal device containing water with and without a “mobile magnet” over a period of more than 8 minutes at an angular velocity of 240 rpm. A 20 point moving boxcar has been applied. ....	246
Figure E-4. Schematic of the magnet spinning upon its own axis. ....	247
Figure E-5. Schematic of the magnet shaking back and forth in the chamber. ....	249
Figure F-1. Reproduced from Amine <i>et al.</i> <sup>2</sup> : General method to establish LOD for enzyme inhibition assays .....	263
Figure G-1. One set of chambers of soil analysis centrifugal device .....	271

## List of Tables

Table 1-1. Summary of magnetic properties and corresponding units.....	7
Table 2-1. Motor specifications.....	34
Table 2-2. CCD camera specifications .....	39
Table 2-3. Close focus zoom lens specifications .....	40
Table 2-4. Summary of controller cards, circuits and breakout boxes .....	43
Table 2-5. LabVIEW software and drivers .....	50
Table 2-6. Magnet composition, strength and thermal stability .....	58
Table 2-7. Comparison of Teflon and Tefzel properties according to DuPont™	61
Table 2-8. ICP-AES operating parameters .....	64
Table 2-9. Scorecard comparing “mobile magnets” for acid medium experiments .....	69
Table 3-1. Solvents used for chemical resistivity test of 3D structures .....	83
Table 3-2. Design and purpose of 3D test structures .....	86
Table 3-3. Summary of 3D printers manufacture specifications .....	91
Table 3-4. Dimensions and weights of 3D structures .....	93
Table 3-5. Diameter and volume of well of Structure 2 .....	94
Table 3-6. Chemical resistivity solvent testing (visual and UV-Vis spectra observations).....	100
Table 3-7. Scorecard comparing 3D printers .....	109
Table 4-1. Liquid addition and distribution of CLAD.....	124
Table 6-1. Comparison of extraction methods .....	161
Table 7-1. Enzyme inhibition-based technique reagents details.....	171
Table 7-2. Spin sequence detailing steps for sample treatment and liquid movement for both the automated vegetable and soil disk methods.....	183
Table 7-3. Comparison of extraction methods for the analysis of <i>vegetable</i> samples.....	190
Table 7-4. Comparison of extraction methods for the analysis of <i>soil</i> samples	190
Table F-1. Summary of error propagation.....	254
Table F-2. Summary of signal and noise equations for classical absorbance and inhibition experiments .....	257
Table F-3. Sample pesticide determination data with propagation of error.....	261
Table G-1. Experimental conditions used to calculated the settling velocities and rates. ....	272
Table G-2. Settling velocities of soil in water .....	272
Table G-3. Time needed for soil particles to settle to bottom of chamber in water .....	273
Table G-4. Comparison of time needed for soil particle to settle in hexane and water .....	273

## List of Equations

Equation 1-1. Magnetic force .....	7
Equation 1-2. Reynolds number .....	9
Equation 1-3. Flow rate of solutions pumped by centrifugal forces.....	15
Equation 1-4. Centrifugal pressure .....	17
Equation 1-5. Capillary burst pressure.....	17
Equation 1-6. Capillary burst frequency.....	18
Equation 1-7. Stokes' Law .....	18
Equation 1-8. Settling velocity by centrifugation .....	19
Equation 7-1. Relationship between absorbance and percent inhibition .....	185
Equation 7-2. Logarithmic relationship between percent inhibition and concentration.....	185
Equation 7-3. Pesticide concentration related to $\ln(\%)$ .....	185
Equation 7-4: Limit of detection (enzyme inhibition assay).....	185
Equation 7-5. Stokes' Law .....	189
Equation 7-6. Settling velocity by centrifugation .....	189
Equation E-1. Work done in one second due to spinning magnet .....	248
Equation E-2. Work done in one second due to shaking magnet .....	249
Equation F-1. Beer's Law .....	251
Equation F-2. Transmittance .....	251
Equation F-3. Absorbance .....	251
Equation F-4. Relationship between percent inhibition and absorbance .....	252
Equation F-5. Relationship between percent inhibition and concentration .....	252
Equation F-6. Logarithm of concentration related to percent inhibition .....	253
Equation F-7. Pesticide concentration related to percent inhibition .....	253
Equation F-8. Pesticide concentration related to signal intensity (complex) ....	253
Equation F-9. Error propagation (addition and subtraction).....	254
Equation F-10. Error propagation (multiplication and division) .....	254
Equation F-11. Error propagation (exponential).....	254
Equation F-12. Error propagation (logarithm) .....	254
Equation F-13. Error propagation (antilogarithm) .....	254
Equation F-14. Absorbance noise .....	255
Equation F-15. Transmittance noise (complex) .....	255
Equation F-16. Transmittance noise (simplified).....	256
Equation F-17. Percent inhibition noise (complex) .....	256
Equation F-18. Percent inhibition noise (simplified).....	256
Equation F-19. Pesticide concentration noise.....	257
Equation F-20. Signal-to-noise (general).....	258
Equation F-21. Relative standard deviation (from Signal-to-Noise) .....	258

Equation F-22. Relative standard deviation (from Standard Deviation) .....	258
Equation F-23. Signal-to-Noise (absorbance).....	258
Equation F-24. Relative standard deviation (absorbance).....	259
Equation F-25. Signal-to-Noise (pesticide concentration).....	259
Equation F-26. Relative standard deviation (pesticide concentration) .....	260
Equation F-27. Limit of detection (general).....	262
Equation F-28. Limit of detection (enzyme inhibition assay).....	263
Equation F-29. F-test.....	264
Equation F-30. Student's t-test .....	265
Equation F-31. Pooled standard deviation .....	265
Equation F-32. Ratio for multiwavelength ratiometric blank estimation technique .....	266
Equation F-33. Transmittance using multiwavelength ratiometric blank estimation technique.....	266
Equation G-1. Stokes' Law .....	268
Equation G-2. Weight of a spherical particle.....	268
Equation G-3. Buoyant force .....	269
Equation G-4. Conditions for terminal velocity .....	269
Equation G-5. Settling velocity by gravity .....	269
Equation G-6. Radial acceleration .....	270
Equation G-7. Settling velocity by centrifugation .....	270

## Abbreviations

$a_c$	radial acceleration (due to centrifugal force) ( $\text{rad}^2 \text{ cm s}^{-2}$ )
$A$	absorption
$A_0$	absorption of blank
$A_s$	absorption of sample
$b$	path length (cm)
$B$	magnetic flux density or magnetic induction ( $\text{T} = \text{N A}^{-1} \text{ m}^{-1}$ )
$B$	buoyant force (N)
$\gamma$	liquid surface tension ( $\text{N cm}^{-1}$ )
$c$	concentration
$d_h$	hydraulic diameter of a channel (cm)
$\varepsilon$	molar absorption coefficient ( $\text{L mol}^{-1} \text{ cm}^{-1}$ )
$f$	frequency (Hertz = $\text{s}^{-1} = \omega/2\pi$ )
$F_{mag}$	magnetic force (N)
$F_r$	resistive frictional force (N)
$g$	acceleration due to gravity ( $\text{cm s}^{-2}$ )
$H$	magnetic field strength ( $\text{A m}^{-1}$ )
$I_{0\%T}$	0% transmittance (light source off) signal
$I_{blk}$	blank reference signal
$I_s$	sample signal
$In(\%)$	percent inhibition
$m$	slope
$\Delta p_b$	burst pressure ( $\text{N cm}^{-2}$ )

$\Delta p_c$	centrifugal pressure ( $\text{N cm}^{-2}$ )
$\rho_f$	density of a fluid ( $\text{g mL}^{-1}$ )
$\rho_p$	density of a particle ( $\text{g mL}^{-1}$ )
$r$	distance of a particle from the centre of rotation (cm)
$\bar{r}$	average distance from the centre of rotation of a liquid subjected to centrifugal pressure (cm)
$\Delta r$	radial extent of fluid subjected to centrifugal pressure (cm)
$R$	Stokes' radius (cm)
Re	Reynolds number (unitless)
rpm	revolutions per minute ( $60 \text{ rev min}^{-1} = 1 \text{ Hertz}$ )
$\sigma$	standard deviation
$\sigma^2$	variance
$\sigma_A$	noise in absorbance measurement
$\sigma_{blk}$	standard deviation of blank
$\sigma_T$	noise in transmittance measurement
$T$	transmittance
$U$	velocity of a liquid ( $\text{cm s}^{-1}$ )
$\mu$ or $\eta$	dynamic viscosity (centipoise = cP = $10^{-2} \text{ g cm}^{-1} \text{ s}^{-1}$ )
$\mu_o$	permeability of free space ( $4\pi \times 10^{-7} \text{ N A}^{-2}$ )
$\nu$	kinematic viscosity (centistokes = cSt = $\text{cm}^2 \text{ s}^{-1}$ )
$\nu$	velocity ( $\text{cm s}^{-1}$ )
$\nu_s$	settling velocity ( $\text{cm s}^{-1}$ )
$\nu_t$	terminal velocity ( $\text{cm s}^{-1}$ )

$V$	volume (mL)
$w$	weight (N)
$\omega$	angular velocity ( $\text{rad s}^{-1}$ )
3D	three dimensional
ABS	acrylonitrile butadiene styrene
ASE	accelerated solvent extraction
CAD	computer-aided design
CCD	charge-coupled device
CD	compact disc
CFD	computational fluid dynamics
CLAD	centrifugal liquid addition distributor
CNC	computer numerically controlled
CSC	China scholarship council
DAQ	digital acquisition
DCAM	1394-based Digital Camera Specification
DDW	distilled deionized water
DL	detection limit
DLP	digital light processing
DVD	digital versatile disc or digital video disc
ESC	enzyme-substrate-chromatic reagent complex
ETFE	ethylene-tetrafluoroethylene copolymer (Tefzel)
FDM	fused deposition modeling
FTI	film transfer imaging
GMO	genetically modified organisms

HMX	oxtahydro-1,3,5,7-tetrenitro-1,3,5,7-tetrazocine
ICP-AES	inductively-coupled plasma atomic emission spectrometer
ID	inner diameter
LBP	liquid binding powder
LED	light emitting diode
LLE	liquid-liquid extraction
LLME	liquid-liquid micro-extraction
LOC	lab-on-a-chip
LOD	limit of detection
LSE	liquid-solid extraction
MAE	microwave-assisted extraction
microTAS	micro-Total Analysis Systems
MGOe	megaGauss Oersteds
NI	National Instruments
NSERC	national science and engineering council of Canada
OD	outer diameter
PAH	polycyclic aromatic hydrocarbons
PCI	peripheral component interconnect
PDMS	polydimethylsiloxane
PFE	pressurized fluid extraction
PJM	polyjet modeling
PMMA	poly(methyl methacrylate)
PTFE	polytetrafluoroethylene (Teflon)
RDX	hexahydro-1,3,5-trinitro-1,3,5-triazine

RSD	relative standard deviation
SBSE	stir-bar-sorptive extraction
SFE	supercritical fluid extraction
SLS	selective laser sintering
SPE	solid-phase extraction
SPME	solid-phase micro-extraction
STL	stereolithography
μTAS	micro-Total Analysis Systems
UE	ultrasonic extraction
UV	ultra-violet
VI	virtual instrument

## CHAPTER 1: Introduction

Automating and miniaturizing analytical techniques to meet heightened environmental monitoring challenges is an important topic in analytical instrument design research.<sup>1</sup> A growing number of pollutants are being shown to have a large environmental and health impact resulting in stricter legislative limits. There is a need for an accurate understanding of the type and extent of contamination. Unfortunately, inherent to the current standard operating procedures is the high cost of operations due to the labour, time required for many analysis and large amounts of solvent used, ironically creating additional environmental issues. Though industrial laboratory testing will continue to play an important part of environmental monitoring, most samples that get shipped to the laboratory are negative for the contaminant of interest. Many agree that if an initial analysis would be quickly performed in the field, fewer or at least more targeted contaminated samples would be shipped and analyzed.<sup>2</sup> That way, laboratory testing could focus on problematic sites instead of dealing with a large overhead of “clean” samples. This would also help environmental monitoring in remote areas, which is both expensive and difficult to perform. The most time intensive step for both field and laboratory based analyses is sample preparation. Though autosamplers have become the norm in industry to free technologists’ time, crushing, grinding, filtering and extracting solid samples are often still performed manually or by dedicated instruments after which samples must be transferred to the detection system. Automating, miniaturizing and integrating these steps on a

single potentially field portable device would provide more timely and cost efficient results while reducing sample and reagent volumes.

## **1.1 Theoretical Concepts & Literature Review**

### **1.1.1 Sample Preparation and Extraction**

Environmental samples pose a continuing challenge to analytical chemists. Effective preparation of air, water and solid samples is crucial before analytes of interest can be identified and quantified. Solid samples in particular are difficult to analyze and are characterized by even larger variability than liquid samples.<sup>3, 4</sup> A representative and ideally homogenous sample is therefore needed to reflect the properties of interest of the target area. Solid sample preparation includes but is not limited to grinding and crushing of samples and isolating the target analyte from a matrix often by extraction.

A typical environmental solid sample is soil. Currently standard methods normally call for some kind of extraction procedure to isolate and concentrate contaminants from soil. A large fraction of the soil in question is sampled and then thoroughly mixed. A subsample, of the order of 10 grams, is then placed in an extraction solvent and agitated for as long as 24 hours or treated to extreme temperatures or pressures. The extraction solvent is then removed and filtered. A series of reagents may be added, and other physical processes such as separation may be required. Finally, a detection procedure is used, usually involving some form of spectrometry. These multiple steps are performed at

different work stations and each introduces a source of error and requires the time of a skilled operator making them a prime target for advanced techniques.

Classical analytical techniques for sample preparation and extraction include the use of mortar and pestle, shakers, vortex mixers and separatory funnels. First proposed in 1879 for the determination of milk fat,<sup>5</sup> the Soxhlet extractor and its variations such as the Dean Stark extractor<sup>6</sup> have become the benchmark liquid-solid extraction techniques to which most new techniques are compared. Unfortunately, inherent to the design of most classical techniques are long extraction times and the use of large amounts of solvent. Consequently, miniaturization of these techniques has become a very active branch of research. In 2003, Janusz Pawliszyn, in his article titled "Sample preparation: *Quo Vadis?*" (Latin for "Where are you going?"), discussed the general trend towards smaller, autonomous sample preparation techniques which would consume less solvent, less sample and take less time.<sup>7</sup> Shortly after, Ramos *et al.*<sup>2</sup> and Namieśnik *et al.*<sup>8</sup> both reviewed the miniaturization in sample handling with a particular focus on environmental samples. Many techniques have been suggested including liquid-solid extraction (LSE), liquid-liquid extraction (LLE), liquid-liquid micro-extraction (LLME), microwave-assisted extraction (MAE), ultrasonic extraction (UE), supercritical fluid extraction (SFE), pressurized fluid extraction (PFE) also called accelerated solvent extraction (ASE), solid-phase extraction (SPE), solid-phase micro-extraction (SPME), and stir-bar-sorptive extraction (SBSE). A variety of review papers comparing the advantages and disadvantages of each of these techniques is available.<sup>9-12</sup>

Many of the extraction techniques have been classified as either exhaustive, in that all of the analyte is removed from the sample, or non-exhaustive, in which only a representative fraction is removed for analysis. This was graphically summarized by Pawliszyn and is reproduced in Figure 1-1.<sup>7</sup>

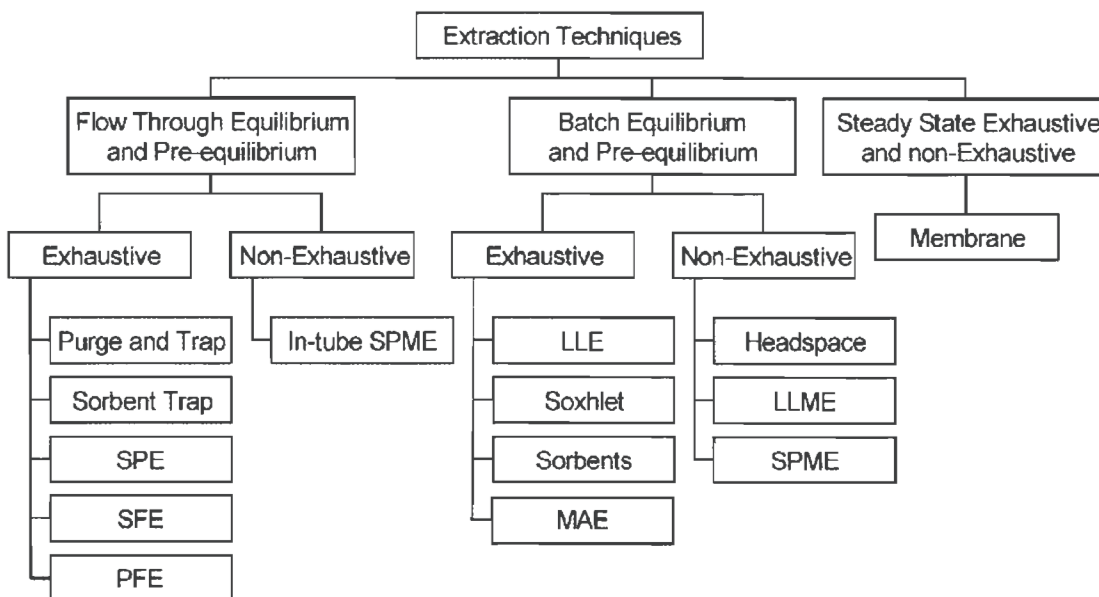


Figure 1-1. Classification of extraction techniques (reproduced from Pawliszyn 2003)

Modern commercially available laboratory-based solid sample preparation instruments include the ASE200 Accelerated Solvent Extractor (Dionex Corporation, Sunnyvale, CA) and the Soxtherm automated Soxhlet extractor (Gerhardt, distributed by Lab Synergy, Goshen, NY). These instruments are expensive and very much limited to laboratory use but provide unsurpassed extraction efficiencies. Other solid sample preparation instruments include the Mars microwave digester (CEM Corporations, Matthews, NC) and autofusers such as TheOx (Corporation Scientifique Claisse, Quebec, QC) in which solids dissolve in a molten flux material such as lithium metaborate.

In regards to field testing, sample preparation has been mostly limited to solid-phase microextractors (SPME) with simple samplers sold by a variety of companies including Sigma-Aldrich. Hach Company (Loveland, CO) has a whole variety of field tests but these are limited to liquid samples. Finally the only true on-site solid sample preparation techniques are those being done using tools such as mini-grinders or blenders to powder samples.

### **1.1.2 Magnetism<sup>13</sup>**

Magnetic fields are provided from either electric currents or from characteristic magnetic moments of certain materials that contain unpaired electrons in their orbitals. Permanent magnets are made of ferromagnetic materials which retain their magnetic properties after an external magnetic field has been removed. Ferromagnetic materials such as iron, nickel and cobalt contain unpaired electrons resulting in a net magnetic moment. If all of the sections or magnetic domains are randomly organized the ferromagnetic material as a whole has a zero net magnetic field. A strong magnet is made when all the domains align parallel to one another, for example when exposed to an external magnetic field. A hysteresis loop or "BH curve" measures the material's magnetic flux density (B) as it is exposed to an increasing external magnetic field (H) as shown in Figure 1-2.

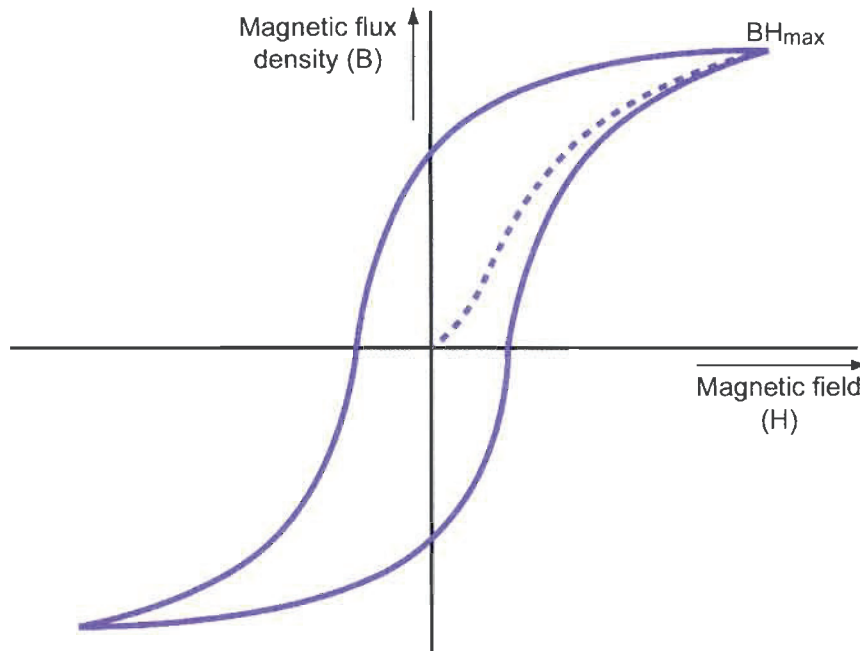


**Figure 1-2.** Magnetization BH curve (hysteresis loop). Dotted line is for a ferromagnetic material that is exposed to a magnetic field for the first time.

As the magnetic field is increased, the magnetic flux density increases until almost all of the magnetic domains are aligned at which point the magnetic energy product ( $BH_{\max}$ ) or saturation point is reached. This maximum is characteristic for each type of magnet. Increasing the external magnetic field beyond this point will not significantly increase the magnetic flux density of the ferromagnetic material. As the external magnetic field is removed, the magnetic flux density decreases to a lesser degree than the original increase. Even if the external magnetic field is completely removed, some magnetic domains remain aligned in the ferromagnetic materials resulting in permanent magnets. The units used to measure these magnetic properties are summarized in Table 1-1.

Table 1-1. Summary of magnetic properties and corresponding units

Magnetic Property	Units	Conversion
	Imperial \ SI	
Magnetic flux density or magnetic induction (B)	Gauss (G) \ Tesla (T)	1 G = $10^{-4}$ T
Magnetic field (H)	Oersteds (Oe) \ Amperes per meter ( $A\ m^{-1}$ )	1 Oe = $79.6\ A\ m^{-1}$
Maximum energy product ( $BH_{max}$ )	megaGauss Oersteds (MGOe) \ kilojoules per cubic meter ( $kJ\ m^{-3}$ )	1 MGOe = $7.96\ kJ\ m^{-3}$

The force of a given magnet ( $F_{mag}$ ) is associated with the square of its magnetic flux density (B), its area (A) in square meters, and the permeability of free space ( $\mu_0$ ) given as  $4\pi \times 10^{-7}$  newton per square amps.

$$F_{mag} = \frac{B^2 A}{2\mu_0} \quad (\text{Equation 1-1})$$

This force can be harnessed to provide a variety of functions in both microfluidics and centrifugal microfluidics as discussed below.

### 1.1.3 Microfluidics

Micro Total Analysis Systems ( $\mu$ TAS or microTAS),<sup>14</sup> also called “lab-on-a-chip” (LOC), is a branch of analytical chemistry dealing with small instrumentation. An active area of research within this field is microfluidics, devices containing channels, structures and fluids on the micro scale. Such microfluidic devices offer striking advantages over conventional analysis systems and have the potential for revolutionizing analytical methods. For example, low reagent and sample volumes translate to lower operational costs and less waste, which is particularly important from an environmental point of view where there are many drawbacks to using large solvent volumes common to most standard

methods. Many microfluidic devices can be mass produced by techniques such as hot embossing resulting in the possibility of disposable, low cost units. Likewise, due to the short diffusion distances, reactions occur quickly resulting in short analysis times. These devices also have minimal power and space requirements make them economically and environmentally very attractive for both clinical point-of-care diagnostics and environmental field use.

Many “perspective” articles have been written detailing the great potential of microfluidic technology.<sup>15, 16</sup> In 1990, Andreas Manz published his first article dealing with microfluidics<sup>14</sup> and since 2002 his group has published a bi-annual review of the latest advancements and trends in this field with their next edition due in December of 2012.<sup>17-22</sup> Topics included in these reviews range from fabrication, through fluid handling procedures and mixing to detection techniques. The development of microfluidic technology has implications in many diverse areas including fuel cells, ink jet printing, microreactors, DNA extraction, PCR amplification and analysis, cosmetics and pharmaceuticals. Manz also discusses the advantages of using microfluidics for environmental analysis highlighting systems that have been developed for the determination of sulfite, nitrite, chlorine, ammonium, lead and copper.<sup>22</sup> Likewise, as an example of extreme field portability, a microfluidic analysis system is currently on route to Mars where it will analyze soils for amino acids using fluorescence detection.<sup>23</sup> Other excellent reviews detailing the global advantages of microfluidics are also available.<sup>24, 25</sup>

Due to the micron size channels, the flow of liquids in microfluidic devices is characterized by low Reynolds (Re) numbers (below 2100) and is therefore almost always laminar.<sup>26</sup> This contrasts with turbulent flow encountered in larger

size channels which generally have Reynolds numbers above 4000. The Reynolds number is a dimensionless number which depends on the density of the fluid ( $\rho_f$ ), the average velocity of the liquid ( $U$ ), the diameter of the channel ( $d$ ) and the dynamic viscosity of the liquid ( $\mu$ ).

$$Re = \frac{\text{inertial forces}}{\text{viscous forces}} = \frac{\rho_f U d}{\mu} \quad (\text{Equation 1-2})$$

Since laminar flow is prevailing in microfluidics, thorough mixing is often a challenge and is the focus of ongoing research. An overview of microfluidic mixing strategies has been recently published by Naher *et al.*<sup>27</sup>

With any new technology come inherent disadvantages. In the case of microfluidics, the devices (or chips) are so small that interfacing with the real world, sometimes called “world-to-chip” interface, remains a challenge.<sup>28, 29</sup> Another major challenge is forcing liquid to flow through the network of channels since, as channel size decreases, the resistance to flow increases and the need for higher pressures arises. Pumping fluids in microfluidics therefore requires comparatively large external pumps, integrated micromachined pumps or high voltage potentials. Electrokinetic pumping with high voltage potentials is quite popular due to its relative ease of implementation and pulse free flow, but it does place strict limits on the pH and ionic character of the mobile solution.<sup>30</sup>

### 1.1.3.1 Magnetism in Microfluidics

Since magnetic interactions are generally not affected by surface charges, pH or ionic strength, an increasing number of microfluidic applications are making use of magnetic forces. The ability to externally control structures inside microchannels is a unique advantage of magnetic forces. In an excellent review

by Nicole Pamme,<sup>31</sup> a long list of microfluidic applications that use magnetism are shown to include pumping, mixing, switching, valving, transporting, positioning, separating and sorting. Superparamagnetic beads are becoming common in a multitude of microfluidic biological and biomedical applications.<sup>32</sup> Specific examples of the use of magnetism in centrifugal microfluidics are detailed below.

#### 1.1.4 Centrifugal Microfluidics

A subsection of microfluidics research that uses centrifugal forces to pump liquids has become very active in the past decade. This area of research referred to in this text simply as “centrifugal microfluidics” has been known under many different names such as “LabCD”,<sup>33</sup> “lab on a CD”,<sup>34</sup> “lab-on-a-disc”,<sup>35</sup> “lab-on-a-disk”,<sup>36</sup> “Bio-Disk platform”,<sup>37</sup> “microfluidic compact disc platforms”,<sup>38</sup> “compact disk-like microfluidic platform”,<sup>39</sup> “CD-like microfluidic platform”,<sup>40</sup> “centrifuge-based fluidic platforms”,<sup>41</sup> “centrifugal microanalysis system”<sup>42</sup> and “microfluidics on a rotating disk”.<sup>43</sup>

Though the automation of sample processing using centrifugal forces dates back to the work by Anderson in 1969<sup>44</sup> and by Scott *et al.* in the 1970s,<sup>45-48</sup> the integration of microfluidic reservoirs and channels on a new generation of centrifugal devices was first presented by Marc Madou’s group in 1998.<sup>33</sup> Since that time research in centrifugal microfluidics has rapidly grown. As seen in Figure 1-3, the number of publications in “centrifugal microfluidics” has increased at a rate similar to that of “microfluidics” as a whole and probably faster if all of the different terms mentioned above were included.

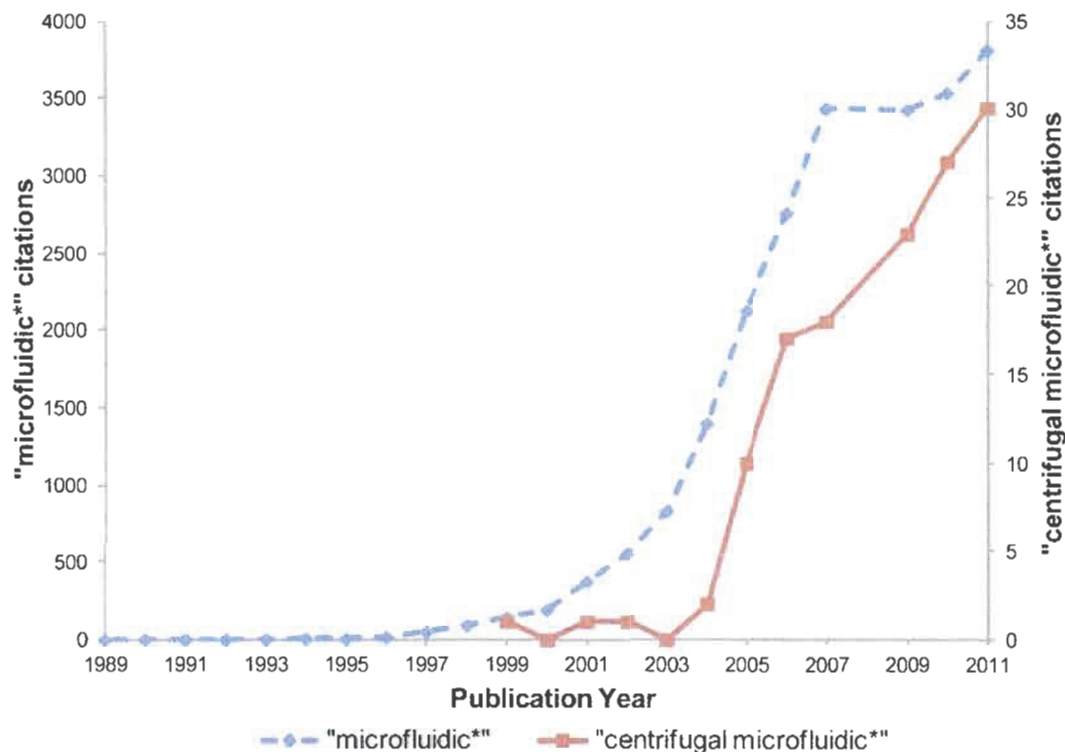


Figure 1-3. The number of publications per year containing the terms “microfluidic\*” and “centrifugal microfluidic\*” found in a search of the Scopus™ database in 2012.

From the Latin *centrum* meaning centre and *fugere* meaning “to flee”,<sup>49</sup> “centrifugal” accurately describes the movement of liquid being pumped radially outward from the centre of spinning devices. This pumping mechanism offers unique advantages over other microfluidic devices in that it eliminates the need for external pumps, integrated micromachined pumps or high voltage potentials. Consequently essentially any liquid can be pumped on these devices<sup>50</sup> which in turn allows one to use almost any chemistry. Likewise, these systems are well suited for field work only requiring a simple motor to provide this pumping force. The centrifugal propulsion force generates a pulse free flow which is mainly influenced by the density and viscosity of the liquid (see Equation 1-3 below).

Centrifugal microfluidic devices are commonly, though not exclusively, the size of a compact disk of varying thicknesses. The advantages of these devices also include the low consumption of sample and reagents, the ease of handling, minimal power and space requirements (small instrument footprint), the robustness and simplicity of its configuration, the high degree of parallelization (either one test of many samples or different tests of one sample; performed simultaneously), the low cost of mass fabrication, the freedom of solvents and rapid prototyping.<sup>41</sup> A number of excellent review articles on centrifugal microfluidics are available.<sup>25, 34, 51</sup> Likewise the growing number of commercially launched devices (e.g. Gyros, Sweden; SpinX, Switzerland; Bio-Disk; Germany) clearly demonstrates the economic prospects of centrifugal microfluidics.

Just as with microfluidic devices, interfacing with spinning centrifugal microfluidics devices is a challenge. Adding samples and reagents, actuating valves and moving objects within spinning devices is difficult. Similarly, visualizing the liquid flow and acquiring real-time data from the spinning devices are continuing challenges. Other disadvantages include space restrictions as sequential operations normally must be placed radially outwards from the centre; only recently have liquids been successfully transported radially inwards to address this challenge.<sup>52, 53</sup> Pre-loaded or pre-stored reagents are common; however, this also reduces the space available on the devices, have a limited shelf-life, and in the case of liquid reagents, have a tendency to move throughout the microfluidic network or evaporate from vent holes.

Many different groups have published research in centrifugal microfluidics. Three main groups have been particularly active over the past decade. First,

from the University of California, Irvine (USA), Prof. Marc Madou's group including Dr. Horacio Kido and Dr. Jim Zoval pioneered the development of centrifugal microfluidic devices, mainly for biological applications. They have collaborated with many other groups including Prof. Michel Bergeron from the Université Laval (Canada), Prof. Ángel Maquieira from the Universidad Politécnica de Valencia (Spain) and the Samsung Advanced Institute of Technology (South Korea). Since 2003, a great number of publications have come from a large group from the University of Freiburg in the Laboratory for MEMS Applications (Germany), notably made up of Prof. Roland Zengerle, Dr. Jens Ducreé, Dr. Stefan Haeberle and Dr. Markus Grumann. This group has focussed on new functionalities and liquid point-of-care biological applications. Finally, Prof. Eric D. Salin's group has developed new functionalities with a unique focus on environmental applications.

As Ducreé *et al.* have described, a growing toolbox of “unit operations” now exist allowing highly precise liquid handling.<sup>37</sup> These “unit operations” add functionalities to the devices and currently include capillary valving, hydrophobic valving, siphon valving, laser-triggered valving, centrifuge-pneumatic valving, metering, aliquoting, mixing, Coriolis switching, detection, sedimentation and reagent storage.<sup>25, 54</sup> A selection of these operations is sequentially integrated on single device depending on the desired function and application. Some devices are capable of simultaneously running hundreds of small volume analyses.<sup>55</sup>

A diverse number of clinical and environmental applications of centrifugal microfluidics have been reported. In regards to clinical and biological point-of-care systems,<sup>56</sup> centrifugal microfluidics has been used for a great variety of

assays including colorimetric glucose assays<sup>57</sup>, PCR amplification,<sup>58</sup> extraction of plasma<sup>59, 60</sup> and hemoglobin<sup>61</sup> from whole blood, biochemical analysis and sandwich type immunoassay from whole blood<sup>62</sup> as well as multiplexed bead-based fluorescence immunoassays<sup>63</sup> and enzyme-linked immunosorbent assays (ELISA).<sup>39, 64, 65</sup> Centrifugal microfluidic devices have also been used in a variety of environmental applications such as the determination of trace metals<sup>66</sup> such as chromium (VI),<sup>42</sup> nitrates and nitrites,<sup>67</sup> and polycyclic aromatic hydrocarbons (PAHs)<sup>68</sup> from aqueous samples.

Generally speaking, solid and particulate samples have been strictly avoided in microfluidic systems due to the potential for channel blockage and their poor behavior in electric fields. This is extremely unfortunate because many interesting environmental analyses involve solid or particulate samples. A strong advantage of centrifugal processing is the ability to integrate solid sample analysis with the clear advantages that microfluidic systems offer. Due to its inherent design, centrifugal microfluidic devices act as a centrifuge on particle which can be made to sediment quickly. To date the analysis of solid samples in centrifugal microfluidics has been limited to small cells<sup>69-71</sup> and no work has been reported on harder solid environmental samples.

#### *1.1.4.1 Liquid Flow Rates*

Duffy *et al.*<sup>50</sup> and Zoval *et al.*<sup>41</sup> experimentally characterized the flow rates of aqueous solutions pumped by centrifugal forces in a open microchannel as being equal to:

$$U = \frac{d_h^2 \rho \omega^2 \bar{r} \Delta r}{32 \eta L} \quad (\text{Equation 1-3})$$

Consequently, the velocity of a liquid ( $U$ ) is shown to be proportional to square of the angular velocity ( $\omega$ ), and is affected by the density ( $\rho$ ) and viscosity ( $\eta$ ) of the liquid as well as the length of the liquid in the channel ( $L$ ), the average distance of the liquid in the channel from the centre of the device ( $\bar{r}$ ) and the radial extent of fluid subjected to a centrifugal pressure ( $\Delta r$ ). These distances are shown in Figure 1-4. The term  $d_h$  is the hydraulic diameter of the channel related to the cross-sectional area and perimeter of the channel.

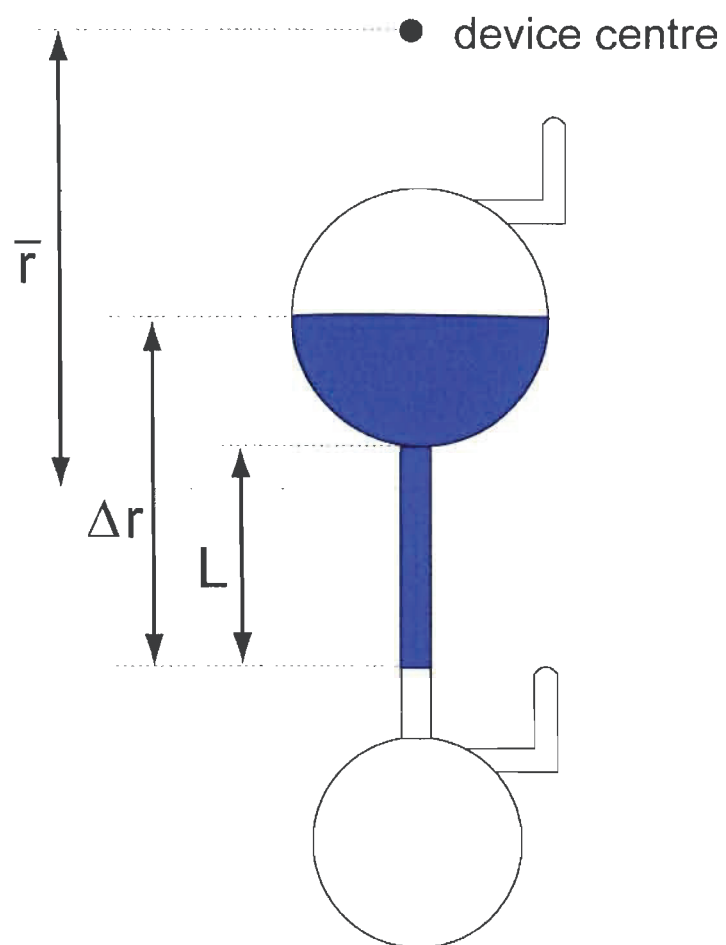


Figure 1-4. Visual representation of variables affecting the flow rate of solution in centrifugal microfluidic devices.

### 1.1.4.2 Capillary Burst Valves

An important feature of centrifugal microfluidic devices is the incorporation of valves for metering sample volumes and timing purposes. There are many different types of both active (requiring external energy) and passive (not requiring external energy) valves. Passive capillary burst valves are the most common and useful in centrifugal microfluidics.

A variety of models characterizing capillary burst valves exists in the literature. From the above expression for the flow rate (Equation 1-3), the centrifugal pressure ( $\Delta p_c$ ) on a column of liquid is given by:

$$\Delta p_c = \rho \omega^2 \bar{r} \Delta r \quad (\text{Equation 1-4})$$

When a moving liquid encounters a rapid expansion, the liquid is described as being “pinned at the discontinuity”<sup>50</sup> between the narrow capillary channel and the relatively large lower reservoir due to the surface tension that develops at this abrupt change in geometry. This is called the pressure barrier or burst pressure described by Zeng *et al.*<sup>72</sup> as being equal to:

$$\Delta p_b = \frac{4\gamma \sin \theta_c}{d_h} \quad (\text{Equation 1-5})$$

Where  $\gamma$  is the liquid's surface tension and  $\theta_c$  is the contact angle between the liquid and the channel. More complex models are available such as that by Chen *et al.*<sup>43</sup> which takes into consideration the menisci in three dimensions

The capillary valve bursts when the centrifugal pressure is greater than or equal to the burst pressure, achieved by increasing the angular velocity.

$$\Delta p_c \geq \Delta p_b. \quad (\text{Equation 1-6a})$$

$$\rho \omega^2 \bar{r} \Delta r \geq \frac{4\gamma \sin \theta_c}{d_h} \quad (\text{Equation 1-6b})$$

Isolating the angular velocity term and substituting for frequency (where  $f = \omega/2\pi$ ) yields an expression for the capillary burst frequency:

$$f \geq \sqrt{\frac{\gamma \sin \theta_c}{\pi^2 d_h \rho \bar{r} \Delta r}} \quad (\text{Equation 1-6c})$$

Although mathematical theory and equations help to calculate the theoretical capillary burst valve frequencies, actual experiments were found to be best to determine these values due to the differences in shape (round versus rectangular), materials (plastic versus glass) and solvents used.

#### 1.1.4.3 Sedimentation

The velocity at which a small spherical particle sediments in a liquid is described by Stokes' Law<sup>73</sup> which states that the magnitude of the resistive frictional force ( $F_r$ ) on the particle of a given Stokes' radius ( $R$ ) sedimenting through a fluid of a given viscosity ( $\eta$ ) with a given velocity ( $v$ ) is equal to:

$$F_r = 6\pi\eta Rv \quad (\text{Equation 1-7})$$

From this Law the settling velocity ( $v_s$ ) of a particle by centrifugation can be derived taking into consideration the density of the particle ( $\rho_p$ ), the density of the fluid ( $\rho_f$ ), the average distance of the particle from the centre of rotation ( $r$ ) and the angular velocity ( $\omega$ ).

$$v_s = \frac{2R^2\omega^2r}{9\eta}(\rho_p - \rho_f) \quad (\text{Equation 1-8})$$

Details of this derivation are available in Appendix G.

#### 1.1.4.4 Magnetism in Centrifugal Microfluidics

The unique advantage of using magnets in centrifugal microfluidics is the ability of externally controlling components that are integrated inside spinning devices. For example, Haeberle *et al.*<sup>74</sup> describe a centrifugo-magnetic pump in which paramagnetic material is enclosed within flexible elastomer lids and is made to move in a magnetic field creating an incorporated pump.

Three other systems are of particular interest. First, Kido *et al.*<sup>69, 70</sup> demonstrated two different configurations in which a fixed magnet base is used to actuate metal disks within spinning devices. These disk agitators combined with glass beads were found to be effective for cell lysis in preparation for PCR amplifications. Second, Grumann *et al.*<sup>75</sup> accelerated the mixing process of liquid samples by placing very small magnetic beads in a mixing chamber which were then deflected by fixed permanent magnets located above. The devices were also spun in a back-and-forth motion by rapidly alternating the rotational direction. As a result, mixing was greatly accelerated from about 7 minutes for mere diffusion to a few seconds. Third, Cho *et al.*<sup>71</sup> achieved complex cell movements using magnetic capture-beads. An integrated movable magnet controlled the position of the magnetic beads. As a result, an automated cell capture, lysis and DNA purification device was developed.

In these three systems, magnetically actuated motion was used for cell transport, cell lysis and liquid mixing. Of note is the lack of applications to solid environmental samples in the literature.

#### *1.1.4.5 Spectroscopic Detection*

A key feature of a true centrifugal “micro total analysis systems” is to include all or nearly all steps of the analysis on one device, including detection. Most centrifugal microfluidic devices are transparent to visible light, allowing the last reservoir to serve as an integrated spectrophotometric detection cell. Both UV-Vis absorbance<sup>59-61</sup> and fluorescence<sup>63, 76</sup> detection have been reported. UV-transparent materials have also been used as top and bottom window layers for greater wavelength range.<sup>68</sup>

The main drawback of performing UV-Vis absorbance measurements on a centrifugal microfluidic device is the relatively short optical path length which is limited by the inherent thickness of the device. Several approaches to increase the optical path length by guiding the light beam through a cross-section of the device have been proposed such as embedding optical waveguides, integrating microlenses, or using optical fibers.<sup>51</sup> In one example in particular, “real-time on-chip beam-guided absorption measurements” were made by reflecting a light beam 90 degrees into and then out of the device’s plane using integrated V-grooves and total internal reflection. The optical path length therefore became the full width of the detection cell instead of only its height, increasing the distance the light passing through the cell by a factor of 10 (from 1 mm to 10 mm).<sup>57</sup>

## 1.2 Objectives

One goal of this thesis is the development of novel instrumentation and sample handling techniques for the automation, miniaturization and integration on a single device of standard analytical procedures. Centrifugal microfluidics was chosen for the advantages outlined in section 1.1.4. These new sample handling techniques will address current challenges in the field of centrifugal microfluidics including the integration of sample introduction, preparation and extraction on devices in motion. As Mark *et al.*<sup>25</sup> mention, the assembly and reagent pre-storage steps increase the cost of devices. A one-step fabrication technique and the elimination of pre-stored reagents will also be addressed.

Another goal of this thesis is the development of new methods for the analysis of environmentally important species such as PAHs and pesticides in solid samples. The automated methods and devices will be cheaper, greener and faster than the corresponding current standard procedures. *Cheaper* in that the possibility to mass produce devices results in a low cost per unit; *greener* in that the small sample and reagent volumes used result in reduced costs and more importantly reduced waste; and *faster*, integrating a variety of operations and processing steps in a single device.

## 1.3 Thesis Outline

**Chapter 2** describes multiple motorized stages with details of the tools necessary to visualize and study centrifugal microfluidic devices in motion. A description of subtractive manufacturing techniques as well as lamination sealing techniques is also included.

**Chapter 3** presents a comparison of 3D printers for the rapid additive manufacturing of parts and entire devices. The study first focuses on the design and manufacturing processes and then compares the resulting parts in terms of precision, accuracy, ability to retain liquids, surface finish, chemical resistivity and ability to print capillary burst valves.

Using the instruments and the fabrication techniques described in Chapters 2 and 3, Chapters 4 to 7 concentrate on new sample handling techniques in centrifugal microfluidics and apply these learnings to the analysis of environmental samples.

**Chapter 4** presents a World-to-Disk interface enabling liquid sample introduction to device in motion. A hybrid centrifugal microfluidic device made from both subtractive and additive manufactured parts is discussed. A gradient is added to the spinning devices to demonstrate the possibility of centrifugal microfluidic chromatography without the use of device space for liquid storage.

**Chapter 5** introduces the use of magnets to enable solid sample preparation on a device in motion. The movement of the “mobile magnets” in close proximity of the fixed magnet base is characterized.

**Chapter 6** evaluates the magnetically actuated liquid-solid extraction technique and method for the automation and miniaturization of the analysis of soil samples for PAHs.

**Chapter 7** expands the use of magnetically actuated liquid-solid extraction for the automated analysis of both soil and vegetable samples for pesticides while greatly reducing sample and reagent volumes.

**Chapter 8** summarizes the main conclusions and includes a discussion of future directions of both the envisioned instrumentation and applications.

## 1.4 References

- (1) de la Guardia, M., Armenta, S., *Comprehensive Analytical Chemistry: Downsizing the Methods*, Vol. 57, Elsevier, **2011**, 157-184.
- (2) Ramos, L., Ramos, J.J., Brinkman, U.A.T., "Miniaturization in sample treatment for environmental analysis", *Analytical and Bioanalytical Chemistry*, **2005**, 381 (1), 119-140.
- (3) Pawliszyn, J., *Comprehensive Analytical Chemistry: Sampling and Sample Preparation for Field and Laboratory*, Vol. 37, Elsevier, **2002**, 1131.
- (4) Ren, J.M., Rattray, R., Salin, E.D., Grégoire, D.C., "Assessment of direct solid sample analysis by graphite pellet electrothermal vaporization inductively coupled plasma mass spectrometry", *Journal of Analytical Atomic Spectrometry*, **1995**, 10 (11), 1027-1029.
- (5) Soxhlet, F.R.v., "Die gewichtsanalytische Bestimmung des Milchfettes", *Dingler's Polytechnisches Journal*, **1879**, 232 461-465.
- (6) Dean, E.W., Stark, D.D., "A Convenient Method for the Determination of Water in Petroleum and Other Organic Emulsions", *Journal of Industrial & Engineering Chemistry*, **1920**, 12 (5), 486-490.
- (7) Pawliszyn, J., "Sample preparation: Quo vadis?", *Analytical Chemistry*, **2003**, 75 (11), 2543-2558.
- (8) Namieśnik, J., Zabiegała, B., Kot-Wasik, A., Partyka, M., Wasik, A., "Passive sampling and/or extraction techniques in environmental analysis: A review", *Analytical and Bioanalytical Chemistry*, **2005**, 381 (2), 279-301.
- (9) Luque de Castro, M.D., García-Ayuso, L.E., "Soxhlet extraction of solid materials: An outdated technique with a promising innovative future", *Analytica Chimica Acta*, **1998**, 369 (1-2), 1-10.
- (10) Assis, L.M., Silva Pinto, J.S., Lanças, F.M., "Comparison among different extraction methods (PFE, SFE, Sonication, Soxhlet) for the isolation of organic compounds from coal", *Journal of Microcolumn Separations*, **2000**, 12 (5), 292-301.
- (11) Morales-Muñoz, S., Luque-García, J.L., Luque de Castro, M.D., "Approaches for Accelerating Sample Preparation in Environmental Analysis", *Critical Reviews in Environmental Science and Technology*, **2003**, 33 (4), 391-421.
- (12) Sporring, S., Bøwadt, S., Svensmark, B., Bjorklund, E., "Comprehensive comparison of classic Soxhlet extraction with Soxtec extraction, ultrasonication extraction, supercritical fluid extraction, microwave assisted extraction and accelerated solvent extraction for the determination of polychlorinated biphenyls in soil", *Journal of Chromatography A*, **2005**, 1090 (1-2), 1-9.

- (13) Moskowitz, L.R., *Permanent magnet design and application handbook*, Krieger, Malabar, Fla. **1995**, p. 946.
- (14) Manz, A., Graber, N., Widmer, H.M., "Miniaturized total chemical analysis systems: A novel concept for chemical sensing", *Sensors and Actuators: B. Chemical*, **1990**, 1 (1-6), 244-248.
- (15) Felton, M.J., "Lab on a chip: poised on the brink", *Analytical Chemistry*, **2003**, 75 (23), 505A-508A.
- (16) Mukhopadhyay, R., "Microfluidics: On the slope of enlightenment", *Analytical Chemistry*, **2009**, 81 (11), 4169-4173.
- (17) Reyes, D.R., Iossifidis, D., Auroux, P.A., Manz, A., "Micro total analysis systems. 1. Introduction, theory, and technology", *Analytical Chemistry*, **2002**, 74 (12), 2623-2636.
- (18) Auroux, P.A., Iossifidis, D., Reyes, D.R., Manz, A., "Micro total analysis systems. 2. Analytical standard operations and applications", *Analytical Chemistry*, **2002**, 74 (12), 2637-2652.
- (19) Vilkner, T., Janasek, D., Manz, A., "Micro total analysis systems. Recent developments", *Analytical Chemistry*, **2004**, 76 (12), 3373-3386.
- (20) Dittrich, P.S., Tachikawa, K., Manz, A., "Micro total analysis systems. Latest advancements and trends", *Analytical Chemistry*, **2006**, 78 (12), 3887-3907.
- (21) West, J., Becker, M., Tombrink, S., Manz, A., "Micro total analysis systems: Latest achievements", *Analytical Chemistry*, **2008**, 80 (12), 4403-4419.
- (22) Arora, A., Simone, G., Salieb-Beugelaar, G.B., Kim, J.T., Manz, A., "Latest developments in micro total analysis systems", *Analytical Chemistry*, **2010**, 82 (12), 4830-4847.
- (23) Skelley, A.M., Scherer, J.R., Aubrey, A.D., Grover, W.H., Ivester, R.H.C., Ehrenfreund, P., Grunthaner, F.J., Bada, J.L., Mathies, R.A., "Development and evaluation of a microdevice for amino acid biomarker detection and analysis on Mars", *Proceedings of the National Academy of Sciences of the United States of America*, **2005**, 102 (4), 1041-1046.
- (24) Haeberle, S., Zengerle, R., "Microfluidic platforms for lab-on-a-chip applications", *Lab on a Chip - Miniaturisation for Chemistry and Biology*, **2007**, 7 (9), 1094-1110.
- (25) Mark, D., Haeberle, S., Roth, G., Stetten, F.v., Zengerle, R., "Microfluidic lab-on-a-chip platforms: requirements, characteristics and applications", *Chemical Society Reviews*, **2010**, 39 (3), 1153-1182.
- (26) Madou, M.J., "Fundamentals of Microfabrication"; 2nd ed.; CRC Press Boca: Raton, Florida, **2002**,
- (27) Naher, S., Orpen, D., Brabazon, D., Morshed, M.M., "An overview of microfluidic mixing application", *Advanced Materials Research*, **2010**, 83 931-939.
- (28) Fang, Q., Xu, G.M., Fang, Z.L., "A high-throughput continuous sample introduction interface for microfluidic chip-based capillary electrophoresis systems", *Analytical Chemistry*, **2002**, 74 (6), 1223-1231.

- (29) Liu, J., Hansen, C., Quake, S.R., "Solving the "world-to-chip" interface problem with a microfluidic matrix", *Analytical Chemistry*, **2003**, 75 (18), 4718-4723.
- (30) Polson, N.A., Hayes, M.A., "Peer Reviewed: Microfluidics: Controlling Fluids in Small Places", *Analytical Chemistry*, **2001**, 73 (11), 312 A-319 A.
- (31) Pamme, N., "Magnetism and microfluidics", *Lab on a Chip - Miniaturisation for Chemistry and Biology*, **2006**, 6 (1), 24-38.
- (32) Shevkoplyas, S.S., Siegel, A.C., Westervelt, R.M., Prentiss, M.G., Whitesides, G.M., "The force acting on a superparamagnetic bead due to an applied magnetic field", *Lab on a Chip - Miniaturisation for Chemistry and Biology*, **2007**, 7 (10), 1294-1302.
- (33) Madou, M.J., Kellogg, G.J., "LabCD: A centrifuge-based microfluidic platform for diagnostics", presented at *Proceedings of SPIE - The International Society for Optical Engineering*, San Jose, CA, USA, **1998**, 80-93.
- (34) Madou, M., Zoval, J., Jia, G., Kido, H., Kim, J., Kim, N., "Lab on a CD", *Annual Review of Biomedical Engineering*, **2006**, 8 601-628.
- (35) Lee, B.S., Lee, J.G., Lee, J.N., Park, J.M., Cho, Y.K., Kim, S., Ko, C., "One-step target protein detection from whole blood in a lab-on-a-disc", presented at *Technical Proceedings of the 2008 NSTI Nanotechnology Conference and Trade Show, NSTI-Nanotech, Nanotechnology 2008*, **2008**, 241-244.
- (36) Steigert, J., Brenner, T., Grumann, M., Riegger, L., Lutz, S., Zengerle, R., Duccée, J., "Integrated siphon-based metering and sedimentation of whole blood on a hydrophilic lab-on-a-disk", *Biomedical Microdevices*, **2007**, 9 (5), 675-679.
- (37) Duccée, J., Haeberle, S., Lutz, S., Pausch, S., Von Stetten, F., Zengerle, R., "The centrifugal microfluidic Bio-Disk platform", *Journal of Micromechanics and Microengineering*, **2007**, 17 (7), S103-S115.
- (38) Martineau, I., Boudreau, D.K., Monfort, L., Bégin, F., Fiola, M.-J., Stewart, G., Morin, H., Huletsky, A., Peytavi, R., Boissinot, M., Picard, F.J., Zoval, J.V., Kido, H., Jia, G., Madou, M., Bergeron, M.G., "Microfluidic compact disc platforms for rapid and sensitive detection and identification of *Candida* yeasts from blood", presented at *Micro Total Analysis Systems 2007, Proceedings of mTAS 2007 11th International Conference on Miniaturized Systems for Chemistry and Life Sciences*, Paris, France, 7-11 October 2007, **2007**, 74-76.
- (39) Lai, S., Wang, S., Luo, J., Lee, L.J., Yang, S.-T., Madou, M.J., "Design of a Compact Disk-like Microfluidic Platform for Enzyme-Linked Immunosorbent Assay", *Analytical Chemistry*, **2004**, 76 (7), 1832-1837.
- (40) Madou, M.J., Lee, L.J., Daunert, S., Lai, S., Shih, C.-H., "Design and fabrication of CD-like microfluidic platforms for diagnostics: microfluidic functions", *Biomedical Microdevices*, **2001**, 3 (3), 245-254.
- (41) Zoval, J.V., Madou, M.J., "Centrifuge-based fluidic platforms", *Proceedings of the IEEE*, **2004**, 92 (1), 140-153.

- (42) LaCroix-Fralish, A., Clare, J., Skinner, C.D., Salin, E.D., "A centrifugal microanalysis system for the determination of nitrite and hexavalent chromium", *Talanta*, **2009**, 80 (2), 670-675.
- (43) Chen, J.M., Huang, P.C., Lin, M.G., "Analysis and experiment of capillary valves for microfluidics on a rotating disk", *Microfluidics and Nanofluidics*, **2008**, 4 (5), 427-437.
- (44) Anderson, N.G., "Computer interfaced fast analyzers", *Science*, **1969**, 166 (3903), 317-324.
- (45) Scott, C.D., Pitt Jr, W.W., Johnson, F., "Centrifugal elution chromatography with eluate monitoring", *Journal of Chromatography A*, **1974**, 99 (C), 35-42.
- (46) Scott, C.D., Burtis, C.A., Johnson, W.F., "A small portable centrifugal fast analyzer system", *Clinical Chemistry*, **1974**, 20 (8), 1003-1008.
- (47) Shumate li, S.E., Scott, C.D., "Centrifugal system for affinity chromatography with eluate monitoring", *Clinical Chemistry*, **1976**, 22 (9), 1493-1496.
- (48) Ingle, J.D., Crouch, S.R., "Spectrochemical analysis"; Prentice Hall: Englewood Cliffs, N.J., **1988**, p. 1-590.
- (49) Merriam-Webster, "Merriam-Webster's Collegiate Dictionary"; 11th ed., **2003**,
- (50) Duffy, D.C., Gillis, H.L., Lin, J., Sheppard, N.F., Jr., Kellogg, G.J., "Microfabricated Centrifugal Microfluidic Systems: Characterization and Multiple Enzymatic Assays", *Analytical Chemistry*, **1999**, 71 (20), 4669-4678.
- (51) Steigert, J., Grumann, M., Brenner, T., Mittenbuehler, K., Nann, T., Ruehe, J., Moser, I., Haeberle, S., Riegger, L., Riegler, J., Bessler, W., Zengerle, R., Ducreé, J., "Integrated sample preparation, reaction, and detection on a high-frequency centrifugal microfluidic platform", *Journal of the Association for Laboratory Automation*, **2005**, 10 (5), 331-341.
- (52) Kong, M.C.R., Salin, E.D., "Pneumatically pumping fluids radially inward on centrifugal microfluidic platforms in motion", *Analytical Chemistry*, **2010**, 82 (19), 8039-8041.
- (53) Abi-Samra, K., Clime, L., Kong, L., Gorkin lii, R., Kim, T.H., Cho, Y.K., Madou, M., "Thermo-pneumatic pumping in centrifugal microfluidic platforms", *Microfluidics and Nanofluidics*, **2011**, 1-10.
- (54) LaCroix-Fralish, A., Templeton, E.J., Salin, E.D., Skinner, C.D., "A rapid prototyping technique for valves and filters in centrifugal microfluidic devices", *Lab on a Chip*, **2009**, 9 (21), 3151-3154.
- (55) Andersson, P., Jesson, G., Kylberg, G., Ekstrand, G., Thorsén, G., "Parallel nanoliter microfluidic analysis system", *Analytical Chemistry*, **2007**, 79 (11), 4022-4030.
- (56) Gorkin, R., Park, J., Siegrist, J., Amasia, M., Lee, B.S., Park, J.M., Kim, J., Kim, H., Madou, M., Cho, Y.K., "Centrifugal microfluidics for biomedical applications", *Lab on a Chip - Miniaturisation for Chemistry and Biology*, **2010**, 10 (14), 1758-1773.

- (57) Grumann, M., Steigert, J., Riegger, L., Moser, I., Enderle, B., Riebeseel, K., Urban, G., Zengerle, R., Ducrée, J., "Sensitivity enhancement for colorimetric glucose assays on whole blood by on-chip beam-guidance", *Biomedical Microdevices*, **2006**, 8 (3), 209-214.
- (58) Amasia, M., Cozzens, M., Madou, M.J., "Centrifugal microfluidic platform for rapid PCR amplification using integrated thermoelectric heating and ice-valving", *Sensors and Actuators, B: Chemical*, **2012**, 161 (1), 1191-1197.
- (59) Steigert, J., Grumann, M., Brenner, T., Riegger, L., Harter, J., Zengerle, R., Ducrée, J., "Fully integrated whole blood testing by real-time absorption measurement on a centrifugal platform", *Lab on a Chip*, **2006**, 6 (8), 1040-1044.
- (60) Haeberle, S., Brenner, T., Zengerle, R., Ducrée, J., "Centrifugal extraction of plasma from whole blood on a rotating disk", *Lab on a Chip*, **2006**, 6 (6), 776-781.
- (61) Steigert, J., Grumann, M., Dube, M., Streule, W., Riegger, L., Brenner, T., Koltay, P., Mittmann, K., Zengerle, R., Ducrée, J., "Direct hemoglobin measurement on a centrifugal microfluidic platform for point-of-care diagnostics", *Sensors and Actuators, A: Physical*, **2006**, 130-131 (SPEC. ISS.), 228-233.
- (62) Lee, B.S., Lee, Y.U., Kim, H.S., Kim, T.H., Park, J., Lee, J.G., Kim, J., Kim, H., Lee, W.G., Cho, Y.K., "Fully integrated lab-on-a-disc for simultaneous analysis of biochemistry and immunoassay from whole blood", *Lab on a Chip - Miniaturisation for Chemistry and Biology*, **2011**, 11 (1), 70-78.
- (63) Riegger, L., Grumann, M., Nann, T., Riegler, J., Ehlert, O., Bessler, W., Mittenbuehler, K., Urban, G., Pastewka, L., Brenner, T., Zengerle, R., Ducrée, J., "Read-out concepts for multiplexed bead-based fluorescence immunoassays on centrifugal microfluidic platforms", *Sensors and Actuators, A: Physical*, **2006**, 126 (2), 455-462.
- (64) Lee, B.S., Lee, J.N., Park, J.M., Lee, J.G., Kim, S., Cho, Y.K., Ko, C., "A fully automated immunoassay from whole blood on a disc", *Lab on a Chip - Miniaturisation for Chemistry and Biology*, **2009**, 9 (11), 1548-1555.
- (65) Chen, Q.L., Ho, H.P., Cheung, K.L., Kong, S.K., Suen, Y.K., Kwan, Y.W., Wong, C.K., "Design and fabrication of automated sedimentation-based separation and siphon-based extraction for detection of allergic reaction on a centrifugal microfluidic disc", *Chinese Optics Letters*, **2010**, 8 (10), 957-959.
- (66) Lafleur, J.P., Salin, E.D., "Pre-concentration of trace metals on centrifugal microfluidic discs with direct determination by laser ablation inductively coupled plasma mass spectrometry", *Journal of Analytical Atomic Spectrometry*, **2009**, 24 (11), 1511-1516.
- (67) Xi, Y., Templeton, E.J., Salin, E.D., "Rapid simultaneous determination of nitrate and nitrite on a centrifugal microfluidic device", *Talanta*, **2010**, 82 1612-1615.

- (68) Lafleur, J.P., Rackov, A.A., McAuley, S., Salin, E.D., "Miniaturised centrifugal solid phase extraction platforms for in-field sampling, pre-concentration and spectrometric detection of organic pollutants in aqueous samples", *Talanta*, **2010**, 81 (1-2), 722-726.
- (69) Kido, H., Micic, M., Smith, D., Zoval, J., Norton, J., Madou, M., "A novel, compact disk-like centrifugal microfluidics system for cell lysis and sample homogenization", *Colloids and Surfaces B: Biointerfaces*, **2007**, 58 (1), 44-51.
- (70) Siegrist, J., Gorkin, R., Bastien, M., Stewart, G., Peytavi, R., Kido, H., Bergeron, M., Madou, M., "Validation of a centrifugal microfluidic sample lysis and homogenization platform for nucleic acid extraction with clinical samples", *Lab on a Chip - Miniaturisation for Chemistry and Biology*, **2010**, 10 (3), 363-371.
- (71) Cho, Y.K., Lee, J.G., Park, J.M., Lee, B.S., Lee, Y., Ko, C., "One-step pathogen specific DNA extraction from whole blood on a centrifugal microfluidic device", *Lab on a Chip - Miniaturisation for Chemistry and Biology*, **2007**, 7 (5), 565-573.
- (72) Zeng, J., Banerjee, D., Deshpande, M., Gilbert, J.R., Duffy, D.C., Kellogg, G.J., "Design Analyses of Capillary Burst Valves in Centrifugal Microfluidics", presented at *Micro Total Analysis Systems 2000, Proceedings of uTAS 2000*, Enschede, The Netherlands, 9-13 October 2005, **2000**, 493-496.
- (73) Serway, R.A., Faughn, J.S., "College physics"; 4th ed.; Saunders College: Fort Worth, **1995**, 1032.
- (74) Haeberle, S., Schmitt, N., Zengerle, R., Duccrée, J., "Centrifugo-magnetic pump for gas-to-liquid sampling", *Sensors and Actuators, A: Physical*, **2007**, 135 (1), 28-33.
- (75) Grumann, M., Geipel, A., Riegger, L., Zengerle, R., Duccrée, J., "Batch-mode mixing on centrifugal microfluidic platforms", *Lab on a Chip*, **2005**, 5 (5), 560-565.
- (76) Badr, I.H.A., Johnson, R.D., Madou, M.J., Bachas, L.G., "Fluorescent ion-selective optode membranes incorporated onto a centrifugal microfluidics platform", *Analytical Chemistry*, **2002**, 74 (21), 5569-5575.

## CHAPTER 2: Instrumentation

Centrifugal microfluidics is a growing field with seemingly endless applications, especially in the medical and environmental monitoring sectors. The potential to automate and miniaturise a wide array of chemistries is of great interest enabling field portable chemical testing for faster and more accurate point-of-care and on-site monitoring. Before this is possible, two types of instrumentation are necessary: 1) fully integrated motorized stages (macroscopic instrumentation) and 2) personalized centrifugal microfluidic devices including different manufacturing techniques and components. The development of these two types of instrumentation is the focus of this chapter enabling the new modes of sample introduction, sample preparation and chemistries described in subsequent chapters.

### 2.1 Motorized Stages

The instrumentation required to observe, quantify and optimized the chemistries occurring in the centrifugal microfluidic devices was developed. In order to integrate more and more complex chemistries to the centrifugal devices, there was a great need to be able to visualize the devices *while in motion*. Consequently a crucial part of the research involved building and interfacing the devices with a motorized stage that included a variety of components such as a motor, drive, spindle, camera, strobe, and computer. A series of stepwise changes to these integrated stages produced very useful and enabling instrumentation. Three different stages (shown in Figure 2-1) were built and are referred to hereafter as Stage v1.0, Stage v2.0 and Stage v3.0.

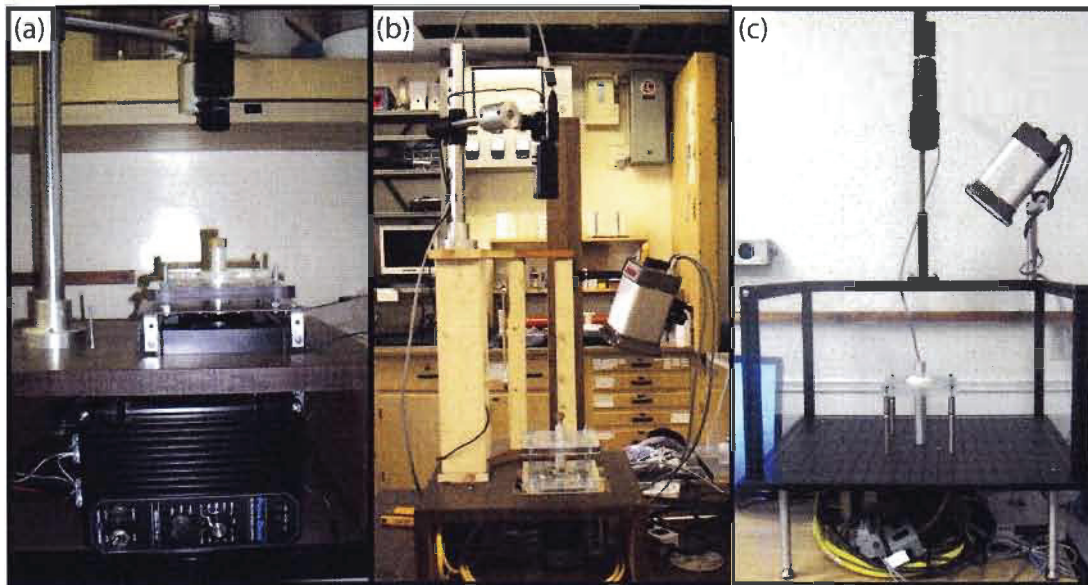


Figure 2-1. Photographs of motorized stages. (a) Stage v1.0, DC motor, (b) Stage v2.0, servo motor, (c) Stage v3.0, servo motor.

These complex integrated stages are intended for research and development laboratory use only. Once a given centrifugal device design has been optimized on a fully integrated motorized stage, smaller and simpler stages which only require automated rotation and detection would be required. A schematic of Stage v1.0 is shown in Figure 2-2. Since Stage v3.0 is basically an updated duplicate of Stage v2.0, the schematic shown in Figure 2-3 applies to both of these stages. The multiple components illustrated in these schematics are described in detail in the following sections.

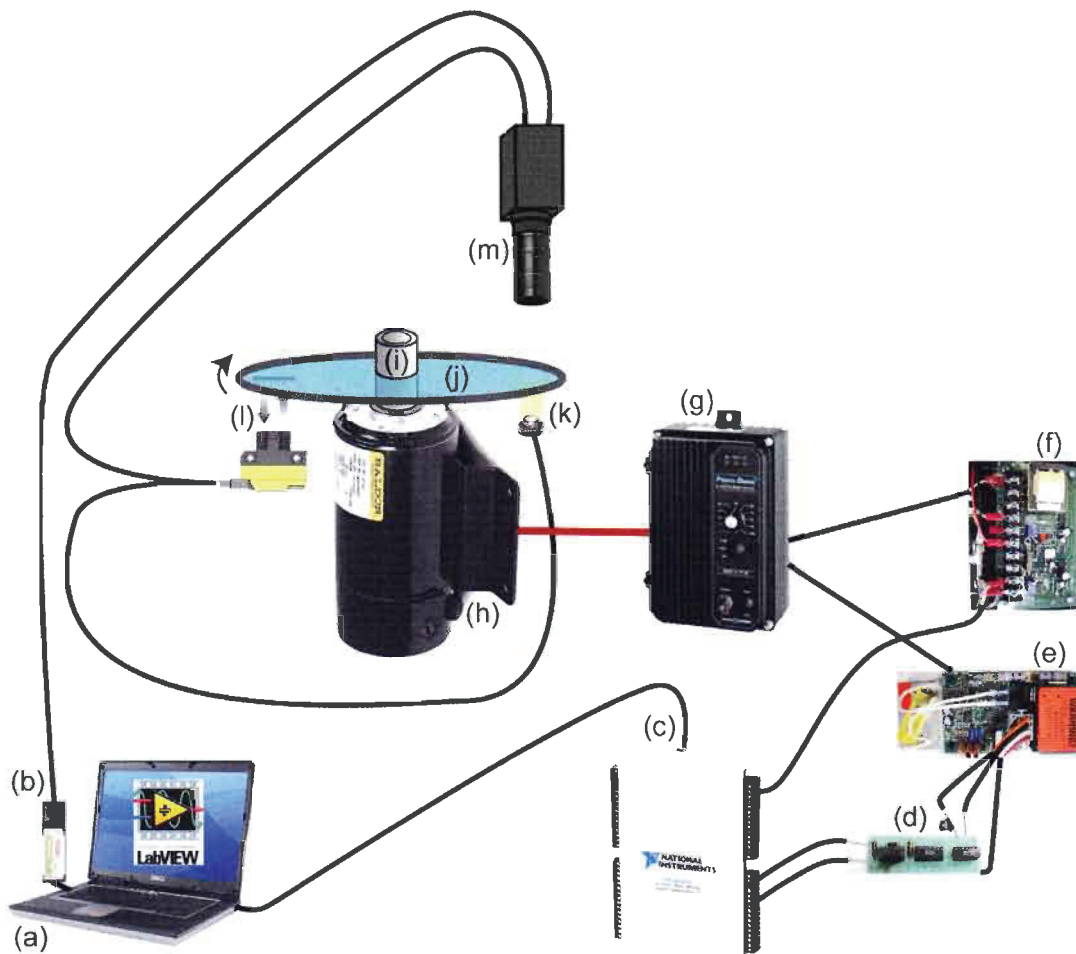


Figure 2-2. Schematic of DC motor Stage v1.0 integrating (a) laptop computer with LabVIEW National Instruments software and drivers, (b) Firewire 800 ExpressCard for interfacing camera, (c) USB6212 data acquisition device, (d) digital direction control circuit, (e) electronic forward-brake-reverse controller, (f) signal isolator controller, (g) DC motor drive, (h) DC motor, (i) spindle shaft, (j) centrifugal microfluidic device, (k) LED (l) retro-reflective sensor and reflective tape, (m) camera and macro lens. Figure components are not to scale.

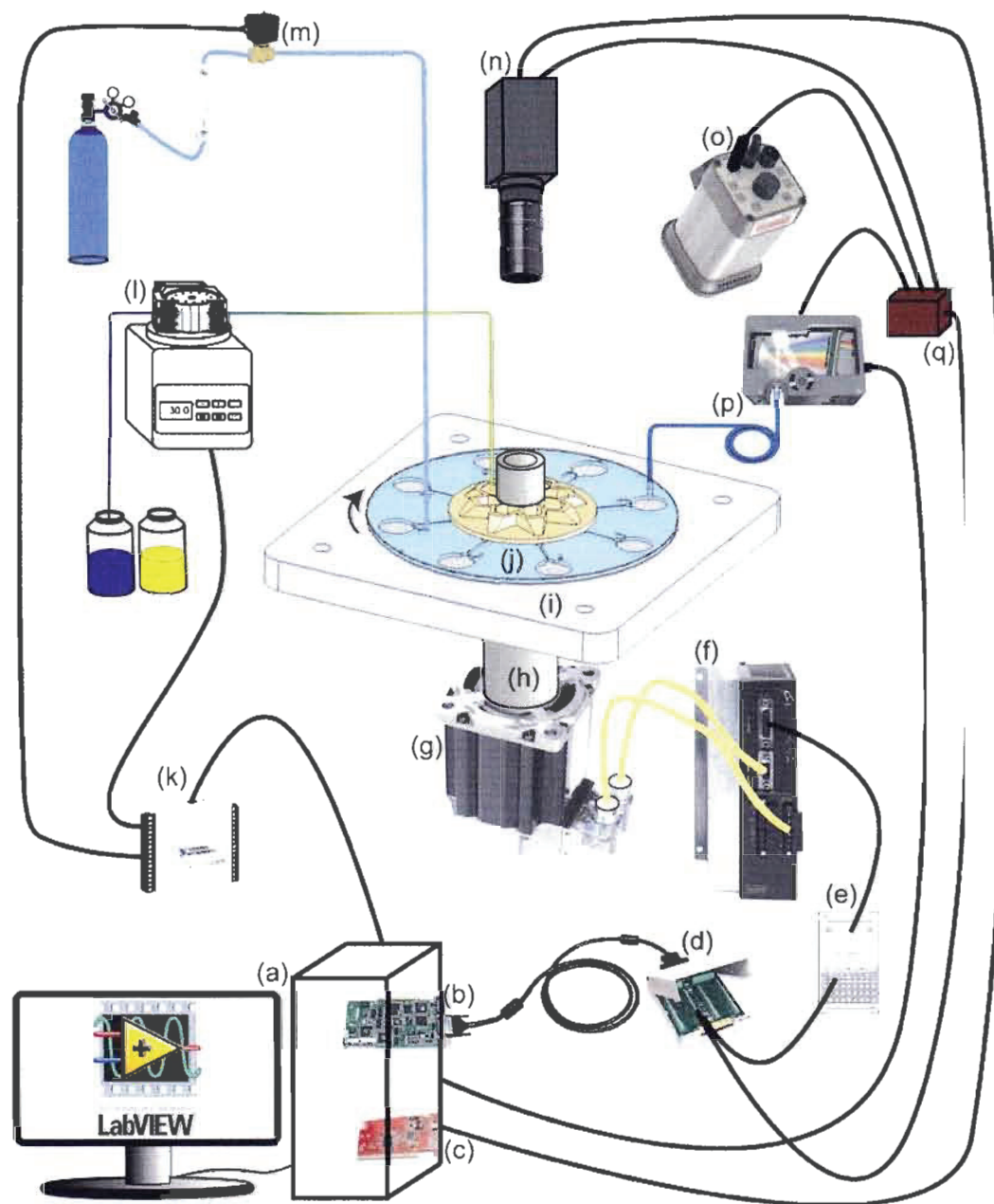


Figure 2-3. Schematic of servo motor Stage v2.0 and Stage v3.0 integrating (a) desktop computer with LabVIEW National Instruments software and drivers, (b) PCI-7342 card for interfacing motor, (c) Firewire 800 PCI card for interfacing camera, (d) UMI-7764 breakout box, (e) VM26-PM breakout box, (f) servo drive, (g) servo motor, (h) spindle shaft, (i) fixed magnets base, (j) centrifugal microfluidic device, (k) USB6009 data acquisition device, (l) peristaltic pump, (m) solenoid valve attached to a rotameter to control and measure gas flow rate, (n) camera and macro lens, (o) strobe light, (p) USB4000 spectrometer and fiber optic, (q) trigger breakout box. Figure components are not to scale.

### 2.1.1 Motors and Drives

The fundamental process of centrifugal microfluidics is the spinning of the devices at a known angular velocity (also referred to as rotational speed). A motor is used to provide this mechanical circular movement. A variety of motors has been reported for use in centrifugal microfluidic research such as modified CD and DVD drives<sup>1, 2</sup>, adapted centrifuges<sup>3</sup>, DC motors<sup>4</sup> and servo motors<sup>5</sup>. It is even envisioned that a commercial drill with a simple adaptor could be used for field work. Both DC motors and servo motors were investigated in the research presented here.

Stage v1.0 was built around a brushless DC motor. This type of motor provided sufficient torque to spin large and heavy devices such as a temperature testing device (see Appendix E). The disadvantage with this type of motor is that no positional feedback information was available. The motor was turned on at a controllable speed and when it was turned off it decelerated to an unknown final position. Likewise no trigger information was output by the motor after each rotation. On the other hand, Stage v2.0 and Stage v3.0 were built around servo motors that provided precise positional feedback information of the centrifugal devices throughout the various spin sequences. This allowed for synchronous acquisition of spectral information from integrated detection cells while the devices were rotating or once the devices had stopped and precisely returned to a given position for a spectrum to be acquired (see section 2.1.7 for additional details). Likewise it was possible to access a trigger signal from the motor after every rotation which permitted the synchronization of other peripherals

components such as a camera (see section 2.1.4) and a strobe (see section 2.1.5). Details of both motors and respective drives are summarized in Table 2-1.

**Table 2-1. Motor specifications**

<i>Part</i>	<i>Description / Function (Model Number)</i>	<i>Provider</i>
DC motor	Permanent magnet type 90V DC motor (AP7402)	TechnoMotion, Montreal, QC
DC motor drive	Manual control of motor speed, (Penta KB Power, KBPC-240D)	TechnoMotion, Montreal, QC
Servo motor	(Parker MPJ0922D3E-NPSN) Max 3000 rpm (120 VAC)	Cadence Automatisation, Ste-Thérèse, QC
Servo drive	(Parker AR-08AE) AR = Aries Digital Drive Series 08 = Maximum Shaft Power (750 Watts) A = Command Interface (Analog +/-10V) E = Motor Feedback (Encoder)	Cadence Automatisation, Ste-Thérèse, QC

### 2.1.2 Spindle Shafts

Each motor spindle required a custom shaft to quickly secure the centrifugal devices for operation. The design evolution of these spindle shafts is shown in Figure 2-4. Increasing the length of the shafts allowed additional access below the centrifugal devices as seen in Figure 2-5. The additional space in Stage v2.0 was introduced by the adaptor being used; however this also introduced a very slight wobble in the devices due to imprecision in the manufacturing. This was corrected in the one-piece spindle for Stage v3.0. The top of each spindle shaft was designed to have a ring that was tightened down onto the centrifugal devices, holding them in place. The addition of a notch or spring loaded ball bearing was envisioned to match a corresponding indentation in the centrifugal devices if they should begin to slip and move on the spindles; however, the tightened ring design seems to be sufficient at maintaining the devices in a fixed position. This ring design also allowed for devices of different

thicknesses to be easily mounted. Later versions included improvements to the securing and tightening mechanisms to allow for even more rapid and easy change of devices. Each spindle shaft was made on a lathe from aluminum using ethanol as lubrication. More detailed specifications are available in Appendix A. A variety of custom adaptors for cameras and strobes was also made.

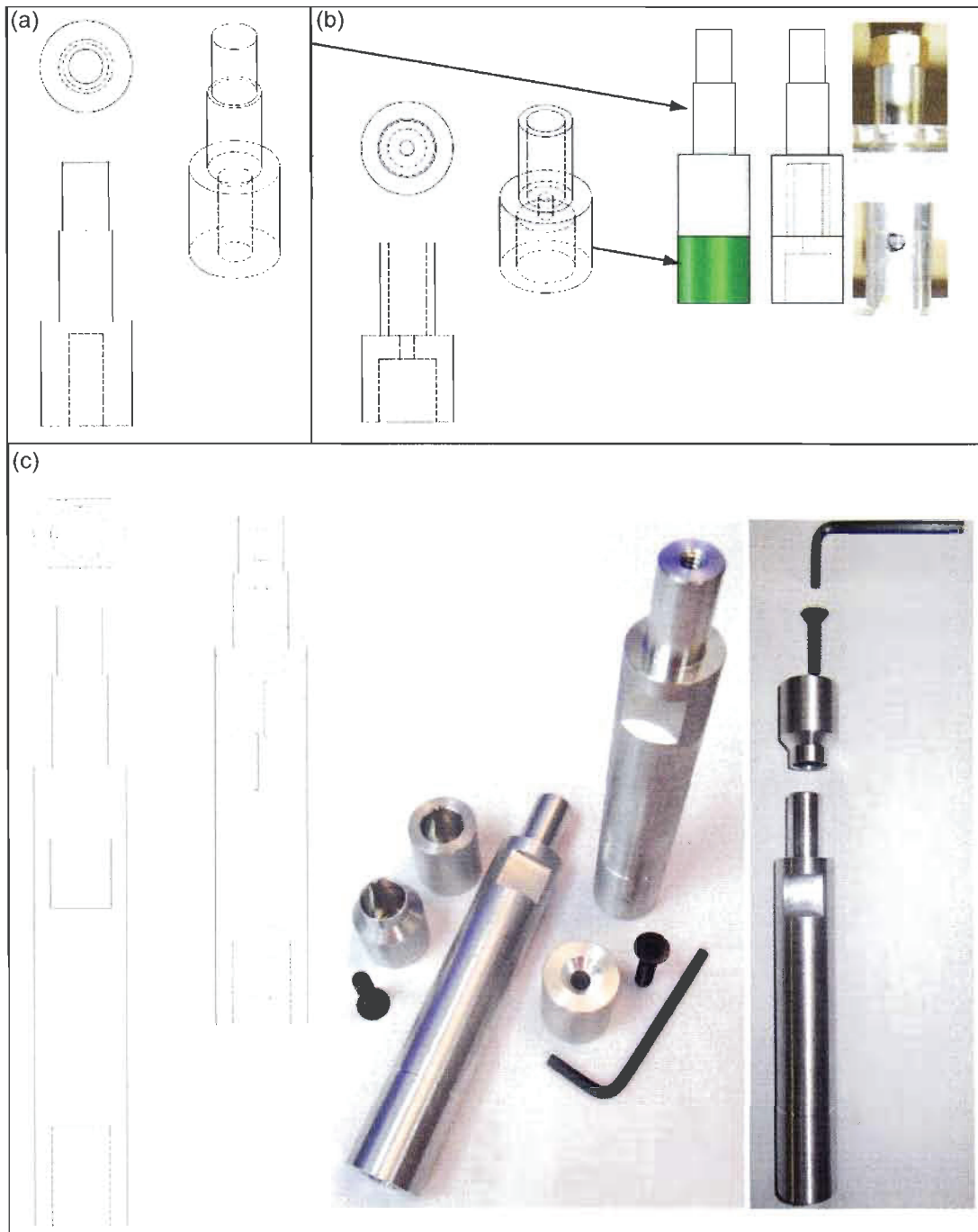


**Figure 2-4.** Custom made spindle shafts. (a) Spindle shaft for Stage v1.0 DC motor. (b) Adaptor show in green to attach the original DC motor shaft to Stage v2.0 servo motor spindle. (c) Redesigned one-piece spindle shaft for Stage v3.0 servo motor.

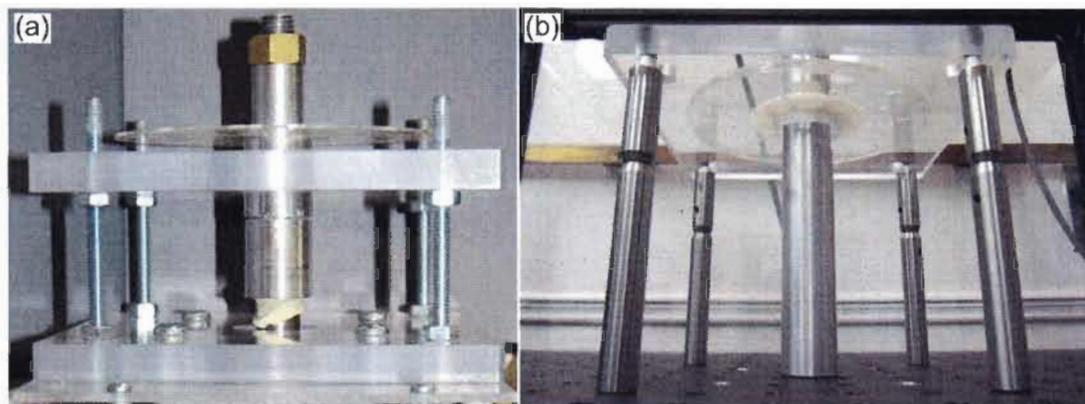


Figure 2-5. Photographs of spindle shafts and relative space below the centrifugal devices on the stages. (a) Stage v2.0 with the combination of the shaft from Stage v1.0 and an adaptor. (b) Stage v3.0 with ease of access to below the centrifugal devices.

### 2.1.3 Fixed Magnet Base

Magnets were used both in a “fixed magnet base” and as “mobile magnets” (see section 2.2.2.1). The interaction of these two sets of magnets is at the heart of the sample preparation and sample extraction experiments described in details in chapters 5 to 7.

Six nickel plated neodymium iron boron (NdFeB) permanent magnets (5862K65, 3/8” diameter, 1/4” thickness, McMaster Carr, Santa Fe Springs, CA) were incorporated into the fixed base and remained immobile during operation similar to a configuration used by Kido *et al.*<sup>5</sup> and also by Grumann *et al.*<sup>6</sup>. As seen in Figure 2-5 this fixed magnet base was placed in very close proximity to the spinning centrifugal devices. The slug-shaped magnets were magnetized parallel to thickness and their resulting magnetic fields are illustrated in Figure 2-6. Detailed specifications of the size of this base are available in Appendix A.

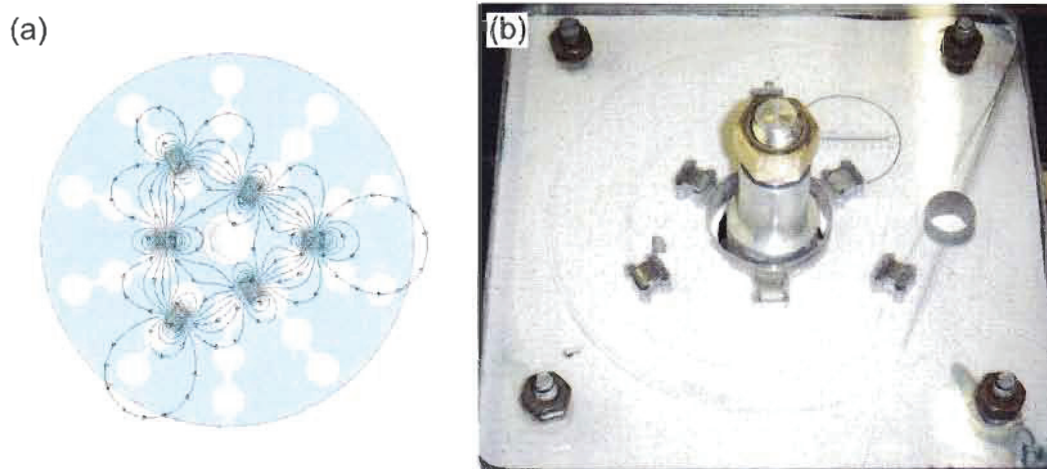


Figure 2-6. Fixed magnet base. (a) Sketch of magnets in fixed base and corresponding flux lines. (b) Photograph of fixed magnet base on Stage v2.0. A reticule is added beneath the base to include relative size and magnification of the acquired images.

#### 2.1.4 Cameras and Lenses

In order to observe the mixing and movement of samples in the spinning centrifugal devices, stop action photography using a synchronized camera and strobe light was used. An alternative would have been to use a high speed video camera which would have allowed continuous monitoring of the devices throughout each revolution; however, stop action photography was more economical and allowed for a magnified view of individual chambers once per revolution.

A variety of cameras were used throughout the evolution of the stages. Work started using a simple handheld digital camera (Pentax Optio) that was limited to 30 frames per second video recording and did not have an external trigger input or a manual contrast mode to be used with the bright strobe light. Next, a high definition video camcorder (Sony Digital HDR-SR1 Handycam) was used in “slow mode” which allowed for 3 seconds of recording at 240 frames per

second. Preliminary results were obtained with this camera in regards to the movement of the “mobile magnets” of Chapter 5. Following this, a research grade black and white charge-coupled device (CCD) digital camera (Sony XCD-V50) was used. Its external trigger input and IEEE 1394b firewire connection allowed for easy integration into the stage. The camera was DCAM compliant (1394-based Digital Camera Specification) required for compatibility with LabVIEW. With time, this camera was replaced with a colour CCD camera (GRAS-14S5C-C, Point Grey, BC, Canada). Both Stage v2.0 and Stage v3.0 now use colour cameras. A comparison of the CCD cameras is summarized in Table 2-2.

**Table 2-2. CCD camera specifications**

<i>Properties</i>	<i>Sony XCD-V50</i>	<i>GRAS-14S5C-C</i>
Colour	Black and white	Colour
Resolution	640 x 480	1384 x 1036
Pixel size	7.4 x 7.4 $\mu\text{m}$	6.45 x 6.45 $\mu\text{m}$
Max frame rate	60 fps	15 fps
Image sensor	1/3"	2/3"
Resolution bits	14	14
Operating temperature	-5 to 45 °C	0 to 40 °C
Interface	IEEE 1394b	IEEE 1394b
Lens mount	C-Mount	C-Mount
DCAM compliant	yes	yes
External trigger input	yes	yes

The CCD cameras were coupled to close focus zoom lenses for convenient focus, zoom and apertures adjustments. This allowed for photographs to be taken of the entire device or of only specific cells at an exposure set in relation to the bright strobe light. A Computar lens (#54-363, Edmund Optics, Barrington, NJ) was purchased for Stage v2.0 for use with the Sony XCD-V50 camera. It was then used on this stage with the GRAS-14S5C-C camera; however, there was a loss of the peripheral part of the images at large fields of view due to the size incompatibility of the image sensor (2/3") and the lens (1/2"). For this reason a Navitar Zoom 7000 (#58-240, Edmund Optics, Barrington, NJ), which matched the lens with the camera sensor, was purchased for Stage v3.0. A comparison of the lenses specifications is summarized in Table 2-3 and detailed dimensions are available in Appendix A.

**Table 2-3. Close focus zoom lens specifications**

<i>Properties</i>	<i>Computar 54-363</i>	<i>Navitar Zoom 7000 58-240</i>
Zoom	10 x	6 x
Focal length (mm)	13 to 130	18 to 108
Total field of view for 1/2" sensor (mm)	7.8 to 280	6.4 to 96
Working distance (mm)	152 to 457	127 to 305
Max CCD Format	1/2"	2/3"
Mount	C-mount	C-mount
Aperture (f/#)	F5.6 - 32Closed	F2.5 – 28Closed
Weight (g)	233	540
Diameter x length (mm)	48 x 98.5	62 x 176

### 2.1.5 Strobes

Another key component of the stages was the strobe that was synchronized with the cameras mentioned above. Two different set-ups of strobes were constructed and tested. The first, used in Stage v1.0, involved using a retro-reflective sensor (Model QS18VP6LV, Banner, Minneapolis, Minnesota), reflective tape and light emitting diodes (LED, Luxeon Star Emitter, Quadica Developments Inc., Brantford, ON) as illustrated in Figure 2-2. A strip of reflective tape was placed on the bottom side of the centrifugal devices and the retro-reflective sensor was placed below the devices. Every time the device rotated once, the tape would reflect the sensor's 660 nm red light beam back towards it activating the LED. At this time the camera was not triggered by the sensor but rather ran at the highest frame rate possible and only the frames that coincided with the LED flash were kept, discarding all dark frames. This set-up was used with the DC motor since no other trigger mechanism was available directly from the motor. Disadvantages with this system were the non-reproducible position and width of the reflective tape and a systematic trigger timing error when the motor was accelerating or decelerating creating a "jitter" in the photographs. Likewise the time that the LED was on was directly related to the time the sensor detected a reflected signal. This created an undesirable relationship between the LED flash time and the tape's width and rotational speed.

Upon designing Stage v2.0 and Stage v3.0 with the servo motors, a second strobe set-up was used as seen in Figure 2-3. This involved using a hardware trigger signal produced directly by the servo motor controllers to trigger

multiple peripherals including the camera and strobe light (also see section 2.1.6.4). A commercially available 10 W xenon flash tube strobe light (Shimpo DT-311A, Primo Instruments, QC) with an external trigger input was used. A fixed 40  $\mu$ s pulse output was possible regardless of the rotational speed and no reflective tape was required. Very reproducible synchronization was achieved even during the acceleration and deceleration portions of the spin sequences. The combination of the camera and strobe made for an effective means of real-time, in-process monitoring and recording of the spinning devices and a greater understanding of the progress of the chemical reactions and processes.

#### **2.1.6 Computer Interfacing**

All of the components of the stages were interfaced and synchronized by either a laptop (Stage v1.0) or desktop (Stage v2.0 and Stage v3.0) computer that controlled a variety of components through controller cards, circuits and breakout boxes. These interfacing cards, circuits and boxes are illustrated in Figure 2-2 and Figure 2-3, summarized in Table 2-4 and detailed below.

Table 2-4. Summary of controller cards, circuits and breakout boxes

	<i>Part</i>	<i>Description / Function (Model Number)</i>	<i>Provider</i>
Stage v1.0	DAQ	Output analog and digital signals (USB6212)	National Instruments, Vaudreuil-Dorion, QC
	Digital direction control circuit	Interface USB6212 to Electronic Forward-Brake-Reverse card	Richard Rossi and Weihua Wang, McGill University
	Electronic Forward-Brake-Reverse card	Provides manual or digital electronic reversing with solid state dynamic braking. (APRM-PC, 9378)	TechnoMotion, Montreal, QC
	Signal isolator card	Digital control of motor (Penta KB Power, KBSI-240D, 9431, plus 9377 installation kit)	TechnoMotion, Montreal, QC
	Firewire ExpressCard	Firewire 800 IEEE 1394b for interfacing camera (PPA 1189)	TigerDirect
Stage v2.0 & Stage v3.0	DAQ	Output digital signals (USB6009)	National Instruments, Vaudreuil-Dorion, QC
	Servo motion controller PCI card	Card for interfacing motor (NI-PCI-7342) 32 bits 1 to 20,000,000 counts/s Encoder rate: 20 MHz	National Instruments, Vaudreuil-Dorion, QC
	Servo motion controller breakout box	National Instruments breakout box (UMI-7764)	National Instruments, Vaudreuil-Dorion, QC
	Servo motor breakout box	Parker Automation breakout box (Parker VM26-PM)	Cadence Automatisation, Ste-Thérèse, QC
	Trigger breakout box	Multiple connector access to trigger signal	David Duford, McGill University
	Firewire PCI card	Firewire 800 IEEE 1394b for interfacing camera	TigerDirect

For Stage v1.0, the USB6212 digital acquisition (DAQ) device served as the heart of the stage controlling both the motor and any additional peripherals. In Stage v2.0 and Stage v3.0, the peripherals were controlled with a simpler USB6009 DAQ and the motor was controlled by a dedicated NI-PCI-7342 servo motion controller peripheral component interconnect (PCI) card and breakout boxes discussed below. Though the original plan was to use a laptop to control

all versions of the stages, servo motion controller cards were only available as desktop PCI cards and not available at that time for laptops.

#### *2.1.6.1 DC Motor Control*

In order to repeatedly run the same spin sequence, digital control of the DC motor was achieved using a “signal isolator” controller card and an “electronic forward-brake-reverse” controller card. After calibration, the “signal isolator” card allowed for precise control of the motor’s rotational speed by simply changing the input analog voltage (from 0 to 10 volts). The “electronic forward-brake-reverse” card permitted control of the direction of rotation during the spin sequence. This was achieved by sending a digital high (5 DC volts) or a digital low (0 DC volts) signal. Both analog and digital voltages were sent using the USB6212 DAQ (see Figure 2-7 for wiring diagram). A custom built “digital direction control circuit” was required to interface the USB6212 to the “electronic forward-brake-reverse card”. As seen in Figure 2-8, this “digital direction control circuit” was made up of an inverting buffer (74LS04N Philips Semiconductors, Digi-Key, Thief River Falls, MN), two NAND gates (7400N, Harris Semiconductor, Melbourne, FL) and two NPN transistors (NTE3041, NTE Electronics, Inc, Bloomfield, NJ). By sending a digital high or low signal to wire labeled “6”, the entire motor was turned on or off. Likewise, by sending a digital high or low signal to the wire labelled “5” the motor turned clockwise or counter-clockwise respectively.

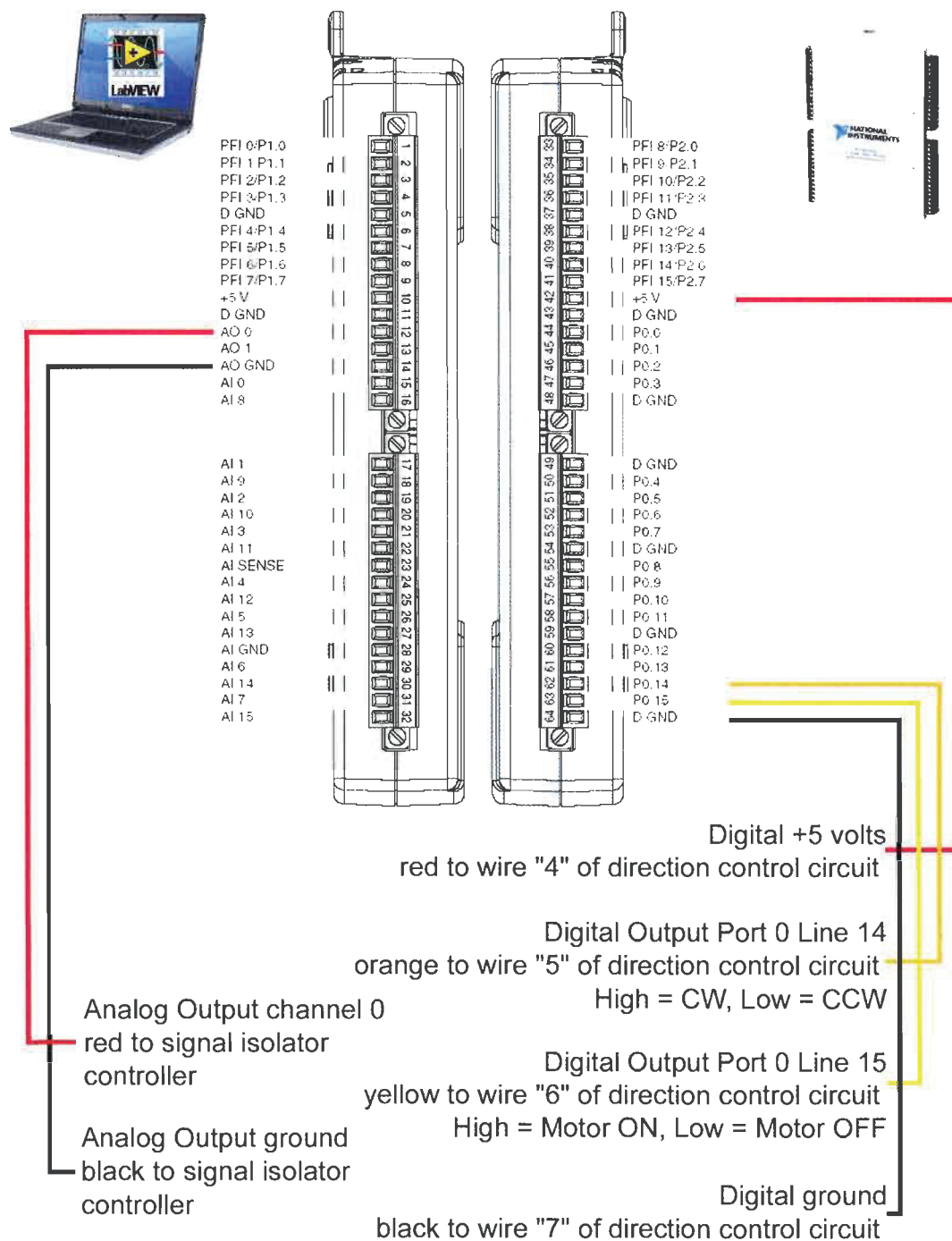


Figure 2-7. Wiring diagram of USB6212 for DC motor control.

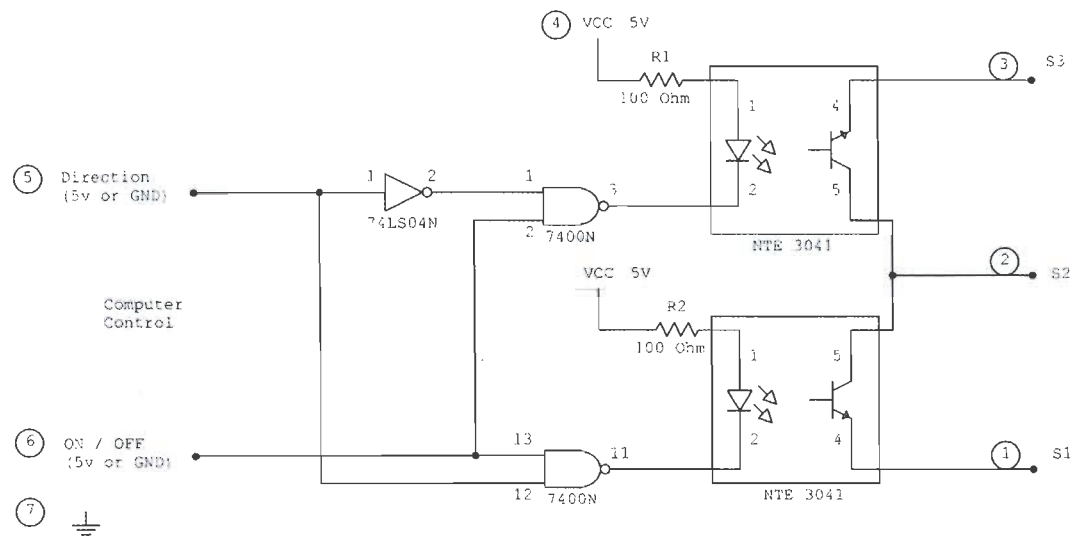


Figure 2-8. DC motor digital direction control circuit diagram.

### 2.1.6.2 Servo Motor Control

In order to precisely run complex spin sequences, computer control of the servo motor was desired. This was accomplished by using LabVIEW software and a servo motion controller PCI card (NI-PCI-7372), both from National Instruments (Vaudreuil-Dorion, QC). Since National Instruments does not sell servo motors, the Parker Automation servo motor and drive detailed in section 2.1.1 were purchased. To connect the components from these two vendors together, two breakout boxes (UMI-7764 from National Instruments and VM26-PM from Parker Automation) and a bridging wire were required as illustrated in Figure 2-3. A bridging wire connection diagram to link these two breakout boxes together is provided in Figure 2-9. Twisted pair shielded wires were used.

Parker Automation  
VD26-PM  
breakout box

National Instruments  
UMI-7764  
breakout box

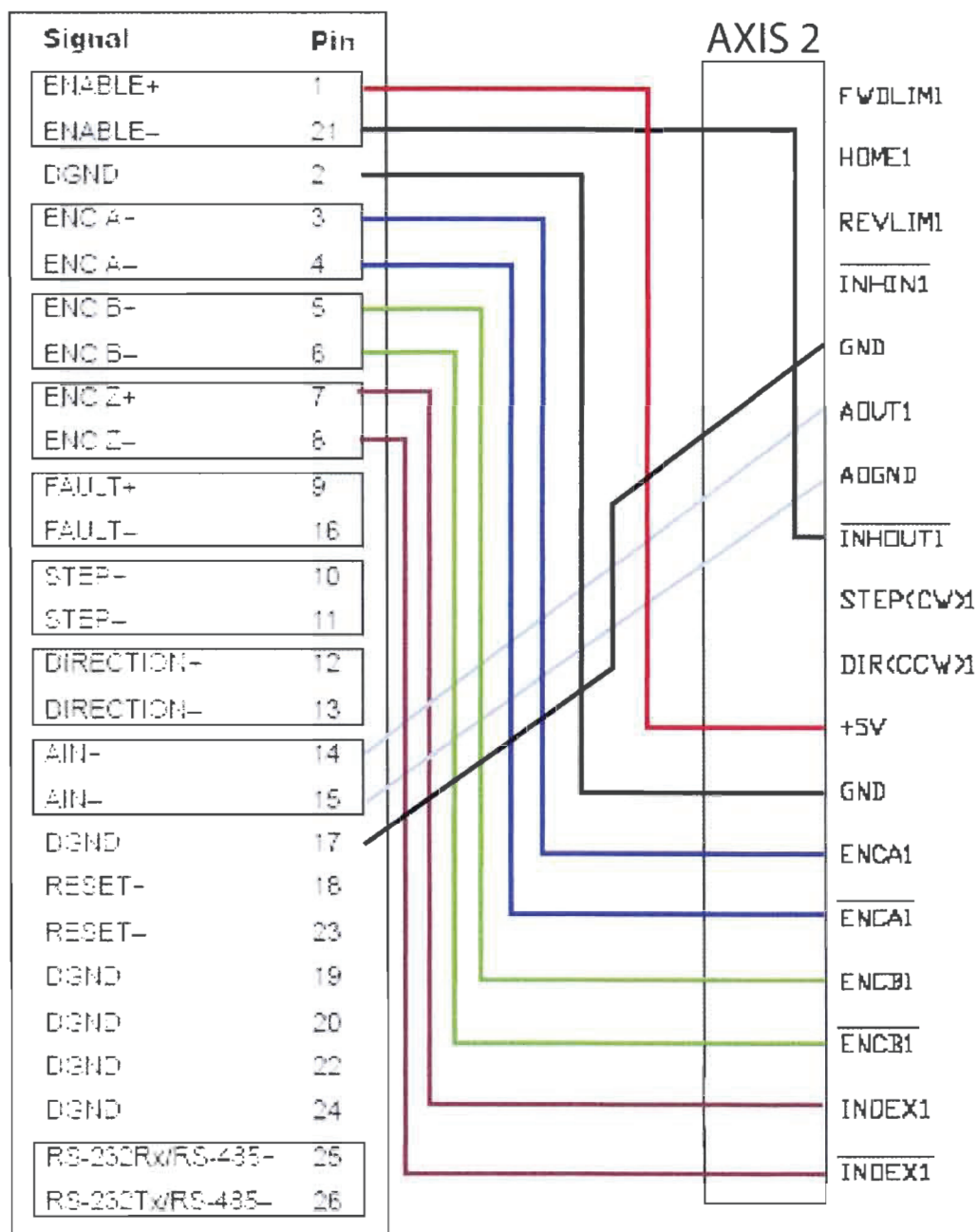


Figure 2-9. Bridging wire connection diagram between Parker Automation VD26-PM breakout box and National Instruments UMI-7764 breakout box.

### *2.1.6.3 Peripherals Control*

Two types of peripheral components were integrated into the stages. One set of components were those that needed to be triggered in accordance with the frequency of the spinning motor and will be considered in the next section. The other set of components that did not need such a trigger were controlled by the DAQ devices (either USB6009 or USB6212). With both digital and analog inputs and outputs, these small portable 14-bit USB DAQ devices were very versatile. Their respective screw terminal configurations are available in Appendix A. Peripheral components such as a peristaltic pump (used in Chapter 4) and a solenoid valve (used by Kong and Salin<sup>7</sup>) were quickly integrated into the stages and program software. Many other external components have the option of being controlled using digital signals or can be interfaced using relays. The stages can therefore be easily adapted to future projects using these DAQ devices.

### *2.1.6.4 Trigger Breakout Box*

The other set of peripheral components that needed to be triggered in synchrony with the motor included cameras, strobes and potentially detectors (such as an Ocean Optics USB4000 spectrometer). As discussed above, Stage v2.0 and Stage v3.0 used a hardware trigger signal produced directly by the servo motor and accessible through the servo motion controller breakout box (UMI-7764). Unfortunately it was observed that if more than two components were connected directly to the trigger signal not enough current was available to feed the signal to all components. For this reason a trigger breakout box made of two NPN transistors (NTE123, NTE Electronics, Inc, Bloomfield, NJ).was

designed and built to enable multiple peripheral components to receive the same trigger signal without circuit loading issues. This trigger breakout box also made connecting peripherals easier and minimized the unintentional disconnect of other peripheral components. A circuit diagram and photographs of the trigger breakout box are shown in Figure 2-10. As seen, if a +5V DC trigger signal from the motor enters the circuit, a +5V signal from the power supply is sent to all of the trigger screw terminals.

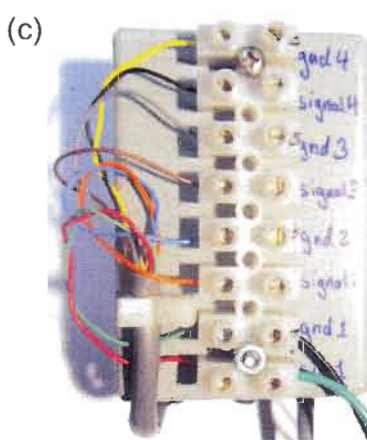
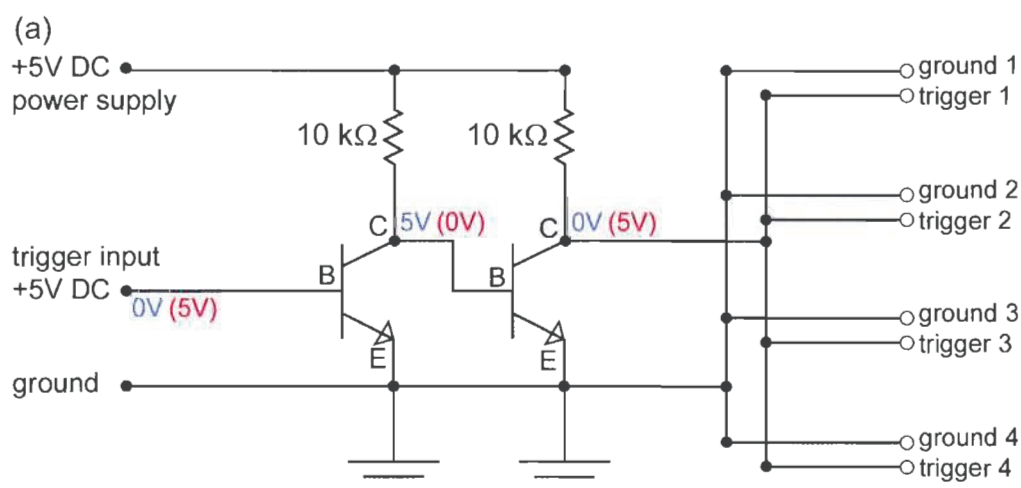


**Figure 2-10. Trigger breakout box. (a) Circuit diagram, (b) Photograph of Stage v2.0 trigger breakout box. (c) Photograph of Stage v3.0 trigger breakout box.**

### 2.1.7 System Software

Computer control of the stages including the motors and all of the peripheral components was achieved using LabVIEW software and drivers (National Instruments, Vaudreuil-Dorion, QC). Details of the different software and drivers and their function are summarized in Table 2-5.

**Table 2-5. LabVIEW software and drivers**

<i>Name</i>	<i>Function</i>
LabVIEW 8.5 to 8.6 Developer Version	Main software platform
NI-Motion Assistant v2.2	Software and drivers for motor
NI-Vision Acquisition	Software to include control of camera
NI IMAQ IEEE 1394 Cameras	Drivers for firewire camera
NI-DAQmx	Drivers for USB6009 and USB6212 DAQ

LabVIEW, a graphical programming language, is industry leading software in the development of new instrumentation. Program code called a Virtual Instrument (VI) was developed to control each component. Icons which represent different programming operations were wired on the “block diagram” (*i.e.* the code) and a user interface was designed on the “front panel”. Many VIs and subVIs (subroutine of code) were programmed. A few stand-alone programs were also made which allowed the VIs to be run on computers that did not have LabVIEW installed; however, these did not have access to the “block diagram”. The main VIs for the stages were not converted to stand-alone programs so as to allow future additions and changes. In these VIs, multiple independent subVIs run simultaneously for control of the motor, camera, and peripherals components. Selected “block diagrams” and “front panels” of the code are available in Appendix B.

The VI user interface provided easy input of the desired spin sequences. Such spin sequences included varying rotational speeds, direction of rotation and “shake” sequences. A shake sequence rotated the devices one half turn at a user defined speed and then back one half turn. This repeated for a user defined amount of time.

Two different operation modes were programmed for the servo motor: 1) “continuous snap” and 2) “stop & snap”. In “continuous snap” mode, a trigger signal was sent to the strobe and camera to take a picture of the device once per revolution (or once per a user-defined number of revolutions) and a concurrently running subVI saved the images in a user defined directory. When viewing the resulting sequence of photographs, great insight into the chemistries, sample addition, sample preparation and liquid movement was acquired. In “stop & snap” mode, a trigger signal was sent, for example, to a detector to acquire a spectrum, with the device at rest and at a precise position. The motor was programmed to return to the same starting position after a specific movement, for example a “shake” sequence. As a result a series of spectra of a given stationary cell in the device could be acquired.

### **2.1.8 Safety Shields**

Considering the high speeds, plastic devices, pulverising forces and solvents being used including concentrated nitric acid, safety shields were included on all three stages. The first safety shield was made out of a modified large pot as seen in Figure 2-11, and was used for both Stage v1.0 and Stage v2.0. The second safety shield was constructed out of 1/4 inch thick Plexiglass

and permitted for a larger enclosed working area (XE25C6, Thorlabs Inc., Newton, NJ).

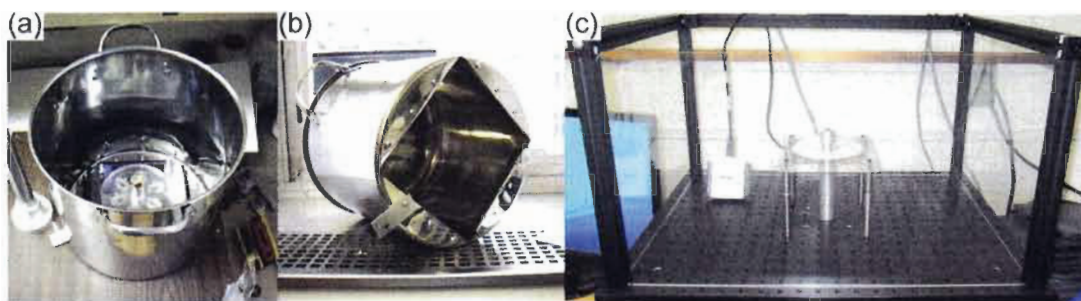


Figure 2-11. Safety shields. (a) Top view of first shield surrounding Stage v1.0. (b) Bottom view of first shield. (c) Side view of second shield surrounding Stage v3.0.

### 2.1.9 Summary of Motorized Stages

The development of the motorized stages has resulted in very useful instrumentation. Future additions and modifications are encouraged and facilitated by the DAQ devices and optical breadboard (MB1824, 18" x 24", Thorlabs Inc., Newton, NJ) used as a base in Stage v3.0. In the end three different stages were built:

- Stage v1.0: DC motor for work that does not require position information.  
This stage may be used in a fume hood for acetone spin coating or monolith filter work.
- Stage v2.0: The original servo motor system on which most stepwise changes were made.
- Stage v3.0 The newest servo motor system with longer spindle shaft, integrated optical breadboard and larger safety shield.

These stages are now in use in the Salin Research Group, enabling current and future chemists in centrifugal microfluidics.

## **2.2 Centrifugal Microfluidic Devices: Subtractive Manufacturing Techniques and Components**

Other than the fully integrated motorized stages, the second type of instrumentation that was developed was the centrifugal microfluidic devices themselves. Both subtractive manufacturing techniques and components were investigated and extensively used in the research described in subsequent chapters.

### **2.2.1 Subtractive Manufacturing Techniques**

Centrifugal microfluidic devices are manufactured by using a number of different techniques. Subtractive manufacturing techniques are discussed here whereas additive manufacturing techniques are discussed in Chapter 3. In all cases, each layer or piece of the centrifugal microfluidic device was designed in the 3D Computer-Aided Design (CAD) software “SolidWorks 2005” (SolidWorks Corp., Concord, Massachusetts, USA) and converted to a \*.DXF file (Data eXchange Files) compatible with most computer numerically controlled (CNC) manufacturing equipment. Both laser cutting and CNC cutting and milling subtractive manufacturing were investigated. After the individual layers were manufactured, they were sealed together using one of the lamination techniques discussed below.

#### *2.2.1.1 Laser Cutting*

Laser cutting or laser beam machining is a common manufacturing technique for industrial applications.<sup>8</sup> Focusing a high power laser beam onto a small spot size, this techniques can quickly cut thick pieces of material. For example, 1/4 inch (6.35 mm) thick poly(methyl methacrylate) (PMMA,

commercially known as *acrylic* or *plexiglass*) was quickly cut according to a specific centrifugal device design using a 100 W CO<sub>2</sub> laser mill (Kern Electronics & Lasers, Minnesota, USA) for the work presented in Chapter 5. Other microfluidic devices manufactured by laser cutting have been reported.<sup>9</sup> Laser cutting offers the potential for micro machining small structures down to 1  $\mu\text{m}$ ; however, the main disadvantage is the high equipment procurement costs. Likewise, some material such as polycarbonate melts under the intense laser beam and highly reflective material cannot be cut.

#### 2.2.1.2 CNC Cutting and Milling

Computer numerically controlled cutting and milling was extensively used to manufacture both the adhesive and plastic layers of the centrifugal microfluidic devices.

Very common in the signage, lettering and car striping industries, a commercially available xurography cutting plotter (CE3000Mk2-60, Graphtec America Inc., Santa Ana, CA) was used to precisely cut double-sided adhesive to the designed dimensions of the processed DXF files. Bartholomeusz *et al.*<sup>10</sup> have extensively discussed these adhesives, equipment and the ability to produce small structures such as passive capillary burst valves in these adhesive layers. Adhesives with a thickness of 100  $\mu\text{m}$  were used in the current set of experiments into which 600  $\mu\text{m}$  to 1000  $\mu\text{m}$  wide channels were cut. In a 1 mm length this provided volumes of 60 to 100 nL placing the volumes well into the microfluidic domain. These channels served as rectangular capillary burst valves discussed in more detail in Chapter 6 and Chapter 7.

Produced for the integrated circuit manufacturing industry, a QuickCircuit 5000 CNC micro-milling machine (T-Tech, Inc. Norcross, GA) equipped with a high speed spindle was used to manufacture the plastic CD-like layers of the centrifugal microfluidic devices. Interchangeable graphite slot-drills (1.00 mm and 1.59 mm = 1/16") and end-mills (1.00 mm and 3.18mm = 1/8") were purchased from Tycom Limited (Mississauga, ON) and T-Tech Inc. and used to mill the designed layers. This milling technique and subsequent cold lamination (see details below) was modified from Kido *et al.*<sup>11</sup>. Other subtractive manufacturing systems include the Roland MDX series four axes (rotational) milling machines capable of producing curved surfaces. Tables of specific speed and feed rates are available for metals and are approximated for plastics to 1/3 of those of copper.<sup>12</sup> "Speeds" refers to the spindle speed or the rate at which the tool spins (proportional to the tool size) and "feeds" refers to how fast the material (or spindle head) moves. These parameters are important to optimize the time it takes to remove the undesired material while not melting the material or increasing the normal wear of the tool. The disadvantages of this manufacturing technique were: 1) the features needed to be carefully offset at the design stage to match half the width of the intended tool, resulting in final piece of the precise size, 2) it was not possible to manufacture internal sharp corners due to the round tools used, and 3) limited to milling a depth of half the width of the end-mill's width making the production of thick pieces very laborious.

The alternating lamination of adhesive layers (for low aspect ratio, low volume structures such as channels) with plastic pieces (for high aspect ratio,

large volume structures such as reservoirs) allowed considerable flexibility in the development of centrifugal systems which typically contained five to seven layers.

#### *2.2.1.3 Lamination Sealing Techniques*

The multiple layers produced by one or more of the manufacturing techniques detailed above and in the next chapter were sealed together to produce the final centrifugal microfluidic devices. Often, before the final layer was added, different components such as capillary burst valves or “mobile magnets” were added to the devices

The first lamination sealing technique used in the manufacturing of the devices was cold lamination. Specially chosen 100  $\mu\text{m}$  thick double-sided adhesive (FLEXmount, DFM 200 Clear V-95 150 poly H-9 V-95 4, FLEXcon, Spencer, MA) and subsequent plastic layer that had been cut and milled were carefully aligned and pressed firmly together using a hand cranked cold laminator (Jet Mounter ML25, Drytac, Concord, ON). This technique was favoured due to both cost and flexibility concerns; however, it is time consuming and required a skilled operator and multiple production stages. As an additional advantage, the double-sided adhesive not only sealed the multiple layer of the devices together but also could include features such as passive capillary burst valves mentioned above.

A second lamination sealing technique used solvents to chemically bond layers together. The resulting seal was stronger than that of double-sided adhesive. This technique was used on a variety of occasions to seal polycarbonate (PC), PMMA and acrylonitrile butadiene styrene (ABS) plastic pieces together using either dichloromethane ( $\text{CH}_2\text{Cl}_2$  - Caledon Laboratories Ltd,

ON, Lot: 22460) or acetone ( $\text{CH}_3\text{COCH}_3$ , Fisher, Napean, ON, Lot F1112). The solvent was either applied drop-wise using a glass pipette or by a fine mist using a commercial touch spray gun or air brush. Next, the pieces were brought together and even pressure applied for 20 to 30 seconds. A good seal was produced though the devices became slightly opaque and small air bubbles were trapped between the layers. Ogonczyk *et al.*<sup>13</sup> have reported a variation of this technique that did not affect the transparency of bonded PC pieces. They used a controlled exposure of the pieces to vapours of solvents using evacuated chambers and heated pressure plates resulting in strong clear bonded layers. Alternatively, epoxy was also used to bond two materials of different properties together or materials that were very resistant such as Teflon.

Reusable lids with loading ports, o-rings and screws were also investigated and showed promise; however, disposable covers with double-sided adhesive were simpler to use.

Other sealing techniques commonly used when dealing with parts made of polydimethylsiloxane (PDMS) include treating the surfaces in an oxygen plasma. Oxidation of the polymer makes the surface hydrophilic increasing its wettability<sup>9</sup> and allowing the formation of a seal with a glass surface without using any additional adhesive or solvent.<sup>14</sup>

### 2.2.2 Components and “Mobile Magnets”

Each centrifugal device was designed to perform a given chemical analysis. By combining different components or “unit operations”<sup>15</sup>, the automation and miniaturization of chemical analyses was achieved. Other than valves, snorkel sedimentation and integrated detection cells used in Chapters 6

and 7, three new “unit operations” were added to a growing toolbox of components. First, sample introduction to the devices while they were in motion was achieved using a “centrifugal liquid addition distributor” (CLAD) described in Chapter 4. Second, magnetically actuated solid sample preparation for crushing and grinding solids was demonstrated in Chapter 5. Third, magnetically actuated liquid-solid extraction was used in the studies presented in Chapter 6 and Chapter 7. The latter two “unit operations” involved “mobile magnets” which interacted with a series of magnets in the “fixed magnet base” described above (section 2.1.3). The magnet composition, coatings and encapsulation of these “mobile magnets” were the subject of advanced study including acid resistivity analysis.

#### 2.2.2.1 “Mobile Magnet” Composition, Coatings and Encapsulation

Many different magnets are commercially available and vary in size, strength, composition, thermal stability, direction of magnetization and coatings. Table 2-6<sup>16</sup> summarizes a few of the more common commercially available magnets.

**Table 2-6. Magnet composition, strength and thermal stability**

<i>Composition</i>	<i>Magnetic Energy Product (MGOe / kJ m<sup>-3</sup>)</i>	<i>Thermal Stability (up to °C)</i>
NdFeB	26 to 48 / 200 to 380	150
SmCo	16 to 32 / 130 to 250	300
Alnico	1.5 to 7.5 / 12 to 60	550
Ceramic (iron oxide, Sr)	1 to 3.5 / 8 to 28	300

Rare earth iron boron magnets such as neodymium iron boron (NdFeB) have the highest magnetic energies of any material but are heat sensitive and cannot be exposed to temperatures higher than 150 °C, after which they will

demagnetize. Rare earth cobalt magnets such as samarium cobalt (SmCo) have slightly less magnetic energies and slightly better thermal stability. Alnico magnets are an alloy of aluminum, nickel, cobalt and iron as well as sometimes other elements and offer the best resistance to high temperature of all magnetic materials

Magnets of each of these compositions can be manufactured to have a number of different directions of magnetisation. The naming convention for the most common bar (rectangular) and slug (ring) magnets is shown in Figure 2-12 (modified from Moskowitz<sup>17</sup>). The magnets used as “mobile magnets” were mainly bar magnets magnetized parallel to width and those used in the “fixed magnet base” were ring magnets magnetized parallel to thickness.

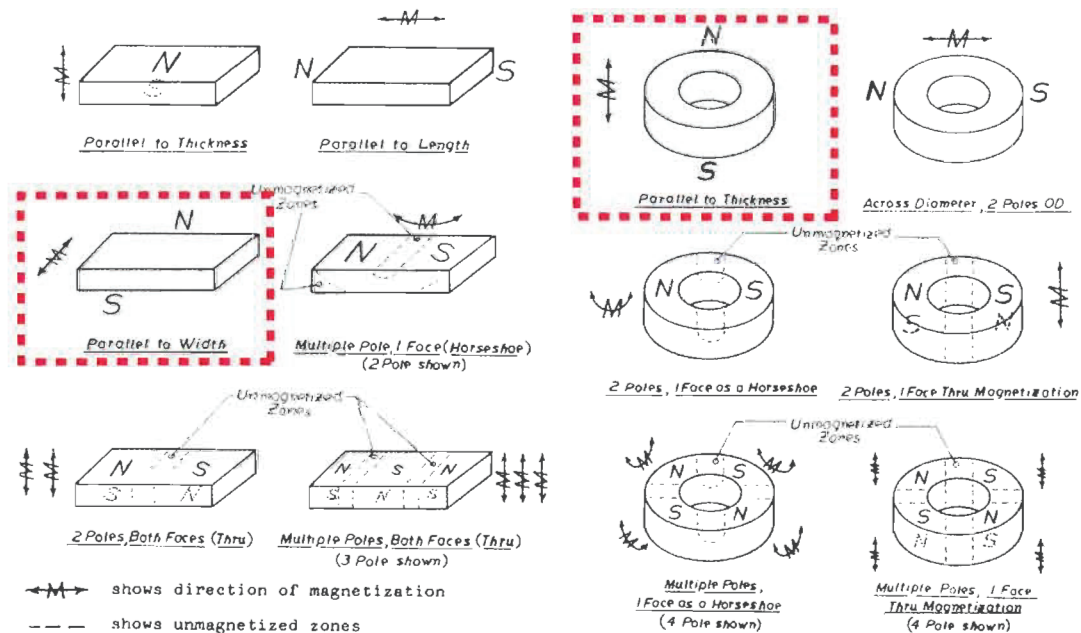
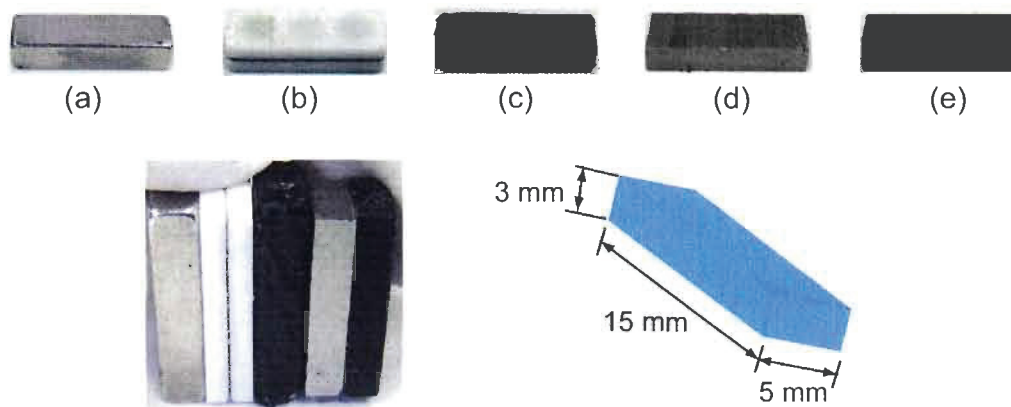


Figure 2-12. Nomenclature for the direction of magnetization of rectangular and ring magnets. Dotted rectangle highlights the direction of magnetization used as “mobile magnets” and in the “fixed magnet base”.

Five different types of “mobile magnets” (Figure 2-13) were compared in terms of strength and acid resistance.



**Figure 2-13.** “Mobile magnets”. (a) Ni plated NdFeB bar, (b) Teflon encapsulated NdFeB discs, (c) Epoxy coated Ni plated NdFeB bar, (d) Alnico bar, (e) Tefzel coated Alnico bar

Nickel (Ni) plated neodymium iron boron (NdFeB) permanent bar magnets were purchased from McMaster Carr (Chicago, IL). These were the strongest magnets tested with and without a severe-environment epoxy coating (coal tar epoxy and activator, 7953T12, McMaster Carr, Chicago, IL). This epoxy is said to withstand severe abrasion and strong chemicals.

To increase the chemical resistivity of the “mobile magnets”, Teflon encapsulated NdFeB discs were also developed in collaboration with V&P Scientific Inc. (San Diego, CA). Six NdFeB discs (VP 782N-3) were incorporated into a Teflon shell in such a way that overall direction of magnetization was the same as the other “mobile magnets”. The two sides of the shell shown in Figure 2-14 were fused together using a proprietary ChemGrip (a PTFE treatment/epoxy formula). Though made of NdFeB magnets, this “mobile magnet” was found not to be strong enough to grind through tough samples. Too much of a volume of

these “mobile magnets” were made of Teflon as opposed to magnetic material. For this reason, Teflon coatings (instead of encapsulation) were investigated next.

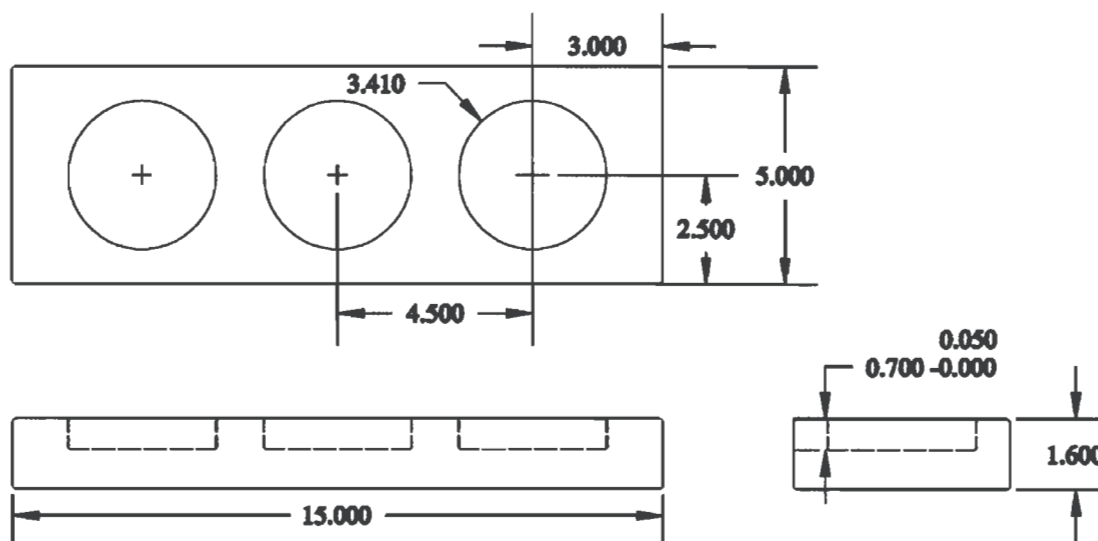


Figure 2-14. Teflon encapsulation schematic diagram. Two halves of the illustrated encapsulation were fused together with a total of six disc magnets inserted into the circular cavities, three on each side.

Coating magnets with Teflon (polytetrafluoroethylene, PTFE) and Tefzel (ethylene-tetrafluoroethylene copolymer, ETFE) was investigated. As seen in Table 2-7, Tefzel coating, the toughest of the fluoropolymers, was preferred over Teflon for its excellent resistance to abrasion and chemicals, though Teflon remains the preferred choice in other applications for its non-stick properties.

Table 2-7. Comparison of Teflon and Tefzel properties according to DuPont™

Properties	Teflon® PTFE	Teflon® FEP <sup>1</sup>	Teflon® PFA <sup>2</sup>	Tefzel® ETFE
Non-Stick	Excellent	Excellent	Excellent	Good
Abrasion Resistance	Fair	Good	Very Good	Excellent
Chemical Resistance	Good	Excellent	Excellent	Excellent

<sup>1</sup>FEP: fluorinated ethylene propylene

<sup>2</sup>PFA: perfluoroalkoxy

All of these coatings, developed by DuPont™, require a high temperature curing step above 370°C. Consequently, the only magnets that could be coated and maintain their magnetization were the Alnico magnets (see Table 2-6 above). After purchasing Alnico magnets (0.096" x 0.178" x 0.529", AB001700, Master Magnetics, Inc., Castle Rock, CO) collaborative work between myself and Boyd Coatings Research Co. Inc., (Hudson, MA) resulted in Tefzel coated Alnico magnets. These had been primed and then coated with three layers (to make sure the pieces were totally covered with the coating material) for a total coating layer thickness of 2 to 8 thousandth of an inch. Both the uncoated and coated Alnico magnets were tested.

#### *2.2.2.2 Acid Resistivity and Elemental Analysis by ICP-AES*

Sample preparation for elemental analysis of many samples often involves digesting or extracting with a strong acid. Consequently, the five different "mobile magnets" were tested in a concentrated acid medium as part of a feasibility study.

Each "mobile magnet" was placed in a centrifugal device chamber (similar to that described in Chapter 5) with 0.8 mL of concentrated nitric acid (HNO<sub>3</sub>, trace metal grade, Fisher, Napean, ON, Lot 1106050) and sealed with a polycarbonate cover with double-face adhesive (FLEXmount DFM 200 Clear V-95 150 poly H-9 V-95 4, FLEXcon, Spencer, MA). The centrifugal device was then placed on Stage v2.0 and spun at 240 rpm (4 Hz) for 120 seconds. The extractant was then quickly pipetted to a vial and analyzed by inductively-coupled plasma atomic emission spectrometer (ICP-AES) for elemental composition.

Replicate runs were made for all magnets and blanks except of the Ni plated NdFeB and of the epoxy coated Ni plated NdFeB since these reacted quite violently in concentrated nitric acid destroying the magnets and posing a safety concern.

A Thermo-Jarrell Ash IRIS ICP-AES (Thermo Electron Corporation, Franklin, MA) was used for these analyses. This system was thoroughly cleaned, repaired (replacing the power supply's high power resistor and high voltage rectifier), the optical pathway aligned and optimized, the detector wavelengths mapped, and overall system calibrated for the 21 elements that were monitored. The ICP-AES operating parameters are summarized in Table 2-8.

Table 2-8. ICP-AES operating parameters

RF power	1150 W
Plasma gas flow rate	14 L min <sup>-1</sup> Ar
Auxiliary gas flow rate	0.50 L min <sup>-1</sup> Ar
Nebulizer gas flow rate	0.70 L min <sup>-1</sup> Ar
Tubing	White/white (0.040" ID)
Flow rate (pump speed)	1.8 mL min <sup>-1</sup> (100 rpm)
Nebulizer	Burgener high-solids
Spray chamber	Cyclonic
Elements and wavelengths monitored	Ag (338.2 nm) Al (309.2 nm) As (228.8 nm) B (249.7 nm) Ca (393.3 nm) Cd (214.4 nm) Co (228.6 nm) Cr (283.5 nm) Cu (324.7 nm) Fe (259.9 nm) K (766.4 nm) Mg (279.5 nm) Mn (257.6 nm) Na (588.9 nm) Nd (406.1 nm) Ni (231.6 nm) Pb (261.4 nm) Se (196.0 nm) Sn (242.9 nm) Sr (407.7 nm) Zn (213.8 nm)

Figure 2-15 shows the element composition of the extractant for all the “mobile magnets”, reagent blank and blanks from elemental leaching from the vials after 2 hours and 5 days in acid. Figure 2-16 limits the results to the poorly performing “mobile magnets” and Figure 2-17 only presents the best performing “mobile magnets”. Note the logarithmic signal scale of the ordinate.

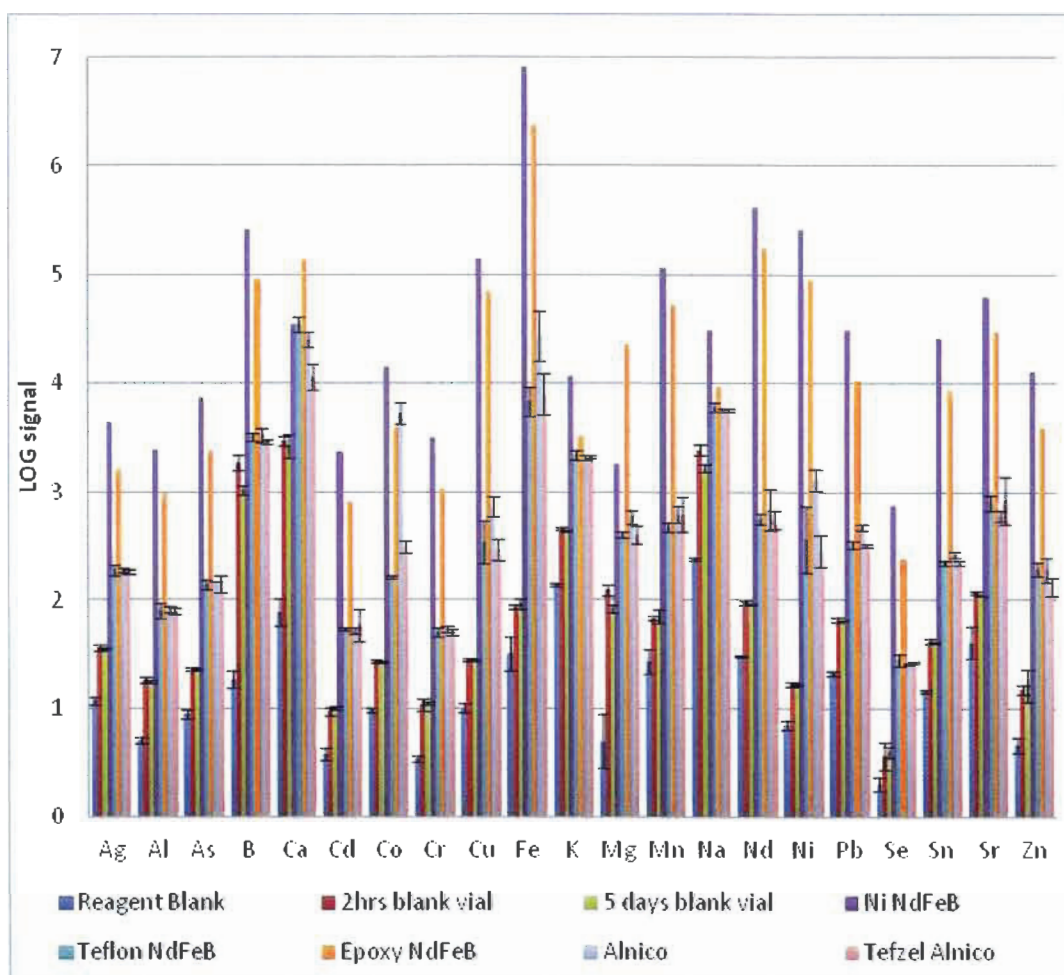


Figure 2-15. Elemental composition of the extractant for the reagent blanks, vial blanks and all of the “mobile magnets”. Error bars  $\pm 1\sigma$ .

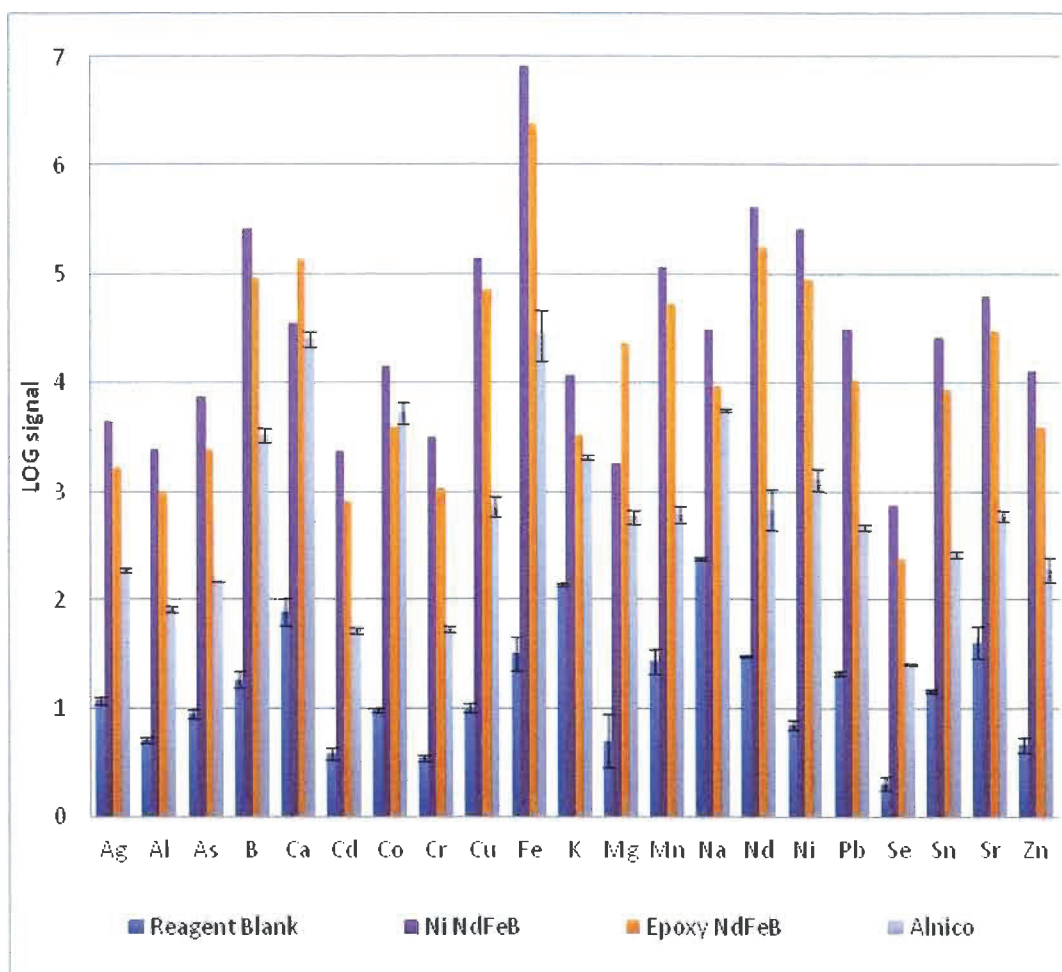


Figure 2-16. Elemental composition of the extractant for the poorly performing “mobile magnets”. Error bars  $\pm 1\sigma$ .

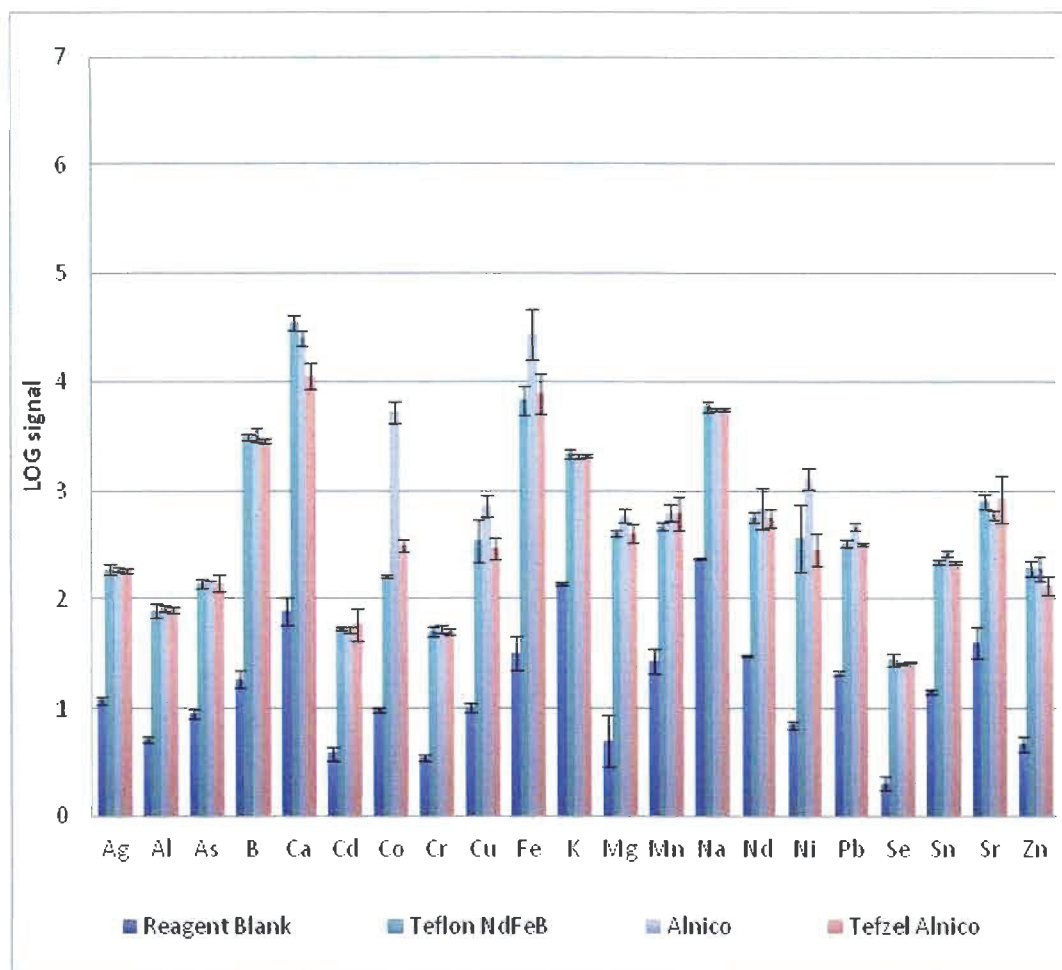


Figure 2-17. Elemental composition of the extractant for the best performing “mobile magnets”. Error bars  $\pm 1\sigma$ .

Though the uncoated and epoxy coated Ni plated NdFeB were intrinsically the strongest magnets, these resisted poorly to acid. Not surprising, high levels of nickel, neodymium, iron, boron as well as mixture of other elements were measured. The epoxy coating seemed to slightly improve the acid resistance of this magnet consistently showing lower leaching of most metals as compared to the same magnet without epoxy, except for calcium and magnesium (no doubt part of the epoxy formulation).

The uncoated Alnico magnets performed surprisingly well. Their extractants had statistically similar signals to those of the Teflon and Tefzel magnets except for higher concentrations of nickel, cobalt and iron. From looking at this magnet's acronym (Alnico), one would not have thought that there should be such a high iron signal; however, as mentioned above, iron is part of this magnet's alloy though it does not appear in its name.

The Teflon encapsulated and Tefzel coated magnets performed the best in regards to acid resistivity with similar low levels of measured extracted contaminants. Most of these contaminants were thought to originate from the process and not from these magnets. Possible sources of contaminants included leaching from the vials used to transfer the samples from the centrifugal devices to the ICP-AES for analysis as seen in the 2 hours and 5 days blank vial runs. Whether the vials were left 2 hours or 5 days before analysis, the signals were of the same magnitude. Other sources of contamination were from the centrifugal devices themselves such as from their plastic structure or from the deterioration of the double-sided adhesive.

A comparison of the Teflon encapsulated NdFeB discs and Tefzel coated Alnico bar "mobile magnets" also demonstrated the marked advantage of coating instead of encapsulating. Coats are much thinner than encapsulations leaving more room for magnetic material in each agitator. For example, though NdFeB is intrinsically a stronger magnet material than Alnico, the Tefzel coated Alnico magnet resulted in a stronger agitator than the Teflon encapsulated NdFeB magnets. Unfortunately the low thermal stability of NdFeB magnets made it impossible to coat and cure them with a Tefzel coating.

Empirically scoring each “mobile magnet” in terms of strength and acid resistance is presented in Table 2-9.

**Table 2-9. Scorecard comparing “mobile magnets” for acid medium experiments**

<i>“Mobile magnet”</i>	<i>Magnet strength</i>	<i>Acid resistance</i>	<i>Total</i>	<i>%</i>
Ni plated NdFeB bar	10/10	0/10	10/20	50
Teflon encapsulated NdFeB discs	3/10	10/10	13/20	65
Epoxy coated Ni plated NdFeB bar	10/10	1/10	11/20	55
Alnico bar	5/10	8/10	13/20	65
Tefzel coated Alnico bar	5/10	10/10	15/20	75

All of the “mobile magnets” worked well in water (used in Chapter 5) and organic solvents such as hexane and ethanol (used in Chapter 6 and Chapter 7). Respective blank runs in those experiments demonstrated that no interfering contaminants originated from the magnetic agitators. Therefore, for acid medium experiments, the best “mobile magnets” were the Tefzel coated Alnico bars for their relative strength and thermal stability allowing for the application of the Tefzel resistive coating. For other experiments where no acid resistance was required, the brute force of the NdFeB bar magnets was preferred. As such the more powerful NdFeB bar magnets were chosen as the “mobile magnets” for the studies presented in subsequent chapters.

## 2.3 References

- (1) Morais, S., Tamarit-López, J., Carrascosa, J., Puchades, R., Maquieira, A., "Analytical prospect of compact disk technology in immunosensing", *Analytical and Bioanalytical Chemistry*, **2008**, 391 (8), 2837-2844.
- (2) Grumann, M., Brenner, T., Beer, C., Zengerle, R., Ducrée, J., "Visualization of flow patterning in high-speed centrifugal microfluidics", *Review of Scientific Instruments*, **2005**, 76 (2), 025101-025101.
- (3) LaCroix-Fralish, A., Templeton, E.J., Salin, E.D., Skinner, C.D., "A rapid prototyping technique for valves and filters in centrifugal microfluidic devices", *Lab on a Chip*, **2009**, 9 (21), 3151-3154.

- (4) Lafleur, J.P., Salin, E.D., "Pre-concentration of trace metals on centrifugal microfluidic discs with direct determination by laser ablation inductively coupled plasma mass spectrometry", *Journal of Analytical Atomic Spectrometry*, **2009**, 24 (11), 1511-1516.
- (5) Kido, H., Micic, M., Smith, D., Zoval, J., Norton, J., Madou, M., "A novel, compact disk-like centrifugal microfluidics system for cell lysis and sample homogenization", *Colloids and Surfaces B: Biointerfaces*, **2007**, 58 (1), 44-51.
- (6) Grumann, M., Geipel, A., Riegger, L., Zengerle, R., Duccrée, J., "Batch-mode mixing on centrifugal microfluidic platforms", *Lab on a Chip*, **2005**, 5 (5), 560-565.
- (7) Kong, M.C.R., Salin, E.D., "A valveless pneumatic fluid transfer technique applied to standard additions on a centrifugal microfluidic platform", *Analytical Chemistry*, **2011**, 83 (23), 9186-9190.
- (8) Dubey, A.K., Yadava, V., "Laser beam machining-A review", *International Journal of Machine Tools and Manufacture*, **2008**, 48 (6), 609-628.
- (9) Weigl, B.H., Bardell, R., Schulte, T., Battrell, F., Hayenga, J., "Design and rapid prototyping of thin-film laminate-based microfluidic devices", *Biomedical Microdevices*, **2001**, 3 (4), 267-274.
- (10) Bartholomeusz, D.A., Boutté, R.W., Andrade, J.D., "Xurography: rapid prototyping of microstructures using a cutting plotter", *Microelectromechanical Systems, Journal of*, **2005**, 14 (6), 1364-1374.
- (11) Kido, H., Zoval, J., Madou, M., "Rapid prototyping of microfluidic systems", *ECS Transactions*, **2006**, 4 101-105.
- (12) Oberg, E., McCauley, C.J., Knoel, "Machinery's handbook a reference book for the mechanical engineer, designer, manufacturing engineer, draftsman toolmaker and machinist"; Industrial Press: New York :, **2004**, 2693.
- (13) Ogonczyk, D., Wegrzyn, J., Jankowski, P., Dabrowski, B., Garstecki, P., "Bonding of microfluidic devices fabricated in polycarbonate", *Lab on a Chip - Miniaturisation for Chemistry and Biology*, **2010**, 10 (10), 1324-1327.
- (14) Duffy, D.C., Schueller, O.J.A., Brittain, S.T., Whitesides, G.M., "Rapid prototyping of microfluidic switches in poly(dimethyl siloxane) and their actuation by electro-osmotic flow", *Journal of Micromechanics and Microengineering*, **1999**, 9 (3), 211-217.
- (15) Duccrée, J., Haeberle, S., Lutz, S., Pausch, S., Von Stetten, F., Zengerle, R., "The centrifugal microfluidic Bio-Disk platform", *Journal of Micromechanics and Microengineering*, **2007**, 17 (7), S103-S115.
- (16) Master Magnetics, I., "Permanent Magnetic Materials", *Brochure*, **2006**.
- (17) Moskowitz, L.R., *Permanent magnet design and application handbook*, Krieger, Malabar, Fla. **1995**, p. 946.

## CHAPTER 3: Comparison of 3D Printing Technologies for Rapid Prototyping and Additive Manufacturing of Centrifugal Microfluidic Devices

Other than subtractive manufacturing and lamination sealing techniques described in Chapter 2 to manufacture devices, recent advances in 3D printing technology have made additive manufacturing of devices an interesting alternative. This chapter deals with the feasibility of manufacturing entire miniaturized chemical analysis devices with microfluidic features using this technique. Additional images and a link to a video compilation are available in Appendix C and Appendix D respectively.

### 3.1 Abstract

Three different additive manufacturing techniques of three-dimensional (3D) printers were compared, and the merits of each technology were investigated for use in centrifugal microfluidics. Having already revolutionized engineering and marketing, 3D printing has now become important in chemistry to enable rapid fabrication of structures for research in new microfluidic experiments. The tested performance parameters of the 3D printers included: precision, accuracy, ability to retain liquids, surface finish, chemical resistivity and the ability to “print” capillary burst valves. The 3D structures were designed to push the limits of each printer. The *Alaris* printer from “Objet Geometries Inc.” (using polyjet modeling technology) performed best followed by the *uPrint* from “Dimension Inc.” (using fused deposition modeling technology) and the *V-Flash* from “3D Systems Corporation” (using film transfer imaging technology). Three

dimensional printing has the potential to reduce the time and skill needed to inexpensively manufacture the next generation of centrifugal microfluidic devices for environmental and medical analyses.

### **3.2 Introduction**

Once limited to making miniature models, rapid prototyping technologies have grown over the past decades into viable and rapid manufacturing tools. No longer are they mere temporary prototypes, structures produced by these technologies are being used as final products in an increasing number of fields including chemistry.<sup>1</sup> Of particular interest to us is the ability to rapidly manufacture centrifugal microfluidic devices by these techniques.

With their evolving technologies and end-use of structures, rapid prototyping nomenclature has become somewhat confusing with panoply of terms being used in both industry and academia. What was once commonly known as “rapid prototyping” is now more precisely called in most cases **“additive manufacturing”**. According to the American Society for Testing and Materials (ASTM), an industry-led standard group, additive manufacturing is defined as the “process of joining materials to make objects from 3D model data, usually layer upon layer, as opposed to subtractive manufacturing methodologies, such as traditional machining. Synonyms include ‘additive fabrication’, ‘additive processes’, ‘additive techniques’, ‘additive layer manufacturing’, ‘layer manufacturing’ and ‘freeform fabrication’”.<sup>2</sup> Office friendly versions of these techniques known as “desktop manufacturing” and **“3D printing”** (three dimensional printing) can also be added to this list of synonyms.<sup>3</sup>

From this definition, two main clarifications have been brought to the field: 1) the distinction between additive and subtractive techniques which can both rightfully be called “rapid prototyping” and 2) the evolution of the technology from simple prototyping to actual manufacturing of end-user production-quality structures. Therefore both “subtractive rapid prototyping” and “subtractive manufacturing” are viable terms such as in the case of the Roland MDX series milling machines. On the other hand, both “additive rapid prototyping” and “additive manufacturing”, which include “3D printing”, more accurately describe the techniques under study here.

Subtractive rapid prototyping evolved from the automation of milling machines that can manufacture parts out of any machinable material. Milling in three or even four axes (rotational) has produced impressive parts; however, 1) inner features cannot be milled easily and 2) fine features are limited to the size of the smallest tool ( $\sim 400\ \mu\text{m}$ , which are very fragile). Additive rapid prototyping is the inverse and involves building up layers of material with the deposition being controlled by printer-type heads or exposure to light. In essence, it is very similar to printing with a modern desktop printer with each successive layer of information being printed on top of those just printed instead of on a separate page. Additive rapid prototyping is an extremely useful technique because, unlike machining, essentially any design that can be drawn in a computer program can be “3D printed” without the need for the skill involved with milling. This has revolutionized engineering, marketing and a growing number of other fields including orthopaedics<sup>4, 5</sup> because complete high precision working models with interior moving parts can be made for testing before investing in more

expensive production methods. An interesting example from George W. Hart and which was fabricated in our lab is provided in Figure 3-1. This is a structure of “six nested truncated icosidodecahedra”<sup>6</sup> and would have been very difficult if not impossible to manufacture by subtractive techniques. Additive manufacturing can be done with a variety of materials, ranging from ceramic through plastics with various properties. The more affordable commercial systems use photopolymers or acrylonitrile butadiene styrene (ABS) plastic and can make designs with sub-millimetre features.

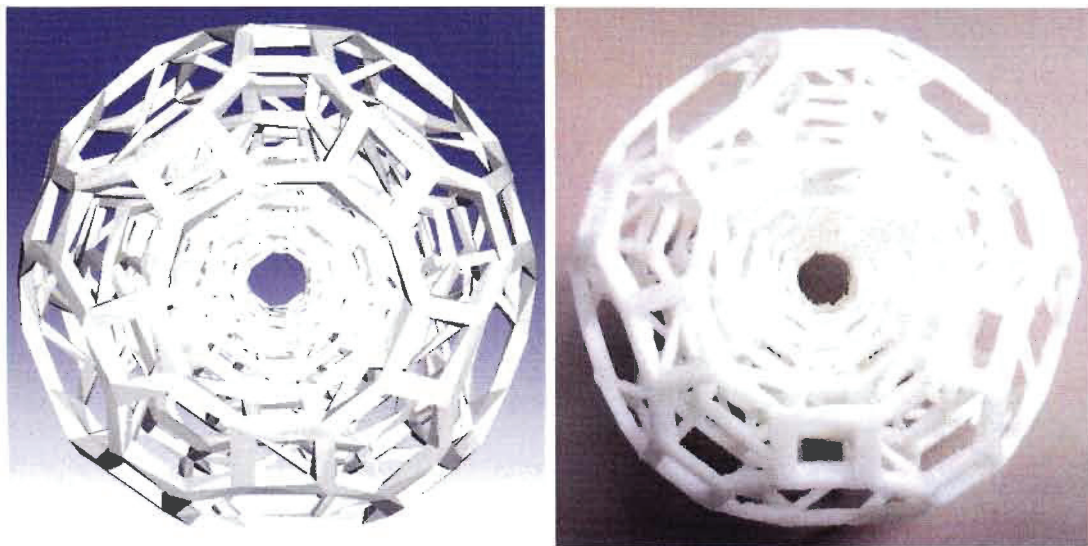


**Figure 3-1.** Example of the complexity possible in structures manufactured by 3D printing taking a computer generated design (left) and rapidly making a finished product (right).

First introduced in 1986 by “3D Systems” in the form of stereolithography,<sup>7</sup> additive manufacturing now includes a variety of techniques and technologies. Some of the most widely used and currently commercially available techniques include:

- Stereolithography (STL)
- Selective Laser Sintering (SLS)
- Liquid Binding Powder (LBP)
- Fused Deposition Modeling (FDM)
- Film Transfer Imaging (FTI)
- PolyJet Modeling (PJM)

Of these techniques, the last three were chosen for the current comparison with the specific application for use as a manufacturing technique for centrifugal microfluidic devices. Since these three additive manufacturing technologies are available as desktop 3D printers, the term “3D printer” or simply “printer” is used in this text to refer to all three systems. These systems are small enough and environmentally friendly enough, as compared to the noxious and toxic chemicals used in some stereolithography, to allow them to operate in an office environment rather than in a production plant or laboratory.

Many factors play an important role when selecting a 3D printer. There is no one 3D printer that will be the best for every engineer, marketing manager and chemist. Factors such as application, cost, build speed, precision and accuracy, need for post-processing, surface finish and chemical resistivity of the produced structures all affect the performance and choice of 3D printer. Some will want structures to fit together according to strict specifications, other will prefer the look and feel of structures, while others still will want resistant and strong structures. At present, no 3D printer can provide all of these characteristics. The best 3D printer will be the one that meets the most of the user’s needs and is a balance between the cost, limitations and performance of each system.

With this in mind, the study presented here compares three 3D printers for the specific application of manufacturing centrifugal microfluidic devices. The global advantages of microfluidics are well documented in a number of excellent reviews<sup>8-11</sup>. The use of centrifugal force as a pumping method in microfluidics offers advantages over some other methods of pumping used in microfluidic systems;<sup>12, 13</sup> however, current manufacturing techniques, especially at the prototyping stage, have relatively long turn-around times between the development of designs and the end of the fabrication process. To date, such devices have been manufactured for example out of polydimethylsiloxane (PDMS) by photolithography,<sup>14</sup> hot embossing,<sup>15</sup> or by cold lamination of multiple layers that were milled and cut (subtractive manufacturing) using a CNC milling machine and xurography cutting plotter.<sup>16, 17</sup> In such devices a series of “unit operations”<sup>13</sup> such as siphons, valves, liquid mixing, volume metering, volume splitting, filtering, solid sample preparation and detection are sequentially integrated radially outwards in order to automate and miniaturize routine chemical assays. The production of a device using cold lamination (favoured in our laboratory due to both cost and flexibility concerns) is time consuming and requires a skilled operator and multiple production stages resulting in devices typically made of five or more layers. Ideally, once the devices have been designed, 3D printers are thought to be able to quickly and easily manufacture the entire device. This is envisioned to be a single step production without the need of an operator supervising the printer. The performance of a design could be tested with real production-quality parts and quickly modified to either optimize performance or to adapt the devices to new problems and intended use. In

addition, each optimized “unit operation” (section of the devices) could be easily combined and integrated at the design level to quickly conceive new and even more complex features and functionalities. Furthermore, a third dimension could be much more easily accessed allowing production of odd structures, overhanging ridges and reproducible channels and liquid flow in this third dimension.

To date, few have used the growing capabilities of 3D printers to build microfluidic devices<sup>18-21</sup> and to our knowledge only two for centrifugal microfluidic devices,<sup>1, 22</sup> one of which is presented in Chapter 4. To our knowledge, no comparison of commercial 3D printers for centrifugal microfluidics has been reported. For other applications such as engineering there are comparisons of the 3D printing techniques available in the literature including an array of performance parameters required for different applications.<sup>23</sup> Some of these were the basis of the studies included here such as accuracy and surface finish.<sup>24, 25</sup> Of the microfluidic applications, most have used the printed structures as moulds for a PDMS mask instead of using the printed structures themselves. Additionally, the utility of 3D printers is not limited to the production of only the microfluidic devices but we and others have expanded this to the production of instrument platforms such as cuvette holders and other small to medium size instruments.<sup>20</sup>

With the continuing advances in 3D printing technology we believe these additive manufacturing techniques can fundamentally alter the way centrifugal microfluidic devices are designed and manufactured. The goal therefore is to determine which commercially available 3D printer is the best suited for

fabrication of all-in-one centrifugal microfluidic devices to be used straight from the printer.

### **3.3 Experimental**

In order to evaluate the potential of applying 3D printing technology to microfluidic studies in analytical chemistry, a comparison was made of the production processes and the resulting structures from three different commercially available 3D printers. The evaluation involved 1) designing 2) manufacturing and 3) studying a series of test structures.

#### **3.3.1 Designing Test Structures**

A series of different test structures were designed in the 3D computer-aided design (CAD) software “SolidWorks” (SolidWorks Corp., Concord, MA, USA) and exported as \*.STL files. Originally developed for stereolithography (STL) CAD software, this file format has become the standard for 3D structure manufacturing. Each \*.STL file is comprised of a set of triangulated surfaces which sum to the designed structure. Each structure was designed with a distinct purpose, each pushing the limits of the 3D printers.

#### **3.3.2 Manufacturing Test Structures**

The designed structures were manufactured by the three distinct commercially available 3D printers. Since \*.STL files can be read by most rapid prototyping machines (printers and mills), identical files were processed on all three printers. Each printer did however use its own proprietary software to process these \*.STL files into a series of cross-sectional slices; each slice was

then printed one on top of the other to create the designed structures. In order to better understand the structures produced by the 3D printers, details of the fabrication process and technology of each of the chosen printers are included below.

It is noteworthy that other than the three printer systems included in this study, there are many more technologies available. An interesting commercially available alternative is that of Z-Corp (Z-Corporation, MA, USA, acquired by 3D Systems in January of 2012), which uses a liquid binding powder (LBP) technology, alluded to in the introduction, in which layers a fine powder are selectively bonded by using an ink jet printer-head to “print” adhesive according to the processed \*.STL file. This technology quickly produces multicoloured parts that fit well into one another. Unfortunately, parts are known to be brittle and fragile. With the specific application of centrifugal microfluidics, in which devices are spun at high speeds, there is a safety and functional need for strong production-quality parts straight from the printer. For these reasons structures were not manufactured for this study using LBP technology.

#### *3.3.2.1 Fused Deposition Modeling (FDM)*

“Fused deposition modeling” was the first of three 3D printing processes studied. In this process long filaments of thermoplastic and support material are molten and extruded out of a resistively heated printer-like nozzle layer upon layer.<sup>25</sup> As the filament is extruded at a constant rate, the printer nozzle follows a computer controlled path according to the processed \*.STL file. The thermoplastic is heated to just above its melting point so that it solidifies quickly after it exits the nozzle. Once one layer is complete, the working platform is

lowered and printing starts on the next layer. This process takes place within a heated chamber allowing successive strips of extruded ABS plastic to cold weld to each other. In order to manufacture overhanging features, a support material (not ABS) is also printed. This material is either snapped off or dissolved away in a caustic bath after printing is complete. The 3D printer chosen for this study that utilizes FDM technology was the “*uPrint*” (Dimension Inc., MN, USA, a division of Stratasys Inc.) which utilizes proprietary “*ABSplus*” plastic.

#### 3.3.2.2 *Film Transfer Imaging (FTI)*

“Film transfer imaging” was the second of three 3D printing processes studied. In this process sequential cross-sections of the desired part are imaged with an ultra-violet (UV) light onto fresh layers of photopolymer. The UV light catalyzes the polymerization, in which the photopolymer cross-links and solidifies. A fresh layer of photopolymer is brought over the previously cured layer using a reciprocating film carriage analogous to classical photography film in a camera. The process is then repeated with the next cross-section of the part being added. Support structures are printed out of the same material and must be cut and sanded away post-production limiting the construction of “inner” structures. The 3D printer chosen for this study that utilizes FTI technology was the “*V-Flash FTI 230*” (3D Systems Corporation, SC, USA). According to the Material Safety Data Sheet (MSDS), the proprietary *V-Flash* photopolymer resin “*FTI-GN*” is an organic mixture containing “phenyl-bis(2,4,6-trimethylbenzoyl)-phosphine oxide”.

### 3.3.2.3 PolyJet Modeling (PJM)

Combining the deposition technique of FDM and material type of FTI, “polyjet modeling” was the third 3D printing process studied in which a liquid photopolymer is deposited through an ink-jet printer head and immediately cured with a UV light. A module of 30 printer heads slides back and forth jetting equal amounts of material in accordance to the processed \*.STL file. Each layer is cured and hardened during the process. For difficult features, a gel support is used and removed post-production by hand or by using a jet of water although some studies report using a sodium hydroxide<sup>20</sup> or a tetramethylammonium hydroxide<sup>18</sup> bath. The 3D printer chosen for this study that utilizes PJM technology was the “Alaris30” (Objet Geometries Inc., MA, USA) which uses the proprietary “FullCure830” photopolymer material.

### 3.3.3 Studying Test Structures

The designed and manufactured structures were used in a series of studies testing their 1) precision, accuracy and ability to retain water 2) surface finish and chemical resistivity and 3) ability to “print” capillary burst valves, an important structure in centrifugal microfluidic devices.

#### 3.3.3.1 Study 1: Precision, Accuracy and Ability to Retain Liquid

In order to assess the precision and accuracy of each 3D printer, multiple replicates of each structure were manufactured by each system. The dimensions of the resulting structures were subsequently measured with an electronic calliper (Mitutoyo 500, QC, Canada) and weighed with an analytical balance (Mettler

AE 163, ON, Canada). One of the structures was also used to ascertain the ability of the parts to retain liquid. Likewise, the structures were observed and photographed at various magnifications (16.8x, 150x, 335x) using a microscope (Carl Zeiss SteREO Discovery V20, ON, Canada) equipped with a boom stand and a CCD colour camera (GRAS-14S5C-C, Point Grey, BC, Canada). These magnifications were equivalent to a field of view of 14.0 mm, 1.5 mm, and 0.7 mm respectively. Pieces were observed at 90 degrees (directly above) and at 22 degrees (see Figure 3-2) using ring lighting, darkfield lighting or backlighting, depending on the desired effect.

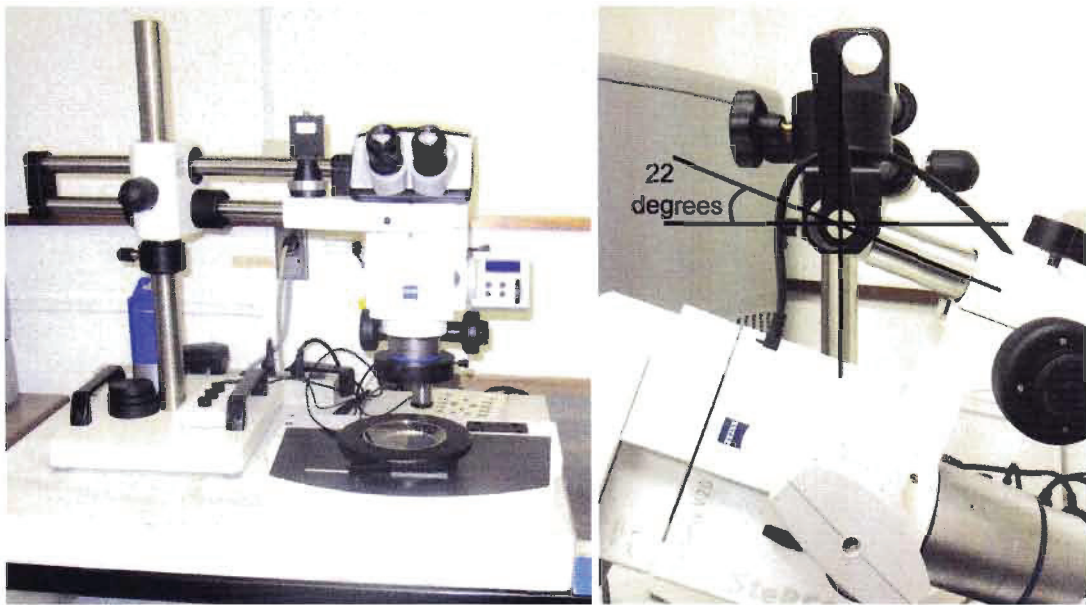


Figure 3-2. Microscope with boom stand and camera. Entire system at 90 degrees to sample (left) and zoom view of boom stand set at 22 degrees to sample (right).

#### 3.3.3.2 Study 2: Surface Finish and Chemical Resistivity

Surface finish was qualitatively compared by both visual and tactile observations. Visual observations were made both with the naked eye and under the Zeiss microscope used in the first study.

Chemical resistivity was performed using a series of ten identical structures from each of the three printers, for a total of 30 test structures. Each structure except the control was placed for 30 minutes in a beaker containing 7 mL of a solvent (solvent details summarized in Table 3-1). Since these structures were essentially identical, they all had the same surface area exposed to the respective solvents. Figure 3-3 shows the experimental setup.

**Table 3-1. Solvents used for chemical resistivity test of 3D structures**

<i>Solvent</i>	<i>Chemical Formula</i>	<i>Grade</i>	<i>Provider</i>
acetone	CH <sub>3</sub> COCH <sub>3</sub>	ACS	ACP, Montreal, QC, Lot H3110
methylene chloride	CH <sub>2</sub> Cl <sub>2</sub>	HPLC	Fisher, Napean, ON, Lot F1112
methanol	CH <sub>3</sub> OH	HPLC	Fisher, Fair Lawn, NJ, Lot 022920
ethanol	CH <sub>3</sub> CH <sub>2</sub> OH	USP	Commercial Alcohols Inc., Brampton, ON, Lot 432526
hexane	C <sub>6</sub> H <sub>14</sub>	HPLC	Fisher, Fair Lawn, NJ, Lot 001109
benzene	C <sub>6</sub> H <sub>6</sub>	ACS	Fisher, Fair Lawn, NJ, Lot 016714
tetrachloroethylene	C <sub>2</sub> Cl <sub>4</sub>	ACS	Sigma-Aldrich, Oakville, ON, Lot 08109JH
nitric acid (≈15.9 M)	HNO <sub>3</sub>	Trace Metal	Fisher, Napean, ON, Lot 1106050
ammonium hydroxide (≈14.8 M)	NH <sub>4</sub> OH	ACS	Fisher, Fair Lawn, NJ, Lot 002754



Figure 3-3. Experimental set-up in fume hood for chemical resistivity study.

Both the test structures (qualitative and photographic comparison) and the solvents (visual and instrumental) were observed in this study. The absorbance spectra of the solvents were acquired using a Varian Cary 5000 UV-Vis-NIR spectrophotometer.

#### 3.3.3.3 Study 3: Ability to “Print” Capillary Burst Valves

The goal of this third study was to determine the feasibility of manufacturing entire devices including microfluidic features such as capillary burst valves using the 3D printers. The first three test structures included individual features such as channels and reservoirs culminating with the fourth test structure which integrated these features into a centrifugal device. To visualize these devices in operation and to determine the burst frequency of the “printed” valves, distilled deionized water dyed with blue commercial food colouring was used as samples and the motorized Stage v2.0 described in Chapter 2 was used.



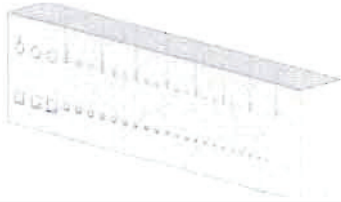

### **3.4 Results and Discussion**

The design, manufacturing and performance of structures produced by 3D printers were evaluated in order to determine which printer was best suited for use in centrifugal microfluidic research.

#### **3.4.1 Designing Test Structures**

As detailed in Table 3-2, four test structures were designed with the intention of pushing the limits of the 3D printers. The purpose of each design is also included. Larger versions of these drawings are available in Appendix C.

Table 3-2. Design and purpose of 3D test structures

SolidWorks CAD design drawing	Purpose
Structure 1	
	<ul style="list-style-type: none"> <li>- Micron size channels</li> <li>- Lengthwise view of capillary valves</li> <li>- Three replicates of each size channel</li> <li>- Decreasing size to an extreme that would not be "printable"</li> </ul>
Structure 2	
	<ul style="list-style-type: none"> <li>- Precise volume well</li> <li>- Ability of the structure to retain liquids (act as a reservoir)</li> <li>- Square base to compare build precision of x-axis and y-axis</li> </ul>
Structure 3	
	<ul style="list-style-type: none"> <li>- Micron size internal features</li> <li>- Imitation of capillary valve</li> <li>- Comparison of square and cylindrical capillaries</li> </ul>
Structure 4	
	<ul style="list-style-type: none"> <li>- Entire device integrating features of Structures 1 to 3 including reservoirs and "printed" capillary valves, all manufactured in one step</li> </ul>

The design of Structure 1 is a more complex version of that of Maher *et al.*<sup>19</sup> and included 21 square channels each 15 mm long. Three replicates of each of the following seven channel sizes were designed: 1000 x 1000  $\mu\text{m}$ , 500 x 500  $\mu\text{m}$ , 400 x 400  $\mu\text{m}$ , 300 x 300  $\mu\text{m}$ , 200 x 200  $\mu\text{m}$ , 150 x 150  $\mu\text{m}$  and 100 x 100  $\mu\text{m}$ . The design of Structure 2 included a precise 100  $\mu\text{L}$

volume cylindrical well (diameter 5 mm, height 5.09 mm) and a 20 x 20 x 2 mm base. The design of Structure 3 included both round and square 5 mm long channels. Three round and three square replicates of each size channel were included for a total of 54 channels. The diameter of the round channels as well as the height and width of the square channels were of the following dimensions: 1000, 500, 400, 300, 200, 150, 100, 75 and 50  $\mu\text{m}$ . The area and corresponding volume of the round channels as compared to the square channels were therefore designed slightly differently (for example the area of the round 500  $\mu\text{m}$  diameter channel was 0.20  $\text{mm}^2$  as compared to the area of the square 500  $\mu\text{m}$  x 500  $\mu\text{m}$  channel which was of 0.25  $\text{mm}^2$ ); however, they are sufficiently similar for the purpose of this study.

Finally, seven different versions of Structure 4 were designed, each with a different size capillary burst valve. Each of the seven versions contained 15 iterations of the same size valve. Figure 3-4 contains a detailed view of one of these 15 iterations. Each version contained cylindrical valves of one of the following diameter: 500, 300, 200, 150, 100, 75, and 50  $\mu\text{m}$ . Each valve was 5 mm long (same as Structure 3) at a radial distance of 28 mm from the centre of the device. This length and radial distance compares with the typically size and placement of burst valves constructed out of double sided adhesive or fused silica capillaries detailed in Chapter 6 and 7. The integrated reservoir giving each valve its head pressure had dimensions of 4 mm x 4 mm x 7 mm for a volume of 112  $\mu\text{L}$ , which is of similar volume to the test well of Structure 2.

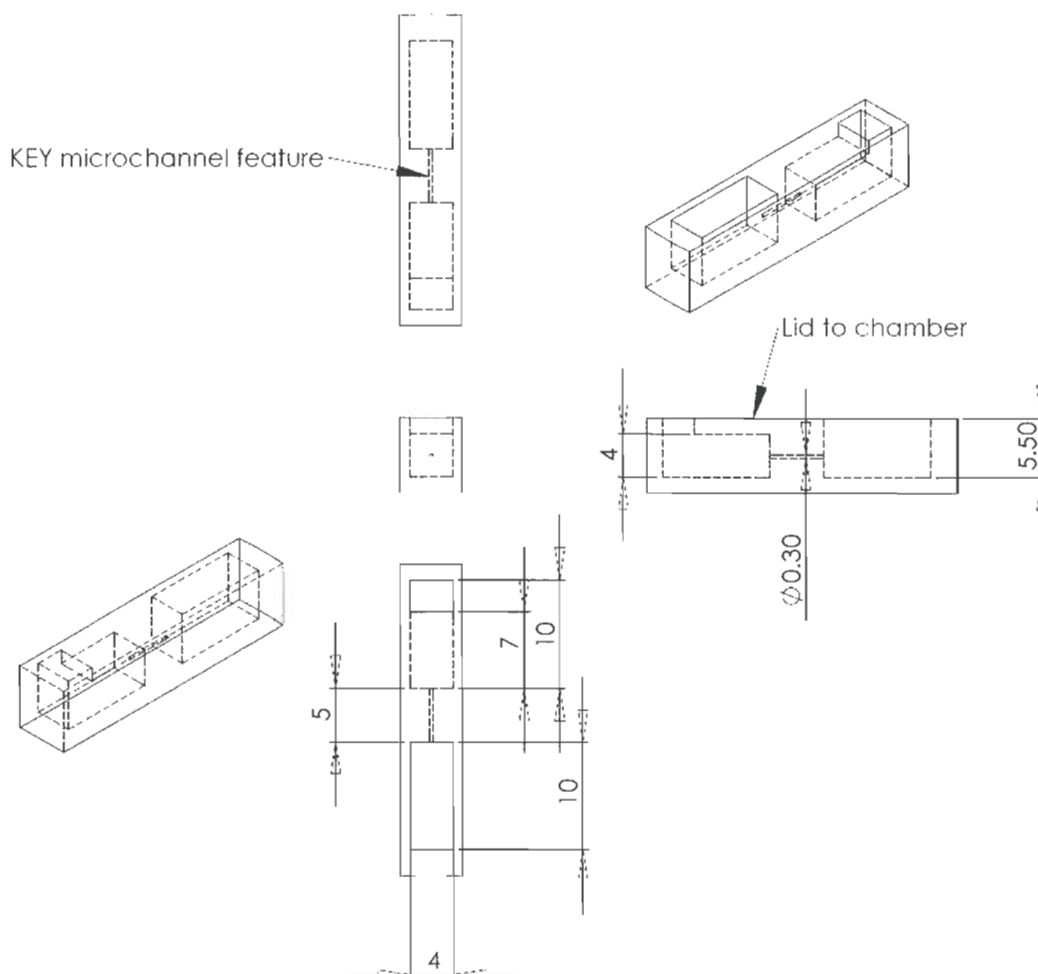


**Figure 3-4.** Multiple views schematic drawing of one set of designed reservoirs and capillary burst valve (dimensions in mm).

The ease with which computer generated designs can become actual working devices frees the chemist from many production limitations. It would seem that essentially any shape that can be conceived can be produced including internal and micro-sized features. More and more intuitive and powerful CAD based software is becoming commercially available facilitating the design of complex and micro-sized chemical platforms. Likewise, the turn-around time is

so fast that the design and production cycles have become more interlinked allowing improvements to be quickly and easily integrated.

### **3.4.2 Manufacturing Test Structures**

Test structures were manufactured on all three 3D printers. FDM parts (*uPrint*) were manufactured in-house using a printer that was on loan to our research group whereas the manufacturing of the FTI (*V-Flash*) and the PJM (*Alaris*) parts were contracted out. Photographs were taken of all structures such as the example in Figure 3-5. More photographs are included in the performance studies in the next section. A comparison of the manufactures' specifications was compiled and is summarized in Table 3-3. Finally, a link to a video compilation of these three printers in action is available in Appendix D.

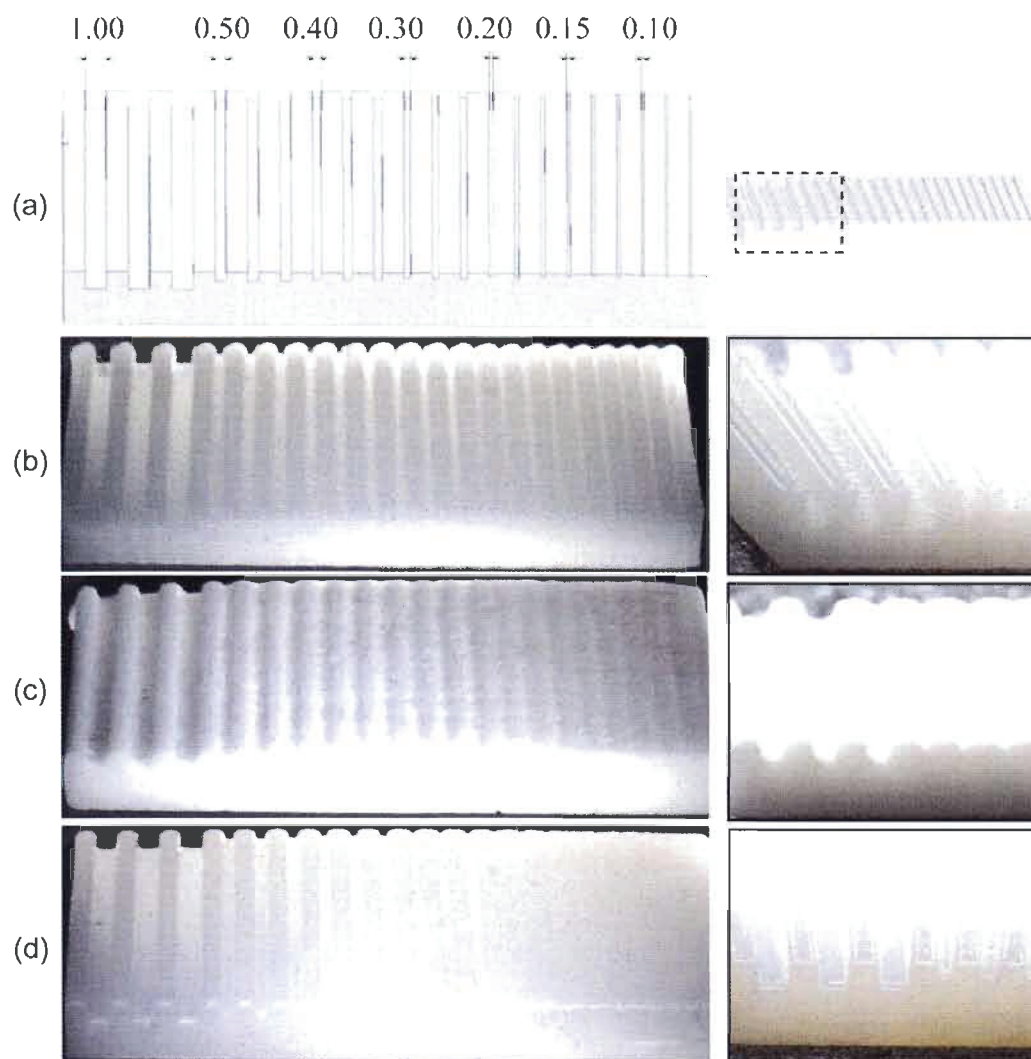











Figure 3-5. Structure 1 (a) Drawings of design that was saved as \*.STL and sent to all three printers (dimensions in mm) dotted area in right hand drawing corresponds to area in right hand photographs taken at 16.8x magnification, (b) photos of *uPrint* part, (c) photos of *V-Flash* part, and (d) photos of *Alaris* part.

Table 3-3. Summary of 3D printers manufacture specifications

Company	 Stratasys Inc. Dimension	 3D Systems Corporation	 Objet Geometries Inc.
Address	7655 Commerce Way, Eden Prairie, MN 55344-2020 U.S.A.	333 Three D Systems Circle, Rock Hill, SC 29730 U.S.A.	5 Fortune Drive, Billerica MA 01821 U.S.A.
Printer name/model		 FTI 230	
Photo of printer			
Technology	Fused Deposition Modeling (FDM)	Film Transfer Imaging (FTI)	PolyJet Modeling (PJM)
Material	Stratasys ABSplus (ABS plastic)	FTI-GN Material (Photopolymer)	VeroWhite FullCure830 (Photopolymer)
Support	Soluble support	none	Gel support
Build Size (inch) (mm)	8 x 6 x 6 203 x 152 x 152	9 x 6¾ x 8 228 x 171 x 203	11.5 x 7.7 x 6 294 x 196 x 150
Layer Thickness (inch) (µm)	0.01 254	0.004 102	0.0011 28
Resolution DPI (xyz)	N/A (dependent on bead size)	768 x 1024 x 2000	600 x 600 x 900
Glass Transition Temperature (°C)	108	N/A	58
Tensile/Flexural Strength(MPa)	36/52	33/53	50/75
Tensile/Flexural Modulus (MPa)	2265/2198	1550/1700	2495/2137
Elongation (%)	4	5	20
Price for printer	\$14,900	\$12,810	\$25,000
Hourly rates*	\$3.62	\$3.03	\$5.67

\* Obtained from Grimm.<sup>23</sup> Factors include the price for the printer, maintenance costs and operational costs including material and solvent baths at an average annual utilization.

All three printers have similar build sizes which are more than adequate for centrifugal microfluidic devices. Depending on future applications of these devices, incorporation of heating such as in a Soxhlet configuration may be difficult due to the low glass transition temperature of the produced parts (especially *Alaris* at 58 °C).

### 3.4.3 Studying Test Structures

The following studies attempted to answer the question: “What is the best 3D printer for the fabrication of centrifugal microfluidic devices?” These performance studies involved an investigation of the precision and accuracy of the fabricated parts, their ability to retain liquids, the surface finish and chemical resistivity, and the integration of capillary burst valves.

#### 3.4.3.1 Study 1: Precision, Accuracy and Ability to Retain Liquid

The dimensions and weights of structures 1, 2 and 3 were all measured. The x and y dimensions were those printed flat on the build platform (lateral resolution) whereas the z dimension was that in which each subsequent layer was printed (vertical resolution). Table 3-4 summarizes the average and standard deviation for the weight and dimensions of each structure manufactured on each of the three printers.

Table 3-4. Dimensions and weights of 3D structures

Structure	Printer	n	Average				Standard Deviation			
			Weight	Dimensions			Weight	Dimensions		
			(g)	x (mm)	y (mm)	z (mm)	(g)	X (mm)	y (mm)	z (mm)
1	Design	--	--	29.95	15.00	3.00	--	--	--	--
	<i>uPrint</i>	13	1.21940	29.84	15.01	3.20	0.00372	0.03	0.02	0.05
	<i>V-Flash</i>	10	1.45639	29.49	15.05	2.97	0.07373	0.12	0.03	0.12
	<i>Alaris</i>	6	1.50652	29.98	15.13	3.00	0.00143	0.01	0.03	0.01
2	Design	--	--	20.00	20.00	7.09	--	--	--	--
	<i>uPrint</i>	12	0.86341	19.88	19.89	7.27	0.00254	0.02	0.02	0.07
	<i>V-Flash</i>	11	1.20942	19.87	20.05	7.17	0.06591	0.10	0.09	0.09
	<i>Alaris</i>	10	1.15715	20.07	20.08	6.97	0.00123	0.03	0.03	0.01
3	Design	--	--	36.33	10.00	5.00	--	--	--	--
	<i>uPrint</i>	9	1.67979	36.32	5.13*	10.24*	0.00483	0.04	0.09	0.10
	<i>V-Flash</i>	10	2.10737	35.80	10.10	5.16	0.05699	0.05	0.06	0.14
	<i>Alaris</i>	8	2.11112	36.34	10.07	5.01	0.00688	0.01	0.04	0.01
Ave	<i>uPrint</i>						0.00370	0.03	0.04	0.07
	<i>V-Flash</i>						0.06555	0.09	0.06	0.12
	<i>Alaris</i>						0.00318	0.02	0.03	0.01

\* This part was printed on its side instead of on its back.

Many conclusions can be drawn from Table 3-4. First, the *V-Flash* and *Alaris* printers produced parts of a similar weight and density. This is no doubt related to their mutual use of photopolymer material. Furthermore, the z-axis was typically the least precise as it was dependent on the systematic addition of layer upon layer to give the final build height. Error in each layer contributed to the total error in this dimension. This was particularly seen in the case of the *V-Flash* and *uPrint*. Variability in size and weight were also greatest on the *V-Flash*. The most accurate printer as compared to the designed dimensions was the *Alaris* (0.5% error) followed by the *V-Flash* (1.2% error) and the *uPrint* (1.8% error). The *uPrint*'s accuracy seemed to depend on whether the final dimension was an

integral of the strand size (0.254 mm) as it was impossible to print half a strand of molten plastic. This will be further discussed in Section 3.4.3.3 below.

Structure 2 was also used to see the precision and accuracy of the well volume and the ability of the parts to retain liquids. Figure 3-6 shows top view photographs of this structure manufactured by the three printers while Table 3-5 summarizes the diameter at the mouth of the well and the volume of each of these (measured by weight of water and converted to volume using a density of 1.00 g/mL).

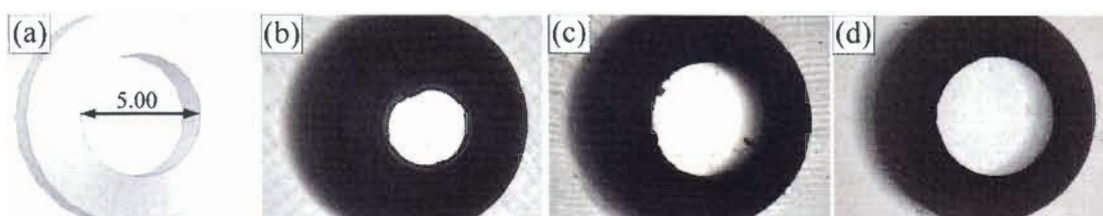


Figure 3-6. Structure 2, top view. (a) Drawing of design that was saved as \*.STL and sent to all three printers (dimension in mm), (b) photo of *uPrint* part, (c) photo of *V-Flash* part, and (d) photo of *Alaris* part. Photographs were taken with backlighting and 16.8x magnification.

Table 3-5. Diameter and volume of well of Structure 2

Printer	n	Average			Standard Deviation		
		Diameter (mm)	Water (g)	Water ( $\mu$ L)	Diameter (mm)	Water (g)	Water ( $\mu$ L)
Design	--	5.00	0.10000	100.0	--	--	--
<i>uPrint</i>	12	3.36	N/A	N/A	0.05	N/A	N/A
<i>V-Flash</i>	11	4.63	0.08040	80.4	0.15	0.00686	6.9
<i>Alaris</i>	10	4.97	0.09746	97.5	0.01	0.00143	1.4

As seen in Table 3-5, the *Alaris* printer was both the most precise and accurate in manufacturing the designed 100  $\mu$ L well with an average of  $97.5 \pm 1.4$   $\mu$ L and only 2.5% error from the designed volume. The *V-Flash* was somewhat precise with an RSD of 8.5%; however, it was not very accurate with an average

well volume 19.6% smaller than designed. Parts produced by both of these printers easily retained the liquid in the well, no doubt related to their being produced out of a hard photopolymer.

The *uPrint* performed very poorly in this study in regards to reservoir size and ability to retain liquid. First, the diameter of the well's mouth was much smaller than the design. A cross-sectional view of this part (Figure 3-7) revealed that the *uPrint* had added a lip or ridge to the top of the wells that was not in the original design. It is unclear why; however, this may be due to the nature of the FDM technology that extrudes strips of ABS plastic and was perhaps programmed not to print such thin edges. Another possibility may be an apparent shrinkage of the *uPrint* parts as they cool. Ippolito *et al.* describe this shrinking effect as "warping due to changes in density"<sup>24</sup>. Other parts, not detailed here, were also designed to connect with one another, similar to Lego<sup>TM</sup> pieces but they did not perform well without compensating for this shrinking effect of the ABS plastic.

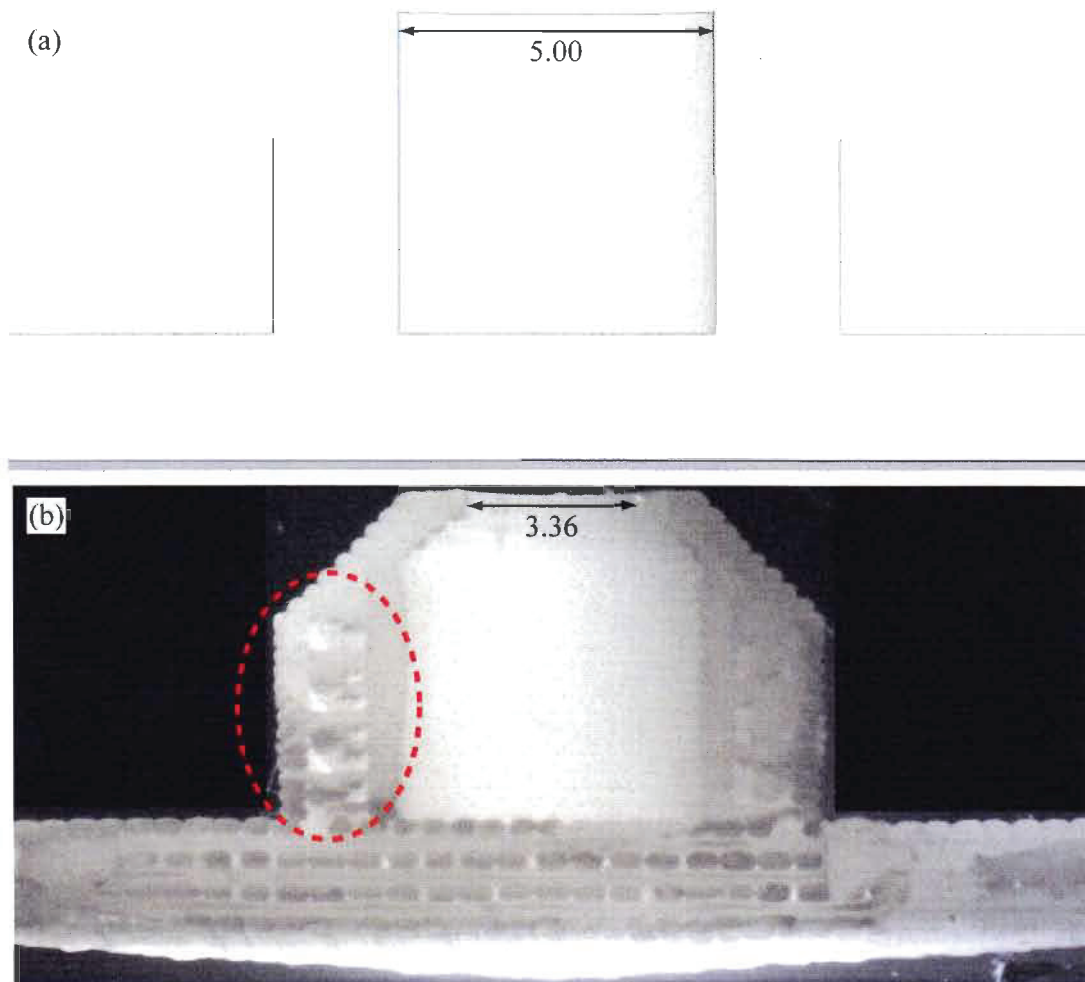


Figure 3-7. Vertical cross-sectional view of Structure 2 (a) Drawing of design, (b) photograph of cut cross section of the *uPrint* part (dimensions in mm). Dotted area highlights the empty spaces within the part.

Also visible in the highlighted area of Figure 3-7 is that the *uPrint* part is not completely “full”. The series of extruded strips trace the outline of the shape and then attempt to fill the area in a cross-hatch design from layer to layer. This inevitably leaves open areas. Other than being made of ABS plastic as opposed to a cured photopolymer, these open spaces help explain the difference in weight as compared to the other printers. Unfortunately this characteristic of *uPrint* parts makes them unable to easily retain liquids. This seeping action took place under

no additional pressure. For the intended application of centrifugal microfluidics in which centrifugal forces add pressure to the liquids, this is a major concern. Furthermore, in order to more precisely record the volume of these wells, the possibility of using a dilute Triton-X solution was considered. This would reduce the surface tension of the liquid and give a flatter meniscus (as opposed to an imprecise liquid dome on top of the well); however, the Triton-X made the solution seep through the layers even more readily. Possible solutions to this seepage problem include sealing the parts post-production with a solvent such as acetone either by spin coating, solvent bath or leaving the parts in an acetone rich vapour such as the system used by Ogonczyk *et al.* to bond polycarbonate parts together.<sup>26</sup> Such treatments do add time and a level of required skill to the process eliminating their immediate use straight from the printer as centrifugal microfluidics devices.

#### 3.4.3.2 Study 2: Surface Finish and Chemical Resistivity

Observation of any of the figures comparing the parts manufactured by all three printers such as Figure 3-5 and Figure 3-6 clearly show marked differences in *surface finish*. Both visual and tactile observations revealed striations on the *uPrint* and *V-Flash* parts. These striations created rough surfaces and were the direct consequence of the manufacturing technique. The surfaces were particularly rough in the z-axis of the build in which small ridges were artefacts of the layering process. Such rough surfaces resulted in uneven flow of liquids over them. These striations were largest in the *V-Flash* parts which also showed further irregularities in the surfaces such as “pock marks” making this printer

unsuitable for centrifugal microfluidics in applications requiring a good surface finish.

It should be noted that post-production treatments such as spin coating with acetone, alluded to when sealing the parts, could also smooth the surfaces of the *uPrint* plastic parts. Similarly, sanding or painting of *V-Flash* parts to a smooth finish is common for other applications. Such treatments would be impractical for application to centrifugal microfluidic devices. It would be very hard to sand microscale features, not to mention the loss in geometry and size.

The parts manufactured by the *Alaris* had very smooth surfaces that did not need any post-production manipulations. This is due to a combination of the effective PJM process and the reported 28  $\mu\text{m}$  layer thickness. The only irregularity was the presence of dust in many of the magnified photographs demonstrating the need for a clean work environment and also indicating a tendency for a build up of static on the parts.

A second element of this study was the *chemical resistivity* of the manufactured parts. This was tested by placing identical pieces (in this case Structure 2) in a series of different solvents. Both the test structures (Figure 3-8) and the solvents (Table 3-6) were closely observed.

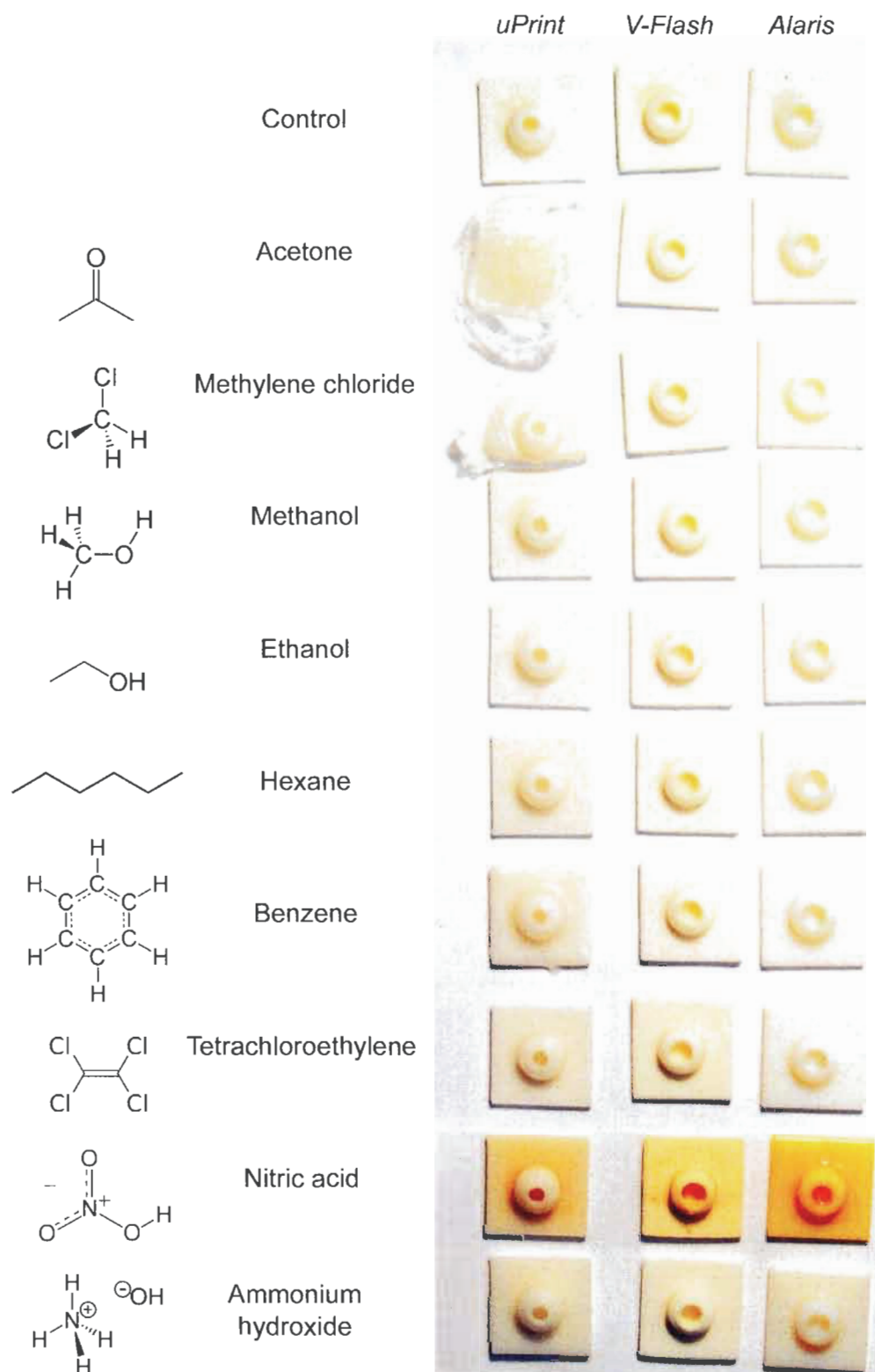





Figure 3-8. Chemical resistivity study effect on structures. Photographs of 30 structures after exposure to different solvents.

Table 3-6. Chemical resistivity solvent testing (visual and UV-Vis spectra observations)

	 <i>uPrint</i> by <i>dimension</i>		 <b>Flash</b> DESKTOP MODELER FTI 230			
	Stratasys ABSplus (ABS plastic)		FTI-GN Material (Photopolymer)		FullCure830 (Photopolymer)	
	Visual of solvent	UV-Vis spectra	Visual of solvent	UV-Vis spectra	Visual of solvent	UV-Vis spectra
Acetone	Cloudy grey	Broad intense abs.	----	Slight increase in abs.	----	Slight increase in abs.
Methylene chloride	Bubbles	Broad abs.	----	Increase in abs	----	Slight increase in abs
Methanol	----	----	----	Slight increase in abs.	----	Slight increase in abs
Ethanol	----	----	----	Slight increase in abs.	----	Slight increase in abs
Hexane	----	----	----	----	----	----
Benzene	----	Large increase in abs.	----	Slight increase in abs.	----	Increase in abs.
Tetrachloro- ethylene	----	----	----	----	----	----
Nitric Acid	Slight colour change	Slight increase in abs.	Slight colour change	Slight increase in abs.	Colour change	Increase in abs.
Ammonium Hydroxide	----	----	----	----	----	----

Blank subtracted UV-Vis spectra for each solvent were compared and the relative broadband increase in absorption was used as a qualitative indicator of the level of dissolution.

Among the worst performing combination of material and solvent is the structures produced in ABS plastic by the *uPrint* with acetone, methylene chloride and benzene. A closer visual comparison shown in Figure 3-9 clearly

demonstrates the ABS plastic dissolved to different degrees in these three solvents. Not surprising, the ABS plastic pieces manufactured by the *uPrint* did not resist well to acetone and methylene chloride, two commonly used polar solvents for chemically bonding plastic pieces together. The methylene chloride was also observed to adversely affect the *Alaris* part and resulted in absorbance readings of the solvent for both the *Alaris* and *V-Flash*. All three parts exposed to concentrated nitric acid suffered discolouration while maintaining structural integrity. Overall, the chemical resistivity of the *V-Flash* and the *Alaris* mirrored each other due to the similar cross-linked photopolymer composition. Hexane, tetrachloroethylene and ammonium hydroxide were not observed to react with any of the three parts.

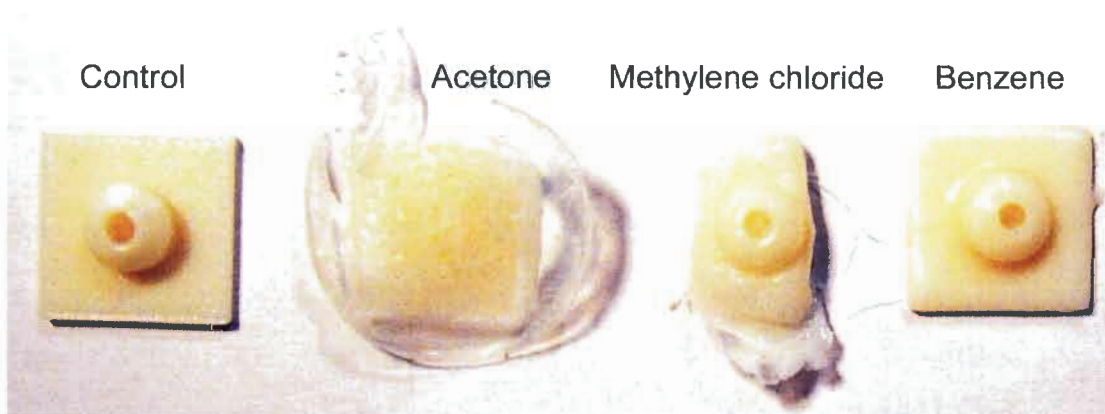


Figure 3-9. Selection of structures manufactured by the *uPrint* by FDM technology after chemical resistivity testing.

#### 3.4.3.3 Study 3: Ability to “Print” Capillary Burst Valves

A key feature of most centrifugal microfluidic devices is the valve system which controls the movement of liquid from one reservoir to the next. Three of the four test structures were designed and manufactured to provide insight into the printers' ability to consistently manufacture capillary burst valves. Structure 1 included an open-faced view of square microchannels, Structure 3 included both square and round channels and Structure 4 integrated the channels as capillary burst valves in an all-in-one test structure of a working centrifugal device to be used straight from the printer. Series of photographs of Structure 1 and Structure 3 are provided in Figure 3-10 and Figure 3-11 respectively.

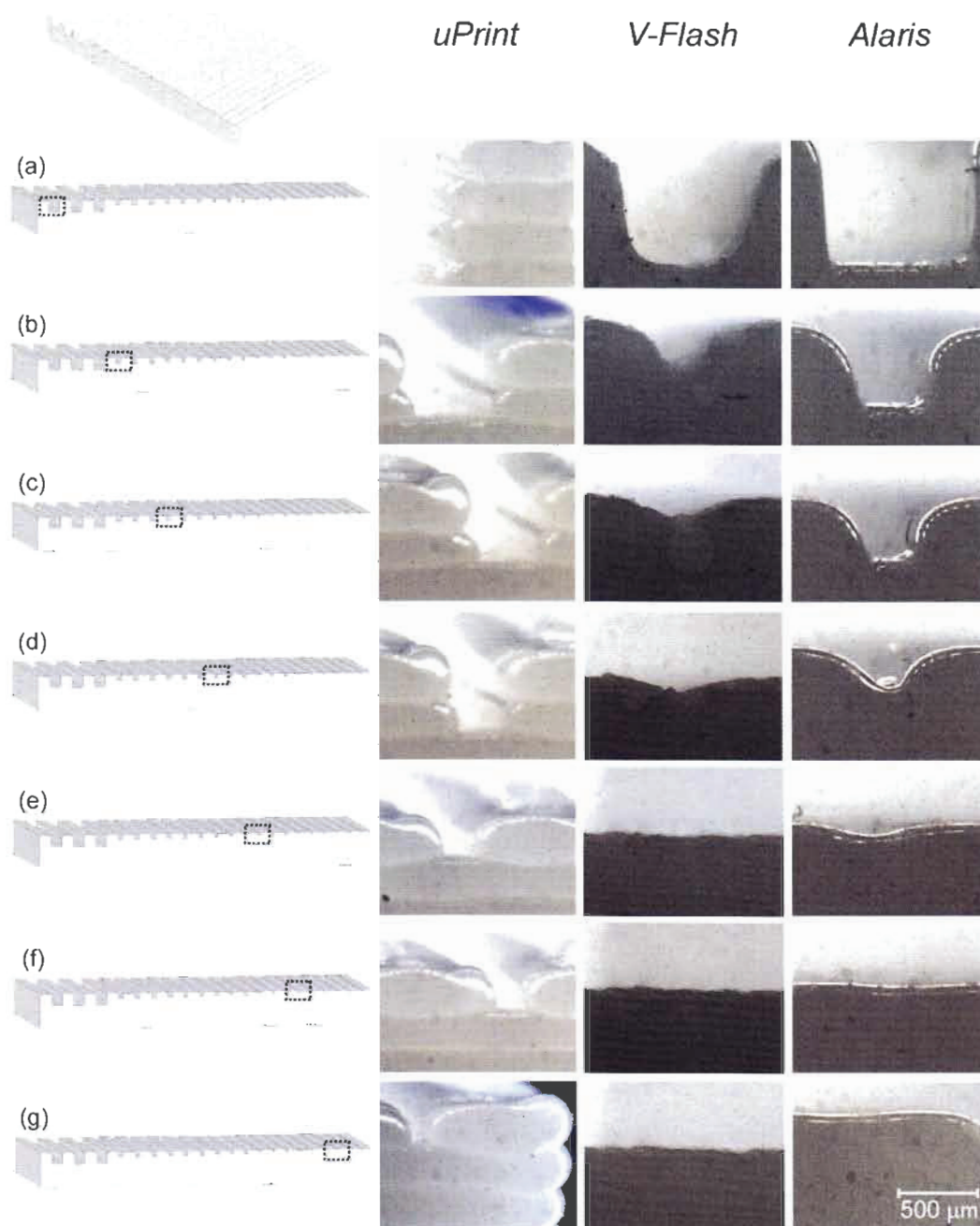


Figure 3-10. Structure 1 at 150x magnification. Dotted rectangles on the left hand drawings represents the magnified area shown in each photograph on the right. Designed dimensions were of (a) 1000 x 1000  $\mu\text{m}$  (b) 500 x 500  $\mu\text{m}$  (c) 400 x 400  $\mu\text{m}$  (d) 300 x 300  $\mu\text{m}$  (e) 200 x 200  $\mu\text{m}$  (f) 150 x 150  $\mu\text{m}$  (g) 100 x 100  $\mu\text{m}$ .

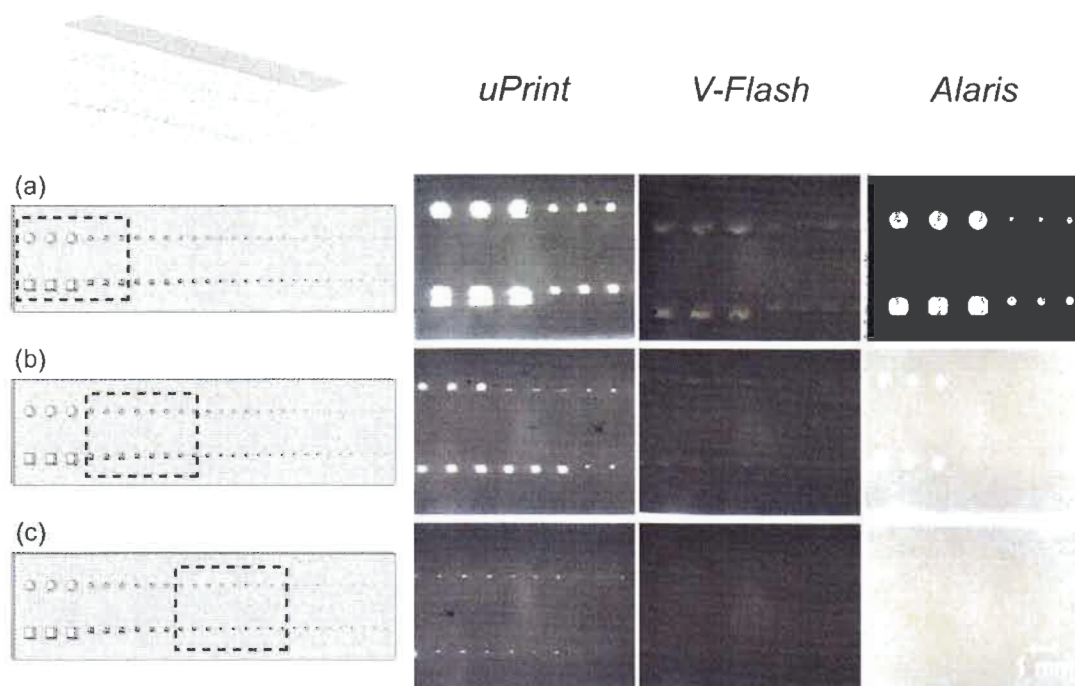


Figure 3-11. Structure 3 at 16.8x magnification. Dotted rectangle on the left hand drawing represents the magnified area shown in each photograph on the right. (a) Magnified view of 1000 and 500  $\mu\text{m}$  round and square sets of three channels. (b) Magnified view of 500, 400 and 300  $\mu\text{m}$  sets of three channels. (c) Magnified view of 300, 200, 150  $\mu\text{m}$  sets of three channels. The smaller 100, 75 and 50  $\mu\text{m}$  sets of three channels are not observed in any all three printers

The purpose of these test structures was to push the limits of each printer starting with dimensions they were thought able to process and moving smaller and smaller with the final dimensions meant to fail. All three printers were able to print the 1000  $\mu\text{m}$  open-faced channels (Figure 3-10a); however, the *V-Flash* was not able to print channels of this dimension (Figure 3-11a). Though light was observed through the *V-Flash* channels, these were all sealed, failing this test even at the larger dimensions.

The *Alaris* performed exceptionally well with channels of 1000  $\mu\text{m}$  and 500  $\mu\text{m}$  and was able to print open-faced channels down to 300  $\mu\text{m}$ . Anything smaller seemed not to have been processed by the proprietary printing software.

In other words what it printed it printed well but it did not print very small channels.

Meanwhile the *uPrint* was unique with its attempts to print even the smallest structures. The *uPrint* was limited to printing features to an integral number of strands (each strand being 254  $\mu\text{m}$  wide). For example, the open-faced channels in Figure 3-10a, the 1000  $\mu\text{m}$  channel was printed as four strands high which in reality came out to be 1016  $\mu\text{m}$  (254  $\mu\text{m}$  x 4 strands). Similarly, the 500, 400 and 300  $\mu\text{m}$  channels were all printed as two strands (508  $\mu\text{m}$ ), and the 200, 150 and 100  $\mu\text{m}$  were all printed as one strand (254  $\mu\text{m}$ ). What was impressive was the *uPrint's* ability of leaving small open areas between printed features. The spaces between the printed strands in the open-faced channels were measured to be approximately 992, 498, 380, 290, 230, 180 and 106  $\mu\text{m}$  which were much closer to the designed dimensions of 1000, 500, 400, 300, 200, 150, 100  $\mu\text{m}$ . The *uPrint* performed equally well with channels in Structure 3 (Figure 3-11), albeit not perfectly round, being observed down to 150  $\mu\text{m}$ . This *uPrint* channel had an area five times smaller than the area of the smallest channel the other printers were able to manufacture (500  $\mu\text{m}$  on *Alaris*).

Structure 3 was also used to compare the ability of the printers to manufacture round and square channels. The *V-Flash* was not able to produce either, while the *uPrint's* channels were very similar to one another but were neither round nor square due to the combination of circular strands used to manufacture the channels. The *Alaris* on the other hand produced very interesting results. As seen in Figure 3-12, the *Alaris* very accurately produced round channels and was able to produce a somewhat square 1000  $\mu\text{m}$  channel

while both round and square designs resulted in being printed round at 500  $\mu\text{m}$ . As Cheong *et al.* mention, the PJM drop printing technology has an intrinsic round shape profile.<sup>18</sup> This is also seen on the edges of the open-faced *Alaris* channels in Figure 3-10.

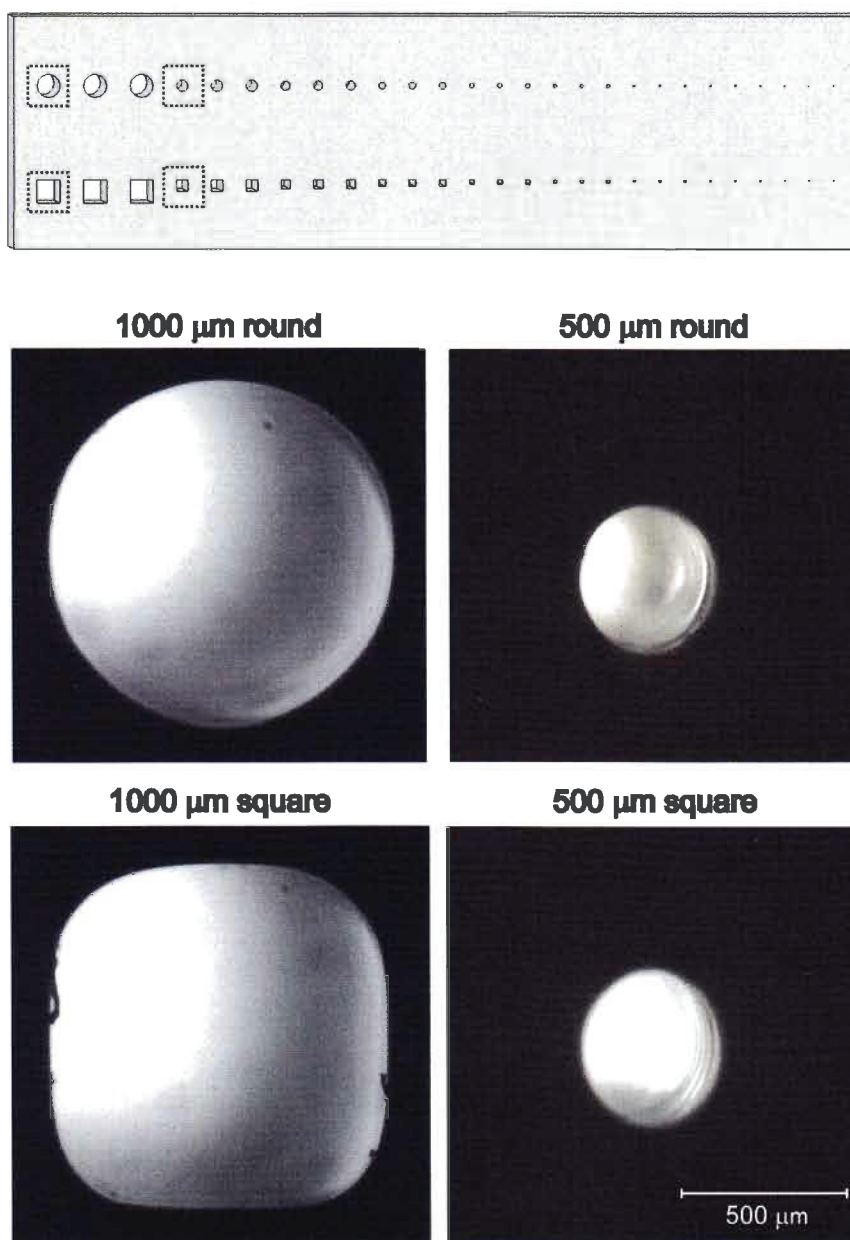


Figure 3-12. Structure 3 comparison of round and square channels of *Alaris part*. Top drawing shows drawing with dotted highlighted channels photographed below.

Finally, Structure 4 was tested to 1) determine if the printers were able to “print” the valves and 2) determine the values of the capillary burst valves frequencies. Based on the other structures described above, both the *uPrint* and the *Alaris* had the greatest potential for success; however, integrating the channels as capillary burst valves in an all-in-one test structure of a working centrifugal device to be used straight from the printer proved challenging for different reasons for each printer.

First, the *uPrint* did seem to effectively print capillary burst valves down to 150  $\mu\text{m}$  as it did for Structure 3. Unfortunately, due to its inability to effectively retain liquids in the integrated reservoir, and worse still when centrifugal pressure was applied by rotating the device on the testing stage, the solvent traveled *between the printed layers of the device*. There was even a noticeable colour change in the device as the coloured water used in this experiment soaked through the disk. There would be a definite need for post-production treatment of *uPrint* devices to seal the reservoirs without sealing the valves.

Second, the *V-Flash* did not provide nearly enough resolution in order to manufacture such fine structures. It was not able to print the features in the simplified test structures 1 and 3 and it was not able to print the integrated capillary burst valves of Structure 4.

Third, from the observations of Structure 1, 2 and 3, the *Alaris* seemed to have the best potential for success, at least at the larger sized valves. Though the 500  $\mu\text{m}$  channels were effectively printed, dry gel support or partly cured photopolymer clogged all of the reservoirs as seen in Figure 3-13 obstructing the burst valve frequency testing. Due to the overhanging lid of the integrated

reservoir this material seemed to have been required as support. Unfortunately neither the manufacturer nor we were able to remove it. Optimizing printing parameters or changing the design might fix this and allow for successful capillary valves to be printed and used.

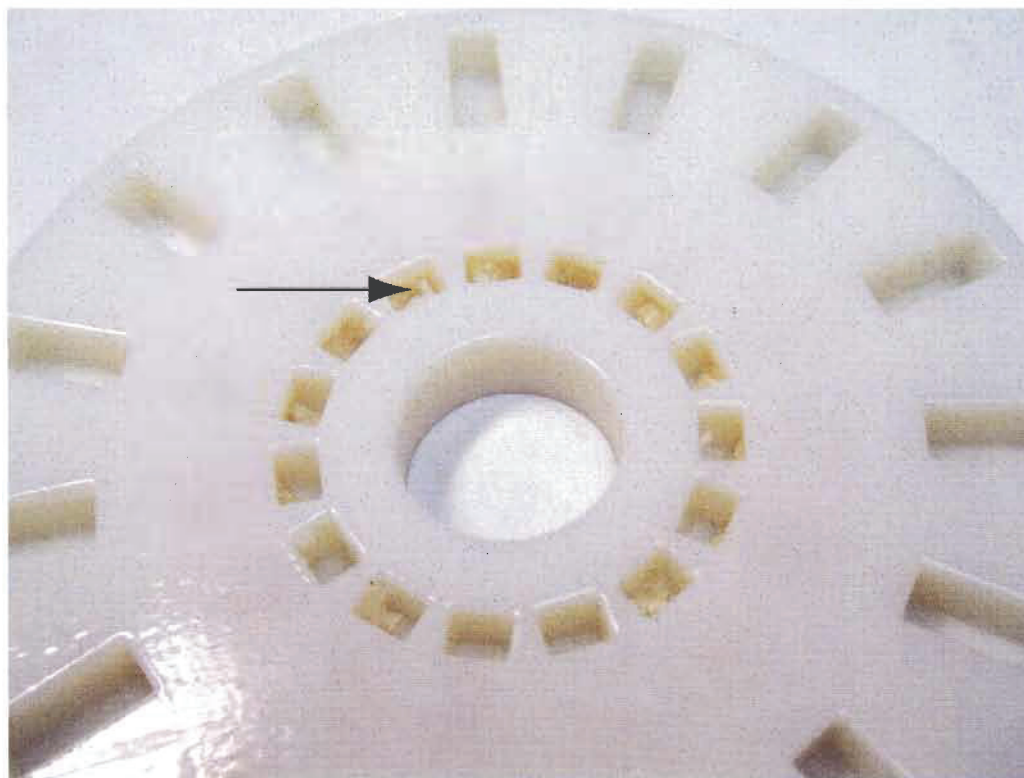





Figure 3-13. Structure 4 built on *Alaris* printer showing material blocking reservoirs and valves.

### 3.4.4 Summary of Results

Based purely on the manufacture's specifications (Table 3-3), one may have concluded that the *V-Flash* was the most suitable 3D printer for centrifugal microfluidics because of its 768 x 1024 x 2000 dot per square inch resolution. Our study indicated that this was not the case. A summary of results of the

studies empirically scoring each printer is presented in Table 3-7. Our general results agree with those from industrial benchmark tests<sup>23</sup> although our tests were specifically focused on questions involving centrifugal microfluidic applications.

Table 3-7. Scorecard comparing 3D printers

			
Precision	8/10	6/10	9/10
Accuracy	8/10	7/10	9/10
Ability to retain liquid	0/5	5/5	5/5
Surface finish	6/10	5/10	9/10
Chemical resistivity	5/10	8/10	8/10
Ability to print capillary valves	8/10	1/10	7/10
Total	35/55	32/55	47/55
%	64%	58%	85%

The question these studies attempted to answer was: “What is the best 3D printer for the fabrication of centrifugal microfluidic devices?” The *V-Flash* was the least able to provide the required fine structures and surface finish. The *uPrint* showed potential with very small spacing between printed strands in the x and y axes effectively creating capillary burst valves. Although “uPrint” probably stands for “you” Print, when it comes to the empty space between strands it could rightfully stand for “micro” Print. Unfortunately, the *uPrint*’s score was very much hindered by weaker chemical resistivity, its inability to retain liquids and

intermediate surface finish. The latter two might be overcome by some sort of post-production treatment. The top ranked 3D printer for centrifugal microfluidic research was therefore the *Alaris* with its superior accuracy and precision and smooth surface finish. It also showed potential in printing functional capillary burst valves producing fine structures intermediate in size between those of the *uPrint* and the *V-Flash*. Working with the manufacturer to print smaller valves and to more effectively remove support structure will make this printer the best option for application in the centrifugal microfluidic field. Future studies with this technology, perhaps with the next generation *Alaris* printer, are well warranted.

### **3.5 Conclusions**

Three different additive manufacturing techniques of 3D printing were compared and the merits of each technology investigated for use in centrifugal microfluidics. The 3D structures were designed to push the limits of each printer. Performance parameters included precision, accuracy, ability to retain liquids, surface finish, chemical resistivity and ability to “print” capillary burst valves. With this deeper understanding, a clearer choice of 3D printer for the specific application to centrifugal microfluidic device prototyping and manufacturing was possible.

These printers allowed for fast, all-in-one builds and geometries not previously possible by milling. Unfortunately, no one printer was able to provide all of the desired characteristics. The *Alaris* performed best but did not print as small a channel as desired whereas the *uPrint* had issues with seepage and surface finish. It was also concluded that the *V-Flash* currently does not

manufacture parts of the required size and finish, though the recent acquisition of the Z-Corporation technology by 3D systems may warrant future testing.

Disadvantages of the 3D printers include limitation to the size of features that can be printed depending on the resolution of the printer. Alternatively, two framework pieces could be printed and micro-features such as capillaries and even electronics could be added before sealing the two parts together. Another limitation is that the produced structures are typically opaque. If integrated spectroscopic detection is desired, spaces for optically transparent plastic, glass or quartz viewing windows would need to be included in the design.

In view of the success of Structure 1 in which open-faced channels were printed and no support material interfered with their functionality, open-faced devices which are then sealed with simple adhesive could be used to produce functional capillary burst valves such as the work by Moore *et al.*<sup>22</sup>

For the moment, it would seem that a hybrid of technologies is the best alternative with only sections of the devices being produced by additive manufacturing and other by subtractive manufacturing (such as the device discussed in Chapter 4).

Future work will take advantage of the blooming 3D printer technology such as that demonstrated here and by the use of other evolving technology such as high resolution Digital Light Processing (DLP) projectors.<sup>27</sup> This technology has already moved beyond rapid prototyping into the additive manufacturing of parts which can be used directly in end-user applications and are durable. Though no conclusive 3D printer was suggested as a result of the current study,

we still believe that this technology will soon fundamentally alter the way many centrifugal microfluidic systems are designed and manufactured.

### 3.6 References

- (1) Bouchard, A.P., Duford, D.A., Salin, E.D., "Non-contact Addition, Metering, and Distribution of Liquids into Centrifugal Microfluidic Devices in Motion", *Analytical Chemistry*, **2010**, 82 (20), 8386-8389.
- (2) ASTM Standard F2792, 2010e1, Subcommittee F42.91, "Standard Terminology for Additive Manufacturing Technologies," ASTM International, 100 Barr Harbor Drive, West Conshohocken, PA 19428, 2010, DOI: 10.1520/F2792-10E01.
- (3) Langnau, L., "Tips on Selecting 3D printers", *Design World*, **2008**, 5 (8), 20-28.
- (4) Vance, A., "3-D Printing Spurs a Manufacturing Revolution", *The New York Times*, **2010**, September 13, A1.
- (5) Tarnita, D., Berceanu, C., Tarnita, C., "The three-dimensional printing - A modern technology used for biomedical prototypes", *Materiale Plastice*, **2010**, 47 (3), 328-334.
- (6) Hart, G.W., "Reticulated geodesic constructions", *Computers and Graphics (Pergamon)*, **2000**, 24 (6), 907-910.
- (7) Wohlers, T., "Additive Manufacturing 101: Part III", *Time Compression*, **2010**, May/June.
- (8) Dittrich, P.S., Tachikawa, K., Manz, A., "Micro total analysis systems. Latest advancements and trends", *Analytical Chemistry*, **2006**, 78 (12), 3887-3907.
- (9) Haeberle, S., Zengerle, R., "Microfluidic platforms for lab-on-a-chip applications", *Lab on a Chip - Miniaturisation for Chemistry and Biology*, **2007**, 7 (9), 1094-1110.
- (10) Mark, D., Haeberle, S., Roth, G., Stetten, F.v., Zengerle, R., "Microfluidic lab-on-a-chip platforms: requirements, characteristics and applications", *Chemical Society Reviews*, **2010**, 39 (3), 1153-1182.
- (11) Gorkin, R., Park, J., Siegrist, J., Amasia, M., Lee, B.S., Park, J.M., Kim, J., Kim, H., Madou, M., Cho, Y.K., "Centrifugal microfluidics for biomedical applications", *Lab on a Chip - Miniaturisation for Chemistry and Biology*, **2010**, 10 (14), 1758-1773.
- (12) Madou, M., Zoval, J., Jia, G., Kido, H., Kim, J., Kim, N., "Lab on a CD", *Annual Review of Biomedical Engineering*, **2006**, 8 601-628.
- (13) Ducrée, J., Haeberle, S., Lutz, S., Pausch, S., Von Stetten, F., Zengerle, R., "The centrifugal microfluidic Bio-Disk platform", *Journal of Micromechanics and Microengineering*, **2007**, 17 (7), S103-S115.
- (14) Duffy, D.C., McDonald, J.C., Schueller, O.J.A., Whitesides, G.M., "Rapid prototyping of microfluidic systems in poly(dimethylsiloxane)", *Analytical Chemistry*, **1998**, 70 (23), 4974-4984.

- (15) Hecke, M., Bacher, W., Müller, K.D., "Hot embossing - The molding technique for plastic microstructures", *Microsystem Technologies*, **1998**, 4 (3), 122-124.
- (16) Kido, H., Zoval, J., Madou, M., "Rapid prototyping of microfluidic systems", *ECS Transactions*, **2006**, 4 101-105.
- (17) Bartholomeusz, D.A., Boutté, R.W., Andrade, J.D., "Xurography: rapid prototyping of microstructures using a cutting plotter", *Microelectromechanical Systems, Journal of*, **2005**, 14 (6), 1364-1374.
- (18) Cheong, W.C., Kuan, Y.K., Li, M.H., Ying, J.Y., "Rapid prototyping of multi-level polydimethylsiloxane-based microfluidic devices", presented at *Proceedings of SPIE - The International Society for Optical Engineering*, Melbourne, December 10-12th 2008, **2008**.
- (19) Maher, P.S., Keatch, R.P., Donnelly, K., "Characterisation of rapid prototyping techniques for studies in cell behaviour", *Rapid Prototyping Journal*, **2010**, 16 (2), 116-123.
- (20) Bonyár, A., Sántha, H., Ring, B., Varga, M., Kovács, J.G., Harsányi, G., "3D Rapid Prototyping Technology (RPT) as a powerful tool in microfluidic development", presented at *Procedia Engineering*, **2010**, 291-294.
- (21) Waldbaur, A., Rapp, H., Länge, K., Rapp, B.E., "Let there be chip - Towards rapid prototyping of microfluidic devices: One-step manufacturing processes", *Analytical Methods*, **2011**, 3 (12), 2681-2716.
- (22) Moore, J.L., McCuiston, A., Mittendorf, I., Ottway, R., Johnson, R.D., "Behavior of capillary valves in centrifugal microfluidic devices prepared by three-dimensional printing", *Microfluidics and Nanofluidics*, **2011**, 10 (4), 877-888.
- (23) Grimm, T., "3D Printer Benchmark: North American Edition"; T.A. Grimm & Associates, Inc.: Edgewood, Kentucky, USA, **2010**, 1-61.
- (24) Ippolito, R., Iuliano, L., Gatto, A., "Benchmarking of Rapid Prototyping Techniques in Terms of Dimensional Accuracy and Surface Finish", *CIRP Annals - Manufacturing Technology*, **1995**, 44 (1), 157-160.
- (25) Chang, D.Y., Huang, B.H., "Studies on profile error and extruding aperture for the RP parts using the fused deposition modeling process", *International Journal of Advanced Manufacturing Technology*, **2011**, 53 (9-12), 1027-1037.
- (26) Ogónczyk, D., Węgrzyn, J., Jankowski, P., Dąbrowski, B., Garstecki, P., "Bonding of microfluidic devices fabricated in polycarbonate", *Lab on a Chip - Miniaturisation for Chemistry and Biology*, **2010**, 10 (10), 1324-1327.
- (27) Zhou, C., Chen, Y., Epstein, D.J., "Additive manufacturing based on multiple calibrated projectors and its mask image planning", *Proceedings of the ASME Design Engineering Technical Conference* **2010**, 1 439-449.

## CHAPTER 4: Non-Contact Addition, Metering, and Distribution of Liquids into Centrifugal Microfluidic Devices in Motion

Hybrid devices incorporating pieces made by both subtractive (Chapter 2) and additive (Chapter 3) manufacturing are shown in this fourth chapter. Exploiting the advantages of each manufacturing technique, the resulting hybrid devices can be quickly manufactured to include both 3D structures and clear cells for viewing. This chapter also tackles the difficulties of interfacing centrifugal microfluidic devices to the laboratory by introducing liquids to spinning devices. The new term “World-to-Disk” is introduced in this chapter to parallel the term “World-to-Chip” used to describe the interfacing to microfluidics device. The described hybrid devices are also a very enabling technology to do simple chemistry while having the potential to allow more advanced gradient chromatography on centrifugal microfluidic devices.

The work presented in this chapter was originally published and is *reproduced with permission from*:

Bouchard, A.P.\*, Duford, D.A.\*, Salin, E.D., "Non-contact Addition, Metering, and Distribution of Liquids into Centrifugal Microfluidic Devices in Motion", *Analytical Chemistry*, **2010**, 82 (20), 8386-8389. Copyright 2010, American Chemical Society.

\* These authors should be considered equal contributors.

This paper had immediate impact with Figure 4-2 being reproduced and highlighted by Petra S. Dittrich<sup>1</sup> (co-worker of Andreas Manz) in the journal “Lab on a Chip” under the subtitle “*World-to-Disk interface for microfluidic devices with disk format*”.

Figure 4-4 was originally published as supporting information but has been placed in the text in this thesis. Also published as supporting information was Video S-1 to which a link is available in Appendix D. The video includes 1) the CLAD being built with a *uPrint* printer 2) chemical bonding with acetone, 3) 3D views of the hybrid device and 4) a collection of high speed digital images of the deposition process. Additional designs and experimental details are also available in Appendix C.

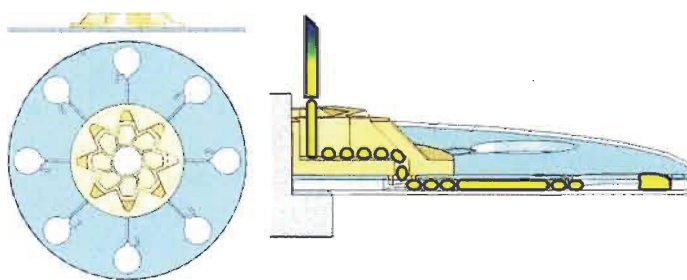


Figure 4-1. Journal's table of content figure of CLAD

- (1) Dittrich, P.S., "Research highlights", *Lab on a Chip - Miniaturisation for Chemistry and Biology*, **2010**, 10 (22), 3011-3012.

## 4.1 Abstract

A three-dimensional structure was constructed to demonstrate contact-free liquid addition and distribution to a conventional centrifugal microfluidic platform. The structure allowed a continuous stream of liquid to be added to the rotating platform where it was dispensed and metered to a series of reservoirs with 9% relative standard deviation of the volume. An off-platform generated gradient was used to demonstrate this design's potential to make gradient centrifugal microfluidic chromatography possible without the use of platform space for liquid storage. The system demonstrates a convenient and versatile "World-to-Chip" or more appropriately, *World-to-Disk*, macro-to-micro interface.

## 4.2 Introduction

In microfluidics, there is a generally recognized problem involving the challenge of interfacing to microfluidic systems.<sup>1</sup> This is sometimes called the "World-to-Chip" problem<sup>2, 3</sup> which, in regards to centrifugal microfluidic platforms,<sup>4-6</sup> we call the *World-to-Disk* problem. This problem includes both pumping liquids in the systems and the addition of samples and reagents to the systems. In regards to pumping, centrifugal systems do not require pump connections to be made for liquid movement due to the inherent centrifugal force. In regards to the addition of liquids, traditionally they have been added beforehand and stored on the disks; however, a practical concern is the shelf-life of these reagents on a preloaded disk. When liquid reagents are placed in a disk, the disk lifetime may be quite short as evaporation and condensation can take place through either vent holes or channels. An alternative is to use

preloaded solid reagents;<sup>7</sup> however, such systems still require the addition of liquid to reconstitute the solid reagents and are at times difficult to manufacture. It is possible at analysis time to add reagents using syringes or possibly other interfaces;<sup>8</sup> however, these techniques require stopping a centrifugal microfluidic platform which can then result in uncontrolled liquid movement. Others have addressed the *World-to-Disk* problem using prefilled ampoules and reservoirs, taking up precious space on the limited size platform.<sup>9</sup>

Space is an important limitation on centrifugal microfluidic systems, and it is called the *real estate* or “footprint” problem.<sup>4</sup> Since centrifugal microfluidic operations are dominated by centrifugal force, the flow must generally move radially outward (“down”) on the platform. Given that reservoirs, transfer channels, mixing chambers, valves, and other structures must take up space on a limited size platform, there is a finite limit to the number of sequential operations that can be implemented on a disk.

Timing of liquid movement from operation to operation is usually controlled by valves in centrifugal microfluidic systems. While some other valve types are used on disks, capillary based passive valves<sup>4</sup> are the most commonly employed. The precision of the valve fabrication dictates to a large extent the range of frequencies over which they will burst. Since the valves at various locations in the platform must burst in a specific sequence, the range of burst frequencies, particularly in prototyping situations, constitutes a significant constraint on the number of valves that can be used in one radially outward centrifugal operational sequence.<sup>6</sup>

The problems posed above could be reduced or overcome if reagents could be added equally to multiple chambers while the disk is rotating. The rotation is critical in many cases, because it provides the force needed to take fluids where the designer intended while minimizing bubble formation, wicking and capillary action. Furthermore, if reagents could be added while the device was operating, there would be no need to have reagent reservoirs or valves. If the reagents could be mixed externally, then there would be some reduction of the need for mixing operations. Indeed, external mixing of reagents would allow dynamic development of the complex mixtures that are at the heart of many separation techniques. Anderson<sup>10</sup> reported a system 40 years ago designed for loading a rotating tray of centrifuge tubes with a density gradient. More recently, Andersson<sup>11</sup> described in a patent application a complex non-contact dispensing system that was capable of depositing droplets into a spinning microfluidic device. The system required careful calibration for fluids with different physical properties. In a mixing experiment, Haeberle<sup>12</sup> showed continuous addition of two liquids to a spinning microfluidic platform; however, they did not demonstrate the ability to distribute these liquids to multiple sets of chambers.

To improve the *World-to-Disk* interface, we introduce here a technique that allows liquid to be transferred directly into a rotating microfluidic platform while simultaneously distributing the liquid into separate microfluidic structures. We believe that this technique can fundamentally alter the way centrifugal microfluidic platforms are designed and increase the number of operations possible.

## **4.3 Experimental Section**

### **4.3.1 Reagents**

Samples were distilled deionized water (DDW) dyed with commercial yellow and blue food coloring. Reagent grade acetone was used to chemically bond plastic parts together.

### **4.3.2 Device Design and Fabrication**

The device was made of two main components: a top Centrifugal Liquid Addition Distributor (CLAD) and a conventional centrifugal disk base. All components were designed in the three dimensional (3D) computer-aided design software “SolidWorks” (SolidWorks Corp., Concord, MA, USA).

#### *4.3.2.1 Centrifugal Liquid Addition Distributor (CLAD)*

The CLAD, as its name implies, was responsible for liquid collection and distribution. This component was fabricated by an additive manufacturing process known as 3D printing using a “*uPrint*” 3D printer (Dimension Inc., MN, USA) which extruded layers of heat sealed strands of proprietary “*ABSplus*” plastic (see video in Supporting Information).

As seen in Figure 4-2, the CLAD was built with eight sections, each made up of a cup and hole (Figure 4-2a(i,ii)). Each hole was at the convergence of the cup walls and went through the CLAD to the underside via a hole extended by a corresponding extruded cylinder (hollow peg; Figure 4-2a(iii)). The cylinders served to (1) align the CLAD component with the disk base component, (2) allow liquid to enter the disk base without escaping between layers, and (3) prevent the sealing of the holes during the chemical bonding of the components. The centre

hole (Figure 4-2a(iv)) is of the same radius as that of the disk base, allowing the composite platform to fit securely on the motor's spindle shaft (see Figure 4-3).

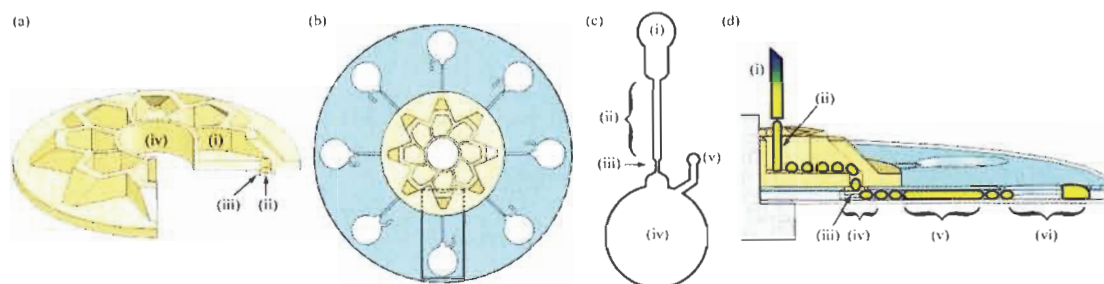


**Figure 4-2.** (a) Cut isometric view of Centrifugal Liquid Addition Distributor (CLAD) including (all in mm): (i) cup, (ii) hole (radius 1.0), (iii) peg (inner radius 1.25, outer radius 1.75) and (iv) centre hole (radius 7.5). (b) Top view of centrifugal microfluidic platform including CLAD and disk base (radius 60.0 mm) – highlighted rectangle is enlarged in (c). (c) Disk base features: (i) Receiving Reservoir (radius 2.59 x 1.40 deep), (ii) Viewing Channel (1.00 wide x 1.40 deep x 10.50 long), (iii) Flow Choke (0.40 wide x 0.10 deep x 1.41 long), (iv) Collection Reservoir (radius 7.00 x 1.40 deep), (v) vent. (d) Cut side view drawing of liquid deposition mechanism: (i) Peristaltic pump tubing, (ii) continuous stream of liquid broken by rough surface of CLAD, (iii) hole in CLAD cup into disk base, (iv) Receiving Reservoir, (v) Viewing Channel and (vi) Collection Reservoir.

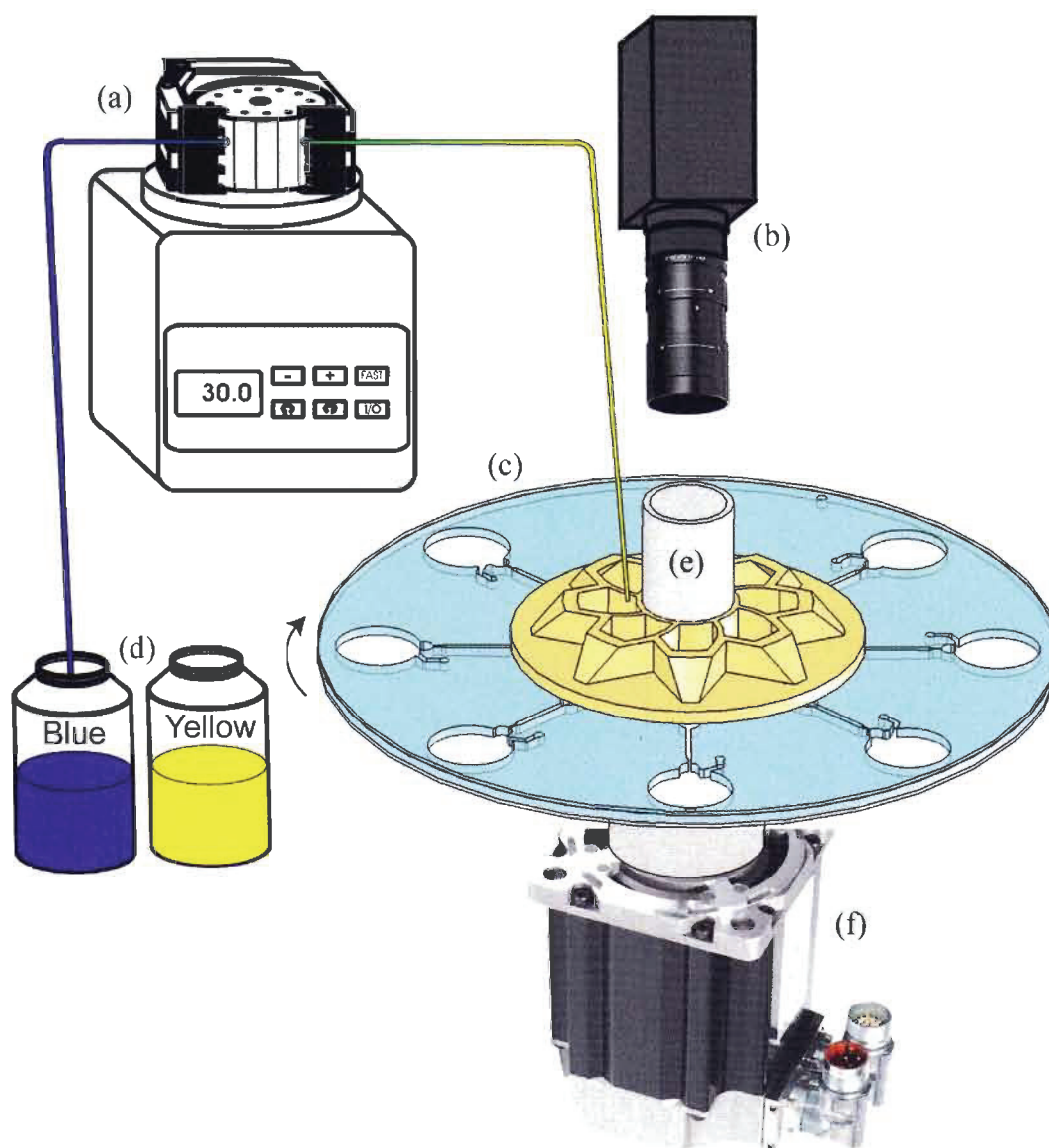


Figure 4-3. Schematic of experimental setup. (a) Peristaltic pump and tubing, (b) camera and lens, (c) centrifugal microfluidic platform including CLAD and disk base, (d) beakers containing dyed water samples, (e) spindle shaft, and (f) servo motor.

#### 4.3.2.2 Centrifugal Disk Base

The conventional centrifugal disk base was responsible for viewing and storing the added liquid. This component was fabricated by a subtractive manufacturing process by milling features out of polycarbonate. A detailed description of the technique and materials is available elsewhere.<sup>13</sup>

The centrifugal disk base (Figure 4-2b,c) is designed with eight sets of features, each containing a Receiving Reservoir, a Viewing Channel, a Flow Choke, a Collection Reservoir and a vent. The Receiving Reservoirs are at the precise locations to accommodate the pegs from the CLAD and act as the female counterparts to the male pegs of the CLAD. The liquid that the CLAD captures and distributes flows through these pegs to the Receiving Reservoirs and then down the Viewing Channel. The liquid flow is restricted by the Flow Choke before entering the Collection Reservoir (Figure 4-2d). These two main components (the CLAD and the disk base) were chemically bonded with acetone to form the complete centrifugal microfluidic platform (see video in Supporting Information).

#### 4.3.3 Instrumentation

In order to optimize the design and performance of the device, it was necessary to control the liquid deposition as the platform rotated. This was facilitated by having all of the system's components controlled by a single computer program. High speed digital images of the experiments were recorded with a color CCD camera (GRAS-14S5C-C, Point Grey, BC, Canada) using a motorized stage and strobe system developed by Duford *et al.*<sup>14</sup>. To that system, a peristaltic pump (Minipuls 3 Model 312, Gilson Inc., WI, USA) was added

(Figure 4-3). All of these components (pump, servo motor, camera and strobe) were synchronized, triggered and controlled via the same LabVIEW program (LabVIEW 8.6, Developer Version, National Instruments, QC, Canada).

A color gradient from yellow to green to blue was produced off-platform as yellow and blue dyed DDW were mixed in the peristaltic pump tubing. The amount of liquid transferred per unit time was gravimetrically calibrated to be  $7.67 \pm 0.03$  mL/min. A total of 1.84 mL was pumped onto the platform over 14.5 seconds. The stream was unbroken when leaving the tubing and oriented perpendicular to the CLAD surface at a radius of 10.5 mm from the platform centre, and 1.5 mm higher than the CLAD cup (see Figure 4-2d and Figure 4-3).

#### **4.4 Results and Discussion**

The CLAD has been developed with its holes at a radius of 23.0 mm, a value that can be decreased in future designs. It has a small “footprint” leaving 85% of the disk area available for subsequent operations.

##### **4.4.1 Liquid Addition and Distribution**

The peristaltic pump was used to meter a precise volume of liquid while the CLAD distributed this volume into eight sets of chambers. Figure 4-2d and Figure 4-3 illustrate the design and operation of the device indicating how the liquid was added to the rotating centrifugal platform and how it followed the designed pathway. The design did not rely on chemical or physical properties of the liquid or of the building material and can, therefore, distribute a large variety of liquids.

The CLAD's design successfully distributed a continuous liquid stream into eight parts, transferring nearly all added liquid into the underlying centrifugal disk base. For the study below (Table 4-1), the volume measurements in the Viewing Channel and Collection Reservoirs were made at the indicated times while still adding liquid. The disk was not spun longer or faster to clear out the system, resulting in approximately 12  $\mu\text{L}$  remaining in each of the CLAD's cups and upper parts the disk structures (e.g. Receiving Reservoir).

**Table 4-1. Liquid addition and distribution of CLAD**

Time (s)	Added volume <sup>a</sup> ( $\mu\text{L}$ per channel)	Measured average volume <sup>b</sup> ( $\mu\text{L}$ per channel)	RSD <sup>c</sup> (%)
4.9	78	68 $\pm$ 14	20
9.7	155	147 $\pm$ 16	11
14.5	232	217 $\pm$ 19	9

<sup>a</sup> Added volume calculated from calibrated flow rate of pump of 7.67 mL/min or equivalent of 16  $\mu\text{L/s}$  per channel.

<sup>b</sup> Actual volume calculated (n=8) from measuring the area on the 2D high speed images and multiplying by the thickness of the channels or reservoirs at each time interval.

<sup>c</sup> 95% confidence.

As seen in Figure 4-4 additions of as little as 15  $\mu\text{L}$  per chamber are possible. If more precise volumes are needed, a specific metering operation could be implemented in the disk base.<sup>15</sup> The use of volumes smaller than that would require special considerations (*i.e.* loss of sample by evaporation or trapped in device); however, for the intended application of the CLAD, such as the introduction of complex gradients, 15  $\mu\text{L}$  is quite small.

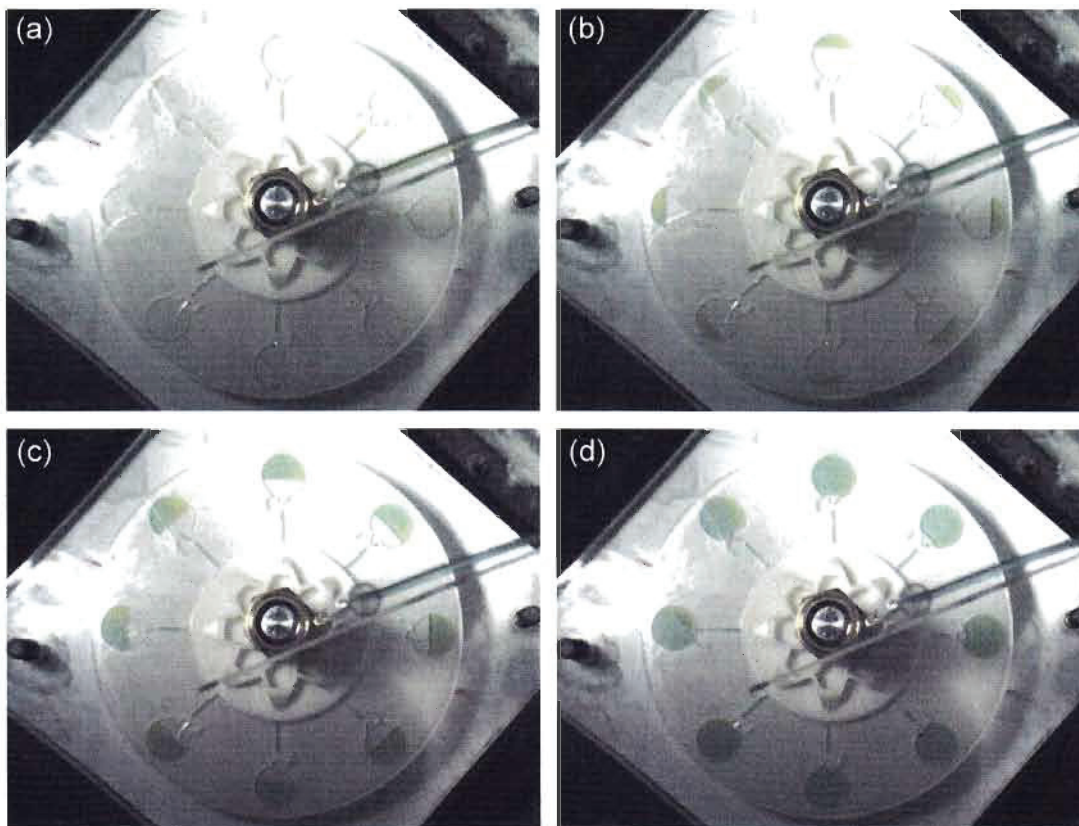


**Figure 4-4.** High speed digital images of rotating CLAD and disk base at 600 rpm (10 Hz) at varying times after pump has started showing deposition process. (a) 1.7 s illustrating minimum liquid addition of 15  $\mu\text{L}$  per channel, (b) 4.9 s, (c) 9.7 s, (d) 14.5 s.

In earlier designs it was noted that the Coriolis pseudo-force directed the flow of liquid on the CLAD surface directly into corners where it would remain somewhat trapped due to surface tension. For this reason, the walls of each cup on which the liquid made contact were designed as curves. Additionally, the design minimized the width of the walls (each wall representing only 1.6% of the total area), thereby maximizing surface area available for liquid addition. Though a small fraction of the liquid must have been added to the top of the CLAD walls, no perceivable loss was observed. This liquid appears to have flowed into one of the adjacent cups. In an ideal CLAD, no droplets would be left behind in the

distribution system. This goal was constrained by the capabilities of the *uPrint* system which generated relatively rough surfaces. A plot of volume pumped versus volume measured produced a linear least-squares regression plot with an  $R^2$  coefficient of 0.993, a slope of 1.03, and an intercept of -11.6, corresponding to the average volume of liquid (in microliters) remaining above the Viewing Channel.

#### 4.4.2 Gradient

The volume and composition of liquid added to the CLAD component was controlled off-platform (Figure 4-3). With such a configuration, adding samples, changing reagents, adding wash cycles and even adding gradients to a centrifugal microfluidic platform are easily envisioned.

For demonstration purposes, an externally generated diffusion gradient was introduced to the CLAD. This gradient solution readily flowed into the disk base Viewing Channels. Since these channels were followed by restrictive Flow Chokes, liquid movement was slowed enough to capture the images before the gradient solution flowed to the Collection Reservoirs (Figure 4-2c). The Flow Chokes required a rotational speed of 600 rpm (10 Hz) to function properly and, thus, defined the frequency. To render the DDW solutions visible, yellow and blue dyes were used to demonstrate the design's ability to deliver a solution gradient. The transition from yellow to blue is seen in Figure 4-5. The set of digital images are of a gradient change as only 220  $\mu\text{L}$  flowed through a single microfluidic Viewing Channel. This indicates that the solution gradient did not

pool on the surface of the CLAD to then travel down the hole but that the added solution flowed freely out of the CLAD to the Flow Choke.

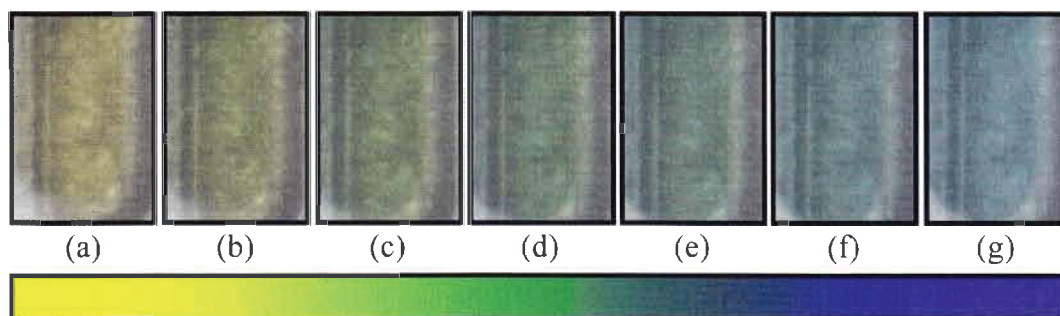


Figure 4-5. Gradient on a disk. (a-g) Series of digital images showing part of the 220  $\mu\text{L}$  Viewing Channel, from yellow to blue.

## 4.5 Conclusions

An efficient and flexible *World-to-Disk* interface for adding, metering, and distributing liquid solutions to rotating centrifugal microfluidic platforms has been built and demonstrated. The addition process was linear and the added liquid volume was reproducible to within 9% with this configuration. The CLAD design consumes only 15% of the available disk real estate. The technique should allow the miniaturization and integration of conventional complex solvent separation techniques onto centrifugal microfluidic platforms. The CLAD concept reduces the need for both valves and reservoirs on microfluidic platforms. We believe that this technique can fundamentally alter the way many centrifugal microfluidic systems are designed and implemented.

## 4.6 Acknowledgments

We thank the National Science and Engineering Council of Canada (NSERC) for scholarship support for D.A.D. and support under the Discovery Grant program.

## 4.7 References

- (1) Mariella, R., Jr., "Sample preparation: the weak link in microfluidics-based biodetection", *Biomed Microdevices*, **2008**, 10 (6), 777-784.
- (2) Fang, Q., Xu, G.M., Fang, Z.L., "A high-throughput continuous sample introduction interface for microfluidic chip-based capillary electrophoresis systems", *Analytical Chemistry*, **2002**, 74 (6), 1223-1231.
- (3) Liu, J., Hansen, C., Quake, S.R., "Solving the "world-to-chip" interface problem with a microfluidic matrix", *Analytical Chemistry*, **2003**, 75 (18), 4718-4723.
- (4) Madou, M., Zoval, J., Jia, G., Kido, H., Kim, J., Kim, N., "Lab on a CD", *Annual Review of Biomedical Engineering*, **2006**, 8 601-628.
- (5) Ducrée, J., Haeberle, S., Lutz, S., Pausch, S., Von Stetten, F., Zengerle, R., "The centrifugal microfluidic Bio-Disk platform", *Journal of Micromechanics and Microengineering*, **2007**, 17 (7), S103-S115.
- (6) Gorkin, R., Park, J., Siegrist, J., Amasia, M., Lee, B.S., Park, J.M., Kim, J., Kim, H., Madou, M., Cho, Y.K., "Centrifugal microfluidics for biomedical applications", *Lab on a Chip - Miniaturisation for Chemistry and Biology*, **2010**, 10 (14), 1758-1773.
- (7) LaCroix-Fralish, A., Clare, J., Skinner, C.D., Salin, E.D., "A centrifugal microanalysis system for the determination of nitrite and hexavalent chromium", *Talanta*, **2009**, 80 (2), 670-675.
- (8) Atencia, J., Cooksey, G.A., Jahn, A., Zook, J.M., Vreeland, W.N., Locascio, L.E., "Magnetic connectors for microfluidic applications", *Lab on a Chip - Miniaturisation for Chemistry and Biology*, **2010**, 10 (2), 246-249.
- (9) Hoffmann, J., Mark, D., Lutz, S., Zengerle, R., Von Stetten, F., "Pre-storage of liquid reagents in glass ampoules for DNA extraction on a fully integrated lab-on-a-chip cartridge", *Lab on a Chip - Miniaturisation for Chemistry and Biology*, **2010**, 10 (11), 1480-1484.
- (10) Anderson, N.G., "Computer interfaced fast analyzers", *Science*, **1969**, 166 (3903), 317-324.
- (11) Andersson, P., Jesson, G., Soderman, T., Sjoberg, J., "Method and instrumentation for micro dispensation of droplets", *US 2003/0094502 A1*, **2003**.

- (12) Haeberle, S., Brenner, T., Schlosser, H.P., Zengerle, R., Duccrée, J., "Centrifugal micromixer", *Chemical Engineering and Technology*, **2005**, 28 (5), 613-616.
- (13) Kido, H., Micic, M., Smith, D., Zoval, J., Norton, J., Madou, M., "A novel, compact disk-like centrifugal microfluidics system for cell lysis and sample homogenization", *Colloids and Surfaces B: Biointerfaces*, **2007**, 58 (1), 44-51.
- (14) Duford, D.A., Peng, D.D., Salin, E.D., "Magnetically driven solid sample preparation for centrifugal microfluidic devices", *Analytical Chemistry*, **2009**, 81 (11), 4581-4584.
- (15) Steigert, J., Grumann, M., Brenner, T., Mittenbuehler, K., Nann, T., Ruehe, J., Moser, I., Haeberle, S., Riegger, L., Riegler, J., Bessler, W., Zengerle, R., Duccrée, J., "Integrated sample preparation, reaction, and detection on a high-frequency centrifugal microfluidic platform", *Journal of the Association for Laboratory Automation*, **2005**, 10 (5), 331-341.

## CHAPTER 5: Magnetically Actuated Solid Sample Preparation for Centrifugal Microfluidic Devices

Most of the utility of centrifugal microfluidics is achieved while the devices are in motion. This motion usually precludes the use of simple direct mechanical force to alter conditions on the devices. Just like liquid samples were introduced in a non-contact manner in Chapter 4, Chapter 5 describes how mechanical movement for solid sample preparation is implemented on moving devices by a non-contact methodology. This is achieved without impairing the motion of the devices but rather by using this motion to magnetically actuate solid sample preparation. This same non-contact methodology is used to magnetically actuate liquid-solid extraction in Chapters 6 and 7. Achieving solid sample preparation on centrifugal devices is of great utility as part of a larger integrated complete analysis system which can include subsequent components such as filtering, metering, and detection with the long term objective of developing a rapid, sensitive and easy-to-use field portable instrument for environmental testing of solid samples.

Additional theoretical and experimental details in regards to the temperature increase within a chamber containing a mobile magnet is available in Appendix E. A link to the video published as supporting information is available in Appendix D. The work presented in this chapter has been published and is *reproduced with permission from:*

Duford, D.A., Peng, D.D., Salin, E.D., "Magnetically driven solid sample preparation for centrifugal microfluidic devices", *Analytical Chemistry*, **2009**, 81 (11), 4581-4584. Copyright 2009, American Chemical Society.

## 5.1 Abstract

A prototype for solid sample preparation on centrifugal microfluidic devices has been designed and characterized. The system uses NdFeB magnets in both the centrifugal device and a fixed base. As the centrifugal device rotates, the magnets move and spin in their chambers creating a pulverizing mechanical motion. This technique was successfully applied to the dissolution of potassium ferricyanide ( $K_3[Fe(CN)_6]$ ), a hard coloured crystal. A 0.10 g sample was completely dissolved in 3 seconds in 1.0 mL of water while rotating at 1000 rpm. This is a 300 fold improvement over static dissolution.

### Keywords

Solid sample preparation, Magnetic pulverization, Centrifugal microfluidics, Lab-On-a-Chip, Instrumentation

## 5.2 Introduction

In the past decade, miniaturization of classical analytical techniques has become a very active branch of research. In 2003, Janusz Pawliszyn, in his "Perspective" article titled "Sample preparation: *Quo Vadis?*" (Latin for "Where are you going?"), discussed the general trend towards smaller, autonomous sample preparation techniques which would consume less solvent, less sample and take less time to process.<sup>1</sup> That same year, Michael J. Felton previewed in his A-pages article "Lab on a chip: Poised on the brink" the clear advantages of microfluidic devices for the integration of sample processing to meet the increasing needs of modern environmental monitoring.<sup>2</sup> Noting the lack of miniature solid sample preparation techniques and the clear advantages of

microfluidic devices, these researchers, among others, admit the need for advances in solid sample preparation linking with the analytical miniaturization concept.

In recent years, growing environmental concerns have resulted in stricter legislative limits of contaminants and heightened environmental monitoring. Traditionally, solid samples are collected in the field and shipped to a laboratory for analysis. Unfortunately many current standard procedures are expensive due to the amount of time, space and labour required as well as the large amount of reagent required. The device that we discuss shows considerable potential for preparing solid samples in the field for immediate analysis by centrifugal microfluidic techniques.

### **5.2.1 Centrifugal Microfluidics**

A centrifugal microfluidic device, sometimes called a “Lab-on-a-Disk”<sup>3-5</sup>, uses the centripetal force imparted by rotation to provide a pumping action for liquids. Most microfluidic devices operate with external connections (eg. electrical) to provide a pumping action. Centrifugal devices, usually disks, can operate without connections of any kind and consequently may be well suited to certain processes conducted in the field. These devices may be cheaper and greener than some conventional procedures because the disks may be mass produced and use smaller reagent volumes with the resulting benefits of reduced reagent consumption and waste. Finally, they offer the potential for being faster, by integrating a variety of operations and processing steps into a single device. While some work has been done demonstrating cell lysis using small paramagnetic beads<sup>6</sup> or small thin metal disks<sup>7</sup> in centrifugal microfluidic devices,

until now, no system has shown the potential to process solids such as tissues and soils.

As Ducreé *et al.* have described, a growing toolbox of “unit operations” such as valving, siphoning, liquid mixing as well as volume metering and splitting are now available and can be sequentially integrated into total analysis systems.<sup>5</sup> The present paper adds solid sample preparation to that toolbox for centrifugal microfluidic devices.

### 5.2.2 Magnets

Magnetic particles have been increasingly used in separations and are commercially available.<sup>8</sup> Magnetic forces and magnets have been utilized for a variety of functions in microfluidic devices; from magnetohydrodynamic flow to valves and solid support for bioreactions.<sup>9</sup> Magnetic particles have also found use in centrifugal microfluidic devices for the mixing of liquids.<sup>10</sup>

In addition to shape, composition and manufacturing process, a key element in the performance of a magnet is the direction of magnetization.<sup>11</sup> Very little work has shown the potential for magnetically induced mechanical movement in centrifugal devices that have the capacity to grind solid samples. This motion and its potential will also be the focus of this report.

The system discussed below is planned as only one of a series of steps to be used in sample preparation and analysis on centrifugal microfluidic systems.

## 5.3 Experimental

### 5.3.1 Instrumentation

The entire system is made of a macroscopic stage (motor, strobe, camera, fixed magnet base) and of disposable centrifugal devices (containing the extraction chamber, solid sample, solvent and “mobile magnets”).

#### 5.3.1.1 Macroscopic Stage

A servo motor (Parker MPJ0922D3E-NPSN, Cadence Automatisation, Quebec, Canada) and servo drive (Parker AR-08AE, Cadence Automatisation, Quebec, Canada) are used for the precise positioning of the centrifugal devices and to run various spin programs. A high speed digital imaging system allows real-time, in-process monitoring and recording of the spinning devices and the movement of the enclosed “mobile magnets” in the extraction chambers. This was achieved by synchronizing the servo motor with a strobe light (Shimpo DT-311A, Primo Instruments, Quebec, Canada) and a CCD camera (SONY XCD-V50). As opposed to similar reported systems,<sup>7, 12</sup> our system is completely controlled via “LabVIEW 8.6” (Developer Version, National Instruments, Quebec, Canada). This includes the triggering of the strobe light. Others have reported the use of retroreflective tape<sup>7</sup> or the alignment of a light spot emitted from fiber optic sensors.<sup>12</sup> Both of these options result in an alignment error and the need to add tape to the devices. This is avoided in our system by electronically triggering both the strobe and camera to grab one image frame at either every rotation or every second rotation, as needed. This also easily enables the

integration of future devices such a spectrometer for simultaneous spectral acquisition.

#### *5.3.1.2 Magnets*

Six permanent magnets are fixed to the motor base and remain immobile during operation. Each extraction chamber on the rotating device contains a magnet, referred to as a “mobile magnet” (see Figure 5-1, Figure 5-2, Figure 5-3 and Video S-1). The rotational shaft of the motor passes through the middle of the fixed base. All of the magnets were neodymium iron boron (NdFeB) permanent magnets (McMaster Carr, Santa Fe Springs, California, USA). The six fixed magnets (slug-shaped, magnetized parallel to thickness) in the base have dimensions of 3/8 inch (9.525 mm) diameter and 1/4 inch (6.35 mm) thickness and their resulting magnetic fields are illustrated in Figure 5-1(d) (created using “Vizimag 3.141” software, Ayrshire, United Kingdom). The “mobile magnets” (rectangular-shaped, magnetized parallel to width) have dimensions of 5 mm (W) x 3 mm (H) x 15 mm (L) and take up 14% of the extraction chamber’s 1.6 cm<sup>3</sup> volume (see Figure 5-3). The dotted line of Figure 5-1(d) illustrates the radial position of the extraction chamber above the base and the path that it would make during rotation through the magnetic fields. It is apparent that the “mobile magnets” moving along that line would alternately be subjected to stronger magnetic fields pulling inward and outward during the rotational cycle. Furthermore, since the “mobile magnets” themselves are magnetized parallel to width, as the device rotates they are made to spin upon their axes. The resulting spin and shake motion is illustrated in Figure 5-3 and Video S-1. Grinding

intensity and period are controlled by 1) setting the proximity of the fixed base magnets relative to the rotating device and 2) the rotational speed.

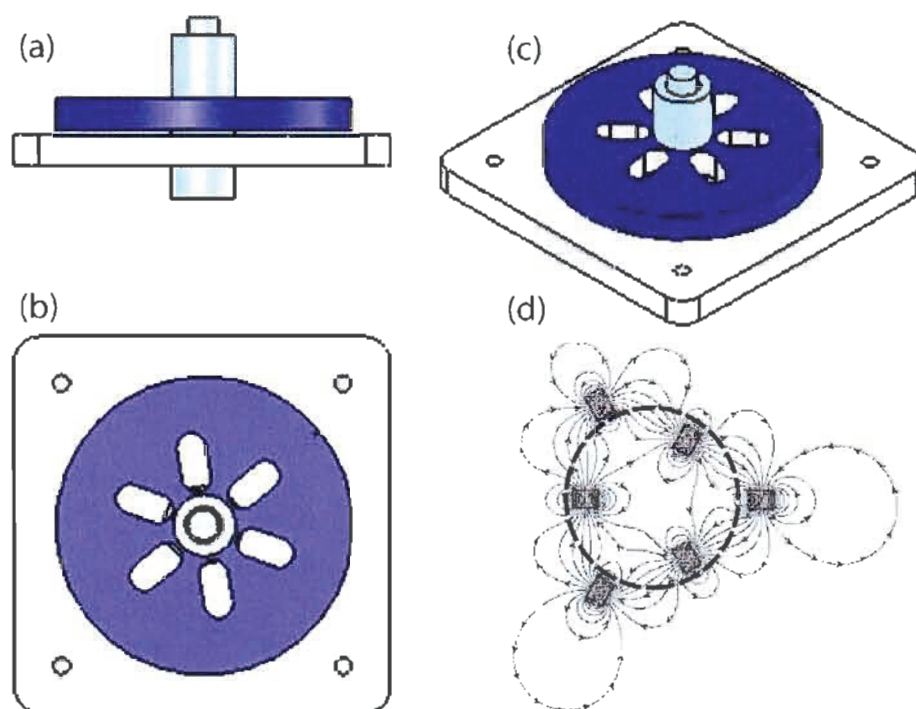


Figure 5-1. (a,b,c) Centrifugal device and macroscopic stage (motor shaft and fixed magnet base).  
 (d) Fixed magnet base: magnet position and flux lines (circle indicate trajectory of extraction chamber above base).

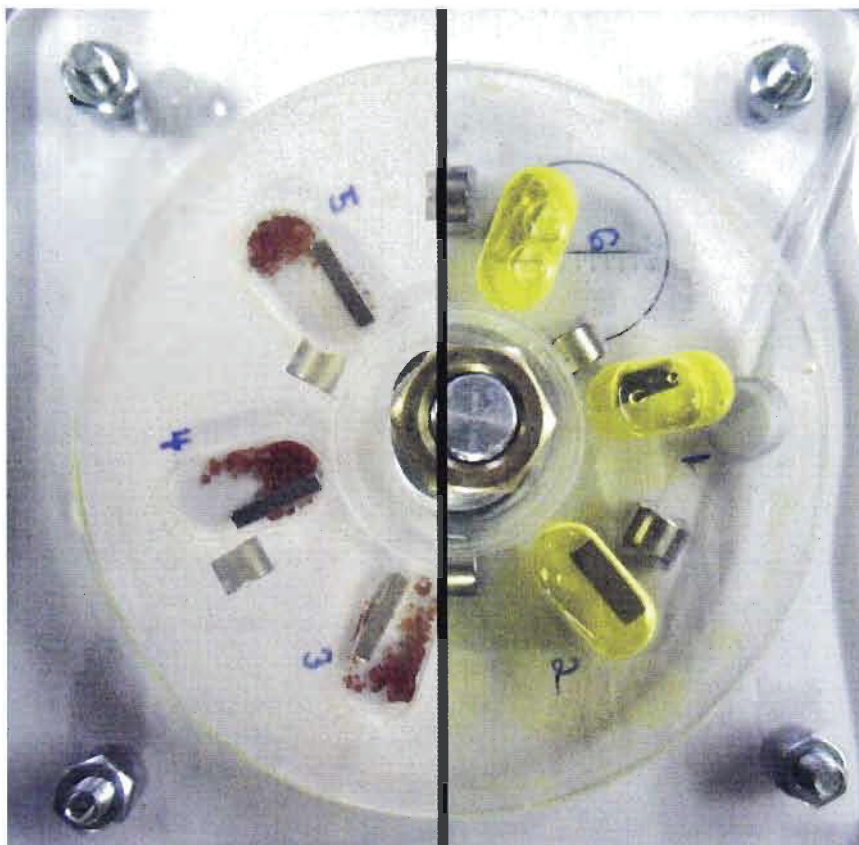


Figure 5-2. Photograph of device including magnets, solvent and solid sample before (left) and after (right) rotation.

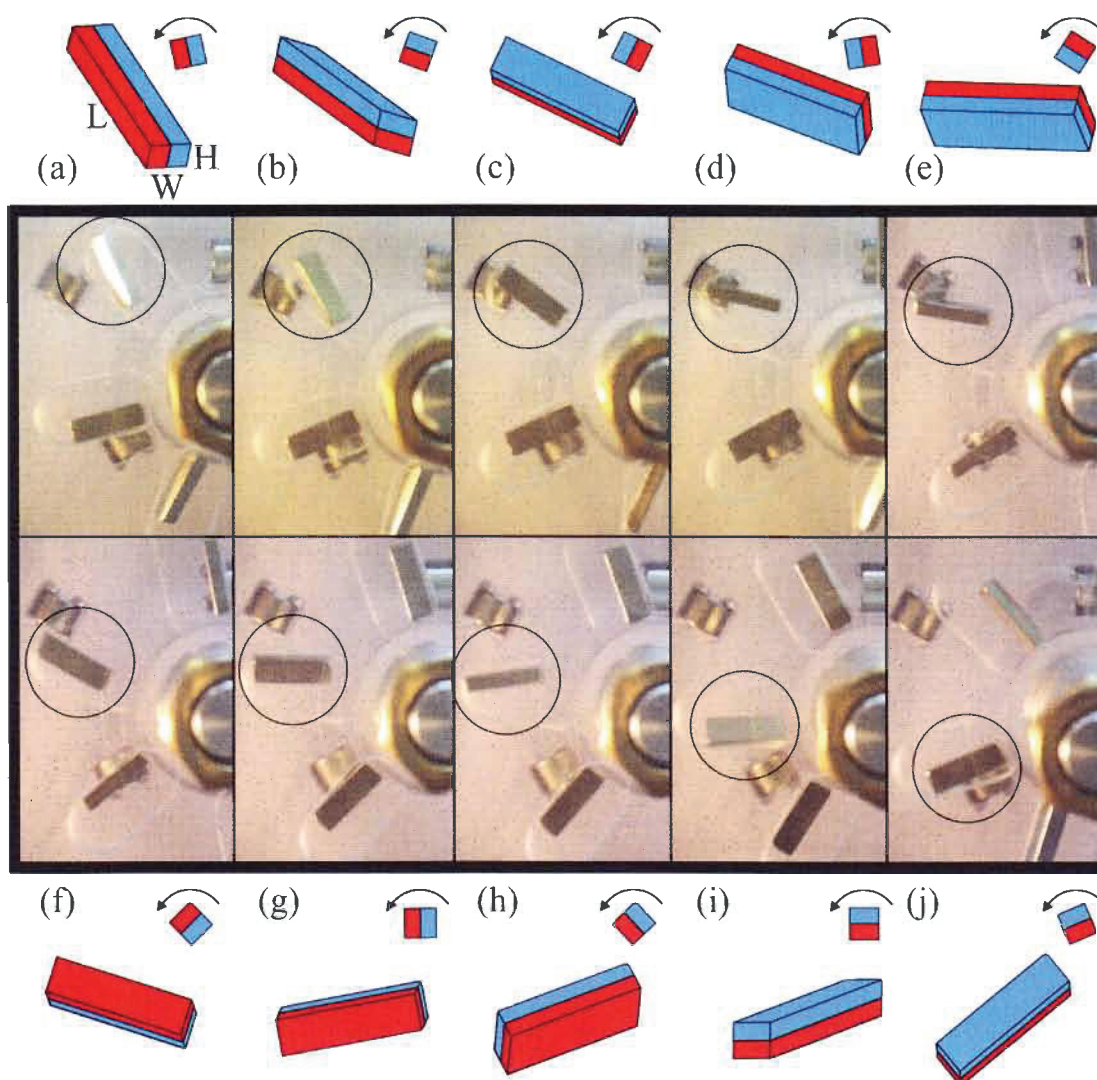


Figure 5-3. Movement of “mobile magnets” enclosed in extraction chamber. Magnet positions in circled regions are illustrated in adjacent drawings.

### 5.3.1.3 Manufacturing Centrifugal Devices

The main bodies of the centrifugal devices were designed in the 3D Computer-Aided Design (CAD) software “SolidWorks 2005” (SolidWorks Corp., Concord, Massachusetts, USA), converted to a \*.DXF file (Data eXchange Files) and laser milled out of 1/4 inch (6.35 mm) thick poly(methyl methacrylate) using a 100 W CO<sub>2</sub> laser mill (Kern Electronics & Lasers, Minnesota, USA). Bottom and

top layers made of 1.2 mm thick polycarbonate disk (material and size of a regular CD but without the metal coating – U-Tech Media Corp., Taiwan, China) were added to these main bodies. The bottom layers were chemically bonded using dichloromethane ( $\text{CH}_2\text{Cl}_2$  - Caledon Laboratories Ltd, Ontario, Canada, Lot: 22460) while the top layers were rapidly affixed using a 100  $\mu\text{m}$  thick double-sided adhesive (FLEXmount, DFM 200 Clear V-95 150 poly H-9 V-95 4, FLEXcon, Spencer, Massachusetts, USA) which had been cut using a cutting plotter (CE3000Mk2-60, Graphtec America Inc., Santa Ana, California, USA) from the original DXF files.

### 5.3.2 Reagents

The hard coloured crystal chosen as the test solid sample was potassium ferricyanide ( $\text{K}_3[\text{Fe}(\text{CN})_6]$  - Caledon Laboratories Ltd, Ontario, Canada, Lot: 62826). The solvent was distilled deionised water (Milli-Q water, 18  $\text{M}\Omega$ , Millipore Co., Bedford, Massachusetts, USA).

### 5.3.3 Procedure

To test for the *enhanced dissolution*, a 0.10 g sample of  $\text{K}_3[\text{Fe}(\text{CN})_6]$ , 1.0 mL of water and one rectangular “mobile magnet” were placed in one of the extraction chambers of the centrifugal device. The top layer described above sealed the chamber. The device was spun at a set rotational speed (between 40 and 1000 rpm). The resulting sets of digital photographs were analyzed to determine at which point the dissolution was complete.

It was also hypothesized that the mechanical motion of the magnets in the extraction chambers would result in an increase in temperature. To test for this

*induced temperature*, a digital thermometer (model HH81 - Omega, Laval, Quebec, Canada) with a type K thermocouple was firmly fastened to the centrifugal device. The extraction chamber containing water was slightly modified to protect the inserted thermocouple tip from the “mobile magnet”. The device was spun at 240 rpm for ten minutes. The temperature change was monitored by reading the digital display of the thermometer from the resulting set of photographs captured by the high speed digital imaging system described above.

## **5.4 Results & Discussion**

The performance of the magnetically driven solid sample preparation centrifugal device revolves around the motion of the “mobile magnets” in response to the fixed magnets. The magnets in the fixed base are responsible for the time-oscillating magnetic forces which induce the back-and-forth motion of the “mobile magnets” in the spinning devices (Figure 5-3). Concurrently, the poles of the “mobile magnets” in the chambers are attracted and repulsed by the magnets in the fixed base resulting in the rapid rotation of the magnets in the chambers upon their own axes (Figure 5-3). Once this motion was optimized and understood, it was used to pulverize solid samples on the spinning devices. The time to dissolve  $K_3[Fe(CN)_6]$  crystals at varying rotational speeds as well as the induced temperature increase in the chamber were also determined.

### **5.4.1 Enhanced Dissolution**

The dissolution of  $K_3[Fe(CN)_6]$  crystals was successfully enhanced by the magnetically driven solid sample preparation centrifugal system. As seen in

Figure 5-4 and Figure 5-5, a 0.10 g sample was completely dissolved in 3 seconds in 1.0 mL of water while rotating at 1000 rpm resulting in a 300 fold reduction in dissolution time. This is a 99.7% reduction in time with respect to static dissolution (found to be equivalent to spinning without the “mobile magnet”), which took 15 minutes. Lutz *et al.*<sup>6</sup> also quantified the efficiency of their cell lysis centrifugal system using the same ratio of  $K_3[Fe(CN)_6]$  crystals to water that we employed. Their “shake mode protocol” would induce frequent reversal of the spinning direction resulting in a complete dissolution with a 70% reduction in time with respect to static dissolution.

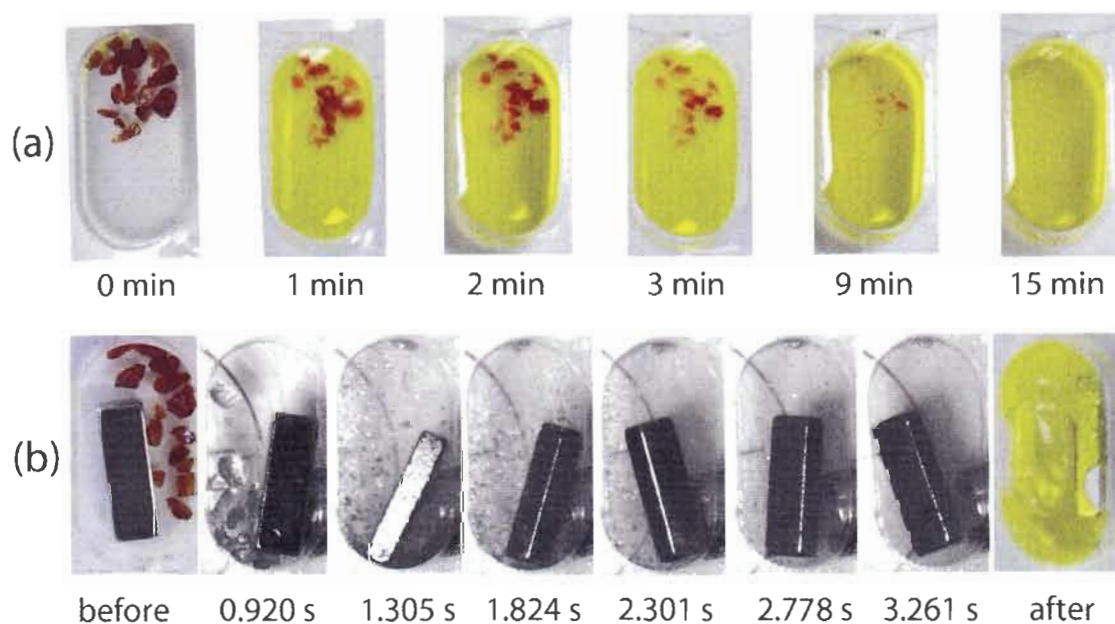


Figure 5-4. Visual comparison of extraction chambers containing 0.10 g  $K_3[Fe(CN)_6]$  and 1.0 mL water (a) without “mobile magnet” (b) with “mobile magnet” (device rotating at 1000 rpm).

It is desirable that the initial components on centrifugal devices (such as sample preparation) require relatively low rotational speeds to operate so that

fluid movement to the next component only occurs at higher rotational speeds. Figure 5-5 illustrates that after an initial steep decrease in dissolution time, increasing the rotational speed of the centrifugal device above roughly 300 rpm does not induce a great increase in efficiency. Valve burst frequencies which regulate fluid movement from one component to the next are typically higher than 300 rpm (or 5 Hz).<sup>13</sup> This bodes well for integrating this solid sample preparation component, or “unit operation”, with subsequent components on a single centrifugal microfluidic device.

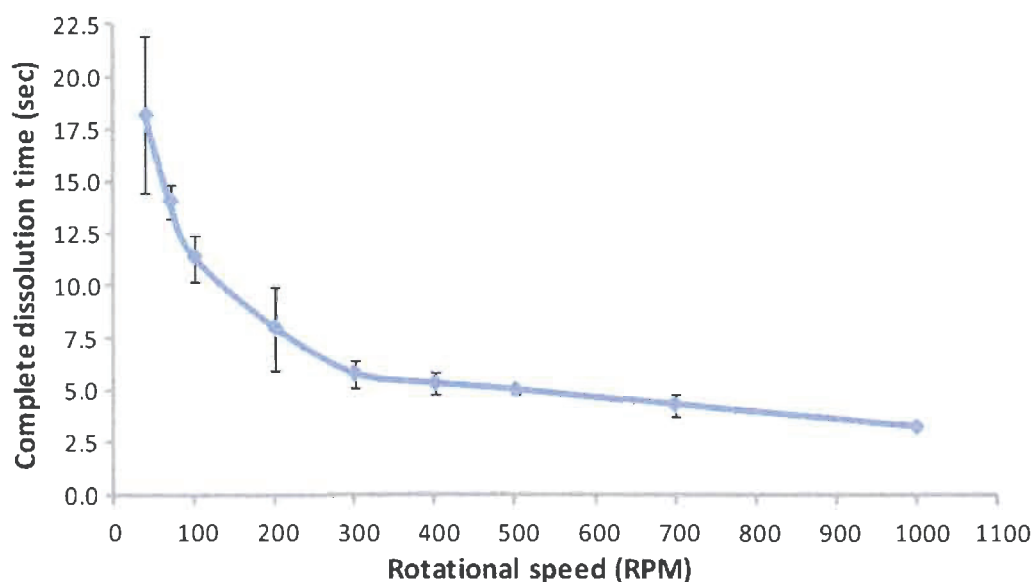


Figure 5-5. Dissolution time of 0.10 g  $K_3[Fe(CN)_6]$  in 1.0 mL of water at different rotational speeds using the magnetically driven solid sample preparation centrifugal device.

#### 5.4.2 Induced Temperature

The temperature inside these extraction chambers was also monitored. At a relatively slow rotational speed of 240 rpm, a 0.7°C/min increase in temperature in water was observed due to the mechanical motion of the rotating magnets. This is equivalent to 3 J/min of work or 12 mJ per revolution of the device.

Additionally, since each “mobile magnet” spins upon its axis 6 times per revolution, this increase in temperature equates to 2 mJ/spin. This generated heat will promote the extraction process. There will also be cooling through conduction into the device's body.

## **5.5 Conclusions**

The system demonstrates the ability to pulverize a hard crystal and mix a solution in a time two orders of magnitude faster than static dissolution or spinning without the “mobile magnets”. This suggests that a solid sample preparation step may be integrated on centrifugal microfluidic devices.

## **5.6 Acknowledgment**

We thank the National Science and Engineering Council of Canada (NSERC) for scholarship support for D.A.D. and support under the Strategic Grant program (STPSC 357011 - 07). Supporting Information Available: This material is available free of charge via the Internet at <http://pubs.acs.org/ac>.

## **5.7 Supporting Information**

### **Abstract**

Very little work has shown the potential for magnetically induced mechanical movement on centrifugal devices that have the capacity to grind solid samples. This motion and its potential is one of the focuses of the primary research article. To better visualize the magnetically driven solid sample preparation on the centrifugal devices, a composite of various videos and photographs has been compiled into a short video. A description of each section of that video follows.

### **Description of Video S-1 (see Appendix D for a link to this video)**

Following the title screen, an introductory photograph of the device lists the various parts of interest that will be the focus of the subsequent sections of the video. This includes the centrifugal device (six extraction chambers each containing one “mobile magnet”, hard crystals and solvent) and the fixed base below (including the six fixed magnets).

Next, a video of the centrifugal device rotating at 5 rpm above the fixed base is seen. The spinning and shaking motion of the “mobile magnets” is clearly observed.

After that a video of the centrifugal device rotating at 240 rpm is seen. The force and ability of the device to grind solid samples is illustrated.

Subsequently, we have displayed a series of eighteen photographs taken by the high speed digital imaging system while the device rotated at 400 rpm. The extraction chamber on the left contains a “mobile magnet” while the extraction chamber on the right does not. Upon rotation, the solid sample on the left is quickly dissolved while the solid sample on the right simply accumulates on the bottom of the chamber due to the centrifugal force. A 25 mm reticule fixed to the base is also discerned on the left side of the photographs. This video sequence provides a further example of the enhanced dissolution shown in Figure 5-4.

Following this, a video with a close up of the centrifugal device rotating at 1000 rpm is followed with a general view of the system. The system includes the servo motor and drive, a camera, a strobe and a safety shield.

Finally a series is displayed of six photographs taken by the high speed digital imaging system while the device rotated at 1000 rpm. The solid sample is completely dissolved in 3 seconds.

## 5.8 References

- (1) Pawliszyn, J., "Sample preparation: Quo vadis?", *Analytical Chemistry*, **2003**, 75 (11), 2543-2558.
- (2) Felton, M.J., "Lab on a chip: poised on the brink", *Analytical Chemistry*, **2003**, 75 (23), 505A-508A.
- (3) Steigert, J., Grumann, M., Brenner, T., Mittenbuehler, K., Nann, T., Ruehe, J., Moser, I., Haerberle, S., Riegger, L., Riegler, J., Bessler, W., Zengerle, R., Ducreé, J., "Integrated sample preparation, reaction, and detection on a high-frequency centrifugal microfluidic platform", *Journal of the Association for Laboratory Automation*, **2005**, 10 (5), 331-341.
- (4) Madou, M., Zoval, J., Jia, G., Kido, H., Kim, J., Kim, N., "Lab on a CD", *Annual Review of Biomedical Engineering*, **2006**, 8 601-628.
- (5) Ducreé, J., Haerberle, S., Lutz, S., Pausch, S., Von Stetten, F., Zengerle, R., "The centrifugal microfluidic Bio-Disk platform", *Journal of Micromechanics and Microengineering*, **2007**, 17 (7), S103-S115.
- (6) Lutz, S., Lang, P., Faltin, B., Haerberle, S., von Stetten, F., Zengerle, R., Ducreé, J., "Towards a comprehensive centrifugal process integration by rotationally induced lyophilisate dissolution and cell lysis", presented at *Micro Total Analysis Systems 2007, Proceedings of mTAS 2007 11th International Conference on Miniaturized Systems for Chemistry and Life Sciences*, Paris, France, 7-11 October 2007, **2007**, 1516-1518.
- (7) Kido, H., Micic, M., Smith, D., Zoval, J., Norton, J., Madou, M., "A novel, compact disk-like centrifugal microfluidics system for cell lysis and sample homogenization", *Colloids and Surfaces B: Biointerfaces*, **2007**, 58 (1), 44-51.
- (8) Berensmeier, S., "Magnetic particles for the separation and purification of nucleic acids", *Applied Microbiology and Biotechnology*, **2006**, 73 (3), 495-504.
- (9) Pamme, N., "Magnetism and microfluidics", *Lab on a Chip - Miniaturisation for Chemistry and Biology*, **2006**, 6 (1), 24-38.
- (10) Grumann, M., Geipel, A., Riegger, L., Zengerle, R., Ducreé, J., "Batch-mode mixing on centrifugal microfluidic platforms", *Lab on a Chip*, **2005**, 5 (5), 560-565.
- (11) Moskowitz, L.R., *Permanent magnet design and application handbook*, Krieger, Malabar, Fla. **1995**, p. 946.
- (12) Park, J.M., Cho, Y.K., Lee, B.S., Lee, J.G., Ko, C., "Multifunctional microvalves control by optical illumination on nanoheaters and its application in centrifugal microfluidic devices", *Lab on a Chip - Miniaturisation for Chemistry and Biology*, **2007**, 7 (5), 557-564.
- (13) Cho, H., Kim, H.Y., Kang, J.Y., Kim, T.S., "How the capillary burst microvalve works", *Journal of Colloid and Interface Science*, **2007**, 306 (2), 379-385.

## CHAPTER 6: Automated Liquid-Solid Extraction of Pyrene from Soil on Centrifugal Microfluidic Devices

With the previously described instrumental setup, fabrication techniques, and magnetically actuated solid sample preparation, Chapters 6 and 7 present a non-contact methodology for the magnetically actuated liquid-solid extraction technique on devices in motion. This is used in two different applications using different extraction solvents (hexane and water), different analytes (PAH and pesticide), different solid sample matrices (soil and vegetable) and different analysis techniques (direct absorbance of analyte and colour complex generation for indirect absorbance of analyte using percent inhibition).

The work presented in Chapter 6 was originally published and is *reprinted with permission from Elsevier*:

Xi, Yongqing\*, Duford, David A.\*, Salin, Eric D., "Automated liquid-solid extraction of pyrene from soil on centrifugal microfluidic devices", *Talanta*, **2010**, 82 (3), 1072-1076.

\* These authors should be considered equal contributors.

Additional details in regards to the multiwavelength ratiometric blank correction technique used in Chapter 6 are available in Appendix F. Also available in Appendix F are detailed absorbance, statistical and limit of detection calculations for both Chapters 6 and 7. Finally, a detailed explanation and calculations of the sedimentation rate using Stokes' Law for both chapters are available in Appendix G.

## 6.1 Abstract

Organic pollutants such as polycyclic aromatic hydrocarbons (PAHs) are present in the environment in increasing concentrations and so are of growing concern. Monitoring these species, particularly on-site, can be both difficult and expensive. This paper presents a novel miniaturised magnetically actuated liquid-solid extraction unit integrated in tandem with a filtration unit and a detection unit on a single centrifugal microfluidic device. A demonstration analyte, pyrene, was rapidly extracted and quantified by UV-absorbance from multiple soil samples. The system showed excellent performance for a system designed for field use. Characterization of two types of passive valves was performed along with an extraction time efficiency study. The system provides a factor of 150 reduction in sample weights and extraction solvent volumes and provides statistically similar recoveries to the conventional method with a pyrene detection limit of 1 ppm (0.03  $\mu\text{g}$  absolute detection limit). The reduction in time and solvent and the potential for field use suggest that this device type may be valuable for environmental monitoring.

### Keywords

Centrifugal microfluidics; Solid sample preparation; Liquid-solid extraction; Absorbance; Polycyclic aromatic hydrocarbon (PAH); Environmental analysis

## 6.2 Introduction

Automating and miniaturizing analytical techniques to meet heightened environmental monitoring challenges is an important topic in analytical instrument design research. Microfluidic devices and, in particular, centrifugal microfluidic devices, sometimes known as “Lab on a CD”,<sup>1</sup> offer the potential to meet many of these challenges with features including miniscule reagent consumption, low production costs, short analysis times and freedom from external connections such as pumps. These features provide compelling arguments for the development of these devices. Though centrifugal microfluidic systems are becoming well known,<sup>1, 2</sup> few centrifugal systems prepare and analyze environmental samples on the same integrated device and even fewer microfluidic devices of any type deal with solid samples such as soil.<sup>3</sup>

Liquid-solid extraction is among the most common sample preparation techniques and is used to selectively remove analytes from a sample matrix. Unfortunately, common practice with this procedure involves large sample and solvent volumes and considerable time (labour) to process each sample. From an environmental point of view there are many drawbacks to using large solvent volumes. Microfluidic techniques have considerable advantage in that regard. As we will illustrate, the centrifugal microfluidic device also offers considerable advantage with respect to time.

Pyrene, a polycyclic aromatic hydrocarbon (PAH), is one of many PAHs being regularly monitored in aqueous and soil samples (EPA Method 610) since they are carcinogenic pollutants that are a public health risk. Regular monitoring

represents large time expenditures and costs due to the sampling, shipping, storage requirements as well as an analysis by extraction and quantification by gas chromatography-mass spectrometry. With such a standard procedure, site assessment mapping of the contaminated areas is arduous. For these reasons, a smaller integrated device that could be field portable for fast and precise monitoring is desirable.

As Ducrée *et al.*<sup>4</sup> have described, a growing toolbox of “unit operations” such as valving,<sup>5</sup> siphoning, liquid mixing and volume metering and splitting are now available for microfluidic systems. These “operations” can be sequentially integrated into total analysis systems and in particular centrifugal microfluidic devices. Recently we have demonstrated magnetically actuated solid sample preparation<sup>3</sup> and pre-concentration on miniaturised solid phase extraction columns<sup>6</sup> on centrifugal microfluidic devices. Using pyrene as a demonstration analyte, this paper adds magnetically actuated liquid-solid extraction of an environmental sample to that toolbox in tandem with sedimentation, filtration and detection, all on a single device.

## **6.3 Experimental**

### **6.3.1 Standards and Reagents**

From pyrene powder (84648-1G, purity > 99%, Sigma-Aldrich, Oakville, ON) a 100  $\mu\text{g mL}^{-1}$  pyrene primary standard solution was prepared in hexane (purity > 99.9%, EMD, Gibbstown, NJ). Pyrene working solutions in hexane (2.0, 4.0, 6.0, 8.0, 10.0 and 20.0  $\mu\text{g mL}^{-1}$ ) were made daily from the primary standard solution in clean, dried 10 mL glass bottles. All solutions were stored in darkness

at 4 °C. Soil samples were obtained from Saint-Jean-sur-Richelieu, Quebec, Canada.<sup>7</sup> Each 0.03 g soil sample was manually spiked with 200 µL of a pyrene working solution and allowed to air dry resulting in spiked soil samples with a pyrene concentration of 13 to 133 ppm. A series of blanks were also prepared spiking soil samples with 200 µL of pure hexane.

A 0.1M sodium hydroxide (NaOH, Fisher Scientific, Fair Lawn, NJ) solution was prepared in distilled deionised water (DDW, 18 MΩ, Millipore Co., Bedford, MA) for pre-treating the fused silica capillaries. Ethyl alcohol (EtOH, Commercial Alcohols, Brampton, ON) was used for cleaning and pre-treatment of the capillaries.

### 6.3.2 Device Fabrication

The centrifugal microfluidic devices were fabricated using a rapid prototyping technique similar to that developed by Kido *et al.*<sup>8</sup> Fabrication can be described in three steps: design, manufacture and assembly.

The multiple layers were first *designed* in the 3D computer-aided design (CAD) software “SolidWorks 2005” (SolidWorks Corp., Concord, MA).

Next, each layer was *manufactured* either by xurography as previously described by Bartholomeusz *et al.*<sup>9</sup> or by micro-milling. As seen in Figure 6-1(a), Layers 2 and 4 consisted of 100 µm thick adhesive film (FLEXmount DFM 200 Clear V-95 150 poly H-9 V-95 4, FLEXcon, Spencer, MA) into which channels and vent lines including the passive valves (see valve section below) were cut by xurography with a cutting plotter (CE300Mk2-60, Graphtec America, Inc., Santa Ana, CA). The top, middle and bottom layers (Figure 6-1(a) 1, 3 and 5) consisted of 2.9 mm thick poly(methyl methacrylate) pieces (PMMA, Acrylite OP-1, Cyro

Industries, Rockaway, NJ) which were milled to 120 mm diameter and into which chambers and centre, loading and vent holes were made using a computer numerically controlled (CNC) micro-milling machine (QuickCircuit 5000, T-Tech, Inc. Norcross, GA). This particular PMMA was chosen for its good resistance to hexane and its optical properties being UV-transparent, since Layers 1 and 5 also served as the optical windows for the integrated detection cell (Figure 6-1(d)3 and Figure 6-2). At this point, the fused silica capillary (Figure 6-1(d)5) was added (see valve section below).

Finally the devices were *assembled* by carefully aligning and firmly pressing together the layers using a hand cranked cold laminator (Jet Mounter ML25, Drytac, Concord, ON). Before laminating the final layer, 0.03g of dried spiked soil sample and one “mobile magnet” (Figure 6-1(d)7, 5.08 mm × 2.57 mm × 1.14 mm, nickel plated NdFeB rectangular magnet, magnetized parallel to width; NB045-35, Master Magnetics Inc., Castle Rock, CO) was added to each extraction chamber. The final device was a laminate of 5 layers and is illustrated in Figure 6-1. Prior to extraction, all loading holes were sealed with microplate sealing tape (Nunc sealing tape T9571, Sigma-Aldrich Corp., St Louis, MO) to avoid contamination.

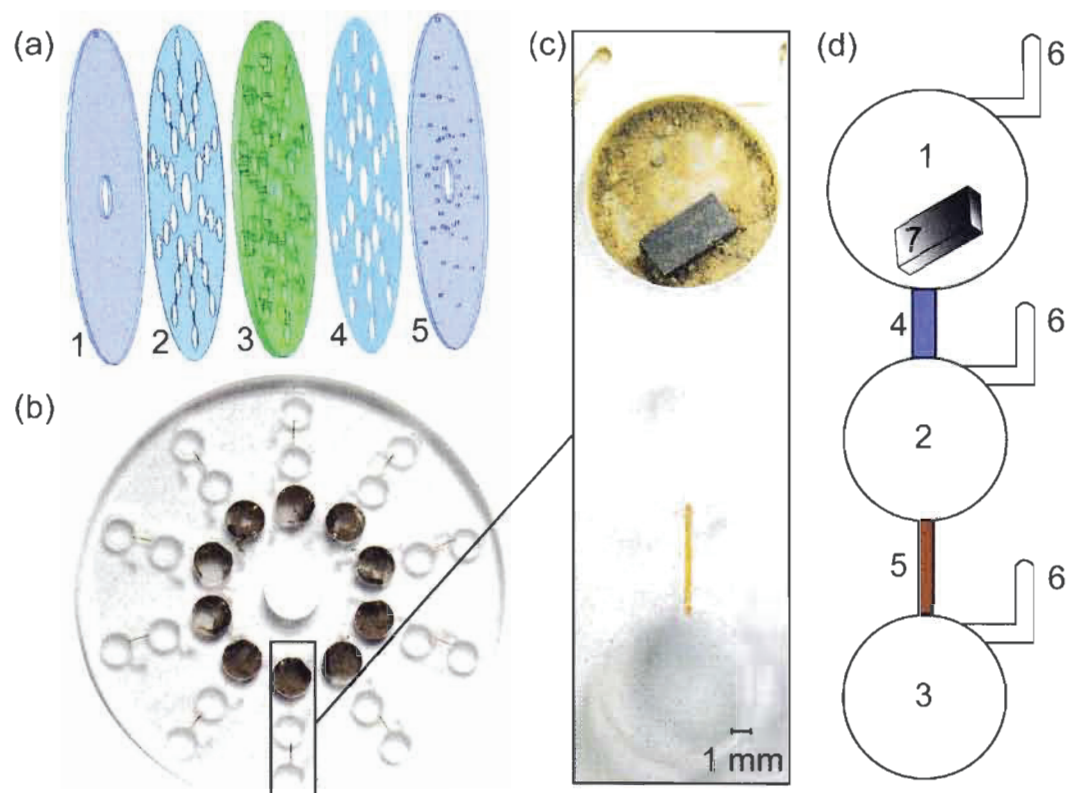


Figure 6-1. (a) Exploded view of device showing following five layers 1) bottom PMMA, 2) adhesive layer including rectangular passive valves, 3) middle PMMA with chambers into which cylindrical capillaries are epoxied, 4) adhesive layer, 5) top PMMA with vent holes. (b) Photograph of device with 10 sets of chambers. (c) Enlarged view of one set of chambers. (d) Schematic of chambers including 1) magnetically actuated liquid-solid extraction unit, 2) filtration unit, 3) detection unit, 4) rectangular passive capillary valve at a radial distance of 29 mm, 5) cylindrical passive capillary valve at a radial distance of 47 mm, 6) vent holes and vent lines (0.1 mm deep x 1 mm wide), 7) "mobile magnet" agitator.

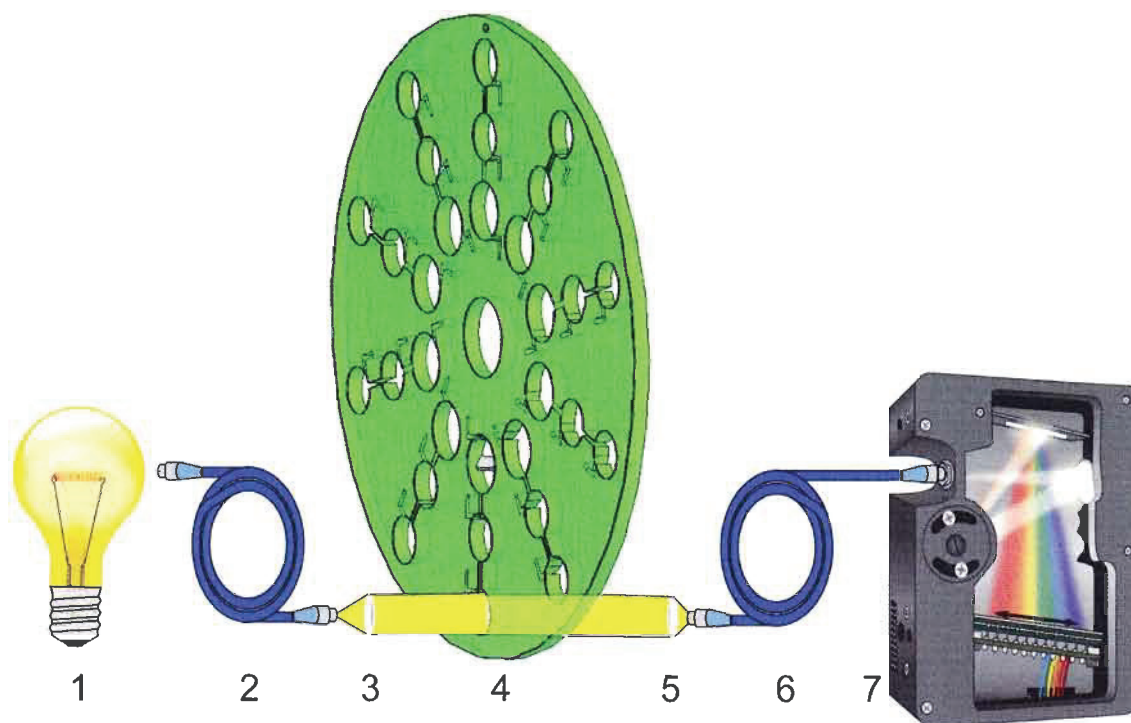


Figure 6-2. Schematic of detection system: 1) light source, 2) fiber optic, 3) collimating lens, 4) integrated detection cell, 5) focusing lens, 6) fiber optic, 7) photodiode array spectrometer for detection at 334 nm.

### 6.3.3 Valves

Two types of passive capillary valves were integrated on the devices and their burst frequencies for hexane were studied.

The first type of valve was a rectangular passive capillary valve (Figure 6-1(d)4) made by cutting fine features in the adhesive layer itself. These valves joined the extraction chamber (Figure 6-1(d)1) and the filtration chamber (Figure 6-1(d)2). As seen in the insert of Figure 6-3(a), these valves had a fixed height of 100  $\mu\text{m}$  (due to the adhesive used) while their widths were controlled by the design and xurographic cutting. Four different widths were studied (600, 800, 1000 and 1200  $\mu\text{m}$ ).

The second type of valve, a cylindrical passive capillary valve (Figure 6-1(d)5), was made of fused silica capillaries (Polymicro Technologies, Phoenix, AZ), similar to those reported by LaCroix-Fralish *et al.*<sup>10</sup> These valves joined the filtration chamber (Figure 6-1(d)2) to the detection cell (Figure 6-1(d)3). As seen in the insert of Figure 6-3(b), these valves had a fixed outer diameter (OD) of 360  $\mu\text{m}$ , while three different inner diameters (ID) were studied (50, 75 and 100  $\mu\text{m}$ ). Before inclusion of the capillaries during the manufacturing step, the capillaries were pre-treated with 0.1 M NaOH, EtOH and air prior to being cut to 5 mm length. They were then glued into milled channels (1.0 mm wide by 400  $\mu\text{m}$  deep) in the bottom side of the middle PMMA layer (Figure 6-1(a)3) using commercially available 5 minute epoxy.

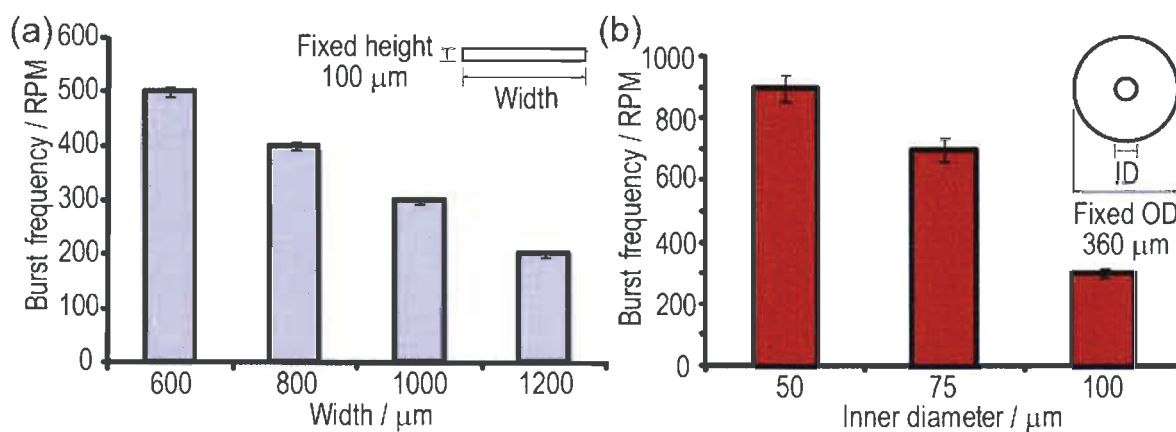


**Figure 6-3.** (a) Burst frequencies of hexane as a function of different channel widths of the rectangular passive capillary valves at a radial distance of 29 mm adhesive. (b) Burst frequencies of hexane as a function of different inner diameter of the cylindrical passive capillary valves at a radial distance of 47 mm. Inserts of both (a) and (b) show cross-sectional geometry of channels.

#### 6.3.4 Centrifugal System

A motorized stage, strobe, camera and fixed magnet base which has previously been described by Duford *et al.*<sup>3</sup> were used to spin the devices and acquire high speed still images (see Figure 6-4(b)).

Each centrifugal device contained ten extraction chambers. To each of these chambers, which contained the dried spiked soil samples and one “mobile magnet” agitator, 200  $\mu$ L of hexane was added. The device was then secured to the spindle of the motorized stage and spun at a series of different speeds as discussed below.

#### 6.3.5 Detection System

After centrifugation, the device was moved from the motorized stage to a detection stage, though these could easily be merged into a single instrument in the future. The detection stage and the multiwavelength ratiometric blank estimation technique are described in detail by LaCroix-Fralish *et al.*<sup>11</sup> and included a deuterium light source (DT-MINI-2-GS, Ocean Optics, Dunedin, FL) and a USB miniature spectrometer (USB4000-UV-VIS, Ocean Optics, Dunedin, FL). Pyrene was determined by absorbance using the 3.1 mm long integrated detection cells, as seen in Figure 6-2. To account for the imprecision of these integrated detection cells, the multiwavelength ratiometric blank estimation technique required monitoring of the signal at 334 nm as the analyte’s absorbing wavelength and the signal at 500 nm as the analyte’s non-absorbing wavelength used to estimate the value of the blank at 334 nm.

Two different studies were completed with this configuration. First, an *extraction time efficiency study* was performed processing three replicate soil samples with the same pyrene concentration (33 ppm) at varying extraction times. With the ideal extraction time determined, the optimized automated extraction was performed as a *comparison to existing methods* processing replicate soil samples with varying pyrene concentrations at a fixed extraction time. The conventional method consisted of extracting from 5.0 g of spiked soil with 25 mL hexane in a separatory funnel, shaking for 20 minutes per sample, transferring the extractant to a 1 cm cuvette and determining pyrene by absorbance at 334 nm using a bench top spectrophotometer (Cary 5000 UV-Vis Near IR Spectrophotometer, Varian, Palo Alto, CA). No spectral correction (multiwavelength ratiometric blank estimation technique) was applied to the results from this double beam instrument.

## **6.4 Results and Discussion**

In order to develop an effective automated controlled sequence of flows through the various stages of the analysis, it was vital to determine the *burst frequencies* using the solvent, hexane, for the two types of passive capillary valves. Typically only one type of valve is used on a device but the interaction of the two types of valves complemented themselves and allowed for greater control. As seen in Figure 6-3(a), the burst frequencies for the rectangular valves ranged from 200 to 500 rpm (3 to 8 Hz) depending on the width. Similarly, as seen in Figure 6-3(b), the burst frequencies for the cylindrical valves ranged from 300 to 900 rpm (5 to 15 Hz). The high reproducibility for both types of valves

meant that implementation of multiple simultaneous runs on a single device could be achieved with the same spin sequence. From these results, the rotational speeds were chosen to be sufficiently above the burst frequency of the desired valve and below that of the subsequent ones to insure a controlled, reproducible transfer of liquid. The following parameters were chosen for the automated liquid-solid extraction: 1) 1200  $\mu\text{m}$  wide (fixed 100  $\mu\text{m}$  height) rectangular valve with a 200 rpm burst frequency, 2) 75  $\mu\text{m}$  ID cylindrical valve with a 700 rpm burst frequency and 3) the following spin sequence:

First, the device was rotated at 50 rpm, well below the burst frequency of the first valve. The solvent and soil were in the inner *magnetically actuated liquid-solid extraction unit* (Figure 6-1(d)1). At this point the magnetic field of the “mobile magnet” interacted with magnetic fields of the magnets in the fixed base of the motorized stage, inducing an efficient and effective movement of the magnet, mixing the liquid and solid. Without this magnetically induced mechanical motion, the soil samples would simply sediment to the bottom of the chambers by centrifugal force with minimal extraction of pyrene.

Next, the device was spun at 400 rpm (greater than the burst frequency of the first valve but less than the second) without the fixed magnetic base of the motorized stage. At this point, sedimentation of the soil in the extraction chamber was achieved by the inherent centrifugal forces and the extractant and some particles were transferred to the *filtration unit* (Figure 6-1(d)2).

Once the extractant was completely transferred to this middle chamber, the device was spun at 1200 rpm at which point a secondary sedimentation process took place and only clear extractant was transferred into the *detection*

cell (Figure 6-1(d)3) for pyrene determination on the device by absorbance at 334 nm. This final transfer could also have been achieved using a 50  $\mu\text{m}$  capillary instead of a 75  $\mu\text{m}$  capillary; however, no advantage is obtained and a lower flow rate results from the smaller diameter.

The extractant was not directly transferred from the extraction chamber to the detection chamber since either the smaller capillaries would have clogged with soil particles or the larger capillaries would have allowed the transfer of soil to the detection cell, increasing undesirable scatter.

The results for the *extraction time efficiency study* are presented in Figure 6-4(a). A pyrene extraction plateau is obtaining in 10 minutes with an efficiency very similar to that of the conventional method.

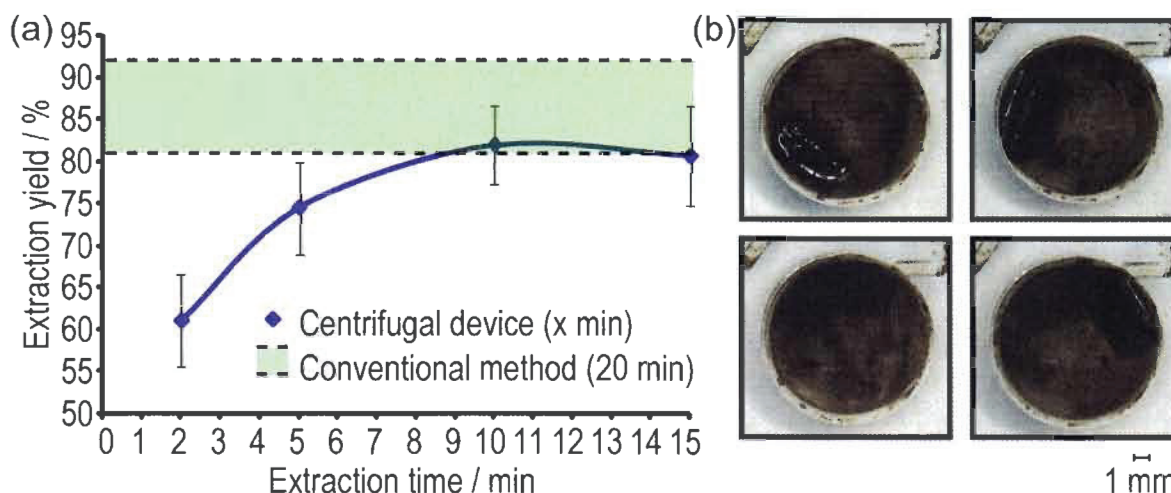


Figure 6-4. (a) Extraction time efficiency study and comparison to conventional method. A pyrene extraction plateau equivalent to conventional method is obtained in 10 minutes. (b) High speed images of spinning device showing the “mobile magnet” movement in top inner extraction chamber. The “mobile magnet” spins upon its own axis as well as back-and-forth in the extraction chamber.

Extracting all subsequent soil samples for 10 minutes, a *comparison to an existing method* was made (Table 6-1). The two methods show linearity over the concentration range.

Table 6-1. Comparison of extraction methods

	Centrifugal microfluidic device	Conventional separatory funnel
$R^2$	0.99	0.99
LOD <sup>a,b</sup> (n=11)	1 ppm (0.03 $\mu$ g)	0.3 ppm (1.5 $\mu$ g)
Linear range <sup>b</sup>	1 to 130 ppm (0.03 to 4 $\mu$ g)	0.3 to 40 ppm (1.5 to 200 $\mu$ g)
Path length / mm	3.1	10.0
Instrument RSD <sup>c</sup> (n=8)	6 % (multiple cells)	0.2 % (single cuvette)
Extraction yield	78 to 84 %	81 to 92 %
Analysis RSD <sup>d</sup> (n=7)	5 %	8 %
Processing time	10 min for 10 samples	20 min for 1 sample
Sample weight / g	0.03	5.0
Solvent volume / mL	0.20	25

<sup>a</sup> Limit of detection as 3 x standard deviation of the blank measured on two different devices

<sup>b</sup> Absolute mass detection limits and absolute linear range are expressed in parentheses for 0.03 and 5.0 g soil samples for the centrifugal and conventional methods respectively

<sup>c</sup> Instrument RSD based on analysis of pure pyrene standard

<sup>d</sup> Analysis RSD based on analysis of pyrene extracted from soil samples

The Instrumental RSD is for the measurement of pure  $5.0 \mu\text{g mL}^{-1}$  pyrene standards either injected into multiple integrated detection cells on the centrifugal device (*i.e.* no extraction) or in a single standard cuvette. As would be expected, very small variations are observed using a single cuvette with alignment fixed by the double beam bench top instrument (0.2% Instrument RSD). Of interest is the 6% Instrument RSD for the multiple cells on the device. This variation is due to slight variations in path length and in surface quality of the different cells, which would affect the light path and the amount of scattering and reflection. An attempt was made to account for this using the multiwavelength ratiometric blank estimation technique. This technique significantly improved the precision but not to the level of the bench top instrument.

The Analysis RSD is for the measurement of pyrene extracted from soil samples. An F-test confirmed that the centrifugal microfluidic device method was statistically more precise than the conventional method, even with a 150 times reduction in sample weights and extraction solvent volumes. The extraction yields of the two methods were also compared. A second F-test confirmed that there was no significant difference in the precision of the yields and a t-test confirmed that the yields of the two methods were statistically similar to a 99% confidence limit. This demonstrates that the techniques are comparable with the exception of the limit of detection (LOD), which is one order of magnitude higher for the device as compared to the bench top instrument. The higher LOD is to be expected given the differences in path lengths though future integration of methods to increase path length on a disk such as those developed by Grumann *et al.*<sup>12</sup> is to be envisioned. It should be emphasized that the present

performance of the centrifugal method is obtained with one order of magnitude improvement in throughput and two orders of magnitude reduction in both sample and solvent consumption. This reduction in sample size is reflected in the one order of magnitude lower absolute detection limit. As is, this device is capable of detecting below the Canadian government limit of 8 ppm pyrene in agricultural, residential and parkland soil <sup>13</sup>.

Pyrene, a PAH, was used as a demonstration analyte. Due to the similar spectral characteristics, we expect that this device could be used for the detection of high to moderate levels polychlorinated biphenyls (PCBs) in, for example, soil in the area of a transformer spill. For the detection of the more noxious benzo(a)pyrene and many other PAHs, a lower detection limit may be required. A variety of alternatives are envisioned to achieve a lower LOD including: 1) using more reproducible cells, 2) integrating a pre-concentration step as demonstrated by Lafleur *et al.*<sup>6</sup>, 3) using a more sensitive detection technique such as fluorescence spectrometry or 4) using longer path length cells as described by Grumann *et al.*<sup>12</sup>. Alternatively, the sample preparation stage can be used as a sample preparation stage for a technique like gas chromatography-mass spectrometry. The reduction in time and solvent use makes this device an advancement and sustainable alternative of great interest for environmental monitoring.

## 6.5 Acknowledgements

Y.X. thanks Huisheng Zhuang and scholarship support from China Scholarship Council (CSC). We thank the National Science and Engineering Council of Canada (NSERC) for scholarship support for D.A.D. and support under the Strategic Grant program (STPSC 357011-07).

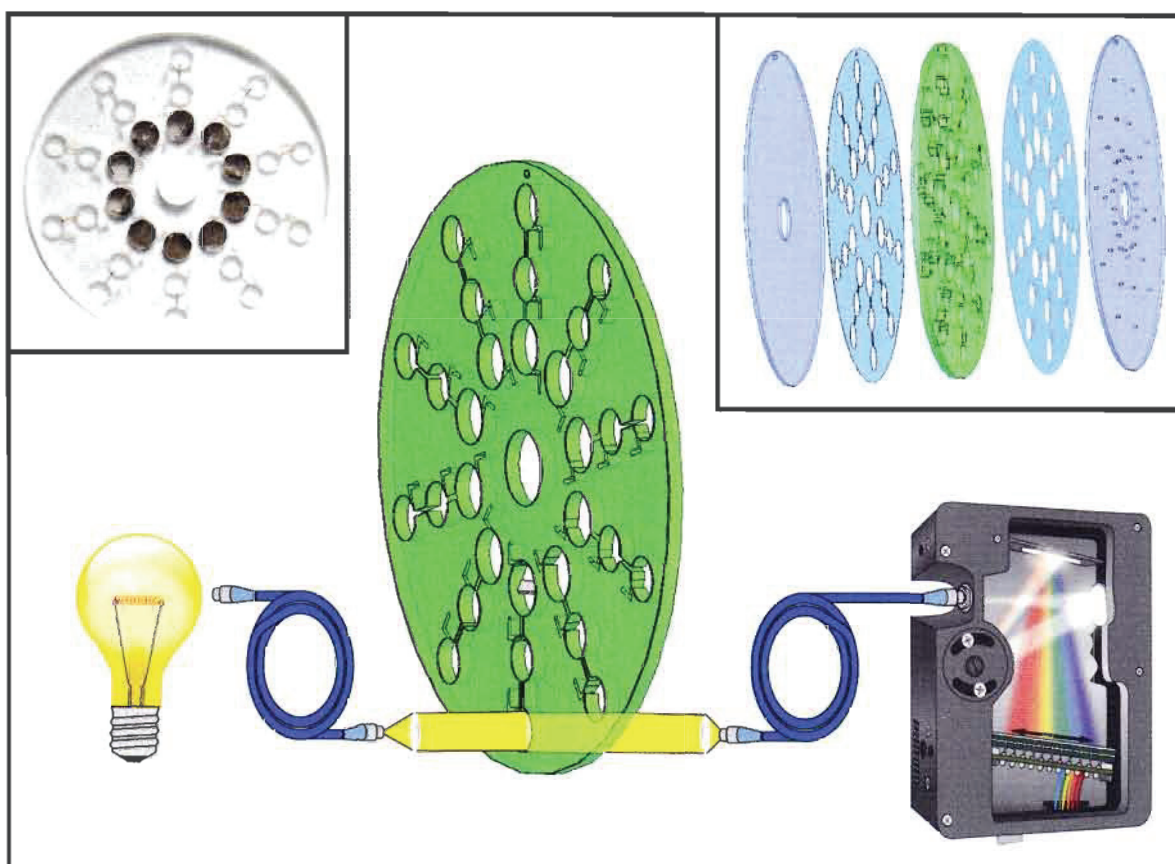


Figure 6-5. Table of Contents Graphical Abstract

## 6.6 References

- (1) Madou, M., Zoval, J., Jia, G., Kido, H., Kim, J., Kim, N., "Lab on a CD", *Annual Review of Biomedical Engineering*, **2006**, 8 601-628.
- (2) Steigert, J., Grumann, M., Brenner, T., Mittenbuehler, K., Nann, T., Ruehe, J., Moser, I., Haerberle, S., Riegger, L., Riegler, J., Bessler, W., Zengerle, R., Ducrée, J., "Integrated sample preparation, reaction, and detection on a high-frequency centrifugal microfluidic platform", *Journal of the Association for Laboratory Automation*, **2005**, 10 (5), 331-341.
- (3) Duford, D.A., Peng, D.D., Salin, E.D., "Magnetically driven solid sample preparation for centrifugal microfluidic devices", *Analytical Chemistry*, **2009**, 81 (11), 4581-4584.
- (4) Ducrée, J., Haerberle, S., Lutz, S., Pausch, S., Von Stetten, F., Zengerle, R., "The centrifugal microfluidic Bio-Disk platform", *Journal of Micromechanics and Microengineering*, **2007**, 17 (7), S103-S115.
- (5) Chen, J.M., Huang, P.C., Lin, M.G., "Analysis and experiment of capillary valves for microfluidics on a rotating disk", *Microfluidics and Nanofluidics*, **2008**, 4 (5), 427-437.
- (6) Lafleur, J.P., Rackov, A.A., McAuley, S., Salin, E.D., "Miniaturised centrifugal solid phase extraction platforms for in-field sampling, pre-concentration and spectrometric detection of organic pollutants in aqueous samples", *Talanta*, **2010**, 81 (1-2), 722-726.
- (7) Skinner, C.D., Salin, E.D., "Determination of lead in soils surrounding a lead-acid battery manufacturer", *Water Quality Research Journal of Canada*, **1995**, 30 (2), 299-304.
- (8) Kido, H., Zoval, J., Madou, M., "Rapid prototyping of microfluidic systems", *ECS Transactions*, **2006**, 4 101-105.
- (9) Bartholomeusz, D.A., Boutté, R.W., Andrade, J.D., "Xurography: rapid prototyping of microstructures using a cutting plotter", *Microelectromechanical Systems, Journal of*, **2005**, 14 (6), 1364-1374.
- (10) LaCroix-Fralish, A., Templeton, E.J., Salin, E.D., Skinner, C.D., "A rapid prototyping technique for valves and filters in centrifugal microfluidic devices", *Lab on a Chip*, **2009**, 9 (21), 3151-3154.
- (11) LaCroix-Fralish, A., Clare, J., Skinner, C.D., Salin, E.D., "A centrifugal microanalysis system for the determination of nitrite and hexavalent chromium", *Talanta*, **2009**, 80 (2), 670-675.
- (12) Grumann, M., Steigert, J., Riegger, L., Moser, I., Enderle, B., Riebeseel, K., Urban, G., Zengerle, R., Ducrée, J., "Sensitivity enhancement for colorimetric glucose assays on whole blood by on-chip beam-guidance", *Biomedical Microdevices*, **2006**, 8 (3), 209-214.
- (13) "Environment Canada: Canadian Council of Ministers of the Environment, Canadian environmental quality guidelines", *Canadian soil quality guidelines for the protection of environmental and human health: Carcinogenic and Other PAHs*, **2008**, 1-11.

## CHAPTER 7: Enzyme Inhibition-Based Determination of Pesticide Residues in Vegetable and Soil in Centrifugal Microfluidic Devices

### 7.1 Abstract

Pesticide residue is of concern as an environmental pollutant when present at medium to high concentrations. Such residue was quantified in both vegetable and soil samples by an enzyme inhibition technique. The multi-step reactions were integrated into centrifugal microfluidic devices allowing automated simultaneous analysis of several samples or replicates to be run. The small sample size inherent to microfluidic devices allowed for less reagent to be used including less of the expensive enzyme which is key to this method. Liquid-solid magnetically actuated extraction, filtration, sedimentation and detection were all integrated on the same device. Several parameters were optimized including the concentration of enzyme, substrate, chromatic agent and reaction time. In this environmental application of centrifugal microfluidics, the percent inhibition of enzyme activity is logarithmically proportional to the demonstration pesticide concentration (in this case carbofuran). This meant that as the pesticide concentration increased in the samples, the reaction was more inhibited and the final product absorbed less light at 525 nm. Two versions of the centrifugal microfluidic devices were made. One version was designed for the analysis of vegetable samples (cabbage) and the other for the analysis of soil samples. Each version provided results that were statistically similar to the conventional bench top method with a carbofuran limit of detection of 0.1 ppm or 0.1  $\mu\text{g g}^{-1}$  (5 ng absolute limit of detection).

## 7.2 Introduction

Many environmental pollutants are routinely released as a result of agricultural activities. Pesticides in particular are used on a very large scale worldwide to protect crops and seeds; however, their presence in foods and soil poses a potential human health threat.<sup>1</sup> Organophosphate and carbamate pesticides in particular are widely used even if they are known to inhibit acetylcholinesterase (AChE), an enzyme participating in nerve impulse transmission.<sup>1</sup> These potential health hazards and corresponding environmental concerns have brought about stricter legislative limits resulting in mounting pressure on analysis laboratories to process an increasing number of samples. In response to the increasing demand for monitoring, there has been a trend to miniaturize and automate classical methods to reduce costs and analysis time.<sup>2</sup>

For laboratory based detection of pesticides, the currently accepted standard methods (e.g. EPA Method 632), are performed by gas chromatography<sup>3</sup> or high-performance liquid chromatography<sup>4</sup> coupled with mass spectroscopy. These methods, though sensitive and effective in detecting pesticides, are complex requiring shipment of samples, long processing times, skilled technicians and expensive instrumentation and thus incur high operational costs. Likewise the consumption of large amount of solvents is the norm with such methods ironically creating additional environmental concerns with the very process used to monitor contamination problems.

As an alternative, a variety of biosensors (biological receptors with selective affinity towards a specific pesticide) have been developed.<sup>5</sup> These

biosensors can be subdivided as either using enzymes (enzyme inhibition-based)<sup>6</sup> or immunosensors (antibodies and antigens)<sup>7</sup> to selectively detect pesticides. The neurotoxic inhibition behaviour of some pesticides is so specific that it has been exploited as a sensitive enzyme inhibition-based spectrometric detection method.<sup>8, 9</sup> Flow injection analysis with potentiometric and amperometric detection of pesticides have also been reported.<sup>1</sup>

Microfluidic devices have the potential for revolutionizing analytical methods due to their low consumption of reagents, low production costs, short analysis times and minimal power and space requirements. These characteristics make these devices economically and environmentally very attractive.<sup>10</sup> The use of centrifugal force as a pumping method in microfluidics has given rise to what is called “Lab on a CD”<sup>11</sup> or simply “centrifugal microfluidics”.<sup>12</sup> This inherent pumping force has facilitated the use of a large variety of solvents and consequently allows the implementation of many known chemistries while keeping the instrumentation footprint small. Centrifugal microfluidic devices have been used in an increasing number of *clinical applications*,<sup>13</sup> including PCR amplification,<sup>14</sup> multiple biochemical analysis and sandwich type immunoassay from whole blood<sup>15</sup> as well as for enzyme-linked immunosorbent assays (ELISA).<sup>16, 17</sup> Centrifugal microfluidic devices have also been used in a variety of *environmental applications* such as the determination of trace metals<sup>18</sup> such as chromium (VI) in water,<sup>19</sup> nitrates and nitrites in water,<sup>20</sup> and polycyclic aromatic hydrocarbons (PAHs) in both water and soil.<sup>21, 22</sup>

In regards to environmental applications, the analysis of both aqueous and solid samples is necessary to effectively monitor pollutants of interest. Before

environmental solid samples can be analyzed they need to be prepared, in other words they need to be mixed, ground up, extracted and/or digested. This is also true of most if not all pesticide residues determination methods, as recently reviewed.<sup>23</sup> To incorporate sample preparation into an automated centrifugal microfluidic device, a magnetically actuated solid sample preparation has been reported<sup>24</sup> and has been applied to the liquid-solid extraction of both PAHs<sup>21</sup> and oil and grease<sup>25</sup> from soil samples. Likewise the ability to sediment and filter soil samples has been reported.<sup>26</sup>

We present here two centrifugal microfluidic devices, one for vegetable analysis and one for soil analysis, for the enzyme inhibition-based determination of pesticides. These two designs are a demonstration of a capability for a broader class of problems. The demonstration pesticide, carbofuran, has one of the highest acute toxicities to humans of any pesticide widely used on field crops. In each device, ten solid samples were simultaneously prepared and then, after an automated series of sequential reactions, were analyzed for the presence of carbofuran. These devices address the unmet need for inexpensive potentially field portable analytical instrumentations and methods for environmental testing of solid samples incorporating a reduction in time and solvent without extensive operator intervention. As such they are a simpler, greener and faster alternative for such essential routine analyses.

### **7.3 Experimental**

The enzyme inhibition-based determination of pesticide residues from solid samples is a multi-step process requiring precise control of timing and liquid

movement. As seen in Figure 7-1, the inhibitor pesticide is first extracted from the sample with buffer. The next step, that is key to the method, is the irreversible interaction of the enzyme with the extracted inhibitor pesticide,<sup>6</sup> before the subsequent addition of the substrate and chromatic reagent in the final step. This precise sequential interaction along with efficient sample extraction and filtration were the main factors in the design and fabrication of the devices as described below.

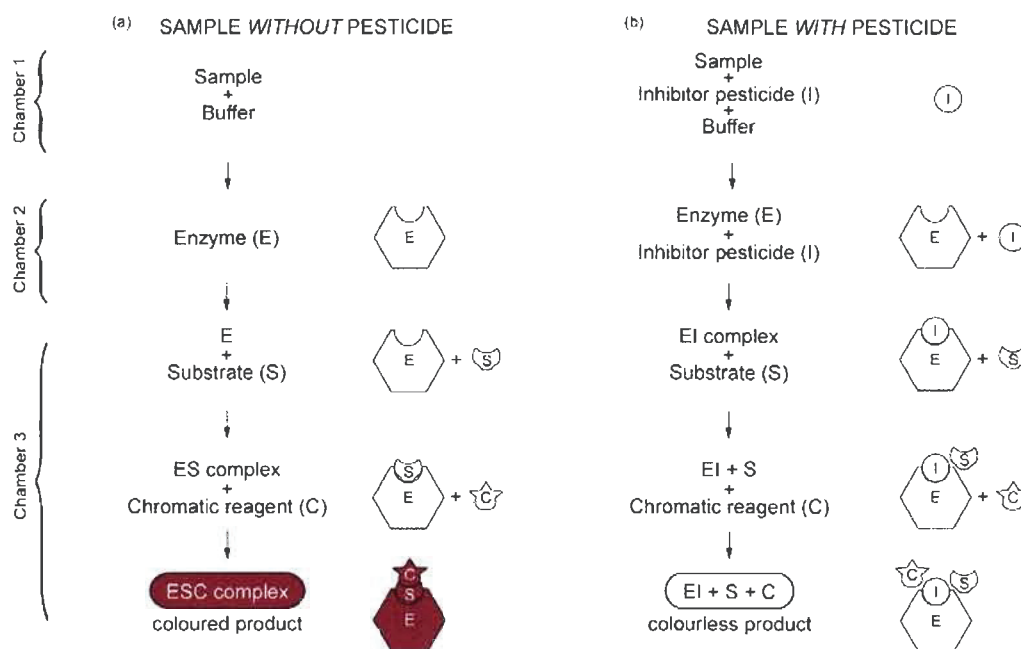


**Figure 7-1. Enzyme inhibition-based determination of pesticide residues.** The multi-step reaction is divided into multiple chambers. (a) Complete reaction process without inhibitor pesticide results in a coloured product. (b) Complete reaction process with high concentration of inhibitor pesticide results in no coloured product. Chamber labels at left refer to chambers of Figure 7-2(iii), location of each subsequent step.

### 7.3.1 Standards, Reagents and Samples

The reagents specific to the enzyme inhibition-based technique and their respective functions are detailed in Table 7-1. From the stock concentration a variety of working standards were prepared as needed in either distilled deionised water (DDW, 18 M $\Omega$ , Millipore Co., Bedford, MA), ethanol (EtOH, Commercial Alcohols, Brampton, ON) or pH 7.7 phosphate buffer. The buffer solution was prepared from 90 mL of 0.07 mol/L disodium hydrogen phosphate (Na<sub>2</sub>HPO<sub>4</sub>, Fisher Scientific, NJ) mixed with 10 mL of 0.07 mol/L potassium phosphate monobasic (KH<sub>2</sub>PO<sub>4</sub>, Fisher Scientific, NJ). A 0.1 M sodium hydroxide (NaOH, Fisher Scientific, Fair Lawn, NJ) solution was prepared in DDW for pre-treating the fused silica capillaries.

Table 7-1. Enzyme inhibition-based technique reagents details

<i>Function</i>	<i>Name</i>	<i>Stock concentration</i>	<i>Working concentrations</i>	<i>Provider</i>
Inhibitor Pesticide (I)	Carbofuran*	Analytical standard, 99.9%	1.00 $\mu\text{g mL}^{-1}$ in DDW	Fluka, Germany
Enzyme (E)	Acetylcholinesterase (AChE) (from electrophorus electricus, electric eel)	425.94 U/mg	2.0 to 40 U/mL in buffer	Sigma-Aldrich, CA
Substrate (S)	1-Naphthyl acetate	Pure, store at -20°C	12.5 to 50 mg/L in EtOH	Sigma-Aldrich, CA
Chromatic reagent (C)	Fast Blue B Salt	Dye 95%	20 to 80 mg/L in DDW	Fluka, Germany

\* Member of the carbamate pesticide family, carbofuran is 2,3-dihydro-2,2-dimethyl-7-benzofuranyl methylcarbamate

In-house synthetic vegetable and soil reference materials were prepared. Vegetable samples (cabbage) were purchased from a local market and stored at 5°C until used whereas soil samples were obtained from Saint-Jean-sur-Richelieu, Quebec, Canada.<sup>27</sup> From the carbofuran stock powder a 100  $\mu\text{g mL}^{-1}$

carbofuran primary standard solution was prepared in DDW, from which a  $1.00 \mu\text{g mL}^{-1}$  (1.00 ppm) carbofuran working solution in DDW was prepared. Distinct bulk batches of known masses of both vegetable and soil samples were manually spiked with varying known amounts the carbofuran working solution, stirred for several minutes to achieve homogeneity and then allowed to dry. This resulted in surface adsorbed bio-available known carbofuran concentration of 0.25 and 0.50 ppm ( $\mu\text{g g}^{-1}$ ) in the spiked vegetable and soil samples. A series of blanks were also prepared by spiking vegetable and soil samples with pure buffer solution and treating them to the same procedure. All of these samples were then standardized by determining their concentration by a conventional macroscale method described below.

### 7.3.2 Device Fabrication

The devices permitted the integration and automation of the multi-step enzyme inhibition-based technique. Photographs of the vegetable and soil devices are seen in Figure 7-2a(i) and Figure 7-2b(i) respectively. These two different centrifugal microfluidic devices were fabricated using a rapid prototyping technique similar to that developed by Kido.<sup>28</sup>

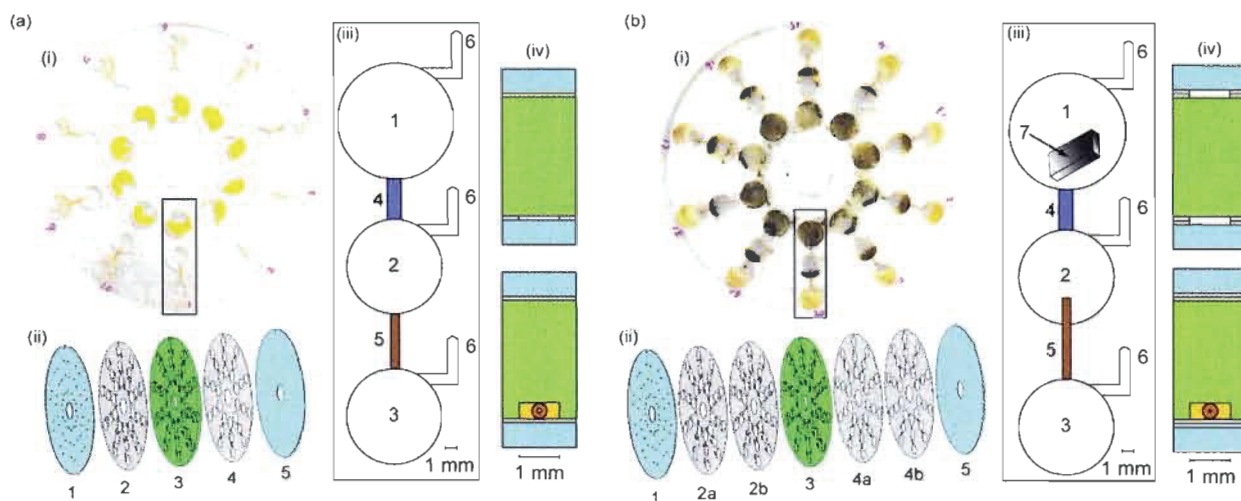


**Figure 7-2.** Centrifugal microfluidic device components and features. (a) Vegetable analysis centrifugal microfluidic device. (b) Soil analysis centrifugal microfluidic device.

*Following description applies to the respective parts of both (a) and (b):* (i) Photograph of device with 10 sets of chambers. Highlighted area is enlarged in (iii). (ii) Exploded view of device showing following layers: (1) Top PC disk with vent holes, (2) adhesive layer including rectangular passive valves, (3) middle PMMA disk with chambers into which cylindrical capillaries are epoxied, (4) adhesive layer, (5) bottom PC disk. (iii) Schematic of one set of chambers including: (1) Chamber 1 - Extraction Chamber, (2) Chamber 2 - for interaction with enzyme, (3) Chamber 3 - for ESC complex formation and detection cell, (4) rectangular passive capillary valve at a radial distance of 29 mm, (5) cylindrical passive capillary valve at a radial distance of 47 mm, (6) vent holes and vent lines (0.1 mm deep x 1 mm wide), (7) "mobile magnet" agitator. (iv) Side cut view of valves

The multiple layers of each device were first designed in the three dimensional computer-aided design (CAD) software "SolidWorks 2005" (SolidWorks Corp., Concord, MA). Next, each layer was manufactured either by xurography<sup>29</sup> or by micro-milling. As seen in Figure 7-2a(ii) and Figure 7-2b(ii), the devices were made of a composite of polycarbonate (PC) disks, adhesive layers and poly(methyl methacrylate) (PMMA) disks. The PC disks were standard 120 mm diameter x 0.6 mm DVDs without reflective coating (U-Tech Media Corp, Taiwan, People's Republic of China) that served as top and bottom layers. The adhesive layers were 100  $\mu$ m thick double-sided film (FLEXmount DFM 200 Clear V-95 150 poly H-9 V-95 4, FLEXcon, Spencer, MA) that were cut

to 120 mm diameter. The middle layers consisted of 2.9 mm thick PMMA pieces (Acrylite OP-1, Cyro Industries, Rockaway, NJ) which were milled to 120 mm diameter. Chambers, centre holes, loading holes and vent holes were made in the PC and PMMA disks using a computer numerically controlled (CNC) micro-milling machine (QuickCircuit 5000, T-Tech, Inc. Norcross, GA) whereas channels, chambers and vent lines including the rectangular passive valves (see valve section below) were cut in the adhesive layers by xurography with a cutting plotter (CE300Mk2-60, Graphtec America, Inc., Santa Ana, CA).

After designing and manufacturing the layers, the devices were assembled by carefully aligning and firmly pressing together the layers using a hand cranked cold laminator (Jet Mounter ML25, Drytac, Concord, ON). During assembly, capillary valves were also added (see valve section below). Before laminating the final layer, sample and one “mobile magnet” (for the soil device only – see below) were added to each Extraction Chamber (Figure 7-2(iii)1). The resulting centrifugal microfluidic devices were a laminate of 5 to 7 layers (Figure 7-2(ii)) containing ten sets of chambers (Figure 7-2(i)). At this point reagents were pipetted into the various chambers and all loading holes were sealed with microplate sealing tape (Nunc sealing tape T9571, Sigma-Aldrich Corp., St. Louis, MO) to avoid contamination.

The design of the vegetable and soil devices differed from one another in terms of thickness, incorporated agitator and valve sizes. These were engineered to optimize the pesticide detection for the two distinct samples (vegetable and soil). In regards to thickness, the final vegetable device had dimensions of 120 mm diameter x 4.3 mm thick with an integrated 3.1 mm

Detection Chamber (Figure 7-2a(iii)3) whereas the soil device had dimensions of 120 mm diameter x 4.5 mm thick with an integrated 3.3 mm Detection Chamber (Figure 7-2b(iii)3); the difference being the double adhesives in the soil device. Another difference was that each extraction chamber of the soil device included one “mobile magnet” (Figure 7-2b(iii)7, 5.08 mm × 2.57 mm × 1.14 mm, nickel plated NdFeB rectangular magnet, magnetized parallel to width; NB045-35, Master Magnetics Inc., Castle Rock, CO)<sup>21, 24</sup>, not present in the vegetable device. Finally the valve sizes and construction differed in the two devices as detail below.

### 7.3.3 Valves

Two types of passive capillary valves (rectangular and cylindrical) were integrated into the devices and their burst frequencies with the use of buffer were determined.

The first type of valve was a rectangular passive capillary valve (Figure 7-2(iii)4) made by cutting fine features in the adhesive layer itself, where each layer was of 100 µm. This valve was another important difference between the vegetable and soil devices. Only one single layer valve (one 100 µm thick x 1000 µm wide) was engineered into the vegetable device between chambers 1 and 2 (Figure 7-2a(iii)4) whereas two double layer valves (two 200 µm thick x 1000 µm wide) were designed and built between these chambers the soil device (Figure 7-2b(iii)4 and Figure 7-3). In other words, the effective total thicknesses of the channels were of 100 µm in the vegetable device and of 400 µm in the soil device. This is illustrated comparing Figure 7-2a(iv) to Figure 7-2b(iv).

The second type of valve, a cylindrical passive capillary valve (Figure 7-2(iii)5), was made from fused silica capillary (Polymicro Technologies, Phoenix, AZ), similar to those reported by LaCroix-Fralish *et al.*<sup>26</sup> These valves had a fixed outer diameter (OD) of 360  $\mu\text{m}$ , while four different inner diameters (ID) were studied (25, 50, 75 and 100  $\mu\text{m}$ ). Before inclusion of the capillaries during the assembly step, the capillaries were pre-treated with 0.1 M NaOH, EtOH and air prior to being cut to either 4.5 or 6.5 mm lengths. They were then glued into small channels (1.0 mm wide by 400  $\mu\text{m}$  deep) that had been milled for this purpose in the bottom side of the middle PMMA layer (Figure 7-2(iv) and Figure 7-3) using commercially available 5 minute epoxy which both sealed the channel and held the capillary firmly in place. This valve was also different in the two devices. A 100  $\mu\text{m}$  ID capillary (by 4.5 mm length) was used in the vegetable device between Chamber 2 and 3 and was flush to the bottom of Chamber 2 (Figure 7-2a(iii)5) whereas a 50  $\mu\text{m}$  ID capillary (by 6.5 mm length) was used in the soil device and protruded 2 mm into Chamber 2 creating an effective “snorkel”<sup>26</sup> for sedimentation and filtration of the soil (Figure 7-2b(iii)5 and Figure 7-3).

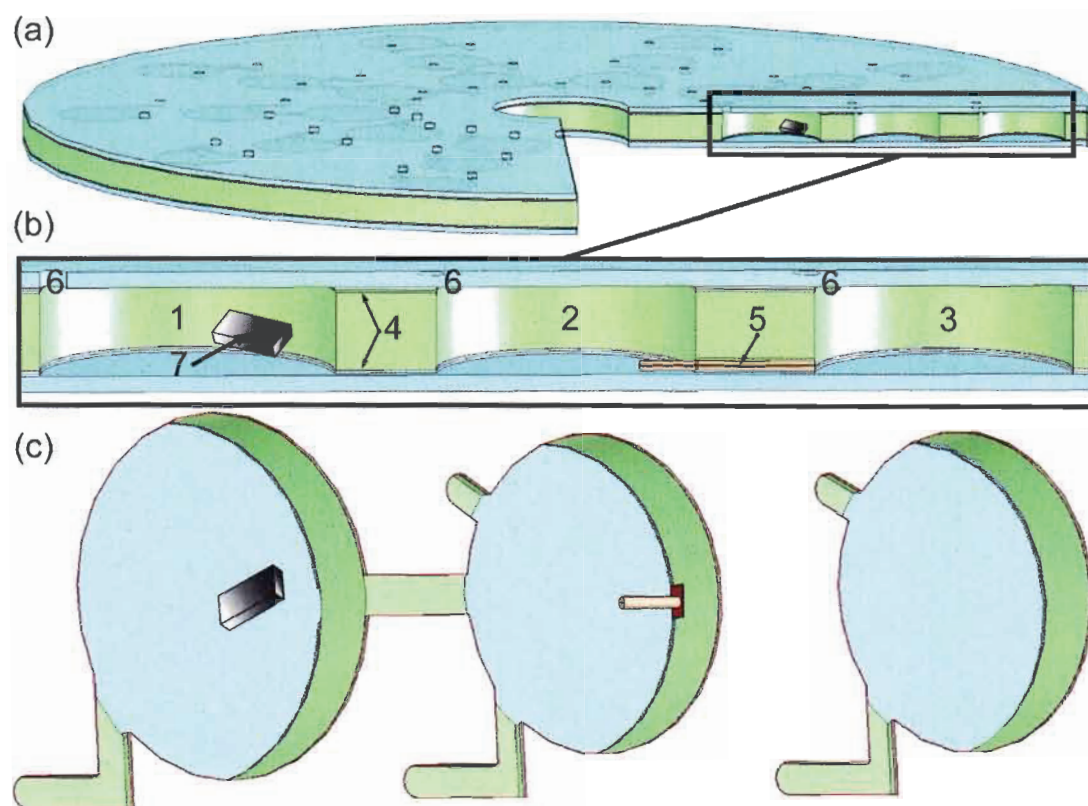


Figure 7-3. Soil analysis centrifugal microfluidic device. (a) Cut isometric side view of device. Highlighted area is enlarged in (b). (b) Zoom side view of one set of chambers (1) Chamber 1 - Extraction Chamber, (2) Chamber 2 - for interaction with enzyme, (3) Chamber 3 - for ESC complex formation and detection cell, (4) two 200  $\mu\text{m}$  rectangular passive capillary valve, (5) cylindrical passive capillary valve with protruding snorkel into Chamber 2, (6) vent holes and vent lines, (7) "mobile magnet" agitator. (c) Isometric view of one set of chambers (shown without top layer).

### 7.3.4 Centrifugal System

High-speed digital images were obtained using a motorized stage and strobe system developed by Duford *et al.*<sup>24</sup> supplemented with a colour digital camera (GRAS-14S5C-C, Point Grey, BC, Canada). The motorized stage, strobe, and camera were controlled by a LabVIEW program (LabVIEW 8.6, Developer Version, National Instruments, QC, Canada). The devices were secured to the spindle of the motorized stage and spun at different speeds as discussed below (Figure 7-4).

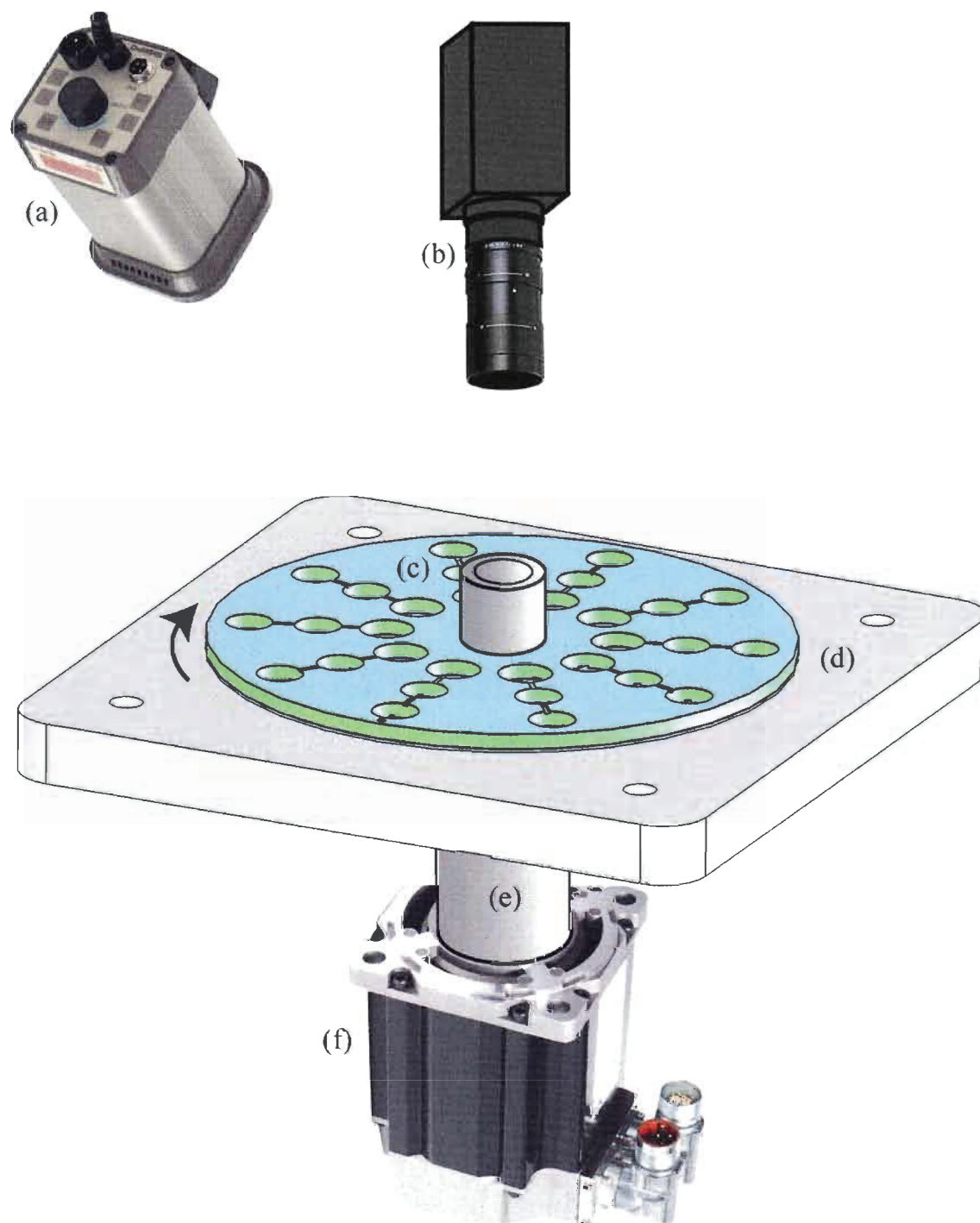
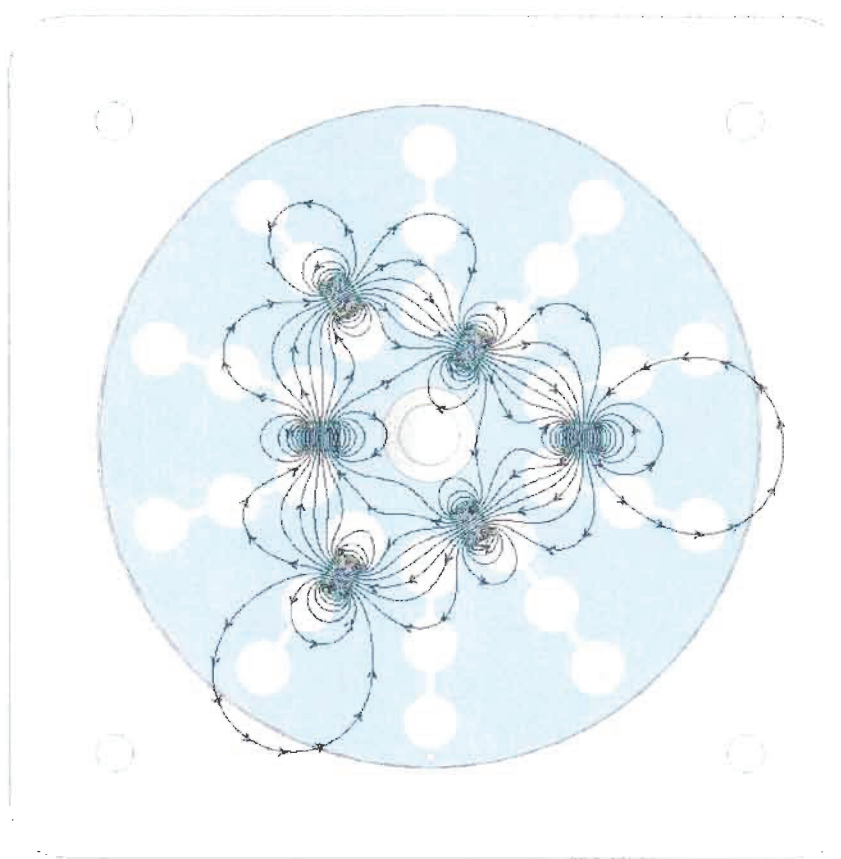


Figure 7-4. Schematic of experimental set-up. (a) Strobe, (b) camera and lens, (c) soil centrifugal microfluidic device, (d) fixed base with six fixed magnets (see also Figure 7-5), (e) spindle shaft and (f) servo motor.

Mixing and liquid-solid extraction in the vegetable device was achieved by alternating the direction of rotation every half turn for 10 minutes at 80 rpm (1.3 Hz). This process was enhanced in the soil device by a magnetically actuated solid sample preparation technique<sup>24</sup> involving the interaction of the “mobile magnets” in the Extraction Chamber of the devices and a non-contact series of six permanent magnets in a fixed base which was in close proximity (Figure 7-4(d) and Figure 7-5). As the devices spun, the “mobile magnets” were alternately subjected to stronger magnetic fields pulling them inward and outward in the chambers during the rotational cycle while simultaneously being made to rotate upon their own axes due to their own magnetic poles. The resulting spinning and shaking mechanical motion increased the agitation of the soil samples. The intensity of the agitation was controlled by 1) the proximity of the fixed base magnets relative to the rotating device and 2) the rotational speed.



**Figure 7-5.** Magnet position and flux lines of the six fixed magnets in fixed base seen through a top semi-transparent view of centrifugal device.

### 7.3.5 Detection System

After automated centrifugation, the devices were moved from the motorized stage to a detection stage, though these could easily be merged into a single instrument in the future. The detection stage is described in detail elsewhere<sup>19, 21</sup> and included a deuterium light source (DT-MINI-2-GS, Ocean Optics, Dunedin, FL) and a USB miniature spectrometer (USB4000-UV-VIS, Ocean Optics, Dunedin, FL) set up at 180 degrees. The pesticide concentration was calculated from the determined absorbance signal through each of the 10 integrated detection cells (Chamber 3) of each device. The integrated intensity of 5 pixels around the maximum 525 nm of the broad absorption peak was used.

### 7.3.6 Methods

The method used was based on the People's Republic of China Standards Method number "GB/T 18630-2002".<sup>30</sup> The sensitivity of the technique was dependent on the following factors: 1) enzyme concentration, 2) substrate concentration, 3) chromatic reagent and 4) incubation time. These parameters were first optimized (see results section below) and then kept stable for all subsequent experiments.

The *conventional macroscale (bench top) method* for vegetable analysis consists of extracting pesticide residue from a 2.0 g subsample of the bulk batch spiked vegetable sample with 5.0 mL buffer and shaking for 2 minutes in a glass vial. Then 2.5 mL of the supernate is pipetted to a second glass vial and to this 0.5 mL of the 40 U/mL enzyme is added and allowed to react. After, 0.2 mL of 0.05% substrate and 0.2 mL 0.08% of chromatic reagent are added and diluted to

a final total volume of 5.0 mL with buffer. Similarly, the conventional macroscale method for soil analysis consists of extracting pesticide residue from a 1.0 g subsample of the bulk batched spiked soil sample with 2.5 mL buffer and shaking for 2 minutes in a glass vial. The entire extractant is then filtered into a second glass vial. To this 0.5 mL of the 40 U/mL of enzyme is added and allowed to react. After, 0.2 mL 0.05% of substrate and 0.2 mL 0.08% of chromatic reagent are added and diluted to a final total volume of 5.0 mL with buffer. Finally, in both analyses the coloured product is transferred to a 1 cm cuvette and the absorbance is measured at 525 nm using a bench top spectrophotometer (Cary 5000 UV-Vis Near IR Spectrophotometer, Varian, Palo Alto, CA). A calibration curve is also prepared from standards treated in a similar fashion. The carbofuran concentrations are therefore determined, effectively standardizing the samples for use in the disk method.

These bench top methods were scaled down for use in the microfluidic devices (*disk methods*). As seen in Figure 7-1, Figure 7-2 and Table 7-2, before executing the spin sequence, the devices were pre-loaded with all the required reagents. This included 120  $\mu$ L of buffer to each Extraction Chamber (Chamber 1) which already contained 0.04 g of dried spiked vegetable or soil sample (and one “mobile magnet” for the soil device only), 60  $\mu$ L of enzyme to Chamber 2 and 20  $\mu$ L mixture of substrate and chromatic agent to Chamber 3. Substrate and chromatic reagent were added separately in the bench top methods whereas it was found to be more convenient for these to be premixed and added together in the disk methods without affecting the results.

**Table 7-2. Spin sequence detailing steps for sample treatment and liquid movement for both the automated vegetable and soil disk methods**

Step	Location	Content	Vegetable device		Soil device		Result
			Action	Time	Action	Time	
1	Chamber 1	- 120 $\mu$ L buffer - Spiked sample	Shake 80 rpm	10 min	Spin 80 rpm with magnets	10 min	Extraction of pesticide from sample
2	Chamber 1 to 2		Spin 400 rpm	30 s	Spin 800 rpm	30 s	Movement of liquid
3	Chamber 2	- 60 $\mu$ L enzyme - contents of chamber 1	Stop 0 rpm	10 min	Stop 0 rpm	10 min	Reaction of pesticide with enzyme
4	Chamber 2 to 3		Spin 700 rpm	60 s	Spin 2000 rpm	5 min <sup>a</sup>	Movement of liquid
5	Chamber 3	- 20 $\mu$ L substrate and chromatic reagent mixture - contents of chamber 2	Stop 0 rpm	10 min	Stop 0 rpm	5 min <sup>a</sup>	Formation of ESC <sup>b</sup> complex
6	Chamber 3	ESC <sup>b</sup> complex	Detection stage		Detection stage		Absorbance recorded at 525 nm

<sup>a</sup> Though the device was spun for 5 min, most of the liquid transferred in a short amount of time. Total development of the coloured complex consequently was almost 10 minutes.

<sup>b</sup> Enzyme-Substrate-Chromatic reagent (ESC) coloured complex

## 7.4 Results and Discussion

The first series of experiments (as seen in Figure 7-6) optimized for the following factors affecting the sensitivity of the method: 1) enzyme concentration, 2) substrate concentration, 3) chromatic reagent concentration and 4) stability of coloured Enzyme-Substrate-Chromatic reagent (ESC) complex. Only one factor was changed at a time in each experiment though in the future a simplex optimization is envisioned. Optimized concentrations were determined to be 12 U/mL enzyme, 50 mg/L substrate and 40 mg/L chromatic reagent. The spectrum of the ESC complex was a broad peak covering the entire visible range and centred around 525 nm. The development of the coloured ESC complex took less than 10 minutes. Once the colour developed, the complex remained

stable for over an hour. These parameters were kept constant for all subsequent experiments.

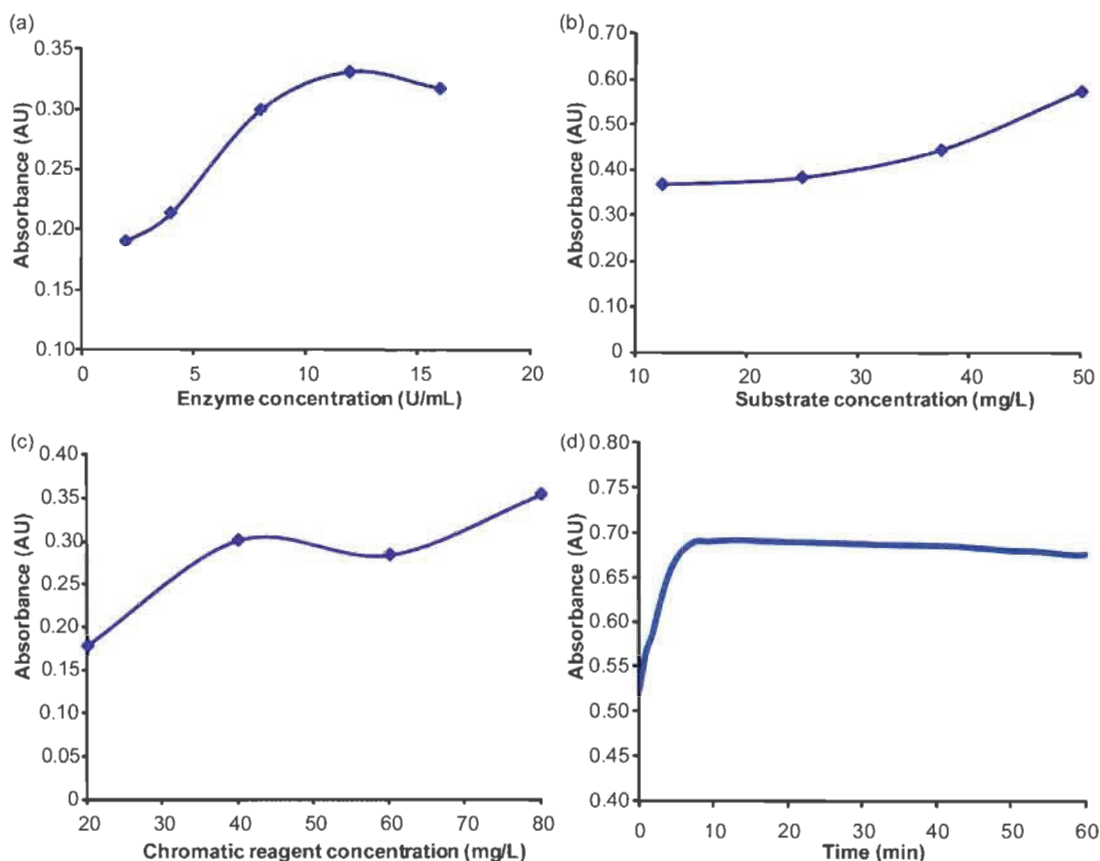


Figure 7-6. Optimization of operating parameters. (a) Effect of enzyme concentration on absorbance. Obtained with pH 7.71 phosphate buffer, 25 mg/L substrate, 40 mg/L chromatic reagent. (b) Effect of substrate concentration on absorbance. Obtained with pH 7.71 phosphate buffer, 12 U/mL enzyme, 40 mg/L chromatic reagent. (c) Effect of chromatic reagent concentration on absorbance. Obtained with pH 7.71 phosphate buffer, 12 U/mL enzyme, 50 mg/L substrate. (d) Stability of the ESC complex. Obtained with pH 7.71 phosphate buffer, 4 U/mL enzyme, 20 mg/L substrate, 32 mg/L chromatic reagent, and detected by Varian UV-VIS spectrometer in kinetic mode.

The pesticide is an enzyme inhibitor. When an inhibited enzyme molecule interacts with the substrate in Chamber 3, no interaction occurs since there is no space for the substrate to form a complex with the enzyme. As a consequence of this, no coloured ESC complex can form. The percent inhibition ( $In(\%)$ ) is consequently calculated from a comparison of the absorbance of the sample ( $A_s$ )

to that of the deeply coloured ESC complex of an uninhibited sample without pesticide ( $A_0$ ), in essence a blank (Equation 7-1).

$$In(\%) = \frac{A_0 - A_s}{A_0} \times 100\% \quad (\text{Equation 7-1})$$

This percent inhibition is logarithmically proportional to the concentration ( $C$ ) of pesticide (Equation 7-2), in other words, the concentration of pesticide is proportional to the antilogarithm of the percent inhibition (Equation 7-3).

$$In(\%) = k \log C + b \quad (\text{Equation 7-2})$$

$$C = 10^{\frac{In(\%) - b}{m}} \quad (\text{Equation 7-3})$$

A plot of percent inhibition versus log base 10 of carbofuran pesticide residue produced a linear least squares regression plot with an  $R^2$  coefficient of 0.989, a slope of 21.7 and an intercept of -12.7. As detailed in Appendix F, the limit of detection for an enzyme inhibition assay ( $LOD_{\text{enzyme inhibition assay}}$ ) must take into consideration both the error in measuring the sample blank and the standard<sup>6</sup> (versus the conventional three standard deviations of the blank) as expressed by:

$$LOD_{\text{enzyme inhibition assay}} = 10^{\frac{(In(\%)_0 + 3\sigma_{In(\%)_0} + 3\sigma_{In(\%)_s}) - b}{m}} \quad (\text{Equation 7-4})$$

The limit of detection (LOD) was thus calculated to be 0.1 ppm or  $\mu\text{g g}^{-1}$  or  $\text{mg kg}^{-1}$  (5 ng absolute limit of detection) with a linear range up to 5 ppm or  $\mu\text{g g}^{-1}$  (200 ng absolute) for both vegetable and soil methods. This is well below the Food and Agriculture Organization of the United Nations (FAO) and World Health

Organization (WHO) limit of  $2 \text{ mg kg}^{-1}$  carbofuran.<sup>31</sup> Likewise for comparison, taking into consideration the small sample volume ( $200 \text{ }\mu\text{L}$ ), this LOD corresponds to  $20 \text{ }\mu\text{g L}^{-1}$  carbofuran which is only one order of magnitude higher than the complex HPLC method (EPA Method 632) LOD of  $3.2 \text{ }\mu\text{g L}^{-1}$  carbofuran in water, while still below the maximum allowable US federal limit of  $40 \text{ }\mu\text{g L}^{-1}$  carbofuran.<sup>32</sup>

Many detection methods are limited by the sample preparation and efficiency of analyte extraction from the matrix. In the enzyme inhibition-base determination of pesticide residues, the first step is a liquid-solid extraction of the inhibitor pesticide carbofuran from either vegetable or soil with buffer. As described, an enhanced extraction method was used for soil samples by adding a “mobile magnet” to the Extraction Chamber which was induced to spin and shake by the fixed magnet base in close proximity. As a comparison, the same extraction of pesticide from soil was performed without the “mobile magnet” and it was clear that the magnetically actuated extraction was more efficient, extracting the same amount of pesticide on average 3 minutes faster than without the “mobile magnet”.

A secondary objective of the investigation was to see if both adsorbed and absorbed pesticide could be extracted from the vegetable samples. To do this, the same “mobile magnets” were used in the vegetable devices. Unfortunately the magnets were so effective in mixing that the sample was quickly pureed and minimal extractant liquid was recoverable with the current valve system. A series of wash and filtering steps would have been needed. Likewise, from the minimal extractant liquid obtained, it was obvious that a matrix effect would significantly

affect the absorbance measurement since many vegetable pigments such as chlorophyll had coloured the extractant as Jin *et al.* have also reported.<sup>1</sup> For this reason, a slower and gentler extraction of adsorbed pesticide from the vegetable samples was achieved by an alternating “washing machine” motion by changing the direction of rotation every half turn for 10 minutes.

Other than the “mobile magnets” in the soil device, the vegetable and soil devices make use of different valve designs. The valves are necessary to restrict liquid flow to fixed predetermined moments in the spin sequence. This allows for effective automated control of liquid movement from one chamber to the next. Typically only one type of valve is used on a device; here however the interaction of the two types of valves complemented themselves and allowed for greater control. The rectangular passive valves were determined to burst (*i.e.* let liquid through) at rotational rates between 200 to 300 rpm. While the devices were spun below that rotational speed (*e.g.* 80 rpm), the buffer remained in the Extraction Chamber. The vegetable sample did not clog or obstruct the thin rectangular passive valve (100  $\mu\text{m}$  thick x 1000  $\mu\text{m}$  wide); however, fine soil (especially after 10 minutes of magnetically actuated extraction) did clog such a small valve. It was finally determined that two thicker rectangular passive valves (200  $\mu\text{m}$  thick x 1000  $\mu\text{m}$  wide each) would burst in a similar range and not be clogged by the fine soil. On the other hand, some soil travelled through these channels to Chamber 2 which contained the enzyme. To remove these finer soil particles, the second set of valves, cylindrical passive capillary valves, were also different in the vegetable and soil devices. First, the burst frequencies of the different sized capillaries were determined (Figure 7-7). In the vegetable device,

the cylindrical capillary valves (Figure 7-2a(iii)5) were flush with the bottom of the chamber to minimize liquid loss and had an ID of 100  $\mu\text{m}$  and a burst frequency of  $410 \pm 25$  rpm. This size was chosen in order not to burst at 300 rpm when liquid is being transferred from Chamber 1 to 2, thus controlling the liquid flow. Once the extractant had reacted with the enzyme, the device was spun at 700 rpm and the liquid was quickly transferred to the Chamber 3. On the other hand, the cylindrical passive capillary valves in the soil device (Figure 7-2b(iii)5) were smaller (50  $\mu\text{m}$  ID), had a higher burst frequency and protruded 2 mm into Chamber 2 creating an effective snorkel for sedimentation and filtration of the fine soil.<sup>26</sup> Once the extractant reacted with the enzyme for 10 minutes, the soil device was spun at 2000 rpm. The smaller capillary (in regards to ID) was chosen to slow the transfer of the liquid to give time to the fine soil particles to sediment to the bottom of Chamber 2 (see details below) leaving only a clear liquid to transfer to Chamber 3 via the capillary. If the liquid transfer had been more rapid with a larger capillary (in regards to ID) the fine soil particles would not have had time to settle past the level of the snorkel and would have transferred and caused undesirable scatter in the absorption measurement taken through Chamber 3. A small reproducible amount of liquid did remain in Chamber 2 due to the snorkel.

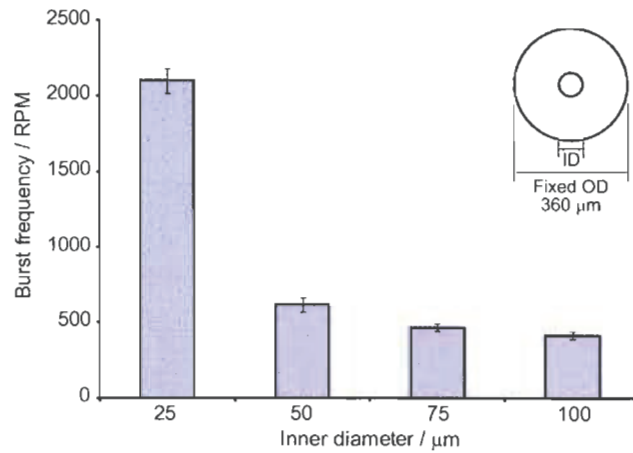


**Figure 7-7.** Burst frequency of buffer as a function of different inner diameter cylindrical passive capillary valves at a radius of 42 mm from the centre of the disk and of length of 4.5 mm

The time it took for fine soil particles to sediment to the bottom of Chamber 2 was calculated using Stokes' Law<sup>33</sup> which states that the magnitude of the resistive frictional force ( $F_r$ ) on the particle of a given Stokes' radius ( $R$ ) sedimenting through a fluid of a given viscosity ( $\eta$ ) with a given velocity ( $v$ ) is equal to:

$$F_r = 6\pi\eta Rv \quad (\text{Equation 7-5})$$

From this Law the settling velocity ( $v_s$ ) of a particle by centrifugation can be derived taking into consideration the density of the particle ( $\rho_p$ ), the density of the fluid ( $\rho_f$ ), the average distance of the particle from the centre of rotation ( $r$ ) and the angular velocity ( $\omega$ ).

$$v_s = \frac{2R^2\omega^2r}{9\eta}(\rho_p - \rho_f) \quad (\text{Equation 7-6})$$

Assuming that the smallest soil particles had a radius of  $3.0 \times 10^{-4}$  mm and settled from an average radial distance of 37.2 mm, it took approximately 82 seconds for the particles to settle 4.8 mm to the bottom of Chamber 2 with the motor spinning at 2000 rpm. The same settling under the force of gravity would have taken 170 times longer (3 hours 53 minutes and 20 seconds). Additional details are available in Appendix G. This further illustrates the advantages of integrating microfluidic techniques for solid sampling on centrifugal devices, since centrifugation is a key operation that is inherent to them.

Next a *comparison to existing methods* was made (Table 7-3 and Table 7-4). The methods show linearity over the concentration range.

**Table 7-3. Comparison of extraction methods for the analysis of vegetable samples**

Vegetable sample	<b>Disk method</b> Sample size: 0.04 g Pathlength: 3.1 mm Solvent volume: 200 $\mu$ L			<b>Bench top method</b> Sample size: 2.0 g Pathlength: 10.0 mm Solvent volume: 7.5 mL		
	Concentration ( $\mu$ g g <sup>-1</sup> )	Abs. RSD (%) (n=8)	Conc. RSD (%) (n=8)	Concentration ( $\mu$ g g <sup>-1</sup> )	Abs. RSD (%) (n=3)	Conc. RSD (%) (n=3)
1	0.23 $\pm$ 0.09	10	39	0.25 $\pm$ 0.05	2	19
2	0.51 $\pm$ 0.13	7	25	0.56 $\pm$ 0.19	3	34

**Table 7-4. Comparison of extraction methods for the analysis of soil samples**

Soil sample	<b>Disk method</b> Sample size: 0.04 g Pathlength: 3.3 mm Solvent volume: 200 $\mu$ L			<b>Bench top method</b> Sample size: 1.0 g Pathlength: 10.0 mm Solvent volume: 5.0 mL		
	Concentration ( $\mu$ g g <sup>-1</sup> )	Abs. RSD (%)	Conc. RSD (%)	Concentration ( $\mu$ g g <sup>-1</sup> )	Abs. RSD (%) (n=3)	Conc. RSD (%) (n=3)
1	0.23 $\pm$ 0.08	4 (n=6)	34 (n=6)	0.23 $\pm$ 0.04	2	19
2	0.47 $\pm$ 0.18	7 (n=4)	39 (n=4)	0.58 $\pm$ 0.17	3	30

The inherent advantages of microfluidic devices are clear when comparing the methods. A series of F-tests and t-tests confirmed that the precision and mean concentrations of the disk methods as compared to the respective bench top methods were statistically similar; though the disk method allowed a two orders of magnitude reduction in sample size, a 25 to 37 times reduction in reagents, including a reduction in the relatively expensive enzyme key to the technique.

These improvements were achieved even if the path length was three times shorter, though future integration of methods to increase path length on a disk such as those developed by Grumann *et al.*<sup>34</sup> are to be envisioned. Alternately, fluorescence detection method are inherently more sensitive and have been reported to greatly eliminate the possible matrix effect originated by the presence of some vegetable pigments.<sup>1</sup> Of concern was the apparently high concentration RSD's between 19 and 39%, though the corresponding absorbance RSD's were of an acceptable 2 to 10%. This is explained through the purely mathematical propagation of error. A detailed step-by-step discussion of this is available in Appendix F, and is summarized by two key factors: 1) the error associated with Equation 7-1 for calculating the percent inhibition compounds the error of the sample blank with that of the sample, due to the nature of the comparison and 2) the error associated with Equation 7-3 for calculating the concentration of pesticide involves the antilogarithm of the percent inhibition which exponentially increases the error.

Sources of error also included the possible inhomogeneity of the in-house reference materials though the bench top method absorbance RSD of only 2 to

3% showed that this was minor. It has been reported that temperature is also a factor that would influence the reactions involved in the enzyme inhibition process.<sup>8</sup> Though not monitored in the performed experiments, future work should include a constant monitoring of the temperature or even a heated environment to speed up the analysis. Error in the soil device was also introduced in the construction of the snorkel using a capillary between Chamber 2 and Chamber 3 (Figure 7-2). If the heights of all the snorkels were not precisely the same, varying amounts of sample volume would have been transferred to the detection cell. Likewise scatter of small soil particles that may have reached the detection cell (Chamber 3) would have increased the error. Meanwhile, pigments from the vegetable sample seem to also have been extracted and have been shown to potentially interfere with the absorbance measurement.<sup>1</sup> The multiwavelength ratiometric blank correction technique used in the PAH determination was not used here due to the broadband absorbance spectrum of the colour complex.

Due to the dependence of the results on many factors, *Amine et al.*<sup>6</sup> note that care should be taken in direct comparison between methods and consideration of the factors used in each case. Small changes in enzyme, substrate and chromatic reagent concentration as well as pH and time are all of importance. The use of a buffer and systematic automation of the devices greatly helped to keep these factors constant.

Future work would not only address detection but would also include better manipulation of samples and reagents. The need to pipette the reagents into the multiple reservoirs (sometimes called “World-to-Chip”<sup>35</sup> or “World-to-Disk”<sup>36</sup>

problem) limits the commercial application of the technique as described here. One alternative is to use lyophilised reagents that could be pre-loaded in the devices<sup>19</sup>; however, such systems still require the addition of liquid to reconstitute the solid reagents and are at times difficult to manufacture. Alternately, fresh reagents could be added to the spinning devices using a “centrifugal liquid addition distributor” or CLAD.<sup>36</sup> Such a distributor could also facilitate field work for easy sample insertion into the devices.

## **7.5 Conclusion**

As Jiang *et al.* concluded, “despite some limitations, biosensors such as enzyme inhibition techniques for pesticide monitoring are becoming more and more relevant in environmental and food analysis”.<sup>7</sup> The disks and methods discussed here add to these emerging monitoring techniques. The scaled down methods take full advantage of centrifugal microfluidics technology such as the minimal reagent and solvent use and the automated spin sequences. Rapid semi-quantitative to quantitative screening is possible with the current design for laboratory and field use making it an alternative of great interest for environmental monitoring.

## 7.6 References

- (1) Jin, S., Xu, Z., Chen, J., Liang, X., Wu, Y., Qian, X., "Determination of organophosphate and carbamate pesticides based on enzyme inhibition using a pH-sensitive fluorescence probe", *Analytica Chimica Acta*, **2004**, 523 (1), 117-123.
- (2) Ramos, L., Ramos, J.J., Brinkman, U.A.T., "Miniaturization in sample treatment for environmental analysis", *Analytical and Bioanalytical Chemistry*, **2005**, 381 (1), 119-140.
- (3) Van Der Hoff, G.R., Van Zoonen, P., "Trace analysis of pesticides by gas chromatography", *Journal of Chromatography A*, **1999**, 843 (1-2), 301-322.
- (4) Núñez, O., Moyano, E., Galceran, M.T., "LC-MS/MS analysis of organic toxics in food", *TrAC - Trends in Analytical Chemistry*, **2005**, 24 (7), 683-703.
- (5) Marty, J.L., Garcia, D., Rouillon, R., "Biosensors: Potential in pesticide detection", *Trends in Analytical Chemistry*, **1995**, 14 (7), 329-333.
- (6) Amine, A., Mohammadi, H., Bourais, I., Palleschi, G., "Enzyme inhibition-based biosensors for food safety and environmental monitoring", *Biosensors and Bioelectronics*, **2006**, 21 (8), 1405-1423.
- (7) Jiang, X., Li, D., Xu, X., Ying, Y., Li, Y., Ye, Z., Wang, J., "Immunosensors for detection of pesticide residues", *Biosensors and Bioelectronics*, **2008**, 23 (11), 1577-1587.
- (8) Mendoza, C.E., Shields, J.B., "Determination of some carbamates by enzyme inhibition techniques using thin-layer chromatography and colorimetry", *Journal of Agricultural and Food Chemistry*, **1973**, 21 (2), 178-184.
- (9) Mendoza, C.E., "Enzyme inhibition and chromatographic techniques: comparative studies and application to pesticide residue analysis", *International Journal of Environmental Analytical Chemistry*, **1974**, 3 (3), 171-183.
- (10) Mark, D., Haeberle, S., Roth, G., Stetten, F.v., Zengerle, R., "Microfluidic lab-on-a-chip platforms: requirements, characteristics and applications", *Chemical Society Reviews*, **2010**, 39 (3), 1153-1182.
- (11) Madou, M., Zoval, J., Jia, G., Kido, H., Kim, J., Kim, N., "Lab on a CD", *Annual Review of Biomedical Engineering*, **2006**, 8 601-628.
- (12) Steigert, J., Grumann, M., Brenner, T., Mittenbuehler, K., Nann, T., Ruehe, J., Moser, I., Haeberle, S., Riegger, L., Riegler, J., Bessler, W., Zengerle, R., Ducreé, J., "Integrated sample preparation, reaction, and detection on a high-frequency centrifugal microfluidic platform", *Journal of the Association for Laboratory Automation*, **2005**, 10 (5), 331-341.
- (13) Gorkin, R., Park, J., Siegrist, J., Amasia, M., Lee, B.S., Park, J.M., Kim, J., Kim, H., Madou, M., Cho, Y.K., "Centrifugal microfluidics for biomedical applications", *Lab on a Chip - Miniaturisation for Chemistry and Biology*, **2010**, 10 (14), 1758-1773.

- (14) Amasia, M., Cozzens, M., Madou, M.J., "Centrifugal microfluidic platform for rapid PCR amplification using integrated thermoelectric heating and ice-valving", *Sensors and Actuators, B: Chemical*, **2012**, 161 (1), 1191-1197.
- (15) Lee, B.S., Lee, Y.U., Kim, H.S., Kim, T.H., Park, J., Lee, J.G., Kim, J., Kim, H., Lee, W.G., Cho, Y.K., "Fully integrated lab-on-a-disc for simultaneous analysis of biochemistry and immunoassay from whole blood", *Lab on a Chip - Miniaturisation for Chemistry and Biology*, **2011**, 11 (1), 70-78.
- (16) Lai, S., Wang, S., Luo, J., Lee, L.J., Yang, S.-T., Madou, M.J., "Design of a Compact Disk-like Microfluidic Platform for Enzyme-Linked Immunosorbent Assay", *Analytical Chemistry*, **2004**, 76 (7), 1832-1837.
- (17) Lee, B.S., Lee, J.N., Park, J.M., Lee, J.G., Kim, S., Cho, Y.K., Ko, C., "A fully automated immunoassay from whole blood on a disc", *Lab on a Chip - Miniaturisation for Chemistry and Biology*, **2009**, 9 (11), 1548-1555.
- (18) Lafleur, J.P., Salin, E.D., "Pre-concentration of trace metals on centrifugal microfluidic discs with direct determination by laser ablation inductively coupled plasma mass spectrometry", *Journal of Analytical Atomic Spectrometry*, **2009**, 24 (11), 1511-1516.
- (19) LaCroix-Fralish, A., Clare, J., Skinner, C.D., Salin, E.D., "A centrifugal microanalysis system for the determination of nitrite and hexavalent chromium", *Talanta*, **2009**, 80 (2), 670-675.
- (20) Xi, Y., Templeton, E.J., Salin, E.D., "Rapid simultaneous determination of nitrate and nitrite on a centrifugal microfluidic device", *Talanta*, **2010**, 82 1612-1615.
- (21) Xi, Y., Duford, D.A., Salin, E.D., "Automated liquid-solid extraction of pyrene from soil on centrifugal microfluidic devices", *Talanta*, **2010**, 82 (3), 1072-1076.
- (22) Lafleur, J.P., Rackov, A.A., McAuley, S., Salin, E.D., "Miniaturised centrifugal solid phase extraction platforms for in-field sampling, pre-concentration and spectrometric detection of organic pollutants in aqueous samples", *Talanta*, **2010**, 81 (1-2), 722-726.
- (23) Kumar, A., Malik, A.K., Picó, Y., "Sample preparation methods for the determination of pesticides in foods using CE-UV/MS", *Electrophoresis*, **2010**, 31 (13), 2115-2125.
- (24) Duford, D.A., Peng, D.D., Salin, E.D., "Magnetically driven solid sample preparation for centrifugal microfluidic devices", *Analytical Chemistry*, **2009**, 81 (11), 4581-4584.
- (25) Xi, Y., Zhuang, H., "Determination of oil and grease in water and soil by liquid extraction on a centrifugal microfluidic device", *Journal of Agro-Environment Science*, **2010**, 29 (10), 2045-2048.
- (26) LaCroix-Fralish, A., Templeton, E.J., Salin, E.D., Skinner, C.D., "A rapid prototyping technique for valves and filters in centrifugal microfluidic devices", *Lab on a Chip*, **2009**, 9 (21), 3151-3154.
- (27) Skinner, C.D., Salin, E.D., "Determination of lead in soils surrounding a lead-acid battery manufacturer", *Water Quality Research Journal of Canada*, **1995**, 30 (2), 299-304.

- (28) Kido, H., Zoval, J., Madou, M., "Rapid prototyping of microfluidic systems", *ECS Transactions*, **2006**, 4 101-105.
- (29) Bartholomeusz, D.A., Boutté, R.W., Andrade, J.D., "Xurography: rapid prototyping of microstructures using a cutting plotter", *Microelectromechanical Systems, Journal of*, **2005**, 14 (6), 1364-1374.
- (30) "Method for simple determination of organophosphorus and carbamate pesticide residues in vegetables - Enzyme inhibition method", **2002**, *GB/T 18630-2002*.
- (31) Food and Agriculture Organization of the United Nations (FAO) and World Health Organization (WHO), Joint Meeting on Pesticide Residues, Geneva, 20-29 September 1993, Carbofuran, p.59
- (32) Federal Register. January 30, 1991. Part II. Environmental Protection Agency. 40 CFR Parts 141, 142, and 143. National Primary Drinking Water Regulations; Final Rule. (56 FR 3526).
- (33) Serway, R.A., Faughn, J.S., "College physics"; 4th ed.; Saunders College: Fort Worth, **1995**, 1032.
- (34) Grumann, M., Steigert, J., Riegger, L., Moser, I., Enderle, B., Riebeseel, K., Urban, G., Zengerle, R., Ducrée, J., "Sensitivity enhancement for colorimetric glucose assays on whole blood by on-chip beam-guidance", *Biomedical Microdevices*, **2006**, 8 (3), 209-214.
- (35) Fang, Q., Xu, G.M., Fang, Z.L., "A high-throughput continuous sample introduction interface for microfluidic chip-based capillary electrophoresis systems", *Analytical Chemistry*, **2002**, 74 (6), 1223-1231.
- (36) Bouchard, A.P., Duford, D.A., Salin, E.D., "Non-contact Addition, Metering, and Distribution of Liquids into Centrifugal Microfluidic Devices in Motion", *Analytical Chemistry*, **2010**, 82 (20), 8386-8389.

## **CHAPTER 8: Conclusion and Suggestions for Future Work**

The objectives of this thesis, the development of instrumentation, fabrication techniques and methods for sample introduction, preparation and extraction in centrifugal microfluidic devices, have been met. A summary of the thesis work and suggestions for future work are described below. For greater details, kindly see conclusions and future directions in the individual chapters.

### ***8.1 Summary of Thesis Work***

This thesis has added to the growing field of research in centrifugal microfluidics with a special focus on environmental monitoring. Several advances in instrumentation, integration of different fabrication techniques and sample handling methods were developed bringing us one step closer to inexpensive field portable analytical instrumentation and methods using centrifugal microfluidics.

In Chapter 2, multiple motorized stages were presented integrating the tools necessary to visualize and study centrifugal microfluidic devices in motion. The characterization of different components and investigation of subtractive manufacturing and lamination sealing techniques enabled the development of the miniaturized chemical analysis devices used in subsequent chapters.

The work in Chapter 3 helps chemists in the field of centrifugal microfluidics to make a knowledgeable choice between the current 3D printer technology for the rapid additive manufacturing of parts and entire devices. The study focused on the design and manufacturing process and compared the

resulting parts in terms of precision, accuracy, ability to retain liquids, surface finish, chemical resistivity and ability to print capillary burst valves.

A World-to-Disk interface enabling liquid sample introduction to a spinning device was presented in Chapter 4. Both subtractive (Chapter 2) and additive (Chapter 3) manufactured parts were used to make the hybrid centrifugal microfluidic devices. A gradient was added to the spinning devices to demonstrate the possibility of centrifugal microfluidic chromatography without the use of device space for liquid storage.

Magnetically actuated solid sample preparation for the crushing and grinding of solids on the integrated devices was demonstrated in Chapter 5. The movement of the “mobile magnets” in close proximity of the fixed magnet base was characterized.

Chapter 6 and Chapter 7 presented studies which used magnetically actuated liquid-solid extraction. The automation of methods and miniaturization of chemical devices was achieved for the analysis of soils and vegetable samples for PAHs and pesticides while greatly reducing sample and reagent volumes.

## ***8.2 Suggestions for Future Work***

The current collection of work is merely what is hoped to be the beginning of the use of centrifugal microfluidics for faster, cheaper and greener solid sample environmental monitoring. Future work improving and expanding both the instrumentation and applications is envisioned.

### 8.2.1 Instrumentation

The instrumentation need not be restricted to those presented here and could be expanded to include a great number of new accessories and peripherals both in the motorized stages and devices themselves.

#### *8.2.1.1 Proposed Additions to the Motorized Stages*

The stages were designed to encourage new ideas and facilitate their development and integration. For example, the acquisition of photographs of the devices in motion has brought great insight into the onboard chemical processes. The next step would be to provide a higher level of information about the chemistry by acquiring spectral information as the analytes travel through the spinning devices. Detection with a USB miniature spectrometer (for example a USB4000-UV-VIS, Ocean Optics, Dunedin, FL) with an external trigger input used to synchronize data acquisition is feasible. Triggering could be achieved either via the trigger breakout box or via a DAQ device (USB 6009 or USB6212). Other than the synchronization, a foreseen challenge is getting sufficient light intensity so that one is not quantum or dark noise limited. Such a set-up would address the limitations with the current detection stage which struggles with air bubbles and scatter from particles. Likewise such a set-up would be ideal for kinetic studies.

Alternatively a detection system could be made to spin with the centrifugal device similar to the work by Chang *et al.*<sup>1</sup> and similar to the spinning temperature test device which obtained real-time temperature readings detailed in Appendix E. It is thought that a reusable spinning instrument base could be affixed to the spindle shaft below the device and contain a variety of battery-

powered sensors. The data could either be stored onboard for subsequent removal or be transmitted in real-time by Wi-Fi or Bluetooth to a nearby computer. For example, commercially available Arduino DAQs are available with SD memory cards readers and Bluetooth capabilities (MKSEED6 SD Card Shield and RB-Ard-04 Bluetooth microcontroller board, Robot Shop Inc, Mirabel, QC). Though this particular system currently only contains a 10-bit analog-to-digital converter<sup>2</sup> which is insufficient to detect small changes in absorbance, it is thought that a simple demonstration would be a good proof-of-concept of the reusable spinning instrument base. Real-time detection would allow the system to feedback information to the sample introduction or pneumatic switches to be able to, for example, add reagents until a detectable colour change (such as pH).

As alluded to in the introduction to Chapter 3, the use of 3D printers is not limited to the manufacturing of the centrifugal devices but can also be used in the production of instrument platforms such as cuvette holders. Such technology could easily manufacture these custom reusable spinning instrument bases.

Likewise, the longer spindle shaft on Stage v3.0 will allow for added flexibility. Space is now available for additional peripherals such as the reusable spinning instrument base. Alternatively, a mirror or white light diffuser could be added at 45 degrees to the devices in order to angle light from below up and through the devices to be detected above by either the current camera or other spectrometer. If the camera is used, software such as "ImageJ"<sup>3</sup> (U.S. National Institutes of Health, Bethesda, MD) is thought to be able to analyze the resulting images for quantitative analysis.

### 8.2.1.2 Future Centrifugal Microfluidic Devices

Having successfully integrated magnetically actuated solid sample preparation and extraction on centrifugal microfluidic devices, the development of effective integrated filters has become a priority. Filter designs could include the use of quartz plugs, filter paper, a series of posts or columns (see Appendix C), modified solid phase extraction (SPE) cartridges, Soxhlet thimbles, frits, or even monoliths. Integrated micro-SPE cartridges are of interest not only to filter but also to preconcentrate analytes. Conditioning, washing, loading, rinsing, and eluting liquids could all be applied using the CLAD.

As Atencia *et al.*<sup>4</sup> discussed, World-to-Disk interfacing remains a weak link in microfluidic research mainly due to the lack of simple, reliable, low-cost reversible connections. The current CLAD addresses many of these concerns except that it is not a reversible connection. Instead of sealing the CLAD components to the centrifugal disk bases with acetone, future versions could include simple magnetic connectors to click on reusable CLAD manifolds. Ring magnets could easily be added around the CLAD's pegs to hold it tightly in place.

Combining the functionality of the different "unit operations" developed here with those already available, new capabilities are at the disposal of chemists to solve challenging problems. For example, a combination of the CLAD with pneumatic flow switching<sup>5</sup> is envisioned to be able to add a liquid through the same inlet to two different reservoirs, all while the devices are in motion. This would provide chemists greater design options and flexibility, effective use of space and greater control of the processes on new versions of the centrifugal microfluidic devices.

For safety and ease of use it may be desirable that water be the only reagent being added to a device. In that case, the centrifugal microfluidic devices could be manufactured with a long shelf-life using lyophilized reagents<sup>6, 7</sup>. In such a case, a combination of the CLAD with “mobile magnets” would be an efficient means of adding the required water and reconstituting these reagents.

Integrating the novel components presented in this thesis into a single hybrid device has been envisioned. As seen in Figure 8-1, a CLAD device with a partially covered reservoir and a “mobile magnet” would create a pocket that could be used for 1) solid and liquid sample introduction, 2) magnetically actuated solid sample preparation and 3) magnetically actuated liquid-solid extraction. Integrating a filter would be necessary to achieve this design and a microcolumn or micro-SPE cartridge could also be added.

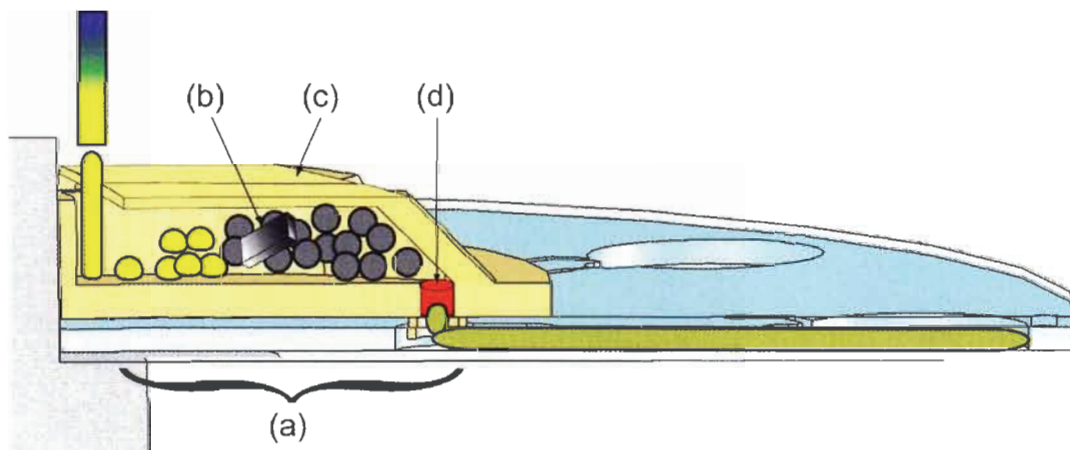


Figure 8-1. Envisioned hybrid centrifugal microfluidic device containing (a) deep pocket for solid and liquid sample introduction, (b) “mobile magnet” for magnetically actuated sample preparation and liquid-solid extraction, (c) partial lid to minimize splash while allowing liquid addition, (d) filter.

Finally, computational fluid dynamics (CFD) simulations have been reported in microfluidic research<sup>8-10</sup> and are now very common in industry. Such CFD simulations could be investigated to help improve the design of the devices

and to corroborate experimental findings. The study of flow patterns, two phase interactions and complex geometries are now possible with commercially available software with built-in standard modules, such as the Fluent software from ANSYS (Canonsburg, PA).

### 8.2.2 Potential Applications

Having been involved in the design of the centrifugal microfluidic devices for the determination of nitrate and nitrite reported by LaCroix-Fralish *et al.*<sup>7</sup>, two advanced versions are envisioned.

First, as reviewed by Marle *et al.*<sup>11</sup>, a wide range of potential analytes and spectroscopic techniques adapted to conventional microfluidics for environmental monitoring have been reported. These even take into consideration the reduced path length typical in microfluidics and the stability of reagents. Many of these could be easily adapted to centrifugal microfluidics including the determination of phosphate and ammonia in water. A combined device that simultaneously determined phosphate, ammonia, nitrate, nitrite and perhaps even pH is envisioned and would be of great use for the monitoring of water quality.

Second, the automation of the EPA method 8510 would provide an ideal opportunity to combine the magnetically actuated liquid-solid extraction to the nitrite system (which used a "NitriVer3" powder pillow).<sup>7</sup> The EPA method involves the colourimetric screening of RDX (hexahydro-1,3,5-trinitro-1,3,5-triazine) and HMX (octahydro-1,3,5,7-tetrenitro-1,3,5,7-tetrazocine) in soil. The method currently involves the liquid-solid extraction of soil samples with acetone, acidification, and reaction with zinc dust. Next, a "NitriVer3" powder pillow is

used to generate a colour product which is monitored by absorbance at 507 nm. A portable field instrument for the screening of these explosive materials would be ideal for site remediation purposes and for the location of the most appropriate sampling points for standard laboratory testing.

A low level fluorescence-based determination of PAHs in soil samples could be accomplished by combining the method and device used for the magnetically actuated liquid-solid extraction of soil samples for the determination of pyrene (Chapter 6) with a micro-SPE column and in-column fluorescence detection similar to that reported by Lafleur *et al.*<sup>12</sup>. Non-resonance fluorescence of pyrene using an excitation wavelength of 238 nm and an emission/detection wavelength of 372 nm is envisioned.<sup>13, 14</sup>

The introduction of liquid gradients to spinning devices using the CLAD, combined with the ability to integrate microcolumns into centrifugal microfluidic devices<sup>15, 16</sup> opens a whole new branch of centrifugal microfluidic chemistries in chromatography and separations science. The miniaturization and integration of conventional complex solvent separation techniques such as molecular and ionic separations by either “elution chromatography” using gradients or the lesser known “frontal chromatography”<sup>17</sup> are envisioned. In centrifugal microfluidic frontal chromatography, the sample solution would be fed continuously as the influent mobile phase into the device using the CLAD to an integrated microcolumn. Meanwhile the effluent mobile phase would be analyzed continuously until its composition was identical with that of the influent creating chromatograms with steps as opposed to peaks.<sup>18</sup>

Other applications include the processing of pharmaceutical tablets and DNA extraction from hard seeds such as corn. Recently, the horses of the New Zealand horse polo team died after being given an incorrectly dosed supplement.<sup>19</sup> A market for field portable, easy to use analytical devices to reduce such sad events is clear. For example, a spectrometric determination of crushed aspirin tablets<sup>20, 21</sup> could feasibly be automated and integrated into centrifugal devices. In regards to DNA extraction, cells need to be broken open to release the DNA before polymerase chain reaction (PCR) and genetic testing can be performed. The analysis of hard samples such as seeds and grains (wheat, corn, rice, soybean, etc) is desirable since the longer term effects and crop cross contamination with genetically modified organisms (GMO) are of growing concern. If a transgenic resistant strain eludes the farmers and crossbreeds with a wild strain, control would be lost. An event like this would have ecological implications. For this reason a rapidly growing market exists for an easy to use field portable device to test for GMO foods. Such a device needs to be able to quickly and efficiently break the grains to liberate the DNA and test for the genetically modified antibody. The magnetically actuated solid sample preparation to crush such hard samples combined to standard ELISA-based methods that have already been developed<sup>22</sup>, similar to the technique described in Chapter 7, would result in a powerful field portable tool.

These are only a few of the possible applications of the instruments and methods developed in this body of work. Applications of this technology outside of environmental monitoring such as for biological, pharmaceutical and forensic samples have been suggested above. The instrumentation, fabrication

techniques and methods for sample introduction, preparation and extraction in centrifugal microfluidics have been developed in an attempt to address the growing need for faster, less expensive, automated and miniaturized alternatives to current standard methods.

### 8.3 References

- (1) Chang, H.C., Tsou, C., Lai, C.C., Wun, G.H., "A real-time dynamic imaging system for centrifugal microflow platforms", *Measurement Science and Technology*, **2008**, 19 (7), Art. No.: 075501.
- (2) McComb, G., "Making Robots With The Arduino, Part 1", *Servo Magazine*, **2010**, (11), 56-63.
- (3) Abramoff, M.D., Magalhaes, P.J., Ram, S.J., "Image Processing with ImageJ", *Biophotonics International*, **2004**, 11 (7), 36-42.
- (4) Atencia, J., Cooksey, G.A., Jahn, A., Zook, J.M., Vreeland, W.N., Locascio, L.E., "Magnetic connectors for microfluidic applications", *Lab on a Chip - Miniaturisation for Chemistry and Biology*, **2010**, 10 (2), 246-249.
- (5) Kong, M.C.R., Salin, E.D., "Pneumatic Flow Switching on Centrifugal Microfluidic Platforms In Motion", *Analytical Chemistry*, **2011**, 83 (3), 1148-1151.
- (6) Madou, M.J., Lee, L.J., Daunert, S., Lai, S., Shih, C.-H., "Design and fabrication of CD-like microfluidic platforms for diagnostics: microfluidic functions", *Biomedical Microdevices*, **2001**, 3 (3), 245-254.
- (7) LaCroix-Fralish, A., Clare, J., Skinner, C.D., Salin, E.D., "A centrifugal microanalysis system for the determination of nitrite and hexavalent chromium", *Talanta*, **2009**, 80 (2), 670-675.
- (8) Zhang, J., Guo, Q., Liu, M., Yang, J., "A lab-on-CD prototype for high-speed blood separation", *Journal of Micromechanics and Microengineering*, **2008**, 18 (12), Article Number 125025.
- (9) Chen, X., Cui, D., Liu, C., Li, H., Chen, J., "Continuous flow microfluidic device for cell separation, cell lysis and DNA purification", *Analytica Chimica Acta*, **2007**, 584 (2), 237-243.
- (10) Lu, L.H., Ryu, K.S., Liu, C., "A magnetic microstirrer and array for microfluidic mixing", *Journal of Microelectromechanical Systems*, **2002**, 11 (5), 462-469.
- (11) Marle, L., Greenway, G.M., "Microfluidic devices for environmental monitoring", *TrAC - Trends in Analytical Chemistry*, **2005**, 24 (9), 795-802.
- (12) Lafleur, J.P., Rackov, A.A., McAuley, S., Salin, E.D., "Miniaturised centrifugal solid phase extraction platforms for in-field sampling, pre-concentration and spectrometric detection of organic pollutants in aqueous samples", *Talanta*, **2010**, 81 (1-2), 722-726.

- (13) Mahanty, B., Pakshirajan, K., Dasu, V.V., "Synchronous fluorescence as a selective method for monitoring pyrene in biodegradation studies", *Polycyclic Aromatic Compounds*, **2008**, 28 (3), 213-227.
- (14) Cai, Z.Q., Zhu, Y.X., Zhang, Y., "Simultaneous determination of dissolved anthracene and pyrene in aqueous solution by synchronous fluorimetry", *Spectrochimica Acta - Part A: Molecular and Biomolecular Spectroscopy*, **2008**, 69 (1), 130-133.
- (15) Moschou, E.A., Nicholson, A.D., Jia, G., Zoval, J.V., Madou, M.J., Bachas, L.G., Daunert, S., "Integration of microcolumns and microfluidic fractionators on multitasking centrifugal microfluidic platforms for the analysis of biomolecules", *Analytical and Bioanalytical Chemistry*, **2006**, 385 (3), 596-605.
- (16) Lafleur, J.P., Salin, E.D., "Pre-concentration of trace metals on centrifugal microfluidic discs with direct determination by laser ablation inductively coupled plasma mass spectrometry", *Journal of Analytical Atomic Spectrometry*, **2009**, 24 (11), 1511-1516.
- (17) Sajonz, P., "Frontal Chromatography", *Encyclopedia of Chromatography*, **2009**, third edition 957-959.
- (18) Cantwell, F.F., "Analytical Separations: Gas Chromatography, Liquid Chromatography, Supercritical Fluid Chromatography, and Electrophoresis", *CHEM421 course notes, University of Alberta*, **1996**, 5-6.
- (19) Padgett, T., "The Dead Polo Ponies and Their Millionaire Owner", *Time CNN*, **2009**, *Miami* (April 23rd), [www.time.com](http://www.time.com).
- (20) Miles, C.I., Schenk, G.H., "Fluorescence of acetylsalicylic acid in solution and its measurement in presence of salicylic acid", *Analytical Chemistry*, **1970**, 42 (6), 656-659.
- (21) Kitamura, K., Majima, R., "Determination of salicylic acid in aspirin powder by second derivative ultraviolet spectrometry", *Analytical Chemistry*, **1983**, 55 (1), 54-56.
- (22) Meyer, R., "Development and application of DNA analytical methods for the detection of GMOs in food", *Food Control*, **1999**, 10 (6), 391-399.

## Appendix A: Additional Instrumentation Details

Chapter 2 discussed the different components of the motorized stages. Additional technical drawings, dimensions and screw terminal configurations are included in this appendix.

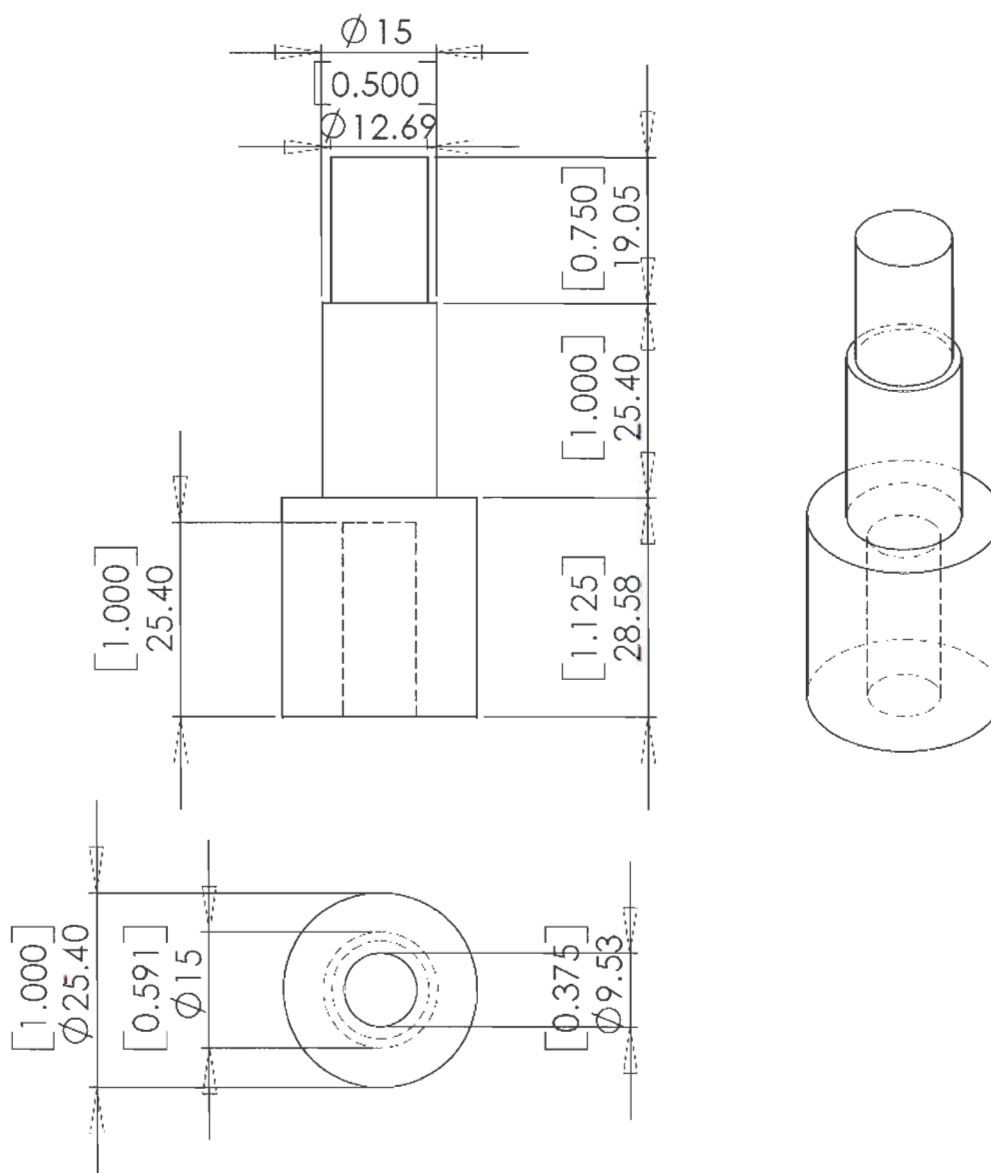


Figure A-1. Dimensions of spindle shaft for Stage v1.0 DC motor.

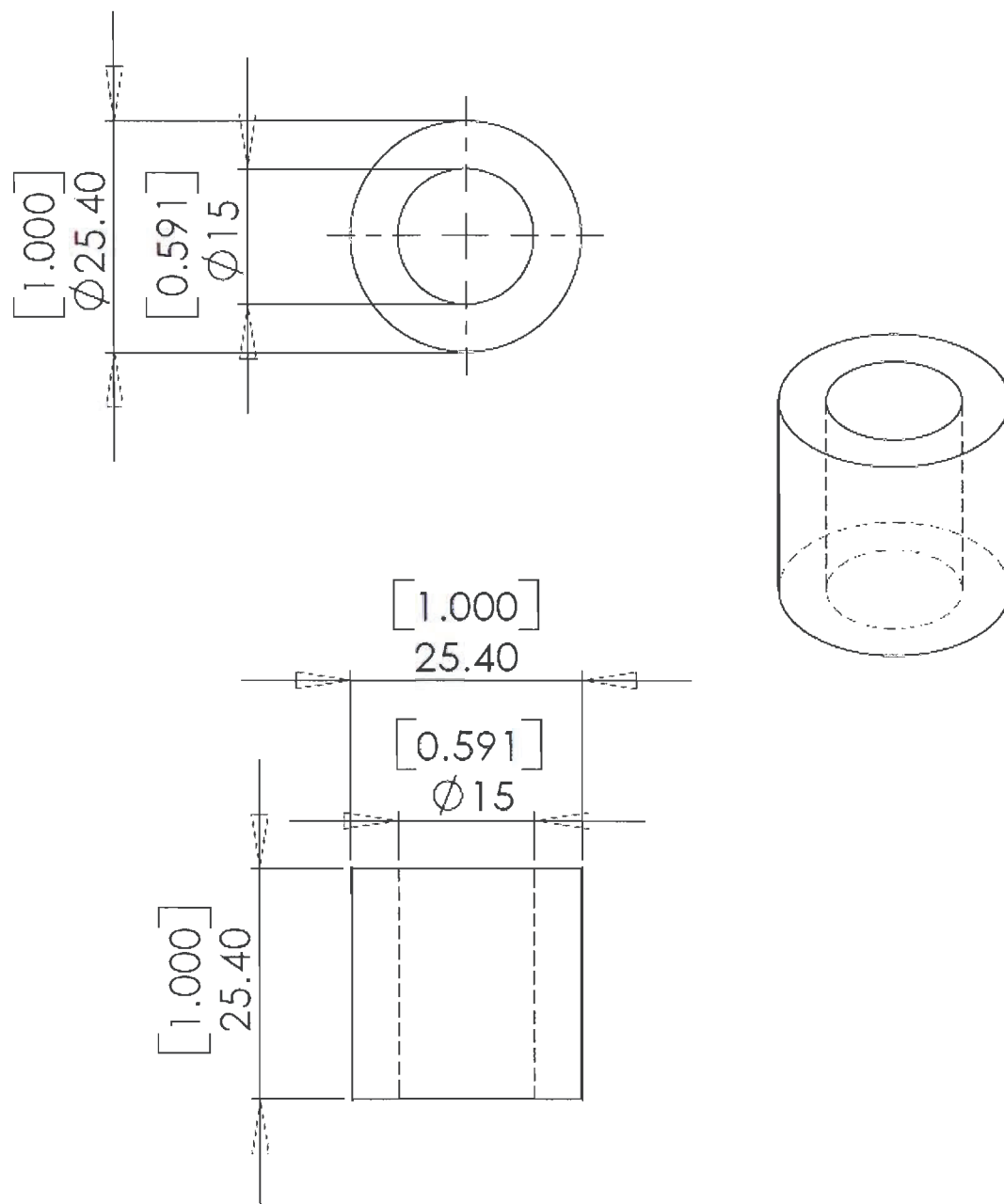


Figure A-2. Dimensions of spindle shaft top ring used to hold centrifugal devices of different thicknesses.

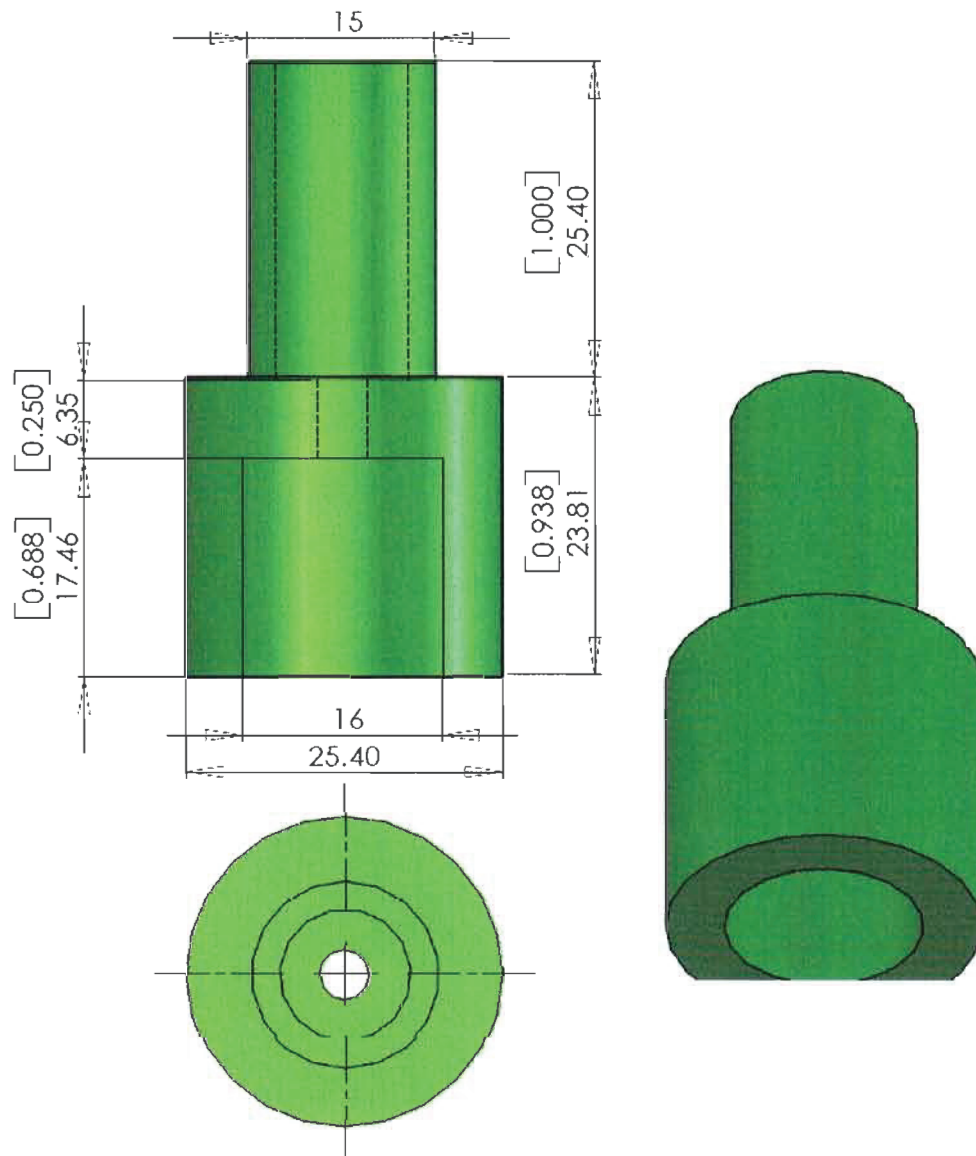


Figure A-3. Dimensions of adaptor used to attach the original DC motor shaft to Stage v2.0 servo motor spindle.

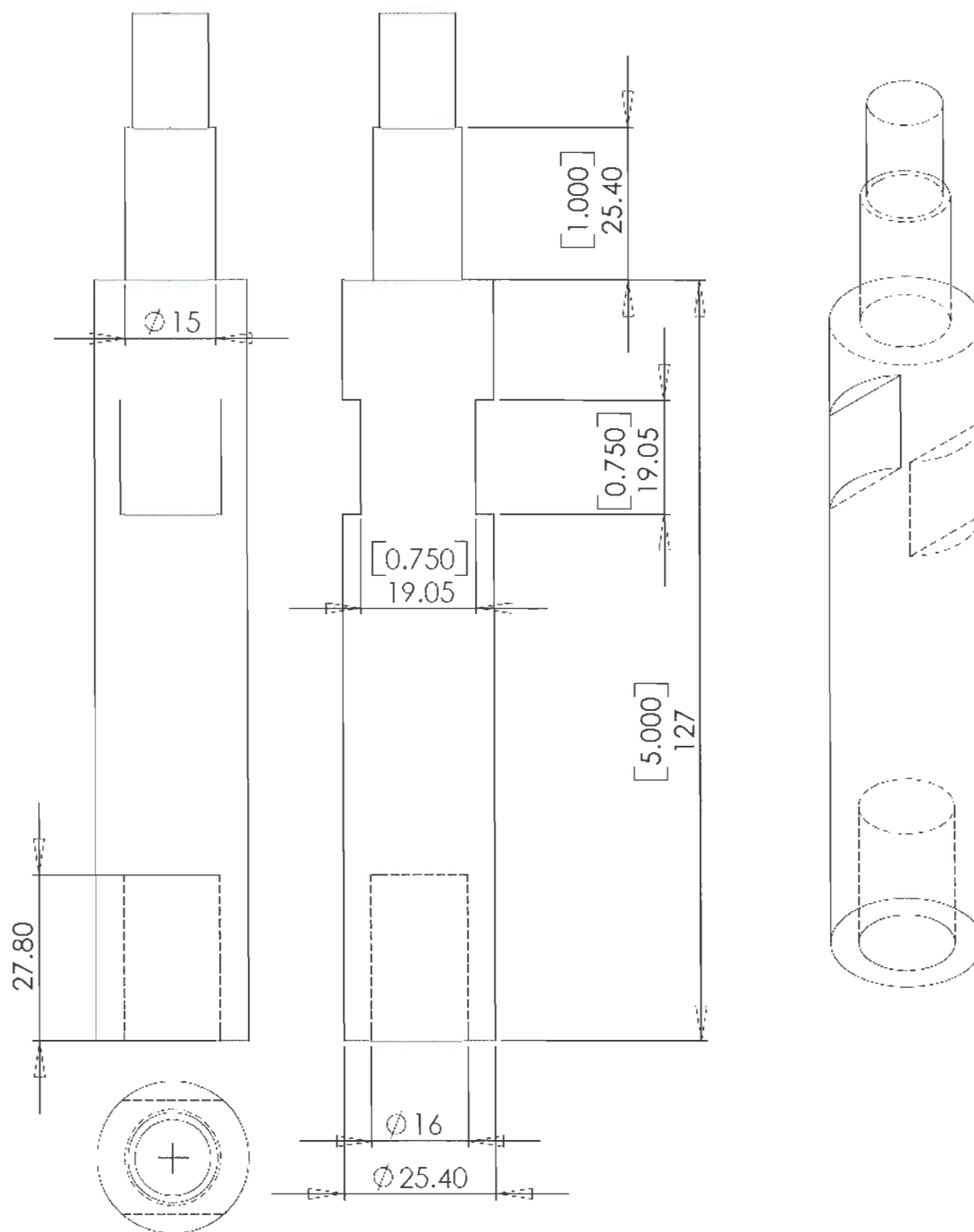
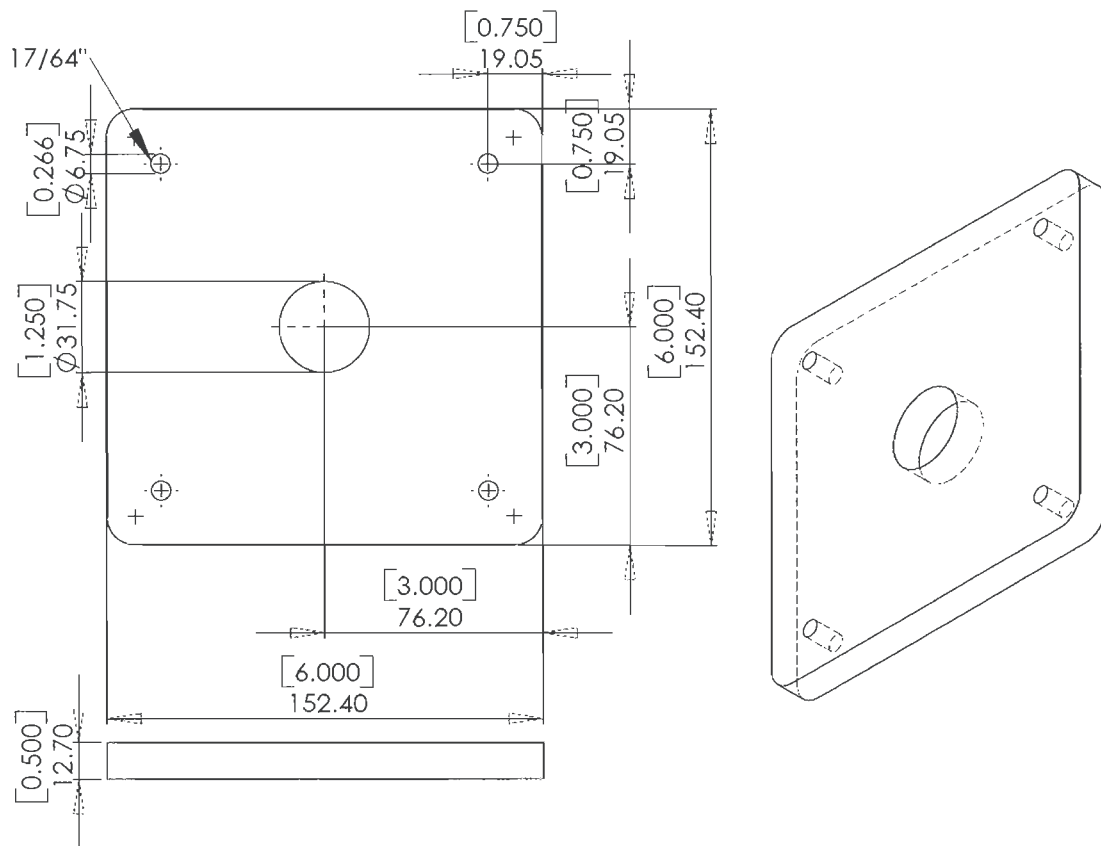


Figure A-4. Dimensions one-piece spindle shaft for Stage v3.0 servo motor.



**Figure A-5. Dimension of fixed magnet base.**

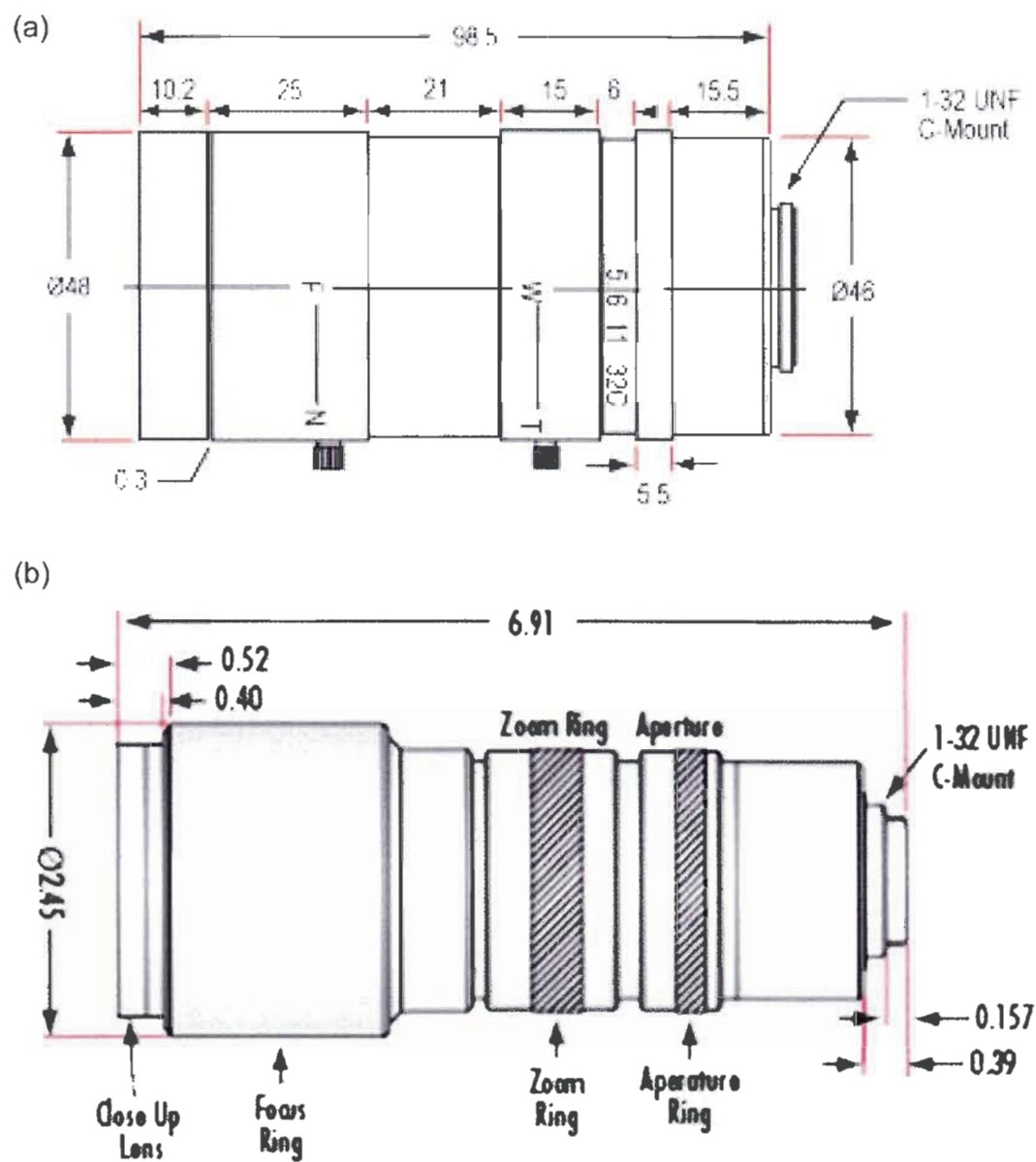


Figure A-6. Dimensions of close focus zoom lenses. (a) Computer #54-363, dimension in mm. (b) Navitar Zoom 7000 #58-240, dimensions in inches.

## USB6009 DAQ



## USB6212 DAQ



GND	1	17	P0.0
AI 0/AI 0+	2	18	P0.1
AI 4/AI 0-	3	19	P0.2
GND	4	20	P0.3
AI 1/AI 1+	5	21	P0.4
AI 5/AI 1-	6	22	P0.5
GND	7	23	P0.6
AI 2/AI 2+	8	24	P0.7
AI 6/AI 2-	9	25	P1.0
GND	10	26	P1.1
AI 3/AI 3+	11	27	P1.2
AI 7/AI 3-	12	28	P1.3
GND	13	29	PFI 0
AO 0	14	30	+2.5 V
AO 1	15	31	+5 V
GND	16	32	GND

PFI 0/P1.0  
 PFI 1/P1.1  
 PFI 2/P1.2  
 PFI 3/P1.3  
 D GND  
 PFI 4/P1.4  
 PFI 5/P1.5  
 PFI 6/P1.6  
 PFI 7/P1.7  
 +5 V  
 D GND  
 AO 0  
 AO 1  
 AO GND  
 AI 0  
 AI 8

AI 1  
 AI 9  
 AI 2  
 AI 10  
 AI 3  
 AI 11  
 AI SENSE  
 AI 4  
 AI 12  
 AI 5  
 AI 13  
 AI GND  
 AI 6  
 AI 14  
 AI 7  
 AI 15

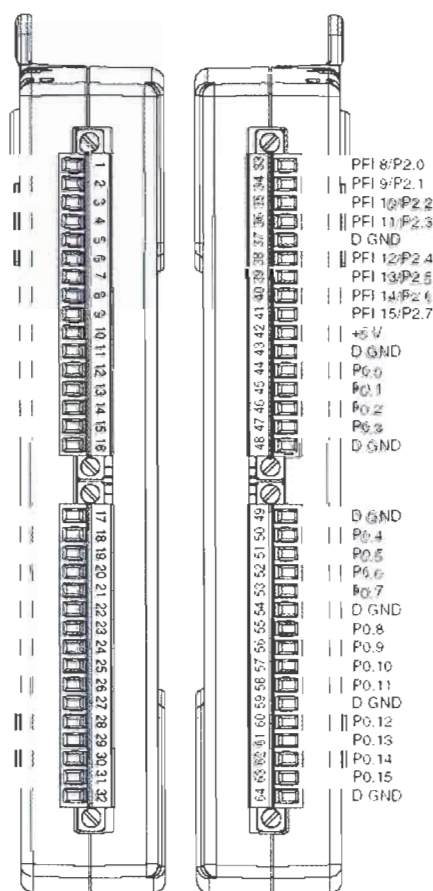


Figure A-7. Digital acquisition (DAQ) screw terminal configuration for both USB6009 and USB6212 (National Instruments User manuals).

## Appendix B: LabVIEW Virtual Instruments Code

Selected “Front Panels” and “Block Diagrams” of the LabVIEW VI code are compiled in this appendix.

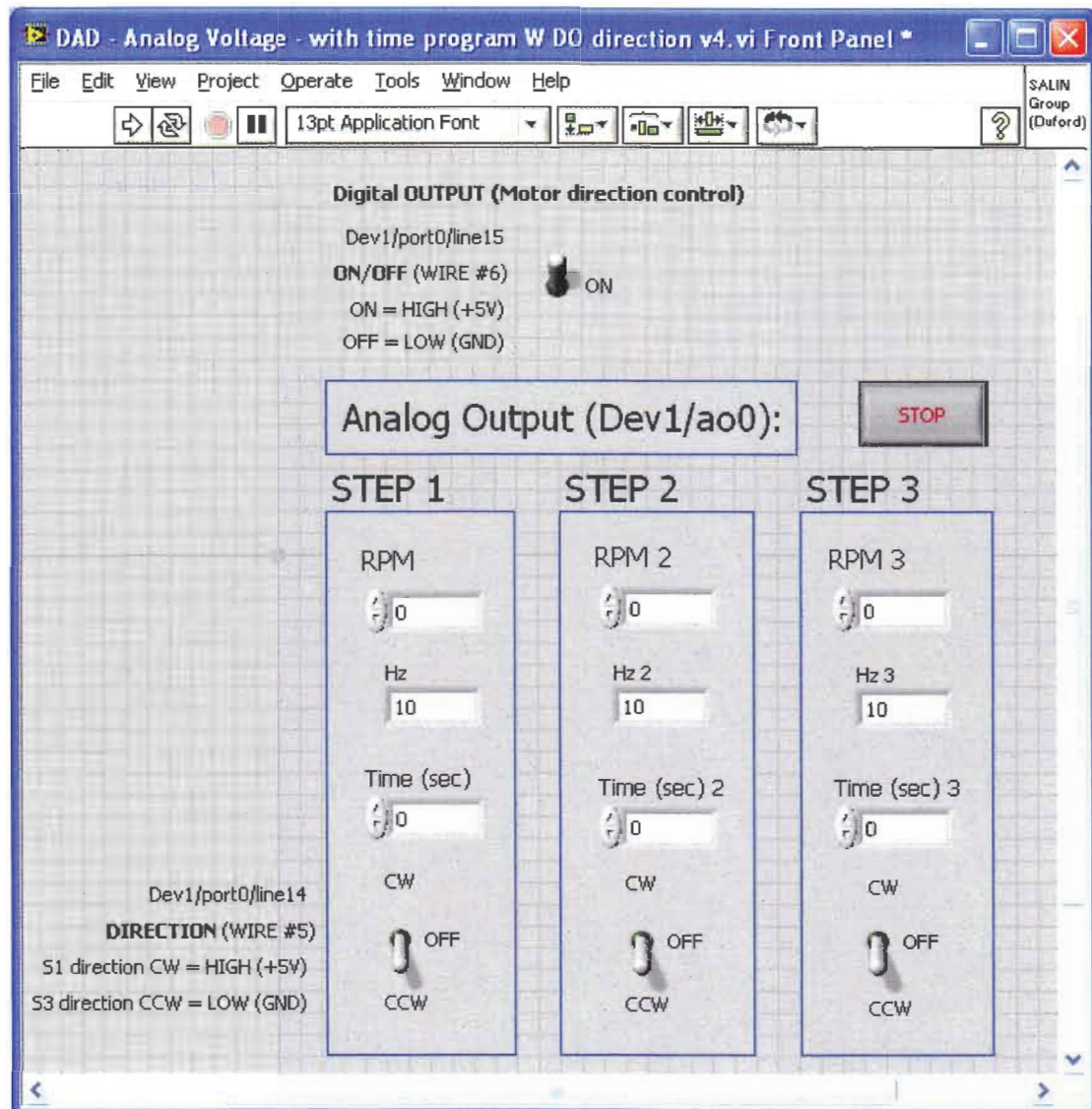


Figure B-1. VI Front Panel for control of DC motor Stage v1.0

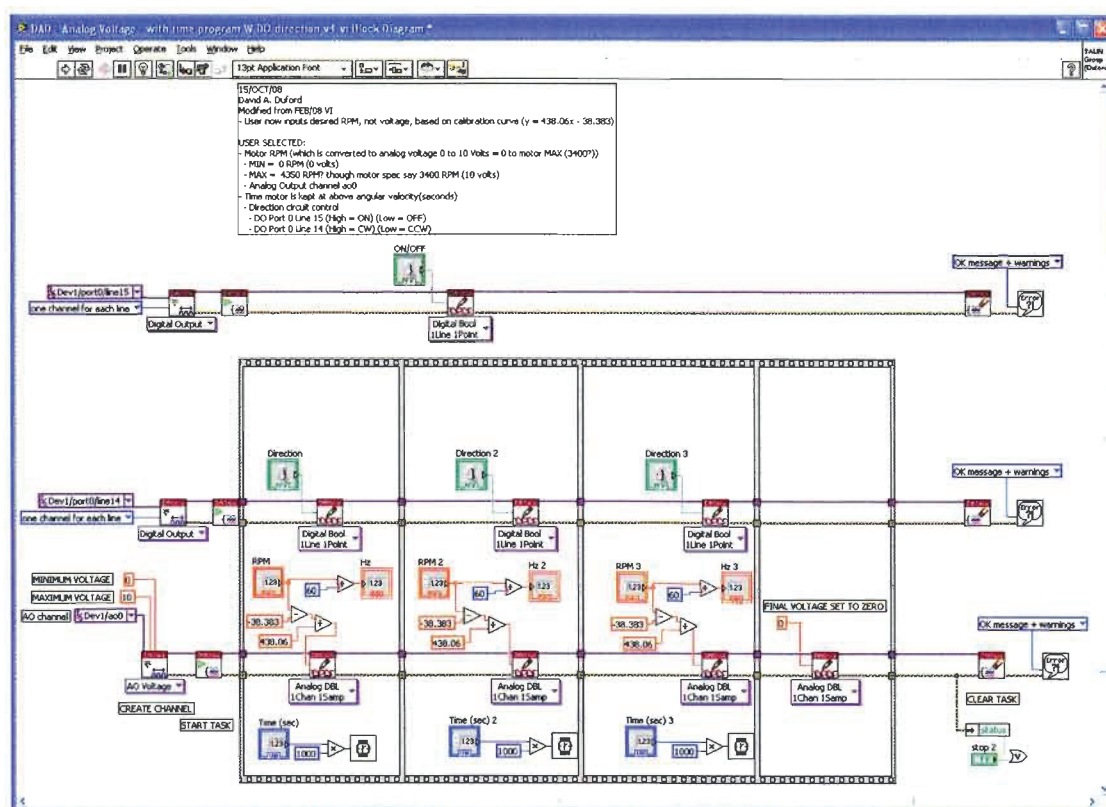


Figure B-2. VI Block Diagram for control of DC motor Stage v1.0

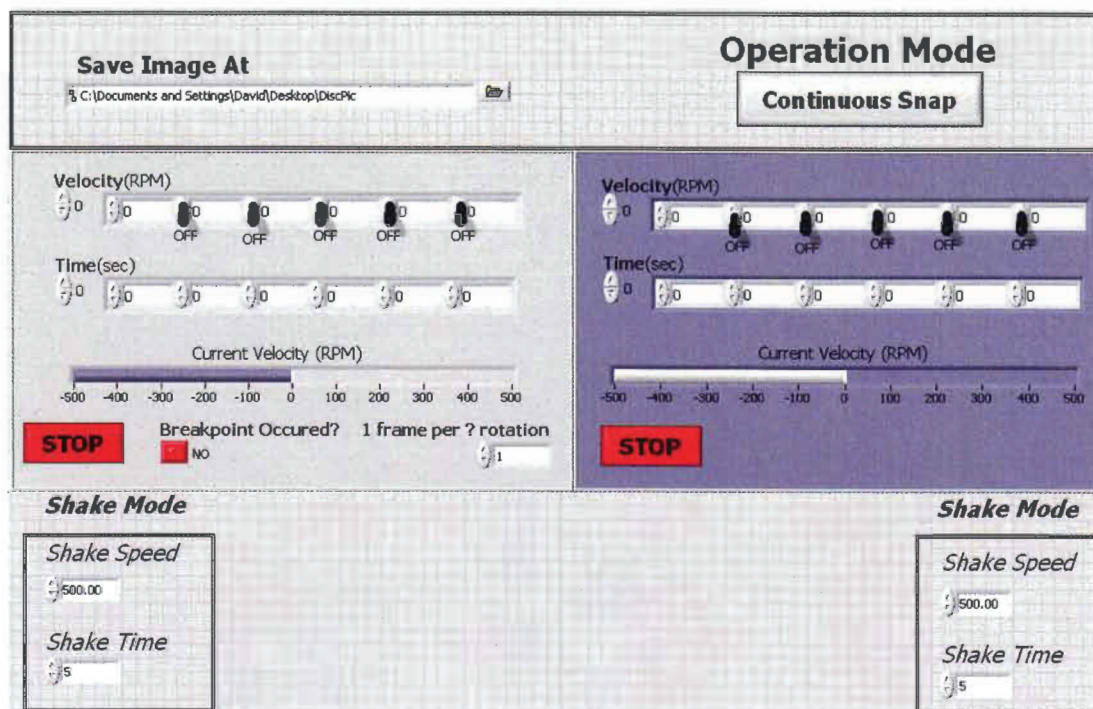


Figure B-3. VI Front Panel for control of servo motors Stage v2.0 and Stage v3.0

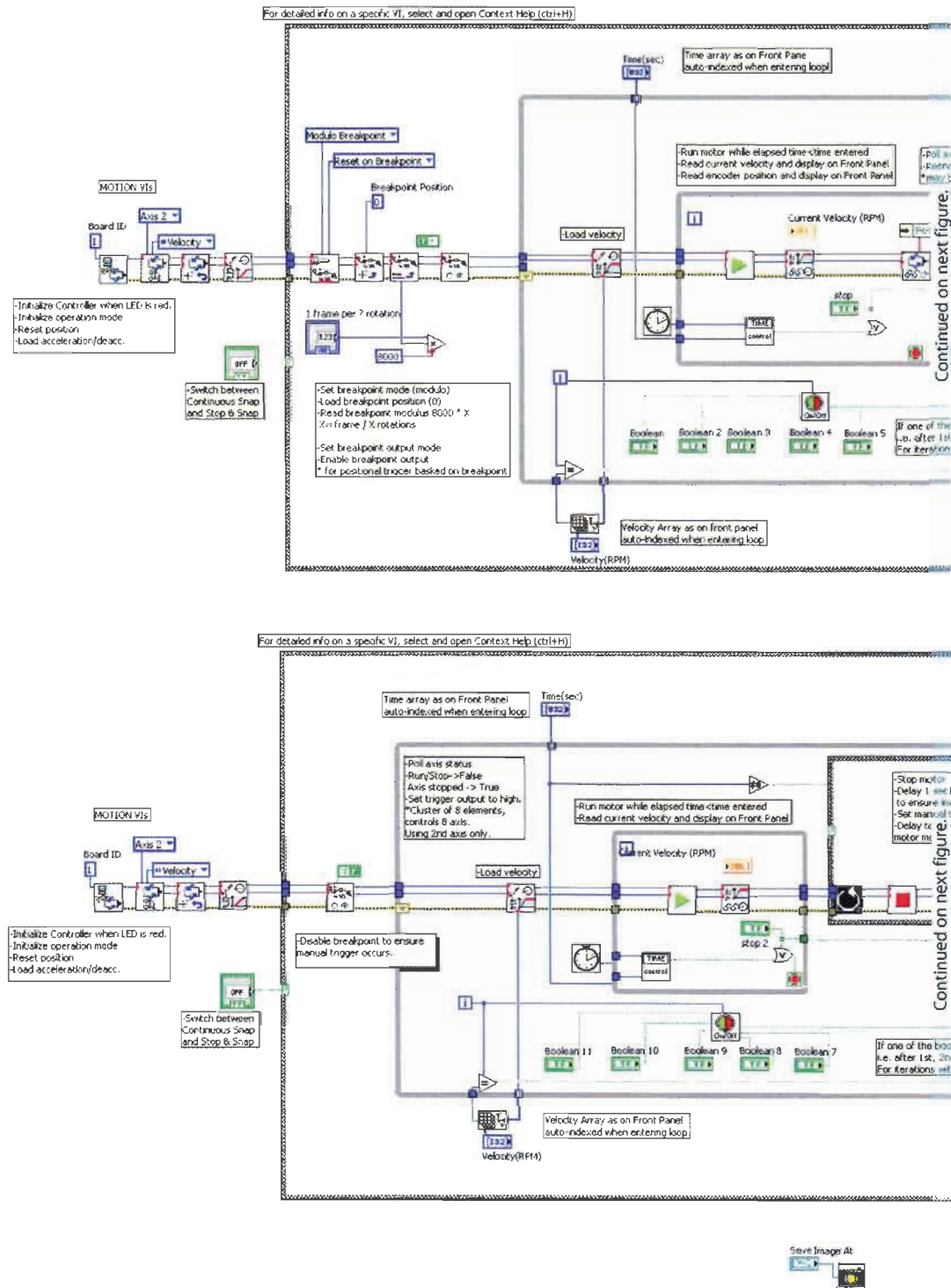


Figure B-4. VI Block Diagrams for “continuous snap” (top) and “stop and snap” (bottom) modes of operation of servo motors (continued in Figure B-5). Bottom “save image at” sub-VI is detailed in Figure B-6

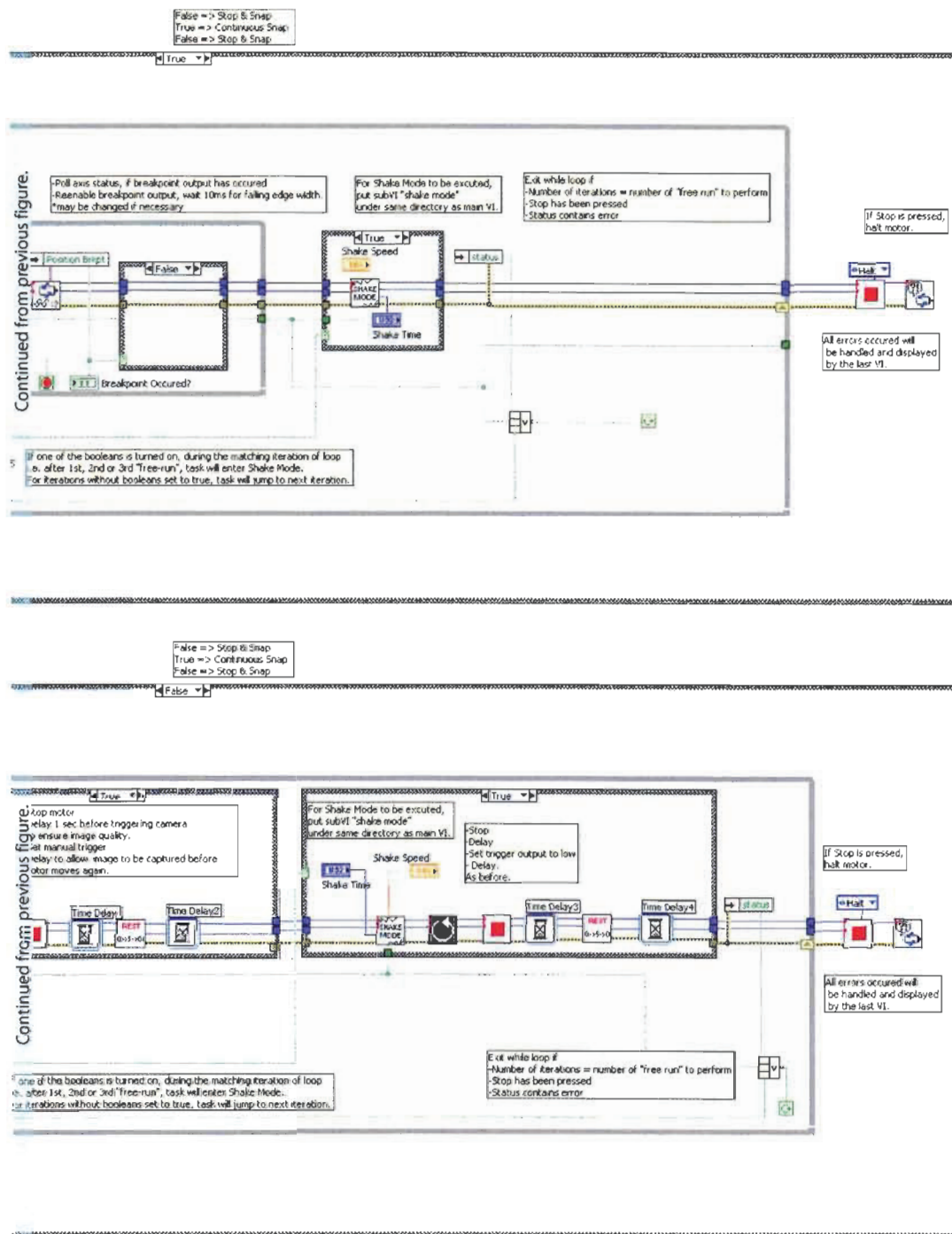


Figure B-5. VI Block Diagrams for "continuous snap" (top) and "stop and snap" (bottom) modes of operation of servo motors (continued from Figure B-4).

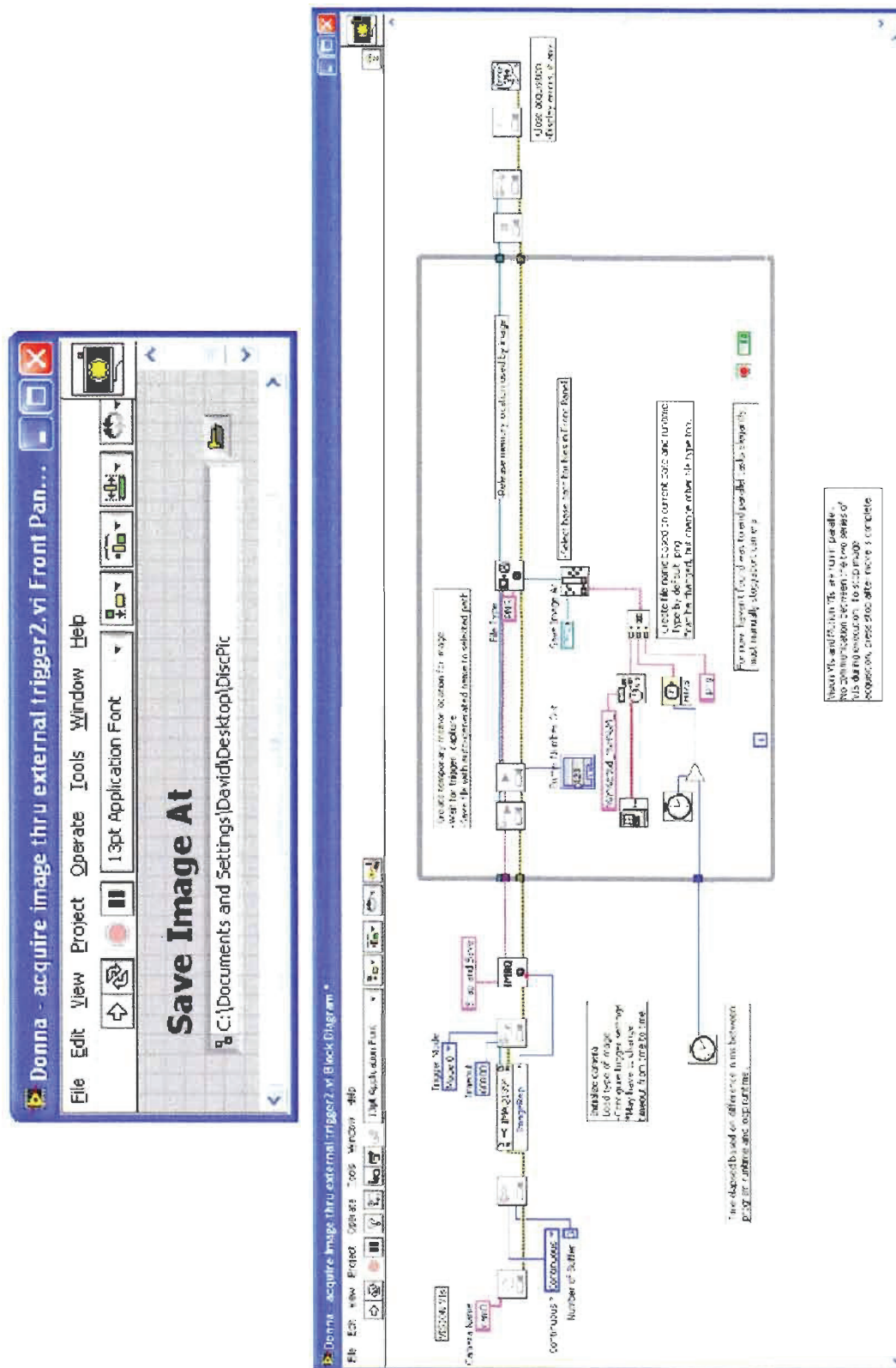


Figure B-6. Sub-VI Front Panel and Block Diagram for control of camera

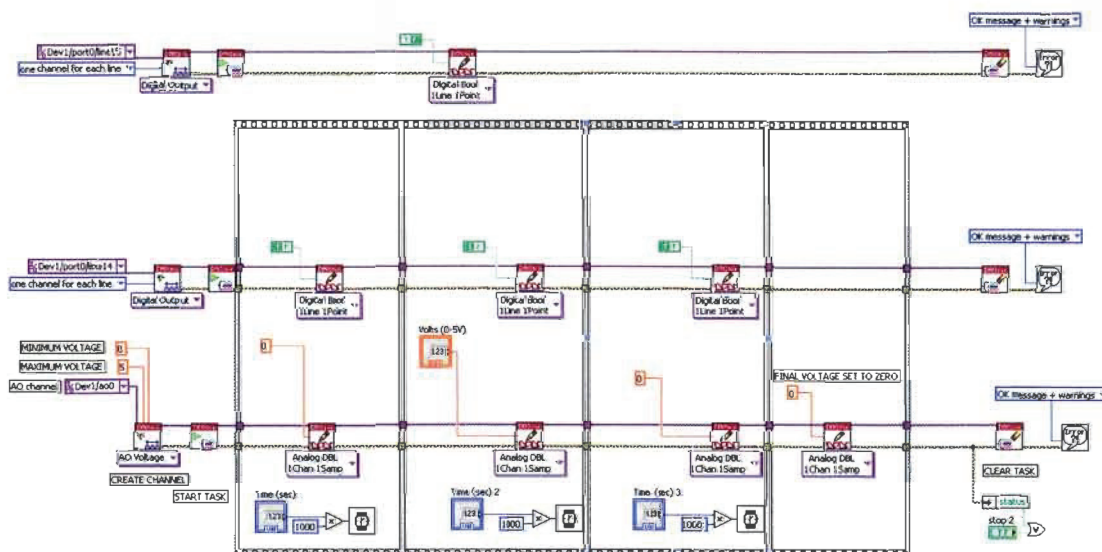
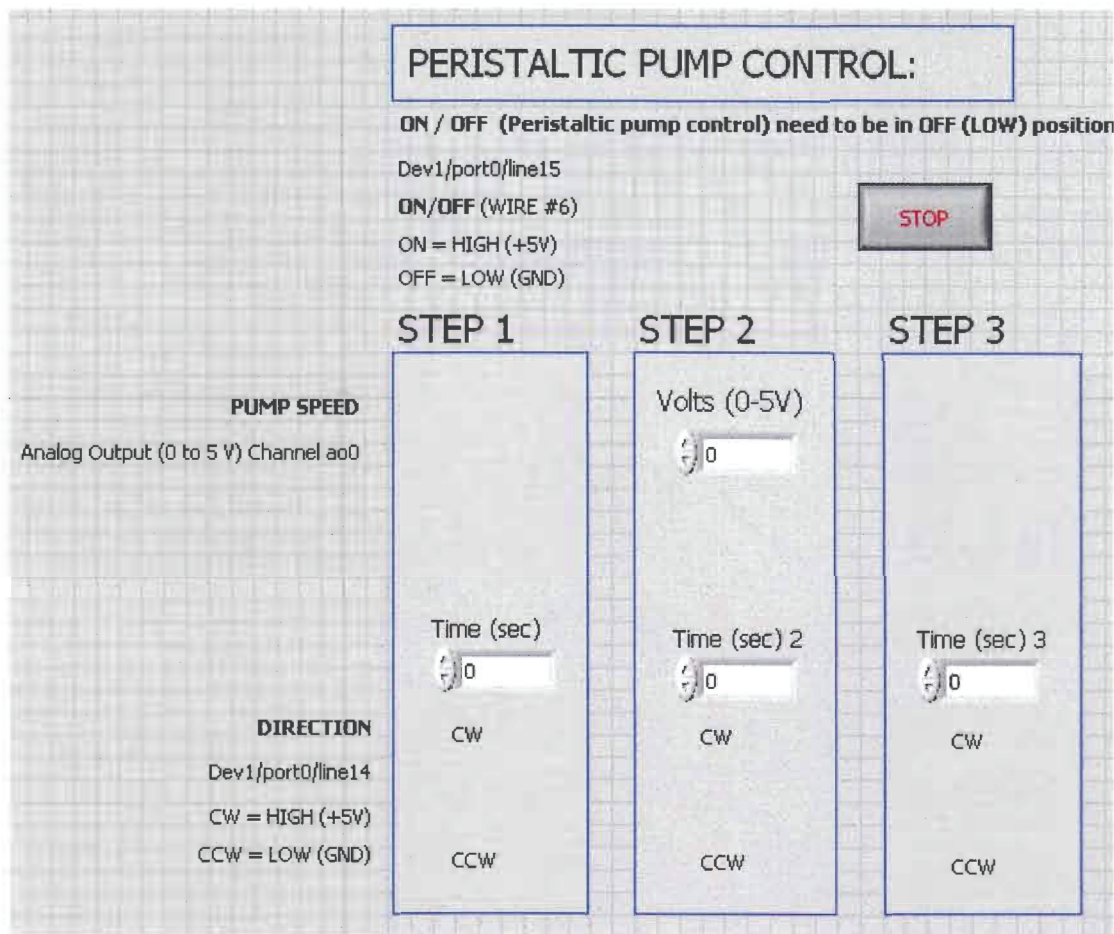


Figure B-7. VI Front Panel and Block Diagram for control of peristaltic pump

## Appendix C: 3D Printing and CLAD – Additional Designs and Details

As detailed in Chapters 3 and 4, recent advances in 3D printing have made additive manufacturing of devices an interesting alternative fabrication technique. The figures and details of this appendix are to complement both of these chapters.

Larger versions of the drawings included in Chapter 3 are shown in the following series of figures in order to add more information in regards to their dimensions.

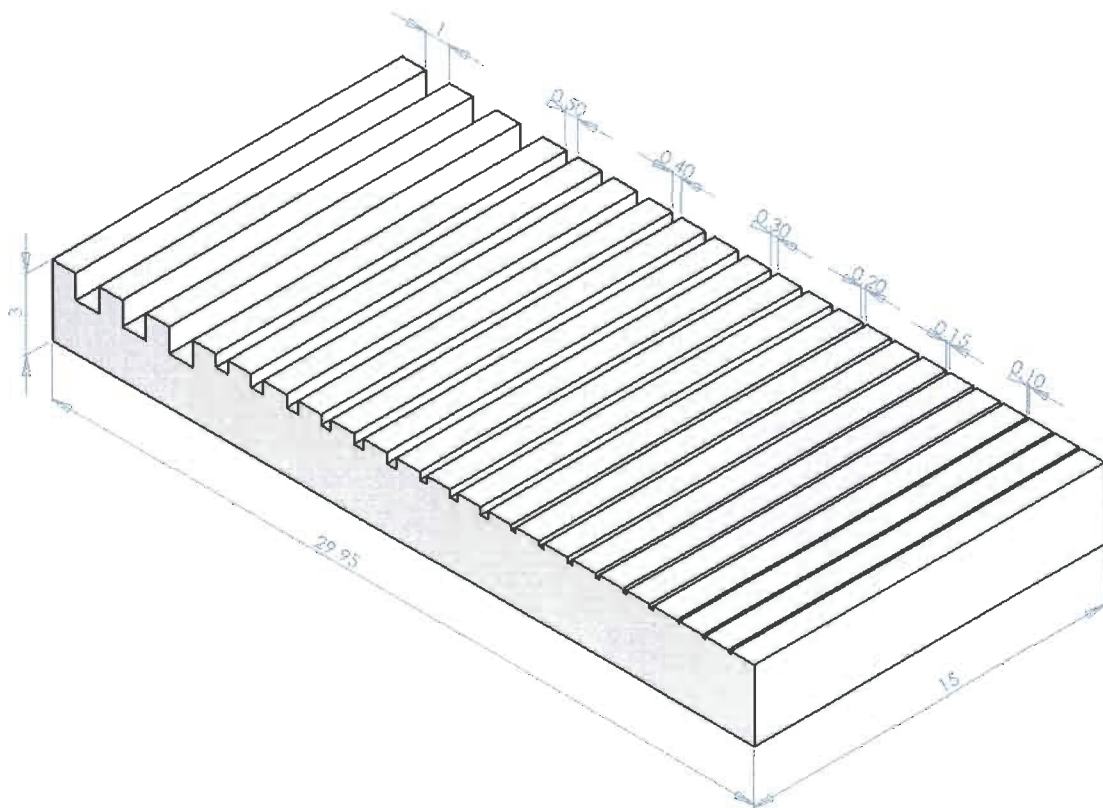


Figure C-1. Structure 1: Dimensions (mm) of square channels (width and height of channels are of 1000, 500, 400, 300, 200, 150 and 100  $\mu\text{m}$  respectively). Each channel was 15 mm long. A 1 mm space was included between each channel.

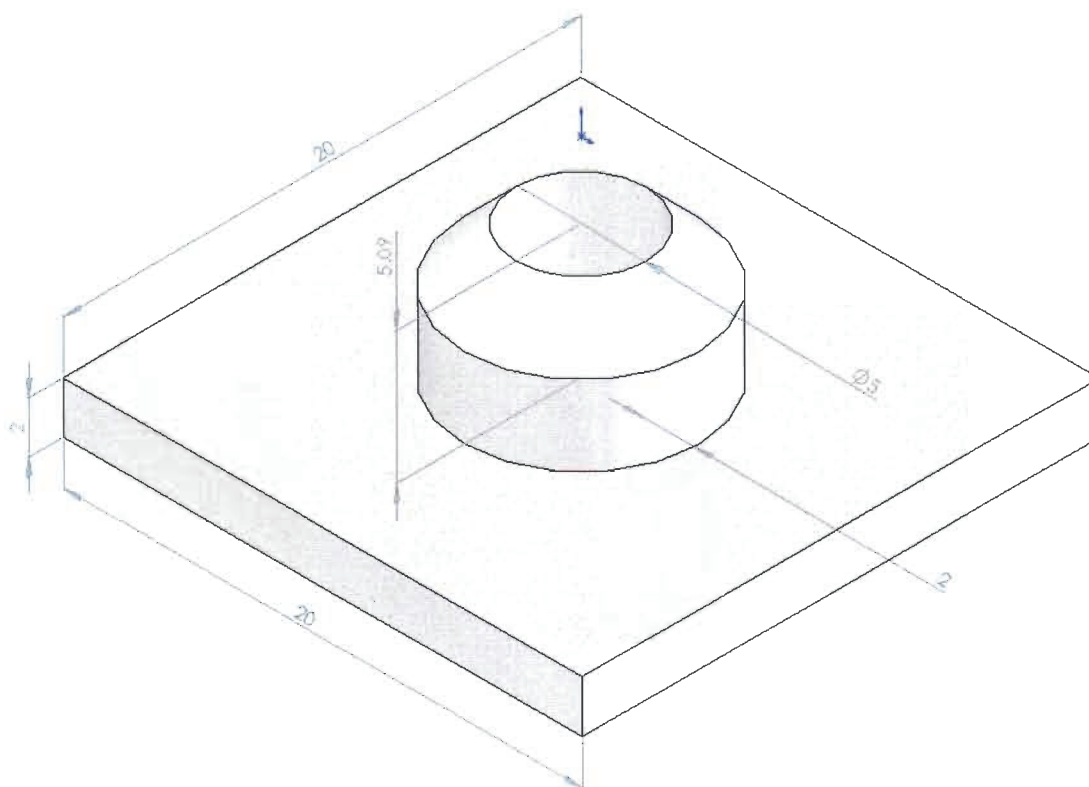
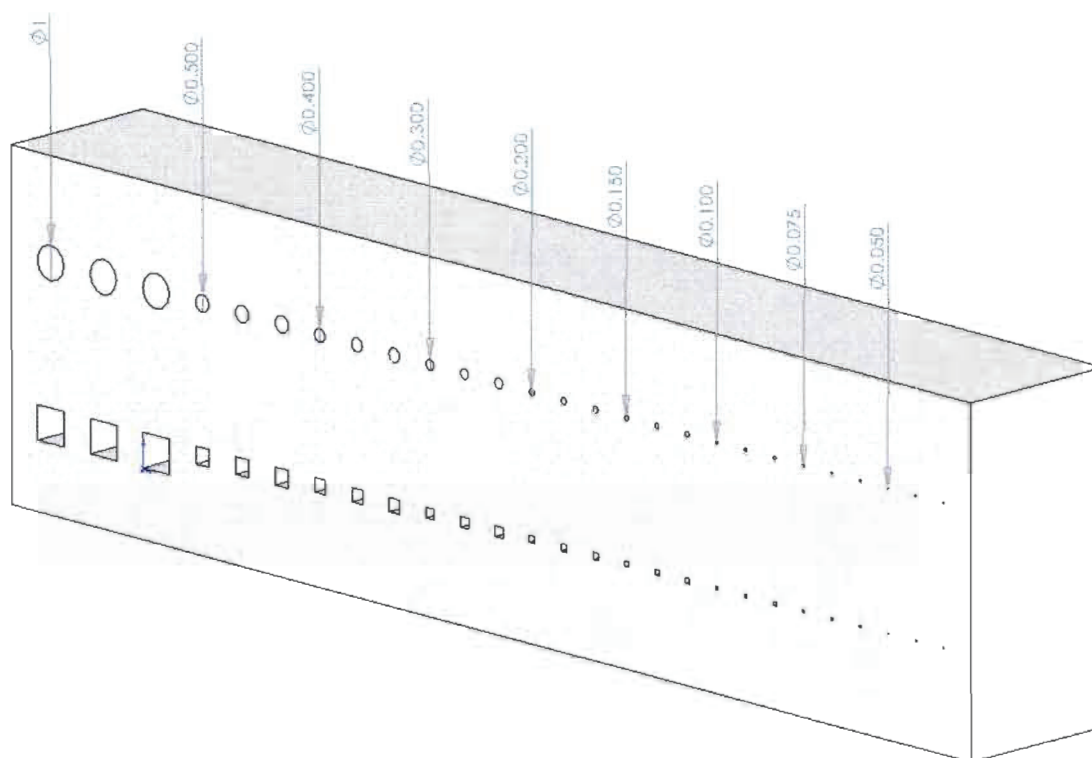


Figure C-2. Structure 2: Precise 100  $\mu$ L volume well with a 20 x 20 mm base



**Figure C-3. Structure 3: Round and square 5 mm long channels. The diameter (for round) or height and width (for square) of the channels were of 1000, 500, 400, 300, 200, 150, 100, 75 and 50  $\mu\text{m}$ . Three replicates of each size were included.**

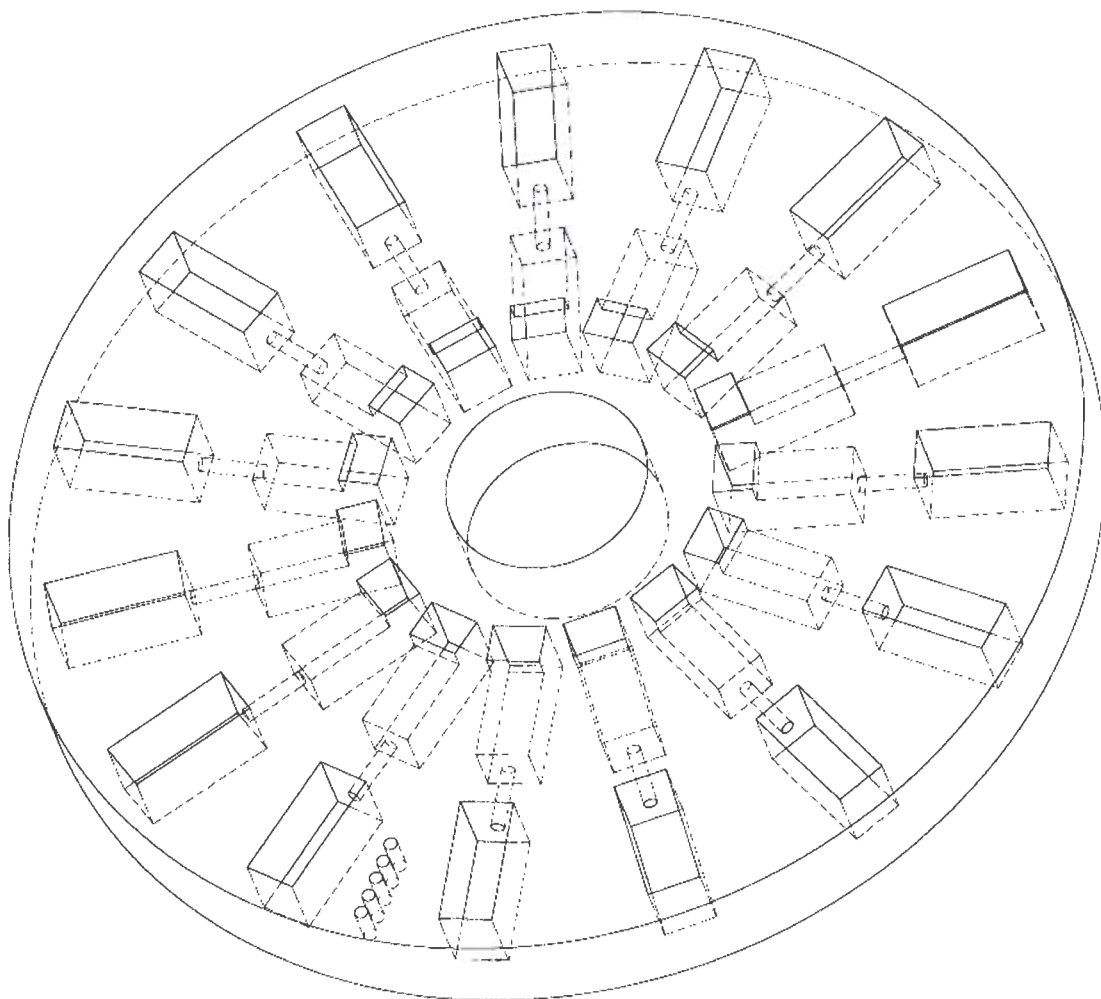


Figure C-4. Structure 4: Entire device including reservoirs and “printed” capillary valves manufactured in one step. Seven different versions of this structure were designed, each with a different size capillary burst valve (500, 300, 200, 150, 100, 75, and 50  $\mu\text{m}$ ). Each of the seven versions contained 15 iteration of the same size valve.

Both the structure and support material used by the *uPrint* printer were examined at a 16.8x magnification. The photograph on the left of Figure C-5 shows the *ABSPplus* material before and after being extruded through the printer nozzle. The uniform shape of the material reflects the efficiency of the extrusion process.



Figure C-5. *uPrint* ABS raw and extruded material (left) and “printed” support structure (right) at 16.8x magnification

Another active branch of research in the lab is the integration of filters in centrifugal devices. These would be of great use following the magnetically actuated solid sample preparation step discussed in Chapter 5. To that end, an attempt was made to “print” filters by combining a series of decreasing size post or columns as seen in Figure C-6. The *uPrint* did not perform well with the combination of small posts. The *V-Flash* performed equally poorly while the *Alaris* did show promising results (not shown here).

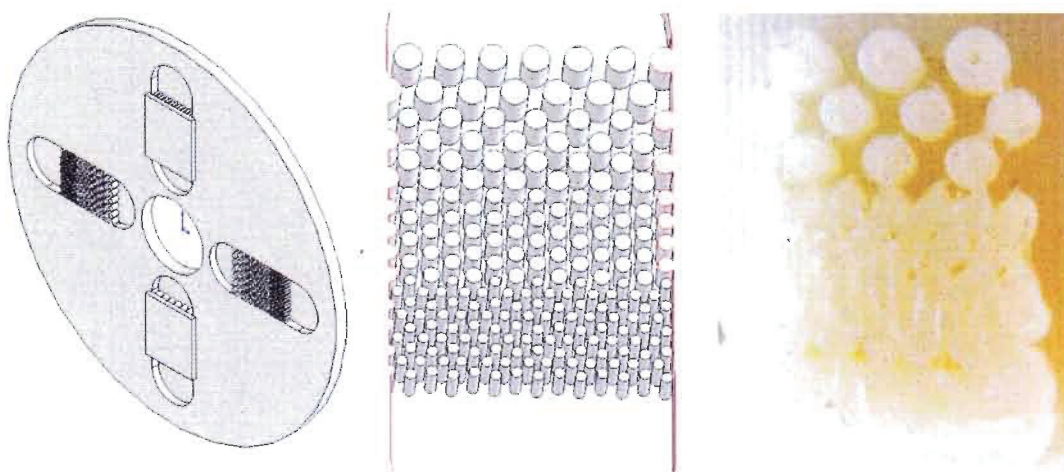
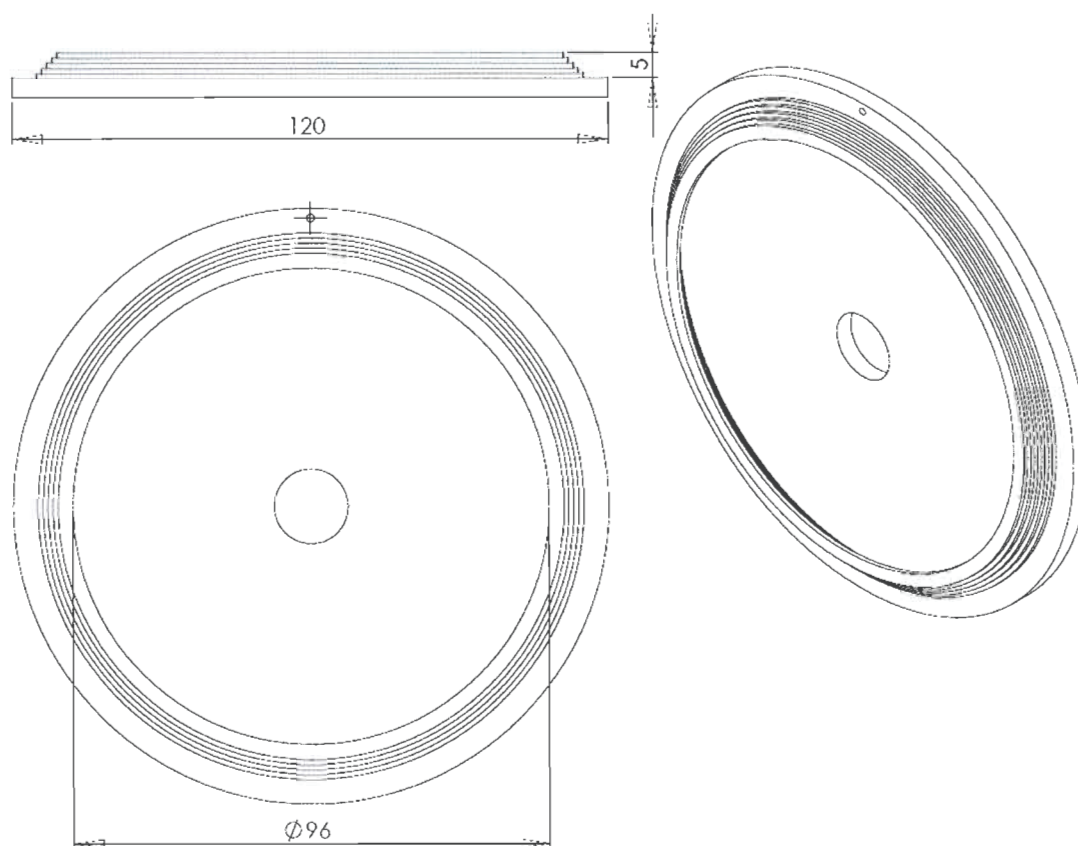


Figure C-6. Design of prototype filters. A series of posts or columns with diminishing diameter and distance between them were staggered over a small area. Entire test device (left), zoom of filter (middle) and *uPrint* failed test print (right) are shown.

Liquid sample introduction to spinning centrifugal devices was also of importance. The first prototypes for capturing liquids while the devices were in motion are shown in the next series of figures. The integration of lips, ridges and scoops in various formats were investigated.



**Figure C-7. First 3D prototype.** The lip design was originally made by stacking a series of smaller concentric circles in SolidWorks.

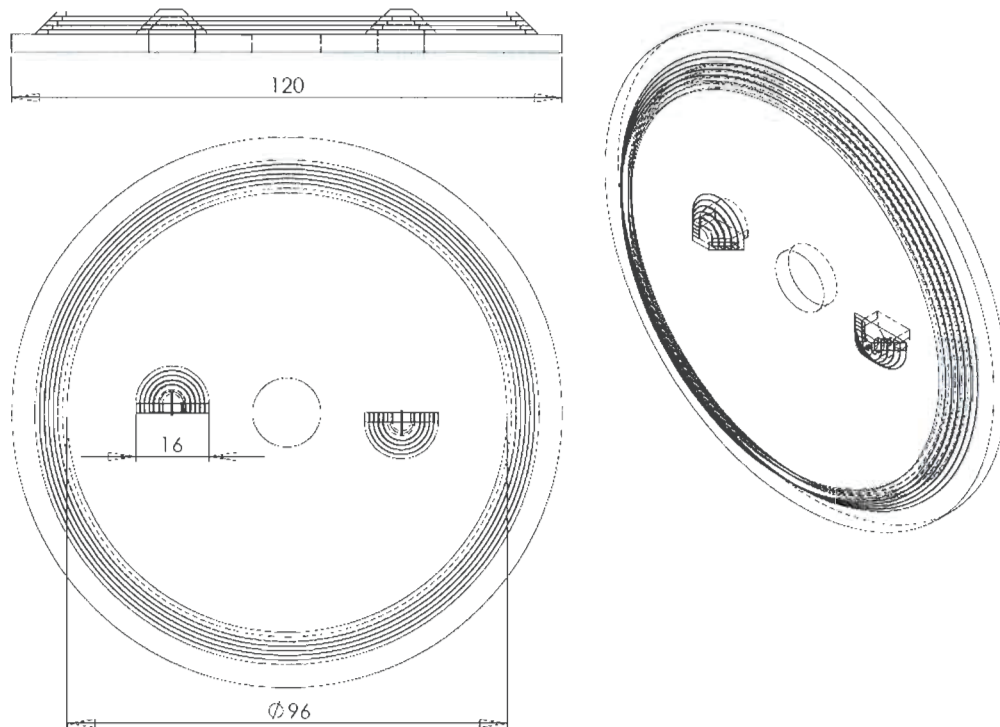


Figure C-8. Second 3D design included the original lip and two scoops which were opposite one another to balance the devices

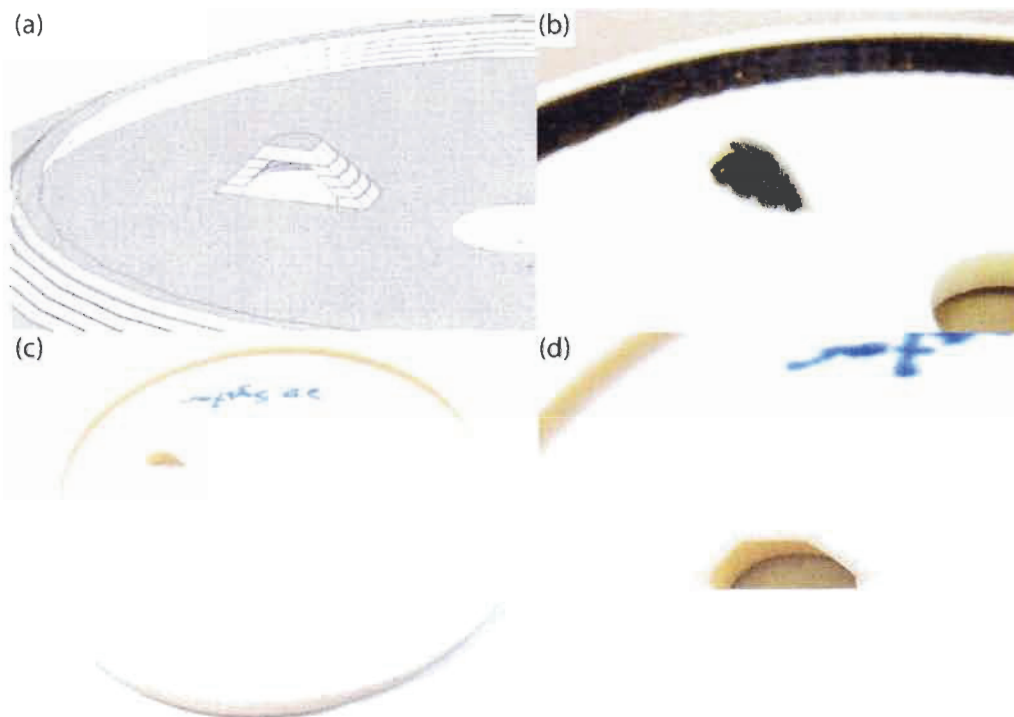
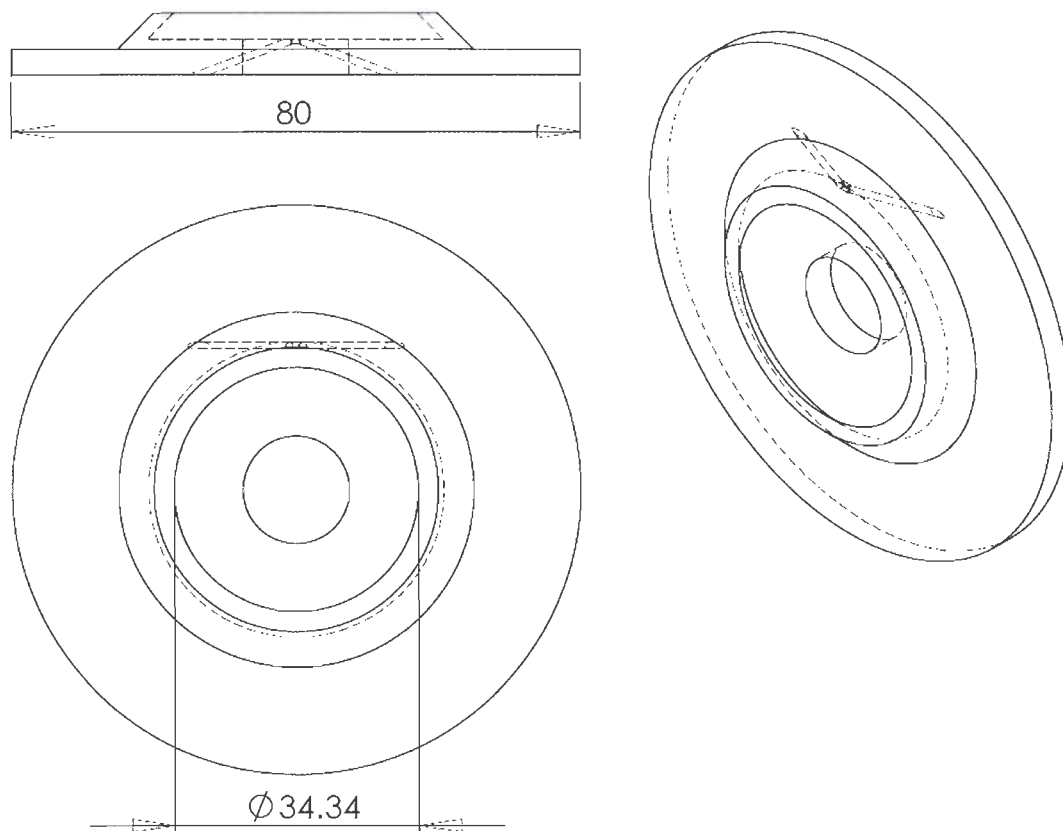
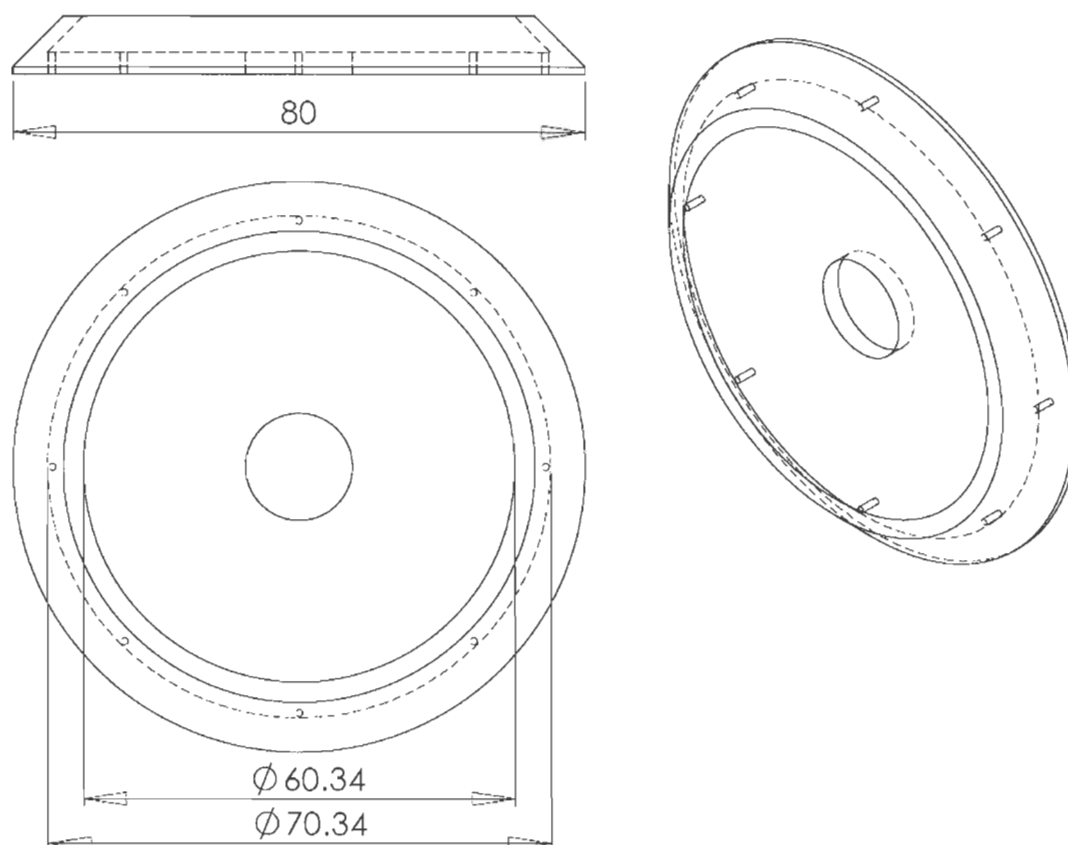


Figure C-9. Lip and scoop design details (a) Zoom view of design lip and one scoop. (b) Zoom view of *uPrint* part after printing but before removal of support structure. (c) Photograph of entire device manufacture on the *V-Flash*. (d) Zoom view of *V-Flash* scoop.

As detailed in Chapter 2, conventional 120 mm diameter CD and DVD polycarbonate disks (or other material cut to this size) have typically been used for centrifugal device fabrication. Another commercially available size disk is the 80 mm diameter mini-CD. Inspired by these, mini-centrifugal microfluidic devices were designed and manufactured (series of figures that follow). The idea was either to have smaller stand alone devices or have these interfaced with larger devices. This work lead to the development of the CLAD detailed in Chapter 4.



**Figure C-10.** First prototype mini-centrifugal device (80 mm diameter) designed with one lip and one test hole that had two drain channels. This design was to deliver liquid to one chamber with the device turning clockwise and a to a second chamber with the device turning counter-clockwise.



**Figure C-11. Second prototype mini-centrifugal device designed with one lip at its perimeter and eight draining holes to segment the added liquid to eight separate chambers.**

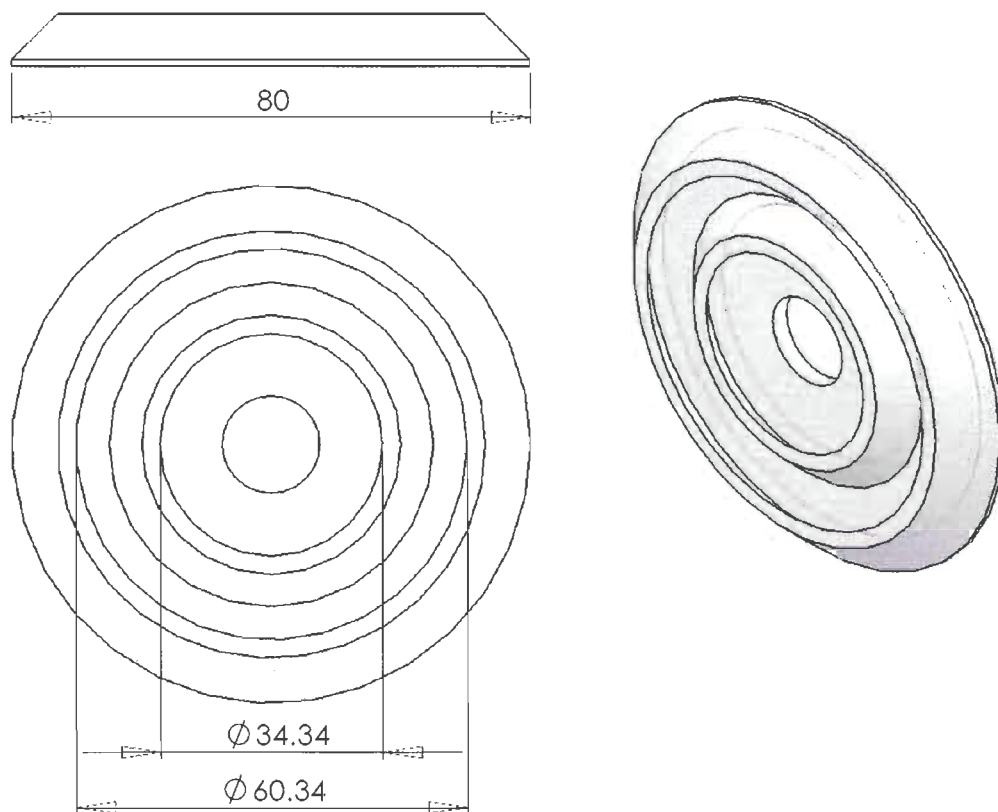


**Figure C-12.** Double lip mini-centrifugal device designed to be able to simultaneously add two different liquids to a moving device.

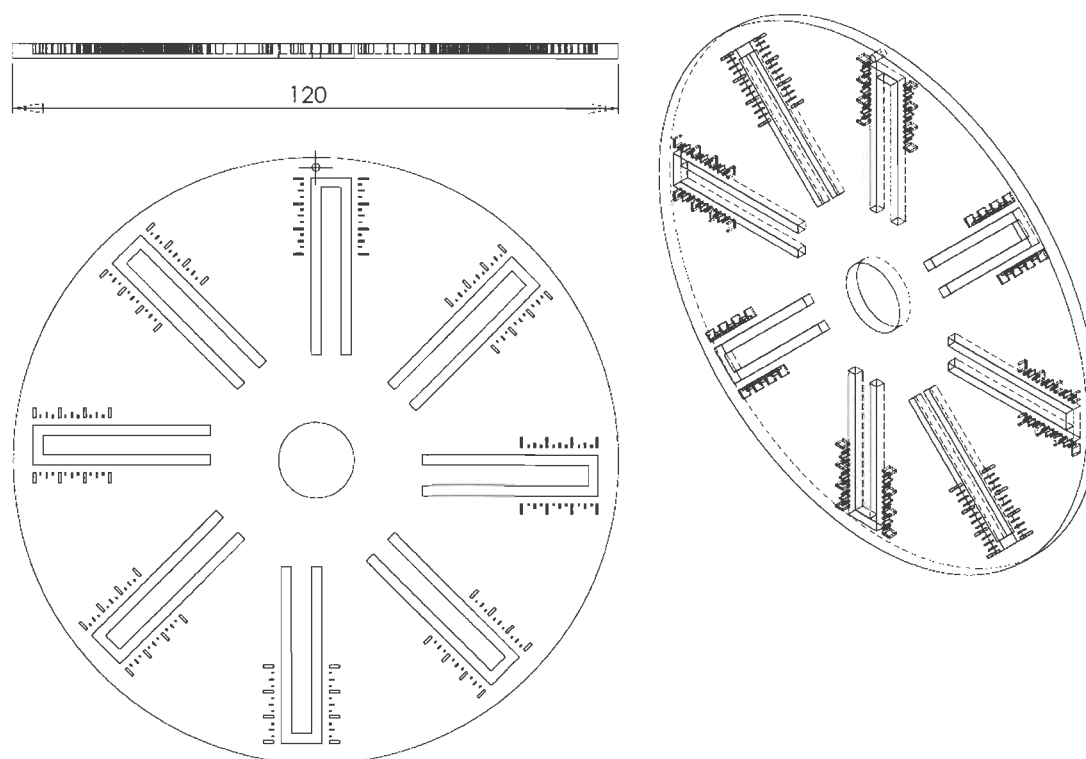


Figure C-13. In order to be able to measure the amount of liquid draining through each hole and to compare the distribution of liquid, U-shaped channels with inlet and vent holes was designed to act as a base for the mini-centrifugal device.

Initial work had both the mini-devices (80 mm) and larger base devices (120 mm) manufactured in a single step (series of figures that follow). Unfortunately, the opaque structures hindered the integration of an effective detection scheme. For this reason hybrid device using the printed mini-devices on clear polycarbonate bases were used in Chapter 4.

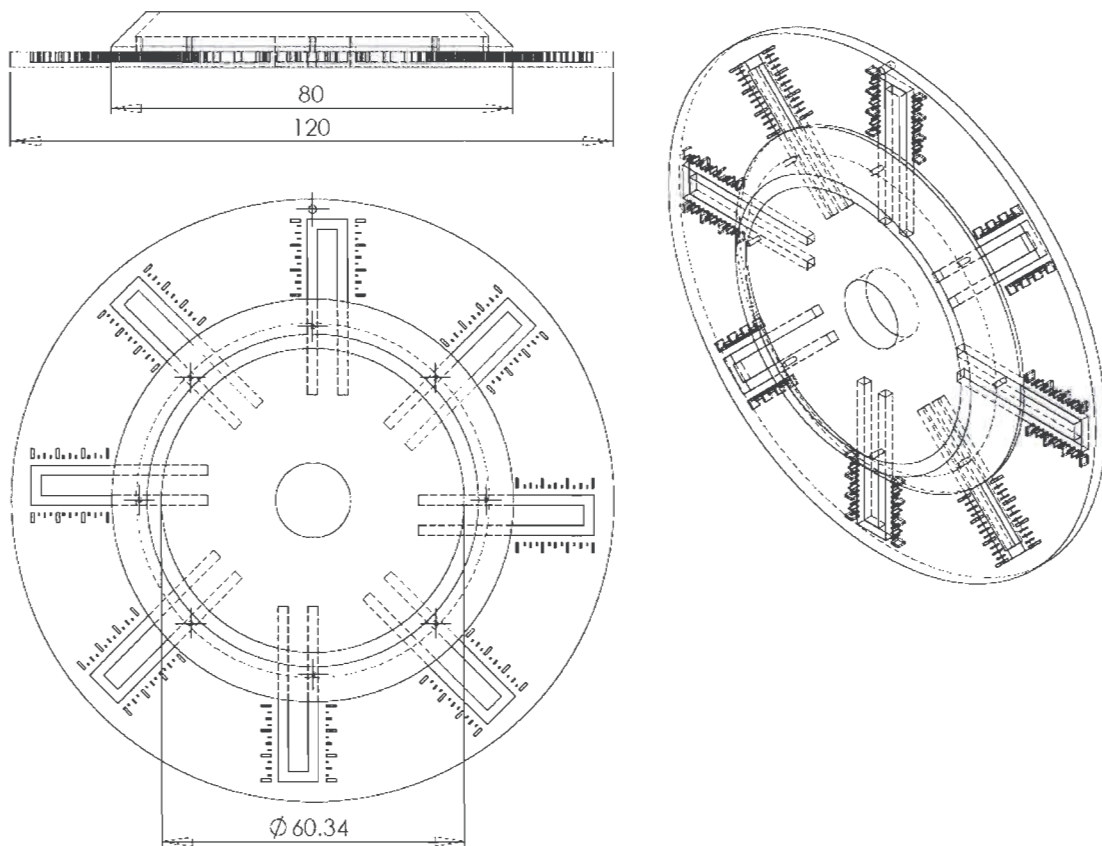
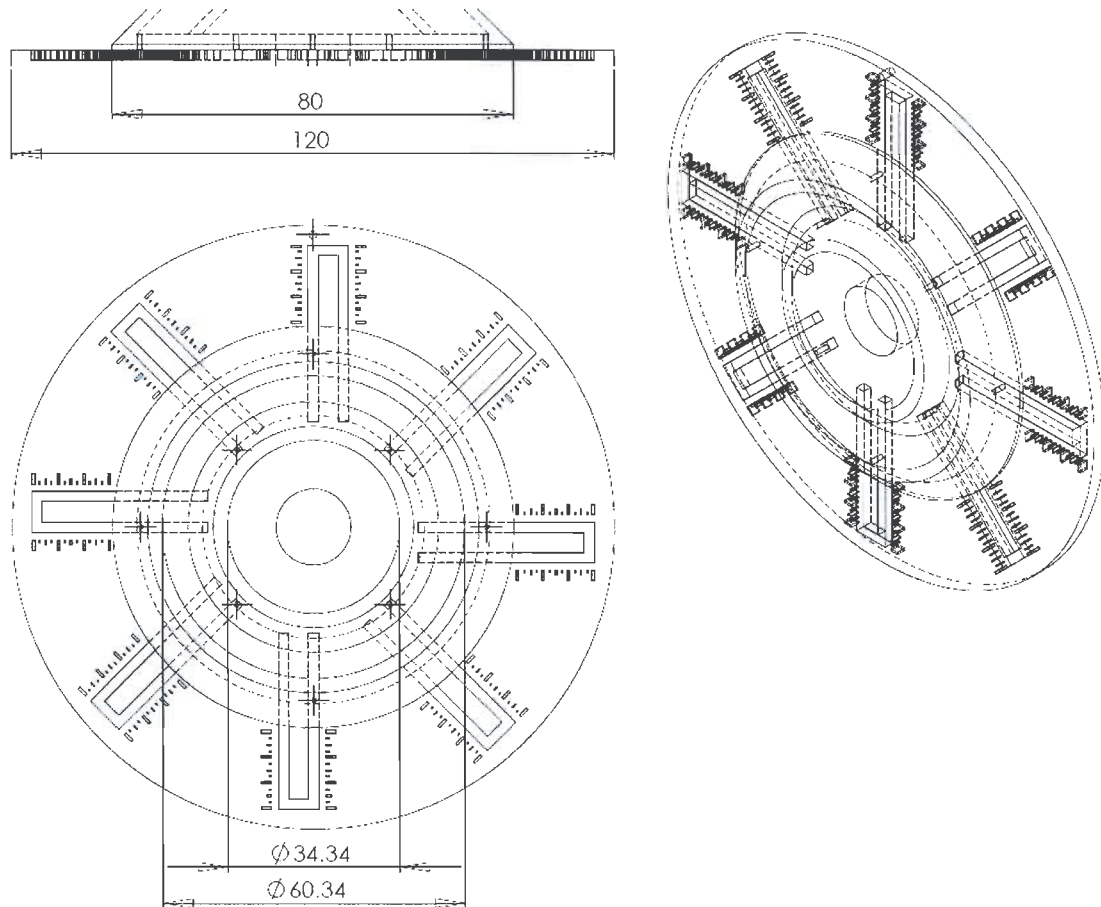


Figure C-14. Joining the 80 mm mini-centrifugal device (here with one lip) and the 120 mm base with integrated U-shaped channels could have been done post-production or as seen here at the design stage and manufacture as a single part.



**Figure C-15.** Composite part joining 80 mm mini-centrifugal device (here with two lips) and the 120 mm base with integrated U-shaped channels at the design stage. Alternating the radial distance from the centre of the inlet holes, four U-shaped channels were to collect liquid from the inner lip and four from the outer lip.

As seen in Figure C-16, imprinted calibrated scale bars were designed to enable the direct visual readout of the liquid level, similar to the visual measurement in the hematocrit report by Riegger *et al.*<sup>1</sup>

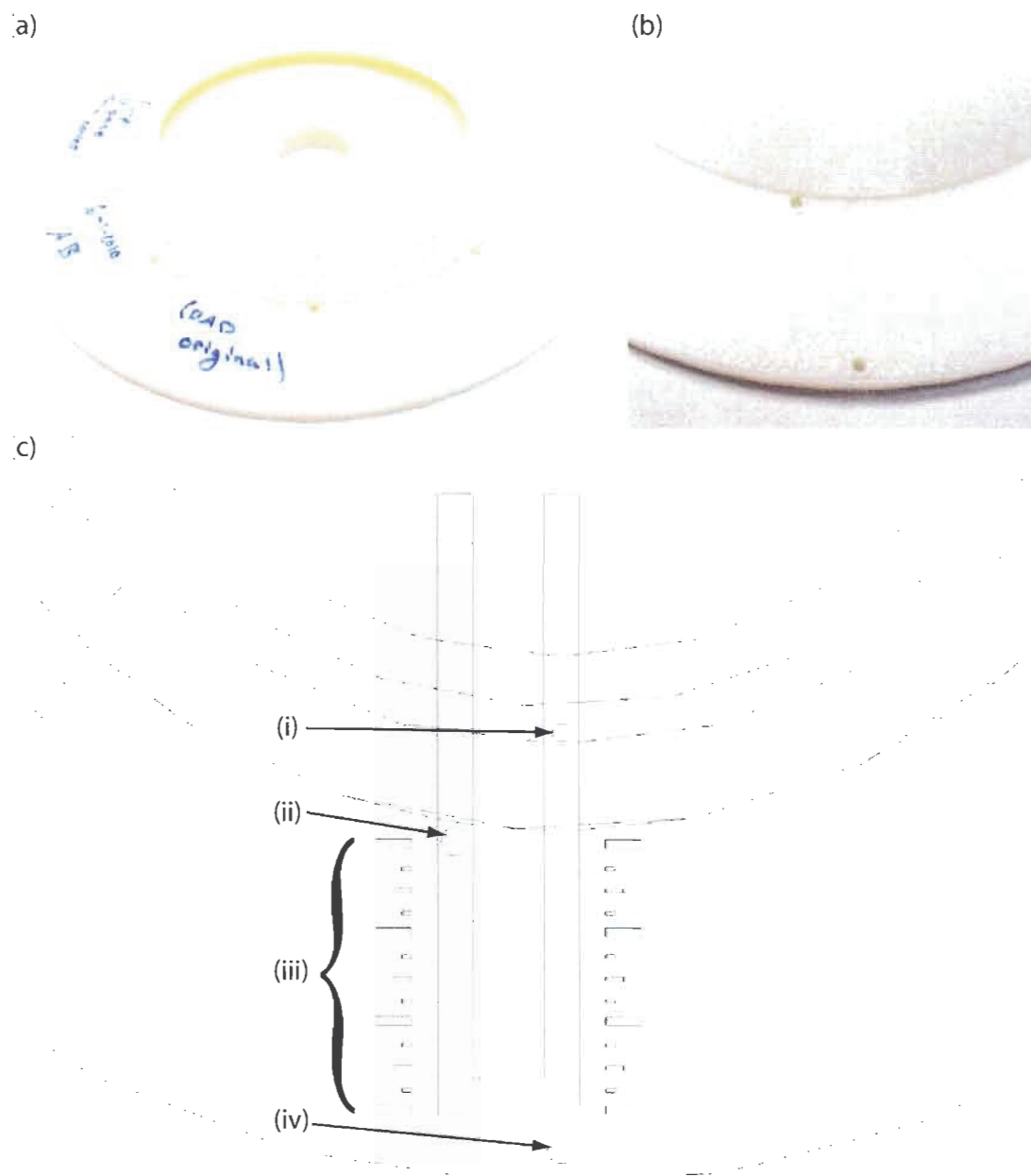


Figure C-16. (a) *uPrint* part with one lip and eight U-shaped channels. (b) Zoom of one U-shaped channel. (c) Schematic of U-shaped channel design including (i) inlet hole inside and under lip, (ii) vent hole and potentially outlet, (iii) integrated scale for measuring and comparing liquid distribution between U-shaped channels and (iv) alignment hole included but not used.

Due to space limitations, Figure C-17 and Figure C-18 were removed from the original published work (chapter 4). These show details of the design and liquid deposition mechanism.

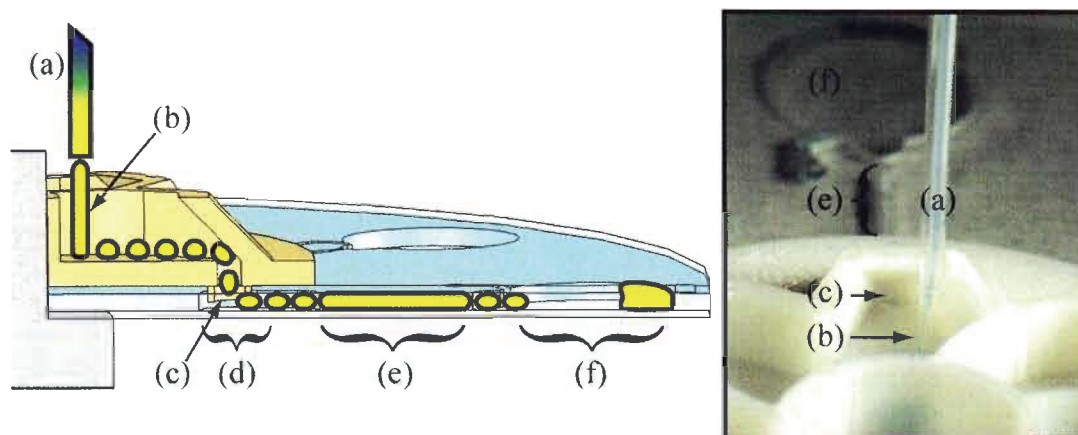


Figure C-17. Liquid deposition mechanism drawing (left – cut side view) and photograph (right). (a) Peristaltic pump tubing, (b) continuous stream of liquid broken by rough surface of CLAD, (c) hole in CLAD cup into disk base, (d) Receiving Reservoir, (e) Viewing Channel and (f) Collection Reservoir.

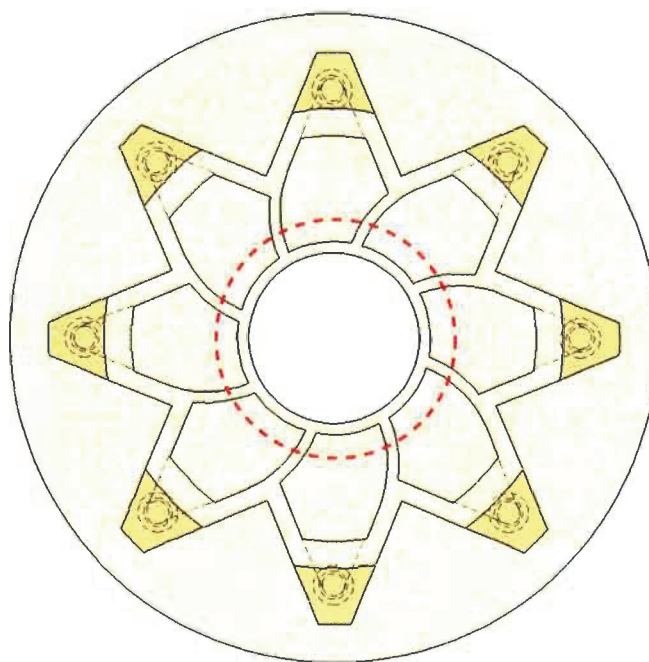


Figure C-18. Top view of CLAD with location of holes. Dotted circle represents the radial distance at which liquid was added (10.5 mm).

In Chapter 4, there is the following statement: “The design minimized the width of the walls (each wall representing only 1.6% of the total area), thereby maximizing surface area available for liquid addition”. This was calculated based on the fact that 1) the liquid was added at a radial distance of 10.5 mm from centre (see dotted circle in Figure C-18) and 2) the thickness of each wall was of 1.05 mm. The calculations used were:

Circumference of a circle	$= 2\pi r$
Circumference of deposition circle	$= 2\pi(10.5 \text{ mm}) = 65.97 \text{ mm}$
Each wall was 1.05 mm thick (8 walls)	$= 8.4 \text{ mm}$
Circumference actually in cups	$= 65.97 - 8.4 \text{ mm} = 57.57 \text{ mm}$
Percent deposition in cup	$= 57.57/65.97 * 100 = 87.3 \%$
Percent deposition on 8 walls	$= 12.7 \%$

Consequently, it was accurate to state that “each wall represent[ed] only 1.6% of the total area.” Notwithstanding this, no splattering was observed and there was no loss of 12.7 % of the added liquid. Rather the liquid that hit the top of the walls seem to fall into the next cup.

A source of error was discerned in regards to the timing of the liquid spray to the moving CLAD. Unless liquid started exactly as the beginning of the first cup passed beneath the tubing, and unless the liquid stopped exactly as the end of the eighth and last cup passed beneath the tubing for the last time, these first and last cups received less volume than the other six cups. This error represented a smaller and smaller fraction of the total volume as the system was run longer. This was a contributing factor to the observed larger RSD at low volumes in Table 4-1.

Precise control of the flow rate was required to obtain repeatable addition and distribution of liquid. A peristaltic pump with small tubing was used in order to obtain a steady stream of liquid instead of inconsistent drops. The pulsating nature of these pumps at low flow rate and the desire to add smaller amount of liquids will necessitate the future use of alternative pumps such as commercially available syringe pumps. The CLAD's linear flow rate is a desirable characteristic for future research into centrifugal gradient chromatography.

### **Reference**

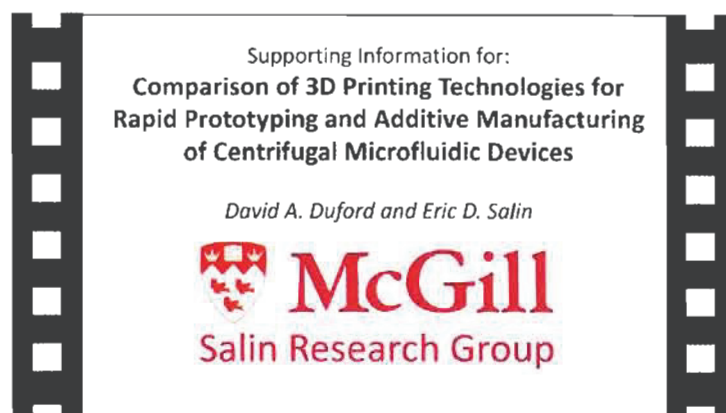
- (1) Riegger, L., Grumann, M., Steigert, J., Lutz, S., Steinert, C.P., Mueller, C., Viertel, J., Prucker, O., Rühle, J., Zengerle, R., Ducrée, J., "Single-step centrifugal hematocrit determination on a 10- $\mu$  processing device", *Biomedical Microdevices*, **2007**, 9 (6), 795-799.

## Appendix D: Links to Supplementary Videos

Video media is among the best to not only explain but to show how centrifugal microfluidic devices and 3D printers work. For this reason three videos were prepared to supplement Chapters 3, 4 and 5.

In this first video, a comparison of the three different additive manufacturing 3D printers in action is compiled showing in order:

- *uPrint* from Dimension Inc. (using fused deposition modeling technology),
- *V-Flash* from 3D Systems Corporation (using film transfer imaging technology),
- *Alaris* from “Objet Geometries Inc.” (using polyjet modeling technology).



QR code to youtube



<http://www.youtube.com/watch?v=vnzmZsrHg3E&feature=youtu.be>

Figure D-1. QR code and link to supplementary video to Chapter 3. The sections of the video showing the *V-Flash* and the *Alaris* were taken from their respective promotional videos.

The second video was published as supporting information to the article of Chapter 4. The video includes 1) the CLAD being built by the *uPrint* 3D printer 2) chemical bonding of the CLAD to the conventional centrifugal disk base with acetone, 3) 3D views of the hybrid platform and 4) collection of high speed digital images of deposition process.



<http://www.youtube.com/watch?v=eMNm6SJako0&feature=youtu.be>

[http://pubs.acs.org/doi/suppl/10.1021/ac1024478/suppl\\_file/ac1024478\\_si\\_002.avi](http://pubs.acs.org/doi/suppl/10.1021/ac1024478/suppl_file/ac1024478_si_002.avi)

Figure D-2. QR codes and links to supplementary video to Chapter 4

The third and final video was published as supporting information to the article of Chapter 5 and illustrates the general experimental set-up that was also used for Chapters 6 and 7. The video includes the centrifugal device rotating above the fixed base at 5, 240 and 1000 rpm. The spinning and shaking motion of the “mobile magnets” and the ability of the device to grind solid samples is clearly observed. A comparison of chambers with and without a “mobile magnet” illustrates the efficiency of the system in which solid samples are quickly and completely dissolved in seconds.



<http://www.youtube.com/watch?v=nZuhX-irGRs&feature=youtu.be>

[http://pubs.acs.org/doi/suppl/10.1021/ac9006733/suppl\\_file/ac9006733\\_si\\_002.avi](http://pubs.acs.org/doi/suppl/10.1021/ac9006733/suppl_file/ac9006733_si_002.avi)

Figure D-3. QR codes and links to supplementary video to Chapter 5.

## **Appendix E: Temperature Increase Within a Chamber Containing a Mobile Magnet – Experimental and Theoretical Calculations**

Section 5.4.2 *“Induced Temperature”* states that “the temperature inside the extraction chambers was also monitored”, with an observed increase of 0.7°C/min due to the induced mechanical motion. The details of that experiment and theoretical calculations are the focus of this appendix.

### ***E.1 Experimental Design and Results***

The determination of the temperature increase within a chamber containing a “mobile magnet” was not trivial. Continuous monitoring of the spinning device was desirable; but interfacing a sensor was difficult. A non-contact infrared sensor was investigated; however the polycarbonate material and the spinning chamber made such a sensor hard to use. Finally, a test device was constructed by adding a type J thermocouple to the top of a centrifugal device and spinning the entire assembly (see Figure E-1). The thermocouple wire inlet was sealed with hot glue and the design assured that the mobile magnet did not touch the thermocouple during the experiment. The objective was to obtain the temperature readout off the thermocouple from the series of synchronised photographs taken by the servo motor stage.

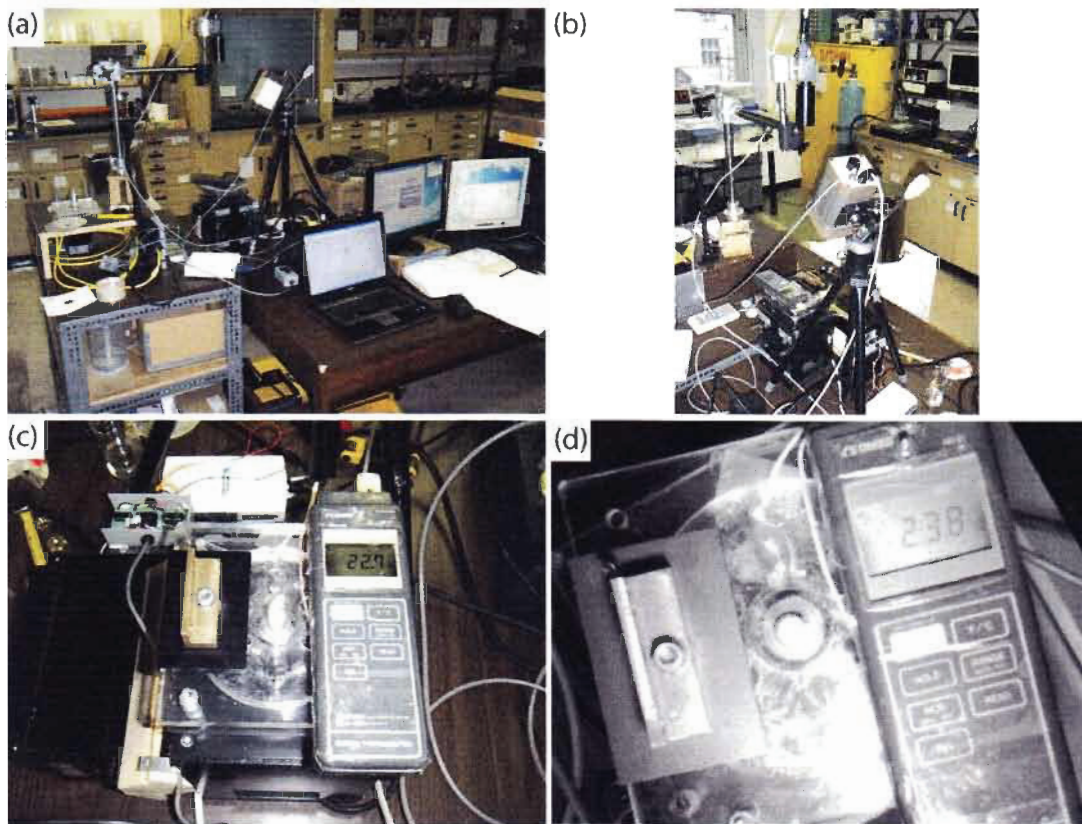


Figure E-1. Experimental set-up for the determination of the temperature in the chamber of centrifugal device with and without a “mobile magnet”. (a) Interfacing components of two stages operated simultaneously. (b) Secondary view of experimental set-up. (c) Temperature determination test device with thermocouple and counter weight. (d) Sample of one of over 4000 pictures obtained displaying the temperature inside chamber.

The final assembly, which required a counter weight for balance, was heavier than any other centrifugal device ever spun in our laboratory. As a result, it was found that the servo motor did not have enough torque to spin the heavy device. Brute force was necessary and for this reason the DC motor was used. The downside to this was that the camera and strobe were synchronized to the servo motor, not the DC motor.

To overcome this, it was thought that the two motors could be ran at the exact same speed and have the camera and strobe take pictures of the DC motor

though being triggered by the servo motor. At that time however, the DC motor had not yet been calibrated for rotational speed (*i.e.* angular velocity). The strobe light set to manual was used and the DC motor was calibrated with exceptional correlation of the voltage to the speed (Figure E-2). This calibration information was then included in the LabVIEW code prompting the user for the desired rpm instead of a non-intuitive voltage. Consequently both motorized stages were ran at the same 240 rpm thus synchronizing the camera and strobe of the servo motor stage to the temperature test device spinning on the DC motor stage.

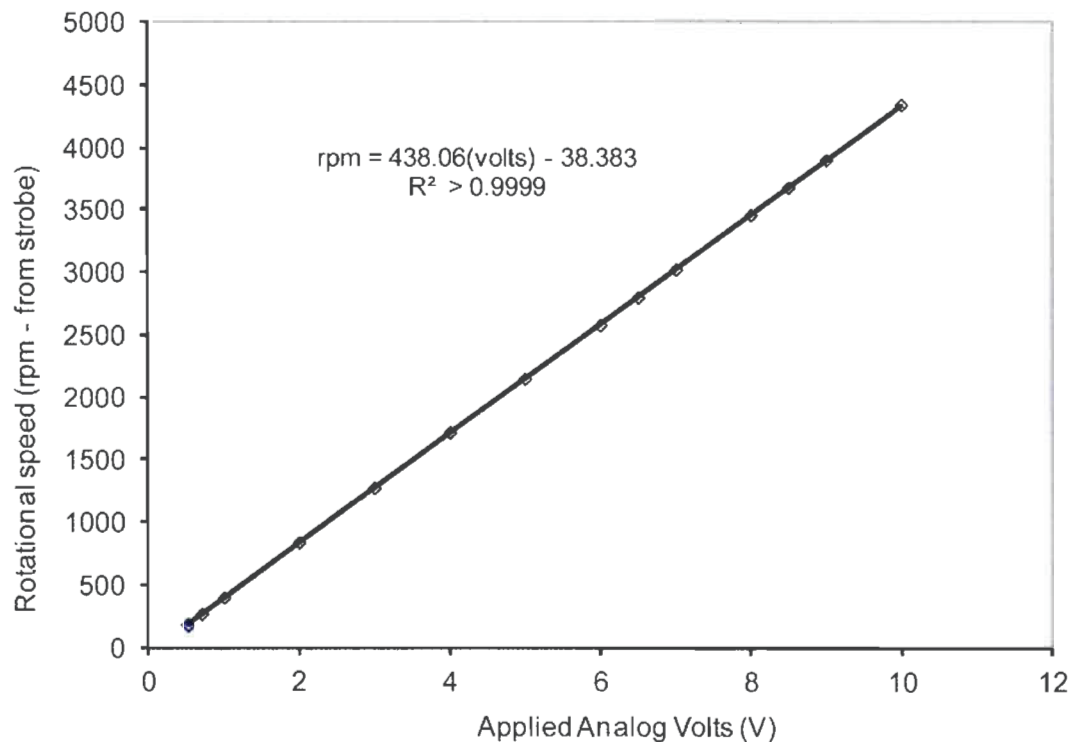


Figure E-2. Calibration curve of the DC motor between the applied voltage and the resulting rotational speed (angular velocity)

With each picture's time stamp and by reading the temperature off each picture taken, the data of Figure E-3 was compiled. From this figure, an average increase in temperature of 0.7°C/min was reported in Chapter 5.

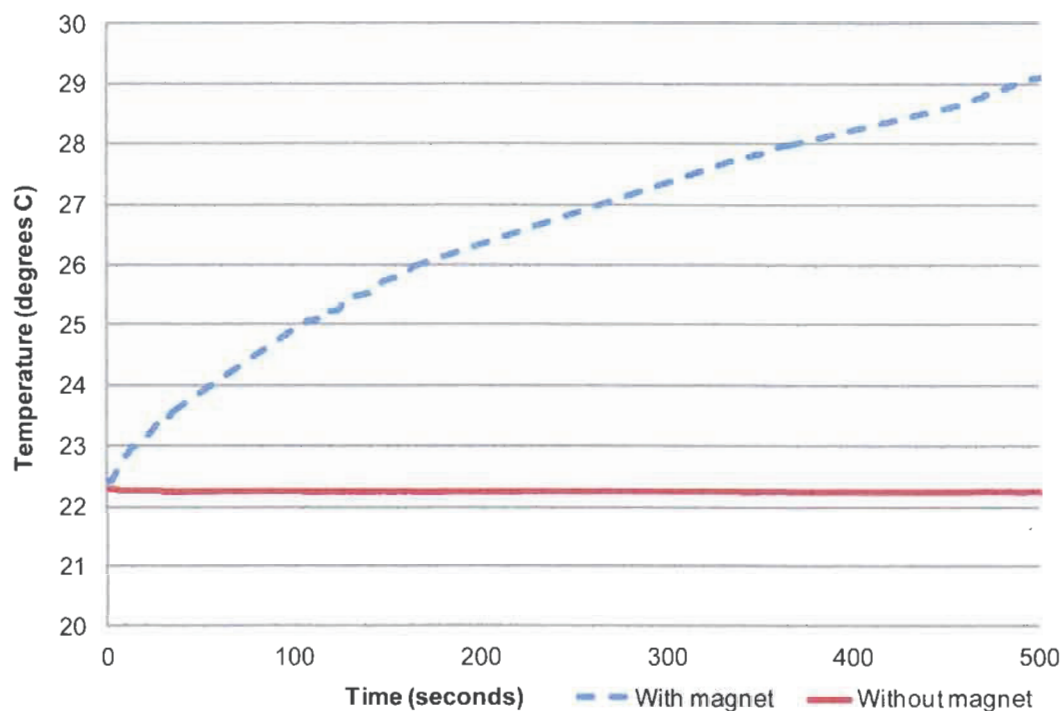


Figure E-3. Plot of temperature in chamber of centrifugal device containing water with and without a "mobile magnet" over a period of more than 8 minutes at an angular velocity of 240 rpm. A 20 point moving boxcar has been applied.

Since the Celsius and Kelvin temperature units are of the same magnitude, an increase of 0.7°C is equal to an increase of 0.7 K. Assuming that roughly 1 mL of water was in the chamber (or 1 g of water assuming a density of 1 g/mL) and knowing the heat capacity of water to be 4.181 J/g K, the amount of work being done resulting in heat was calculated to be:

$$\frac{0.7 \text{ K}}{\text{min}} \times \frac{4.181 \text{ J}}{\text{g K}} \times \frac{1 \text{ g}}{1} = 3 \text{ J/min}$$

## E.2 Theoretical Calculations

Since no temperature increase was observed in the chamber without the “mobile magnet”, the main contributing factor to this increase in temperature was assumed to be the work done by the revolving magnets. As noted in Chapter 5, each magnet underwent a spinning and shaking action due to the interaction of the magnetic fields of the “mobile magnets” with those in the fixed base. Theoretical calculations were made to quantify the amount of work done by each of these movements.

### E.2.1 Work Done by a Magnet *Spinning* on its Own Axis

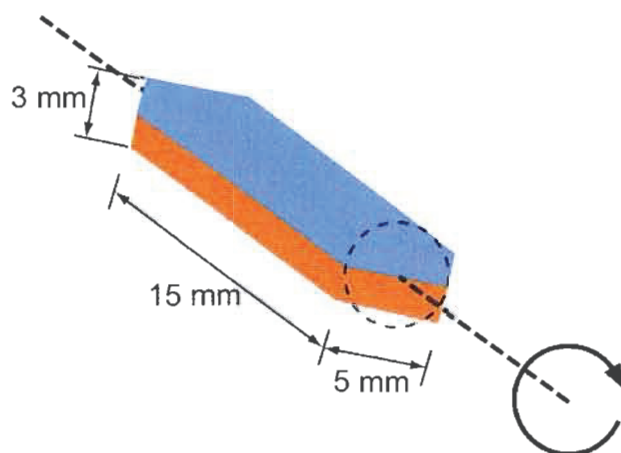


Figure E-4. Schematic of the magnet spinning upon its own axis

In order to be able to compare to the experimental results above, we will assume that the entire device is rotating at 240 rpm and that each magnet weighs 1.7 g.

$$\text{Revolutions of entire device} = \frac{240 \text{ rev}}{\text{min}} \times \frac{1 \text{ min}}{60 \text{ s}} = 4 \text{ rev/s}$$

If the diameter of the assumed path in which the magnet spins on its own axis is approximately 5 mm (see Figure E-4), the radius of that theoretical circle is 2.5 mm and the distance traveled is equal to the circumference of that circle.

$$\text{Circumference of spin of each magnet} = 2\pi r = 2\pi(2.5\text{mm}) = 15.7 \text{ mm/spin}$$

Every revolution of the entire device makes each magnet spin upon its own axis 6 times.

$$\text{Spin frequency} = \frac{6 \text{ spins}}{1 \text{ rev}} \times \frac{4 \text{ rev}}{s} \times \frac{24 \text{ spins}}{s}$$

Given this distance and time, the velocity of each magnet is therefore:

$$\text{Velocity of spinning magnet} = \frac{24 \text{ spins}}{s} \times \frac{15.7 \text{ mm}}{\text{spin}} \times \frac{1 \text{ m}}{1000 \text{ mm}} = 0.38 \text{ m/s}$$

The weight of each magnet is of 1.7 grams. Therefore the theoretical work done every second by each magnet due to its spinning motion is:

$$W_{\text{spin}} = \frac{1}{2}mv^2 = (1.7g) \left( \frac{0.38m}{s} \right)^2 \left( \frac{1 \text{ kg}}{1000 \text{ g}} \right) = 2.5 \times 10^{-4} \frac{\text{kg m}^2}{\text{s}^2} \text{ or Nm or J}$$

(Equation E-1)

### E.2.2 Work Done by a Magnet *Shaking Back and Forth* in Chamber

As described in Chapter 5, the motion of the magnets is not limited to spinning upon their own axis. Due to the staggering of the magnets in the fixed base, the “mobile magnets” are alternately subjected to stronger magnetic fields pulling inward and outward during the rotational cycle. This back and forth shake motion also contributes to the work being done by these magnets and to the observed increase in temperature. The magnets move a distance of 1 cm six

times every revolution, three movements up and three movements down in the chamber (see Figure E-5), accurately described therefore as a shaking motion.

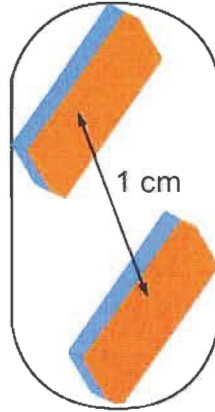


Figure E-5. Schematic of the magnet shaking back and forth in the chamber

$$\text{Distance travelled} = \frac{1 \text{ cm}}{1 \text{ shake}} \times \frac{6 \text{ shakes}}{\text{rev}} \times \frac{1 \text{ m}}{100 \text{ cm}} = 0.06 \text{ m/rev}$$

$$\text{Velocity of shaking magnet} = \frac{0.06 \text{ m}}{\text{rev}} \times \frac{4 \text{ rev}}{\text{s}} = 0.24 \text{ m/s}$$

Therefore the theoretical work done every second by each magnet due to its shaking motion is:

$$W_{\text{shake}} = \frac{1}{2}mv^2 = (1.7g) \left( \frac{0.24\text{m}}{\text{s}} \right)^2 \left( \frac{1 \text{ kg}}{1000 \text{ g}} \right) = 9.8 \times 10^{-5} \frac{\text{kg m}^2}{\text{s}^2} \text{ or Nm or J}$$

(Equation E-2)

It is important to note that more work is done by the magnets as they do not merely maintain a velocity of 3 m/s, but rather repeatedly accelerate to this velocity.

### E.2.3 Total Work Done by a Magnet Spinning and Shaking

Combining the work from both the spinning and shaking motions of the magnets, the total work from these sources is:

$$W_{total} = W_{spin} + W_{shake}$$

$$W_{total} = 2.5 \times 10^{-4} + 9.8 \times 10^{-5} = 3.5 \times 10^{-4} \frac{kg \ m^2}{s^2} \text{ or } Nm \text{ or } J$$

Which in terms of temperature represents:

$$\frac{3.5 \times 10^{-4} J}{s} \times \frac{g \ K}{4.181 J} \times \frac{1}{1 g} \times \frac{60 s}{min} = 0.005 K/min$$

This theoretical total work and corresponding temperature increase of 0.005°C/min only accounts for the spinning and shaking motion of the magnets with the assumptions of the simple model used here. Other forces such as friction contribute to the total work being performed, reflected in both the experimental temperature increase and the sound waves being produced. The key is that a great impacting force is achieved and is concentrated on the solid samples in these chambers.

## Appendix F: Absorbance and Statistics

Spectrochemical analyses are among the most widely used methods for quantifying analytes.<sup>1</sup> Other than merely measuring signals, in such methods the noise and propagation of error must be taken into consideration. This appendix details the absorbance measurements for both the determination of PAHs and pesticides and the corresponding expressions for the signal-to-noise and the limit of detection.

### F.1 Signal Measurements

Absorption spectroscopy involves the measurement of light that is transmitted ( $T$ ) through a cell of fixed path length ( $b$ ), typically 1 cm. In general, a linear relationship is seen between the analyte concentrations ( $c$ ) when such measurements are converted to absorption ( $A$ ), as described by Beer's Law<sup>1</sup>: (where  $\varepsilon$  = molar absorption coefficient)

$$A = \varepsilon bc \quad (\text{Equation F-1})$$

Transmittance ( $T$ ) is defined as:

$$T = \frac{I_s - I_{0\%T}}{I_{blk} - I_{0\%T}} \quad (\text{Equation F-2})$$

Where  $I_s$  = sample signal  
 $I_{blk}$  = blank reference signal  
 $I_{0\%T}$  = 0% transmittance (light source off) signal

Substituting Equation F-2 into Equation F-1 yields the classic absorbance equation summarized here in its various equivalent forms:

$$A = -\log T = -0.434 \ln T = -\log \frac{I_s - I_{0\%T}}{I_{blk} - I_{0\%T}} = \log \frac{I_{blk} - I_{0\%T}}{I_s - I_{0\%T}} \quad (\text{Equation F-3})$$

Equation F-3 was used for the determination of PAHs in Chapter 6.

In Chapter 7, pesticide concentration was determined using an enzyme inhibition-based method. Initially the relationship between concentration and signal is counter-intuitive since it is 1) a logarithmic relationship and 2) based on percent inhibition and not directly on pesticide concentration. From absorbance ( $A$ ) of a sample, the percent inhibition ( $In(\%)$ ) can be calculated from Equation F-4<sup>2</sup> where  $A_0$  is sample without analyte, in essence a blank, which absorbs the most light and  $A_s$  is the sample being analyzed.

$$In(\%) = \frac{A_0 - A_s}{A_0} \times 100\% \quad (\text{Equation F-4})$$

To better understand this equation, take for example a sample without any inhibitor pesticide. In such a sample, there would be minimal or no inhibition (and equivalent percent inhibition) resulting in a high absorbance due to the coloured Enzyme-Substrate-Chromatic reagent (ESC) complex formed. Therefore if  $A_s$  is equal to  $A_0$ , there is zero  $In(\%)$  and if  $A_s$  is half the value of  $A_0$  there is obviously a 50% inhibition rate (see Chapter 7 for more details).

In addition to this, the relationship between pesticide concentration ( $C$ ) and percent inhibition is not linear but rather logarithmic. A linear regression calibration curve is obtained by Equation F-5 and isolating the  $\log C$  term results in Equation F-6:

$$In(\%) = m \log C + b \quad (\text{Equation F-5})$$

$$\log C = \frac{\ln(\%) - b}{m} \quad (\text{Equation F-6})$$

Equation F-4 to Equation F-6 were used for the determination of pesticide concentration in Chapter 7. In addition, in order to better understand the complexity of these relationships (related to propagation of error described in the next section) the pesticide concentration is also described in Equation F-7 in terms of percent inhibition and in Equation F-8 in terms of signal intensity.

$$C = 10^{\frac{\ln(\%) - b}{m}} \quad (\text{Equation F-7})$$

$$C = 10^{\left[ \frac{\left[ \frac{\left( \log \frac{I_{blk} - I_{0\%T}}{I_{sample\ blk} - I_{0\%T}} \right) - \left( \log \frac{I_{blk} - I_{0\%T}}{I_{sample} - I_{0\%T}} \right)}{\left( \log \frac{I_{blk} - I_{0\%T}}{I_{sample\ blk} - I_{0\%T}} \right)} \right] 100\% - b}{m} \right]} \quad (\text{Equation F-8})$$

## F.2 Error Propagation and Noise

Each signal value has an uncertainty or error associated with it. When arithmetic calculations are performed with these signals, the error of the result is a combination of the individual errors. Depending on the arithmetic calculation performed, the error is calculated as summarized in Table F-1<sup>3</sup>.

Table F-1. Summary of error propagation

Type of Calculation	Example	Standard Deviation of $x$
Addition and Subtraction	$x = p + q - r$	$\sigma_x = \sqrt{\sigma_p^2 + \sigma_q^2 + \sigma_r^2}$ (Equation F-9)
Multiplication and Division	$x = pq/r$	$\frac{\sigma_x}{x} = \sqrt{\left(\frac{\sigma_p}{p}\right)^2 + \left(\frac{\sigma_q}{q}\right)^2 + \left(\frac{\sigma_r}{r}\right)^2}$ (Equation F-10)
Exponential	$x = p^y$	$\frac{\sigma_x}{x} = y \frac{\sigma_p}{p}$ (Equation F-11)
Logarithm	$x = \log_{10} p$	$\sigma_x = 0.434 \frac{\sigma_p}{p}$ (Equation F-12)
Antilogarithm	$x = 10^p$	$\frac{\sigma_x}{x} = 2.303 \sigma_p$ (Equation F-13)

The total error or noise observed in a measurement is due to a combination of the noises of each measurement. As seen in Table F-1 their variances ( $\sigma^2$ ) and not their standard deviations ( $\sigma$ ) are additive. This also makes the major source of noise dominate over the other minor sources of noise since its value is squared in this calculation. It is also assumed that the noise sources are non-correlated or independent of each.

Consequently, to each of the signal equations described in section F.1, a corresponding error or noise equation can be elaborated, applying the propagation of error formulae summarized in Table F-1.

For example, the noise associated with an absorbance measurement ( $\sigma_A$ ) is related to the noise in the transmittance measurements ( $\sigma_T$ ). Applying the mathematic propagation of error to Equation F-3 results in the absorbance noise expression of Equation F-14:

$$\sigma_A = \frac{0.434 \sigma_T}{T} \quad (\text{Equation F-14})$$

Theoretically the noise in transmittance ( $\sigma_T$ ) is associated with the noise of all three required measurements (*i.e.* sample, blank and 0%T). Application of the propagation of error would result in the noise of transmittance being described by:

$$\frac{\sigma_T}{T} = \sqrt{\left( \frac{\sqrt{\sigma_{I_s}^2 + \sigma_{I_{0\%T}}^2}}{I_s - I_{0\%T}} \right)^2 + \left( \frac{\sqrt{\sigma_{I_{blk}}^2 + \sigma_{I_{0\%T}}^2}}{I_{blk} - I_{0\%T}} \right)^2} \quad (\text{Equation F-15})$$

However, only  $I_s$  varies with  $T$  and thus the dependence of  $\sigma_T$  on  $T$  is dependent mainly on the noise (or uncertainty) in measuring the sample signal ( $I_s$ ). For this reason, Ingle and Crouch insert the condition: "it is assumed there is no uncertainty in measuring  $I_{blk}$  and  $I_{0\%T}$ ".<sup>1</sup> Mark and Workman<sup>4</sup> do not entirely agree with that statement since "in fact this could happen (or at least there could be no variation in  $I_{blk}$ )". For example, they mention that if one reference spectrum was used in conjunction with multiple sample spectra using an FTIR spectrometer that it would not be a true indication of the total error of the measurement because the effect of the noise in the reference reading would have been removed from the calculated standard deviation, whereas the true total error of the reading would in fact include that source of error, even though part of it was constant. Similarly, in the centrifugal devices, multiple detection cells are used with slight imprecision in path length and imperfections in surface

finish resulting in a cell-to-cell variation that may have significantly contributed to the error; however probably not to  $I_{0\%T}$ .

Notwithstanding this observation, for simplicity we shall also use the same assumption as Ingle and Crouch, that no uncertainty exists in measuring the blank signal and be content with the fact that "the approximation is good to within a factor of  $2^{1/2}$ ."<sup>1</sup> Therefore from the transmittance signal (Equation F-2) the noise in transmittance ( $\sigma_T$ ) is simplified from Equation F-15 to Equation F-16, assuming that  $I_{0\%T}$  is negligible with respect to  $I_{blk}$ :

$$\sigma_T = \frac{\sigma_{I_s}}{I_{blk}} \quad (\text{Equation F-16})$$

Similarly, for the enzyme inhibition-based experiments, the noise associated with calculating the percent inhibition (Equation F-4) is a combination of the noise for the absorbance of the sample blank (no pesticide, high absorbance) and the absorbance of the sample. The resulting noise is expressed as:

$$\frac{\sigma_{In(\%)}}{In(\%)} = \sqrt{\left(\frac{\sqrt{\sigma_{A_0}^2 + \sigma_{A_s}^2}}{(A_0 - A_s)}\right)^2 + \left(\frac{\sigma_{A_0}}{A_0}\right)^2} \quad (\text{Equation F-17})$$

This can be rearranged and simplified to:

$$\sigma_{In(\%)} = \frac{A_0 \sqrt{\sigma_{A_0}^2 + \sigma_{A_s}^2} + (A_0 - A_s) \sigma_{A_0}}{(A_0)^2} \times 100 \quad (\text{Equation F-18})$$

Meanwhile, pesticide concentration (Equation F-7) noise, taking into account the antilogarithm error propagation rule (Equation F-13) is equivalent to:

$$\sigma_C = C \ 2.303 \ \sigma_{\ln(\%)} \quad (\text{Equation F-19})$$

A summary of the main signal and noise equations is presented in Table F-2.

**Table F-2. Summary of signal and noise equations for classical absorbance and inhibition experiments**

Signal equations	Noise equations
$T = \frac{I_s - I_{0\%T}}{I_{blk} - I_{0\%T}}$ (Equation F-2)	$\sigma_T = \frac{\sigma_{I_s}}{I_{blk}}$ (Equation F-16)
$A = -\log T = -0.434 \ln T$ (Equation F-3)	$\sigma_A = \frac{0.434 \ \sigma_T}{T}$ (Equation F-14)
$\ln(\%) = \frac{A_0 - A_s}{A_0} \times 100\%$ (Equation F-5)	$\sigma_{\ln(\%)} = \frac{A_0 \sqrt{\sigma_{A_0}^2 + \sigma_{A_s}^2} + (A_0 - A_s) \sigma_{A_0}}{(A_0)^2} \times 100$ (Equation F-18)
$C = 10^{\frac{\ln(\%) - b}{m}}$ (Equation F-7)	$\sigma_C = C \ 2.303 \ \sigma_{\ln(\%)}$ (Equation F-19)

### F.3 Signal-to-Noise and Relative Standard Deviation

The signal-to-noise ratio is a useful number to determine if a measurement is clearly meaningful or just part of the error associated with the instrument.

$$\frac{\text{signal}}{\text{noise}} = \frac{S}{N} = \frac{\text{mean}}{\text{StdDev}} = \frac{\bar{I}}{\sigma} \quad (\text{Equation F-20})$$

The inverse of the signal-to-noise ratio times 100 percent is equivalent to the precision of the measurement, also known as the relative standard deviation.

$$RSD = \text{precision} = \frac{\text{noise}}{\text{signal}} \times 100\% = \frac{N}{S} \times 100\% = \frac{\sigma}{\bar{I}} \times 100\% \quad (\text{Equation F-21})$$

An alternative way of calculating the relative standard deviation is to calculate the standard deviation of a series of results and divide by the average and multiple by 100%.

$$RSD = \frac{\text{Std Dev}}{\text{Average}} \times 100\% \quad (\text{Equation F-22})$$

Using the signal equations detailed in section F.1 and the noise equations detailed in section F.2, the signal-to-noise ratio expression can be elaborated. For example, the signal-to-noise for absorbance (first merging Equation F-3 and Equation F-14 and then Equation F-16) is:

$$\frac{S}{N} = \frac{A}{\sigma_A} = \frac{T A}{0.434 \sigma_T} = \frac{T \ln T}{-\sigma_T} = \frac{T I_{\text{blk}} \ln T}{-\sigma_{I_{\text{sample}}}} \quad (\text{Equation F-23})$$

There is also a well-known effect on the relative precision of spectral analysis as  $T \rightarrow 0$  and as  $T \rightarrow 1$ . The minimum relative error or optimum %T occurs at 36.8 %T.<sup>1</sup> This is found by taking the derivative of Equation F-23, then setting that derivative equal to zero. Once again however, Mark and Workman state that the true optimum would be of 32.994 %T if we had not assumed that there was no uncertainty in measuring the blank reference signal<sup>5</sup>. Their derivation includes a “transcendental equation” that was solved with the method of successive approximations.

Similarly, the relative standard deviation of an absorbance measurement is equivalent to:

$$RSD_{Abs} = \frac{N}{S} \times 100\% = \frac{-\sigma_{I_s}}{T I_{blk} \ln T} \times 100\% \quad (\text{Equation F-24})$$

In the special case of the pesticide determination, the concentration is related to absorbance via the percent inhibition of the reaction. The corresponding signal-to-noise ratio expression (using Equation F-7 and Equation F-19) for the pesticide concentration is:

$$\frac{S}{N} = \frac{C}{\sigma_C} = \frac{1}{2.303 \sigma_{In(\%)}} \quad (\text{Equation F-25})$$

And the corresponding relative standard deviation of the pesticide concentration including the expression for noise of the percent inhibition ( $\sigma_{In(\%)}$ , Equation F-18) is:

$$\begin{aligned}
 RSD_{conc} &= \frac{N}{S} \times 100\% = 2.303 \sigma_{\ln(\%)} \times 100\% \\
 &= 230.3 \frac{A_0 \sqrt{\sigma_{A_0}^2 + \sigma_{A_s}^2 + (A_0 - A_s)\sigma_{A_0}}}{(A_0)^2} \times 100 \\
 &\quad \text{(Equation F-26)}
 \end{aligned}$$

### F.3.1 Absorbance RSD and Concentration RSD

Upon examining the results from Chapter 7 there seems to be a large error in the concentration in terms of its RSD. The RSD of the concentration is much higher than the RSD of absorbance due to two key factors: 1) compounding the error of absorption of the sample blank to that of the sample (comparing by how much the sample absorbed less light) and 2) the logarithmic relationship between concentration and percent inhibition which exponentially increases the error.

To better understand this point, a sample set of data is presented in Table F-3. As described by the above equations and as seen in this table, a small and reasonable absorbance RSD of 3% mathematically corresponds to a concentration RSD of over 30% (calculated by  $SD/ave \times 100$ ) and over 500% (calculated by  $Noise\text{-}to\text{-}Signal \times 100$ ). This large concentration RSD is inherent to the method and due to the purely mathematical propagation of error.

Table F-3. Sample pesticide determination data with propagation of error

	Signal (I)	Transmittance (T)	Absorbance (A)	Percent Inhibition ( $In(\%)$ )	Conc. (C) ppb	Conc. (C) $\mu\text{g/g}$
	11788	0.282	0.550	24.2	50.2	0.25
	11163	0.258	0.588	18.9	28.8	0.14
	11290	0.263	0.580	20.0	32.4	0.16
Average	11414	0.268	0.572	21.1	37.1	0.19
StdDev	330	0.012	0.020	2.8	11.5	0.06
RSD = SD/ave*100	2.9	4.7	3.4	13	30.9	30.9
noise	330	0.011	0.017	2.4	206	--
S/N	35	25	33	7	0.18	--
RSD = N/S*100	2.9	4.0	3.0	11	554	--

Note:  $I_{\text{blk}} = 30800$ ,  $I_{0\%T} = 4320$ ,  $A_0 = 0.725$ ,  $\sigma_{A_0} = 0.0003$ , Calibration curve:  $In(\%) = 21.7 (\log C) - 12.7$

#### F.4 Limit of Detection

The limit of detection (LOD) or detection limit (DL) of an instrument quantifies the smallest signal or concentration of an analyte being measured that can be distinguished from the noise at a given confidence level. It is generally defined as three times (confidence level of 99%) the standard deviation of the blank ( $\sigma_{blk}$ ) divided by the slope of the calibration curve ( $m$ ).

$$LOD = \frac{3\sigma_{blk}}{m} \quad (\text{Equation F-27a})$$

Once the limit of detection is determined in units of concentration, an absolute mass detection limit can also be determined taking into consideration the sample size used in the determination. For example, for a detection limit of 130 ppm and a sample size of 0.03 g, the absolute mass detection limit would be:

$$\text{Absolute mass LOD} = \frac{130 \mu\text{g}}{\text{g}} \times \frac{0.03 \text{ g}}{1} = 4 \mu\text{g} \quad (\text{Equation F-27b})$$

An exception to this definition for the limit of detection is for enzyme inhibition assays such as the pesticide residue determination. Though Equation F-27a is often applied to such types of determinations, this is incorrect due to the mathematical relationships involved. Amine *et al.* correctly describes the true value of the limit of detection as “the concentration of the inhibitor where the confidence interval does not overlap that of the zero concentration of the inhibitor standard,” which graphically has been expressed as Figure F-1:<sup>2</sup>

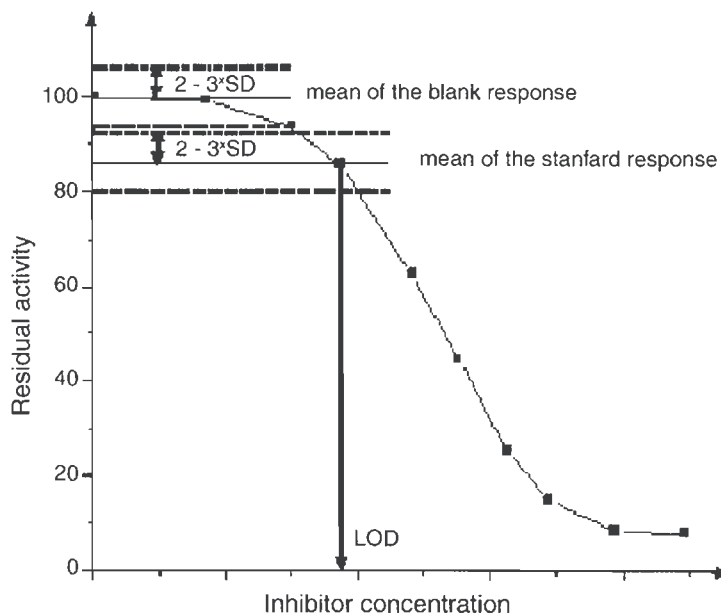


Figure F-1. Reproduced from Amine *et al.*<sup>2</sup>: General method to establish LOD for enzyme inhibition assays

From examination of this figure, the limit of detection for enzyme inhibition assays can be expressed as:

$$LOD_{enzyme\ inhibition\ assay} = 10^{\frac{(In(\%)_0 + 3\sigma_{In(\%)_0} + 3\sigma_{In(\%)_s}) - b}{m}} \quad (\text{Equation F-28})$$

Where  $In(\%)_0$  = percent inhibition of sample without analyte  
 $\sigma_{In(\%)_0}$  = standard deviation of  $In(\%)$  sample without analyte  
 $\sigma_{In(\%)_s}$  = standard deviation of  $In(\%)$  sample

In the case of carbofuran determination this corresponded to a LOD of  $0.1\ \mu\text{g g}^{-1}$  (ppm) or 18% inhibition, well within what is considered typical for enzyme inhibition assay limit of detection of 10 to 20% inhibition.<sup>2</sup>

## **F.5 Comparison Methods**

### **F.5.1 F-test – Comparison of Variance**

An *F*-test is a comparison of the spread of two sets of data to see whether or not their precision is similar.<sup>6</sup> The closer to unity the ratio of the variances of two set of data is, more similar they are. This ratio is compared to a tabulated critical value taking into consideration the respective degrees of freedom of each set. If the calculated *F*-value is less than or equal to the *F*-value of the table (at a given confidence interval, typically 95% or 99%), there is no significant statistical difference in precision. An *F*-test often precedes a student *t*-test since it determines whether or not the standard deviations of the set of data can be pooled or not in the *t*-test.

$$F_{\text{calculated}} = \frac{\sigma_{\text{Set 1}}^2}{\sigma_{\text{Set 2}}^2} \quad (\text{Equation F-29})$$

### **F.5.2 Student's *t*-test – Comparison of Means**

A *student t*-test is a comparison of the two sets of data to see whether or not their means are similar (once the standard deviations of the sets of data have been proven similar, for example via an *F*-test).<sup>6</sup> The calculated *t*-value is then compared to a tabulated *t*-value (with the number of degrees of freedom being equal to  $n_1 + n_2 - 2$ ). If the calculated *t*-value is less than or equal to the *t*-value of the table (at a given confidence interval, typically 95% or 99%), the two sets of data are statistical similar. The calculated *t*-value is equivalent to:

$$t_{calculated} = \frac{|\bar{x}_1 - \bar{x}_2|}{s_p} \sqrt{\frac{n_1 n_2}{n_1 + n_2}} \quad (\text{Equation F-30})$$

Where  $\bar{x}_1$  and  $\bar{x}_2$  are the mean values and  $n_1$  and  $n_2$  are the number of data values in data set 1 and 2, whereas  $s_p$  is the pooled standard deviation of the two sets as defined by Equation F-31. :

$$s_p = \sqrt{\frac{(n_1 - 1) s_1^2 + (n_2 - 1) s_2^2}{n_1 + n_2 - 2}} \quad (\text{Equation F-31})$$

### ***F.6 Multiwavelength Ratiometric Blank Estimation Technique***

For the determination of PAH in soil, a multiwavelength ratiometric blank estimation technique developed in our laboratory was used.<sup>7</sup> Taking advantage of the multiwavelength capabilities of the photodiode array (USB4000-UV-VIS), both an absorbing (334 nm) and non-absorbing (500 nm) wavelengths were monitored. This helped account for the imprecision of the multiple detection cells. This technique was not used for the determination of pesticide since the coloured specie in that case absorbed over the entire available spectral range (*i.e.* no non-absorbing wavelength was available).

Once the absorbing and non-absorbing wavelengths were selected, a blank spectrum was obtained. The ratio of the blank signal at the absorbing wavelength ( $I_{\lambda_{1\text{blank}}}$ ) to the blank signal at the non-absorbing wavelength ( $I_{\lambda_{2\text{blank}}}$ ) was calculated (Equation F-32<sup>7</sup>):

$$\text{Ratio} = \frac{I_{\lambda_1 \text{blank}} - I_{\lambda_1 0\%T}}{I_{\lambda_2 \text{blank}} - I_{\lambda_2 0\%T}} \quad (\text{Equation F-32})$$

Any subsequent sample measurement was corrected by dividing by this ratio (Equation F-33<sup>7</sup>) resulting in an expression for the transmittance using multiwavelength ratiometric blank estimation technique:

$$T = \frac{I_{\lambda_1 \text{sample}} - I_{\lambda_1 0\%T}}{\text{Ratio}(I_{\lambda_2 \text{sample}} - I_{\lambda_2 0\%T})} \quad (\text{Equation F-33})$$

This therefore resulted in an expression equivalent to the general expression for transmittance described earlier:

$$T = \frac{I_s - I_{0\%T}}{I_{blk} - I_{0\%T}} \quad (\text{Equation F-2})$$

Using this technique allowed for the versatile simultaneous measurement of the blank and sample signals, ideal for centrifugal systems and reducing analysis time.

## F.7 References

- (1) Ingle, J.D., Crouch, S.R., "Spectrochemical analysis"; Prentice Hall: Englewood Cliffs, N.J., **1988**, p. 1-590.
- (2) Amine, A., Mohammadi, H., Bourais, I., Palleschi, G., "Enzyme inhibition-based biosensors for food safety and environmental monitoring", *Biosensors and Bioelectronics*, **2006**, 21 (8), 1405-1423.
- (3) Skoog, D.A., Holler, F.J., Nieman, T.A., "Principles of instrumental analysis"; 5<sup>th</sup> ed.; Saunders College Pub.: Fort Worth :, **1992**,
- (4) Mark, H., Workman Jr, J., "Analysis of noise -Part II", *Spectroscopy*, **2000**, 15 (11), 20-23.
- (5) Mark, H., Workman Jr, J., "Analysis of noise - Part III", *Spectroscopy*, **2000**, 15 (12), 15-17.
- (6) van Reeuwijk, L.P., "Guidelines for Quality Management in Soil and Plant Laboratories"; Food and Agriculture Organization of the United Nations: Rome, **1998**, Chapter 6: Basic Statistical Tools.
- (7) LaCroix-Fralish, A., Clare, J., Skinner, C.D., Salin, E.D., "A centrifugal microanalysis system for the determination of nitrite and hexavalent chromium", *Talanta*, **2009**, 80 (2), 670-675.

## Appendix G: Sedimentation Rate and Stokes' Law

In order to effectively integrate solid sample preparation to centrifugal microfluidics, separation of the processed solid particles from the extractant is necessary. Among the techniques to achieve this is the sedimentation by centrifugation inherently present in centrifugal microfluidics. This appendix details the physical properties involved and parameters that were optimized applying Stokes' Law to our devices.

### G.1 Stokes' Law<sup>1</sup>

The velocity at which a small spherical particle sediments in a liquid was first mathematically described by George Stokes in 1845.<sup>1</sup> Stokes' Law states that the magnitude of the resistive frictional force ( $F_r$ ) on the particle of a given Stokes' radius ( $R$ ) sedimenting through a fluid of viscosity ( $\eta$ ) with a velocity ( $v$ ) is:

$$F_r = 6\pi\eta Rv \quad (\text{Equation G-1})$$

Three forces act on a particle in a liquid, 1) the resistive frictional force ( $F_r$ ), 2) the weight of the spherical particle ( $w$ ) and 3) the buoyant force ( $B$ ). The resistive frictional force has just been defined by Stokes' Law. The weight of the spherical particle can be described as:

$$w = mg = \rho_p g V = \rho_p g \left( \frac{4}{3} \pi R^3 \right) \quad (\text{Equation G-2})$$

Where  $\rho_p$  is the density of the particle,  $g$  is the acceleration due to gravity and the  $V$  is the volume.

In regards to the buoyant force, Archimedes' principle states that “any body completely or partially submerged in a fluid is buoyed up by a force equal to the weight of the fluid displaced by the body.”<sup>1</sup> Consequently, the buoyant force ( $B$ ) is described as:

$$B = \rho_f g V = \rho_f g \left( \frac{4}{3} \pi R^3 \right) \quad (\text{Equation G-3})$$

Where  $\rho_f$  is the density of the fluid.

When both the frictional force and the buoyant force equal the weight of the particle, the terminal velocity ( $v_t$ ) or *settling velocity* ( $v_s$ ) of the particle in the fluid is reached:

$$F_r + B = w \quad (\text{Equation G-4a})$$

$$6\pi\eta R v_t + \rho_f g \left( \frac{4}{3} \pi R^3 \right) = \rho_p g \left( \frac{4}{3} \pi R^3 \right) \quad (\text{Equation G-4b})$$

Solving Equation G-4b for velocity gives an expression for the settling velocity by gravity:

$$v_s = \frac{2R^2 g}{9\eta} (\rho_p - \rho_f) \quad (\text{Equation G-5})$$

## ***G.2 Application of Stokes' Law to Centrifugal Microfluidics***

For clinical and environmental applications, particles are often quite small (blood cells in plasma or fine soil particles). Waiting for particles to sediment by gravity in a test tube is neither practical nor common. For this reason a centrifuge is very often used to increase the velocity at which material fall through a fluid, in other words, to increase the *sedimentation rate*. Instead of

experiencing the gravitational acceleration ( $g$ ), particles would experience the much larger radial acceleration ( $a_c$ ):

$$a_c = \frac{v^2}{r} = \omega^2 r \quad (\text{Equation G-6})$$

Consequently, the settling velocity of a particle in a centrifuge would be dependent on both the angular velocity of the motor ( $\omega$ ) – often expressed as revolution per minute (rpm), hertz (Hz) or radian per second ( $\text{rad s}^{-1}$ ), where  $60 \text{ rpm} = 1 \text{ Hz} = 2\pi \text{ rad s}^{-1}$  – and the distance of the particle from the centre of rotation ( $r$ ). Substituting the gravitational acceleration for the radial acceleration in Equation G-5 yields the settling velocity of particle by centrifugation:

$$v_s = \frac{2R^2\omega^2r}{9\eta}(\rho_p - \rho_f) \quad (\text{Equation G-7})$$

### G.2.1 Application to the Sedimentation of Soil

For example, one set of chambers for the soil analysis centrifugal microfluidic device is illustrated here (designed and manufactured for the enzyme inhibition assay for the determination of pesticide residue):

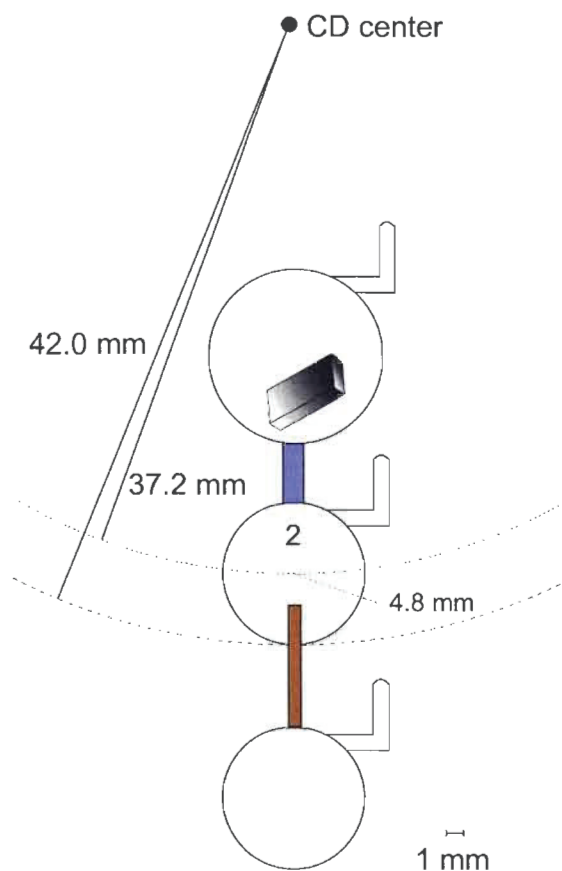


**Figure G-1. One set of chambers of soil analysis centrifugal device**

According to the literature,<sup>2</sup> soil has an average density is of  $2.6 \text{ g cm}^{-3}$ . Likewise, the upper limit of the Stokes radius for coarse sand particles is 1 mm, whereas the smallest particles present in soil typically have Stokes radii of approximately  $3 \times 10^{-5} \text{ mm}$ .<sup>2</sup> Finally, the viscosity of water is  $8.90 \times 10^{-4} \text{ Pa s}$  ( $\text{kg s}^{-1} \text{ m}^{-1}$ ) and the motor was spun at an angular velocity of 2000 rpm (33 Hz or  $209 \text{ rad s}^{-1}$ ) in the spin protocol to sediment the soil for the pesticide determination. The experimental conditions are summarized in Table G-1.

**Table G-1. Experimental conditions used to calculate the settling velocities and rates.**

	Units	Value
Average radial distance	mm	37.2
Distance needed to travel	mm	4.8
Density of particle	$\text{g cm}^{-3}$	2.6
Density of fluid (water)	$\text{g cm}^{-3}$	1.0
Density of fluid (hexane)	$\text{g cm}^{-3}$	0.65
Viscosity (water)	$\text{g m}^{-1} \text{s}^{-1}$	0.89
Viscosity (hexane)	$\text{g m}^{-1} \text{s}^{-1}$	0.29

With these parameters, the settling velocities for a range of Stokes' radii and a range of motor angular velocities were calculated using Equation G-7. These settling velocities for soil in water are summarized in Table G-2 whereas the times needed for soil particles to settle to bottom of chamber in water are summarized in Table G-3.

**Table G-2. Settling velocities of soil in water**

Settling velocities ( $\text{mm s}^{-1}$ )		Angular velocity (rpm)						
		50	80	155*	400	800	1200	2000
Stokes' radius (cm)	0.000003	3.7E-07	9.4E-07	3.5E-06	2.3E-05	9.4E-05	2.1E-04	5.9E-04
	0.00003	3.7E-05	9.4E-05	3.5E-04	0.002	0.01	0.02	0.06
	0.0003	3.7E-03	0.01	0.04	0.2	0.9	2	6
	0.003	0.37	0.9	3.5	23	94	211	587
	0.03	37	94	352	2.3E+03	9.4E+03	2.1E+04	5.9E+04
	0.1	407	1.0E+03	3.9E+03	2.6E+04	1.0E+05	2.3E+05	6.5E+05

\*155 rpm at average radial distance of 37.2 mm is equivalent to the force of gravity ( $9.8 \text{ m s}^{-2}$ )

**Table G-3. Time needed for soil particles to settle to bottom of chamber in water**

Time to settle 4.8 mm (s)		Angular velocity (rpm)						
		50	80	155*	400	800	1200	2000
Stokes' radius (cm)	0.000003	1.3E+07	5.1E+06	1.4E+06	2.0E+05	5.1E+04	2.3E+04	8.2E+03
	0.00003	1.3E+05	5.1E+04	1.4E+04	2.0E+03	511	227	82
	0.0003	1.3E+03	5.1E+02	136	20	5	2	0.8
	0.003	13	5	1	0.2	0.1	0.02	8.2E-03
	0.03	0.1	0.05	0.01	2.0E-03	5.1E-04	2.3E-04	8.2E-05
	0.1	0.01	4.6E-03	1.2E-03	1.8E-04	4.6E-05	2.0E-05	7.4E-06

\*155 rpm at average radial distance of 37.2 mm is equivalent to the force of gravity ( $9.8 \text{ m/s}^2$ )

As mode of comparison, a very small soil particle with a Stokes' radius of  $3.0 \times 10^{-4}$  mm would have taken approximately 82 seconds to settle to the bottom of Chamber 2 (Figure G-1) with the motor spinning at 2000 rpm; however, it would have taken that same particle almost 9 minutes to settle the same distance at 800 rpm.

If the fluid was a different solvent such a hexane, which was used for the PAH determination, the sedimentation rate would change. A comparison of the time needed for particle of the same size to settle in hexane and in water under different forces (gravitational acceleration or radial acceleration) is presented in Table G-4, the difference being in the density and viscosity of the solvent (see values in Table G-1).

**Table G-4. Comparison of time needed for soil particle to settle in hexane and water**

	Hexane	Water
gravity	1.0 hour	3.8 hours
400 rpm	9.1 min	34 min
800 rpm	2.3 min	8.5 min
1200 rpm	1.0 min	3.8 min
2000 rpm	22 sec	82 sec

\* based on particle of Stokes' radius of  $3.0 \times 10^{-4}$  mm settling 4.8 mm from an average radial distance of 37.2 mm

Therefore the sedimentation rate is governed by Stokes' Law and is directly dependent on the location of the particle on the device (radial distance), the motor's angular velocity, as well as the particle's and fluid's physical properties (Stokes' radius, density and viscosity).

### **G.3 References**

- (1) Serway, R.A., Faughn, J.S., "College physics"; 4th ed.; Saunders College: Fort Worth, **1995**, 1032.
- (2) Coutts, J.R.H., "The estimation of the specific surface of a soil from mechanical analysis data", *British Journal of Applied Physics*, **1955**, 6 (3), 90.